Nanomaterials Embedded Nitrogen-Doped Graphene for Advanced Energy Storage and Conversion

A thesis submitted in fulfillment of the requirements for the degree of Doctor of Philosophy

By

Shaikh Nayeem Faisal

School of Chemical and Biomolecular Engineering

Faculty of Engineering and Information Technologies

The University of Sydney

May 2017

DECLARATION

I hereby declare that this submission is my own work and that, to the best of my knowledge and belief, it contains no material previously published or written by another person nor material which to a substantial extent has been accepted for the award of any other degree or diploma of the university or other institute of higher learning, except where due acknowledgment has been made in the text.

Shaikh Nayeem Faisal

May 2017

ABSTRACT

A facile synthesis of nitrogen-doped graphene with high atomic percentage of Nitrogen (9.2 at%) including high ratio of pyridinic N and graphitic N has been reported *via* thermal annealing of graphene oxide with uric acid. The resultant material shows efficient electrochemical properties for capacitances and bifunctional electrocatalysis of oxygen reduction reaction (ORR) and oxygen evolution reaction (OER). In spite of its remarkable electrochemical properties, the major limitation of the two-dimensional graphene like materials for device fabrication or commercial applications is the restacking nature of the layers. Designing a three-dimensional nanostructure via inserting metal nanoparticles or one-dimensional carbonaceous nanomaterials inside the graphene layers can prevent the restacking of the layers and hence enhance the electrochemical properties of the composites by providing higher electroactive surface area for electrolyte permeation, charge storage as well as active sites for electrocatalysis. To enhance the electrocatalytical activity of the synthesized nitrogen-doped graphene, a hybrid of nickel embedded nitrogen-doped graphene is developed. The composite shows superior noble-metal-free quadrafunctional electrocatalysis of oxygen reduction reaction (ORR), oxygen evolution reaction (OER), hydrogen evolution reaction (HER) and hydrogen peroxide oxidation reaction (HPOR) compared to commercial electrocatalysts of Pt/C and Ru/C. Alternatively, the insertion of carbon nanotubes inside the graphene layers and fabricating a lamellar three-dimensional nanostructure exhibit excellent supercapacitor behavior as fabricated as solid-state supercapacitor and high-rate capable anode for Li-ion battery as well as metal-free bifunctional electrocatalysis of ORR and OER. In addition, the decoration of copper nanoparticles in the three-dimensional nanostructured nitrogen-doped graphene/carbon nanotube composite further improves the conductivity and electrochemical properties *via* interconnecting network of copper nanoparticles and carbon nanotubes with the graphene layers and have been evaluated for high performance metal-ion battery applications. The resultant composites show promising electrochemical performances for developing as electrode materials for next generation energy storage and conversion devices like solid-state supercapacitor, metal-ion battery, metal-air battery and rechargeable fuel cells.

LIST OF PUBLICATIONS

Parts of this thesis and some related experiments have been published and submitted for publication as follows:

Patent Application:

1. Electrocatalysis and Electrochemical cell. M. Arab, A. I. Minett, T. L. Church, L. Xiaobo, T. Maschmeyer, N. Noorbehesht, A. T. Harris, **S. N. Faisal**, A. Hussain, Patent Number-WO/2016/141414, Patent Application number-PCT/AU2016/000081.

Journals:

1. Pyridinic and Graphitic Nitrogen-rich Graphene for High-Performance Supercapacitors and Metal-Free Bifunctional Electrocatalysts for ORR and OER**. S. N. Faisal***, E. Haque, N. Noorbehesht, W. Zhang, A. T. Harris, T. L. Church and A. I. Minett*, *RSC Advances* 2017, 7(29), 17950-17958.

2. Three Dimensional Cellular Architecture of Sulfer-doped graphene: Self-standing Electrode for Flexible Supercapacitors, Lithium ion and Sodium ion Batteries. M. M. Islam, C. M. Subramaniyam, T. Akhter, **S. N. Faisal**, A. I. Minett, H. K. Liu, K. Kostantinov and S. X. Dou. *J. Material Chemistry A*, 2017, 5(11), 5290-5302.

3. In-situ Direct Grafting of Graphene Quantum Dots onto Carbon Fibre by Low Temperature Chemical Synthesis for High Performance Flexible Fabric Supercapacitor, M. S. Islam, L. Tong, M. Hasan, A. I. Minett, V. G. Gomes, Y. Deng, A. K. Roy, **S. N. Faisal**, *Materials Today Communication*, 2017, 10, 12-119.

4. Liquid-Crystal-Mediated 3D Macrostructured Composite of Co/Co_3O_4 Embedded in Graphene: Free-Standing Electrode for Efficient Water Splitting. M. M. Islam, S. N. Faisal, T. Akhter, A. K. Roy, A. I. Minett, K. Konstantinov and S. X. Dou, *Particle & Particle Systems Characterizations,* 2017 (Just accepted). *(M. M. Islam and S. N. Faisal are contributed equally*)

5. Doped Graphene/Cu Nanocomposite: A High Sensitivity non-Enzymatic Glucose Sensor for Food, L. Shabnam, **S. N. Faisal**, A. K. Roy, E. Haque, A. I. Minett and V. G. Gomes, *Food Chemistry,* 2017, 221, 751-759.

6. Nonenzymatic Multispecies Sensor based on Cu-Ni Nanoparticle Disperson on Doped-Graphene, L. Shabnam, **S. N. Faisal**, A. K. Roy, A. I. Minett and V. G. Gomes, *Electrochimica Acta*, 2017, 224, 295-305.

7. Self-Assembled N/S Co-doped Flexible Graphene Paper for High Performance Energy Storage and Oxygen Reduction Reaction. T. Akhter, M. M. Islam, **S. N. Faisal**, E. Haque, A. I. Minett, H. K. Liu, K. Konstantinov, S. X. Dou. *ACS Applied Materials and Interfaces,* 2016, 8, 2078-2086.

8. Grafting carbon nanotubes directly onto carbon fibers for superior mechanical stability: Towards next generation aerospace composites and energy storage applications. M. S. Islam, Y. Deng, L. Tong, **S. N. Faisal**, A. K. Roy, A. I. Minett, V. G. Gomes, *Carbon,* 2016, 96, 701-710.

9. Nitrogen doped Graphene *via* Thermal Treatment of Composite Solid Precursors as a High Performance Supercapacitor. E. Haque, M. M. Islam, E. Pourazadi, M. Hassan, **S. N. Faisal,** A. K. Roy, K. Konstantinov, A. T. Harris, A. I. Minett and V. G. Gomes, *RSC Advances*, 2015, 5, 30679-30686.

10. Synthesis of Nitrogen-Doped Graphene via Thermal Treatment of Graphene Oxide within Methylimidazole and its Capacitance Performance as Electric Double Layer Capacitor. M. M. Islam, **S. N. Faisal**, A. K. Roy, S. Ansari, D. Cardillo, K. Konstantinov, E. Haque, *Journal of Nanotechnology and Materials Science,* 2015, 2(1), 1-5.

11. Hierarchical assembly of graphene/polyaniline nanostructures to synthesize free-standing supercapacitor electrode. M. Hassan, K. R. Reddy, E. Haque, **S. N. Faisal**, Samira Ghasemi, Andrew I. Minett, Vincent G. Gomes, *Composites Science and Technology*, 2014, 98, 1–8.

Manuscripts in progress

1. 3D Nanostructured Nitrogen-Doped Graphene/Carbon Nanotube Composites for Large Volumetric Solid State Supercapacitor, Highly Stable Anode for Li-Ion Battery and Metal-Free Bifunctional Electrocatalyst, **S. N. Faisal**, C. M. Subramaniyam, P. Newman, E. Haque, N. Noorbehesht, A. K. Roy, M. M. Islam, M. S. Islam,H. K. Liu, S. X. Dou, A. T. Harris and A. I. Minett, *ACS Nano*, 2017 (to be submitted).

2. Nickel Embedded Nitrogen-Doped Graphene as Quadrafunctional Electrocatalyst for ORR, OER, HER and HPOR**. S. N. Faisal**, N. Noorbehesht, L. Shabnam, A. K. Roy, E. Pourazadi, E. Haque, M. S. Islam, A. T. Harris and A. I. Minett, , *Nano Energy, 2017* (To be submitted).

3. Three-dimensional Copper-confined Nitrogen-Doped Graphene/Carbon Nanotube Composites as High Performance Anode for Li-Ion Battery. **S. N. Faisal**, C. M. Subramaniyam, E. Haque, A. K. Roy, M. M. Islam, H. K. Liu, S. X. Dou, A. T. Harris and A. I. Minett, (Manuscript in preparation).

Conference Presentations:

01. "Nitrogen-doped Graphene with High Nitrogen level for High Performance Supercapacitor Applications and Efficient Electrocatalysis", **Shaikh Nayeem Faisal,** 12th *International Conference on Frontiers of Polymers and Advanced Materials,* 2013 held in Auckland, New Zealand.

02. "3D Nitrogen-doped Graphene/ Carbon nanotube for High Performance Flexible Supercapacitor", **Shaikh Nayeem Faisal,** *Graphene Week,* 2015 held in Manchester, United Kingdom.

03. Nanostructured Material for Advanced Energy Storage and Conversion. **Shaikh Nayeem Faisal,** International Symposium on Graphene Device, 2016 held in Brisbane, Australia (**Awarded as ANN Bursary**)

ACKNOWLEDGEMENTS

I am grateful to my supervisors Prof. Andrew Harris and Prof. Andrew Minett for the patient guidance, expert knowledge, research suggestion and valuable support that they have provided me all through my PhD candidature.

I would like to thank the School of Chemical and Biomolecular Engineering at University of Sydney for the Postgraduate Research Scholarship. Needless to say without this opportunity, this work would not be existed. I also thank the staff in the school for their kind assistance on administrative functions.

Many thanks also go to the staff of the Australian Centre for Microscopy & Microanalysis (ACMM) and Vibrational Specreoscopy Core Facility (VSCF) at University of Sydney, in particular Mr. Joonsup Lee, Dr. Honwei Liu for their patient training and useful discussions on the analysis of nanostructured materials. Also thanks to Dr. Bill Gong of Surface Analysis Laboratory, University of New South Wales for his valuable support for XPS.

I wish also acknowledge the support of my colleagues in the Laboratory of Sustainable Technology led by Dr. Andrew Harris and Dr. Andrew Minett.

Most importantly, I am sincerely grateful to my parents, family members and friends, specially my Mother and Grandparents, for whose inspiration I come to this level and my beloved wife and children who always keep me relax in this stressful journey of life.

TABLE OF CONTENTS

Chapter 1:

INTRODUCTION

1. INTRODUCTION

Nanostructured materials have attracted great interest for developing next generation energy storage and conversion devices due to their unique electrical, optical and mechanical properties. The size, shape, dimensions, surface area and porosity make them suitable for energy storage and conversion, catalysis, gas storage and sensing related applications. [1-3] The fast development of energy storage and conversion devices, specially the portable electronics, hybrid renewable devices, the smart grid and the transport sector, increased the demand of new materials with excellent electrochemical properties. [2] The physical and chemical behavior of the nanostructured materials not only depends on their unique intrinsic properties but also highly depends on the dimension and structure. Such as, even the 0 dimensional fullerene, 1 dimensional carbon nanotube and 2 dimensional graphene all are consist of sp2-bonded hydrocarbons, their physical, chemical and surface properties are different. [4] In the vast sections of nanomaterials, noble metal nanoparticles show superior electrocatalytical properties especially in oxygen reduction reaction, oxygen evolution reaction and hydrogen evolution reaction. [2, 3, 6] transitional metal nanoparticles exhibit efficient electrochemical properties [5-6] and carbon based nanostructured materials are found as electrode materials for energy storage, conversion, gas storage and electrocatalysis. [4, 7-10] The electrochemical energy storage properties of material are crucial for developing high performance energy storage devices and nanostructured materials are getting wide attention for their high conductivity and catalytical activity due to their specific structure, surface area and reduced electron transport length. The noble metal nanoparticles are the state of the art electrode material for energy storage and conversion, however these are often suffered for the scarcity and poisoning. [6, 8] The transition metals have been shown superior electrocatalytic activity but still suffer for the cost and stability for potential applications. [8] Carbon materials are of great interest owing to their abundance, stability and relative environment-friendliness. In particular, the excellent chemical stability across a wide temperature range in either acidic or basic media makes carbon materials extremely attractive for use as electrodes in electrochemical energy devices. [4,8, 10] In particular, nanostructured carbon materials for efficient energy storage and conversion devices have been reported for a wide range of applications including as solar cells, [11] fuel cells, lithium-ion batteries and electrochemical double-layer capacitors. [2-4] Among these energy storage devices, supercapacitors have gained attention due to their orders-of-magnitude-higher

power density, cycle efficiency and charge/discharge rates than batteries. [12, 13] Besides energy storage, energy conversion is also crucial to meeting global energy demands. Fuel cells are among the promising methods of delivering energy in the future, but their widespread implementation is hindered by the expenses of the cathode material (platinum), as well as by their deactivation by the by-products of fuel decomposition (the fuel crossover effect), making the development of alternative, precious-metal-free electrode materials with high priority.[7, 14, 15] Among the different available carbon allotropes, graphene with two-dimensional structure have been emerged as exciting materials for electrochemical energy storage. [16] Graphene consists of a flat monolayer of *sp2*-bonded carbon atoms into a two dimensional (2D) honeycomb lattice with large theoretical surface area (2630 m^2/g), high mobility of charge carriers (200,000 cm^{-2}/ Vs, anomalous quantum Hall effect and mass less relativistic carries. [16]

Chemical dopants can alter the electronic properties of graphene. [17] The introduction of dopants, either by the adsorption of molecules on the graphene surface or by the substitution of dopant atoms into the carbon lattice, can produce a band gap in graphene, and this strategy has led to the development of high-performance energy storage and conversion devices.[18, 19] Various heteroatoms, including N, B, and S, have imparted excellent electrochemical properties,[20-24] and N-doped graphene in particular has shown capacitance suitable for high-performance supercapacitors applications,[25-29] excellent electrocatalytic activity for oxygen reduction in fuel cells [30, 31] and oxygen evolution reaction for rechargeable metal-air batteries.[32, 33] The properties of nitrogen-doped graphene (NG) are conferred by nitrogen atoms within the carbon lattice, where they can exist as pyridinic, pyrrolic, graphitic, and oxidized N (Scheme 1).[34] The roles of the differently configured nitrogen atoms in enhancing capacitance or generating catalytically active sites are still controversial,[35, 36] but both quantum mechanical calculations [37-39] and experimental [27, 40] investigations indicate that graphitic, pyridinic, and pyrrolic N can enhance the capacitance, whereas pyridinic N and graphitic N can be essential to catalyzing oxygen reduction reaction by enhancing the adsorption of O_2 on the adjacent carbon atoms and thus promotes the four-electron pathway.[41-44] Besides the capacitance and oxygen reduction reaction, oxygen evolution reaction has gained a considerable attention due to the promising future of rechargeable metal-air batteries.[45-47] N-doped graphene,[32] NG/CNT composites,[33] N-doped coaxial carbon nanotube,[48] carbon

nitrogen nanotubes[49] and nitrogen and phosphorous co-doped nanocarbons[50, 51] have shown to be promising alternatives to noble and transition metal based OER catalysts.

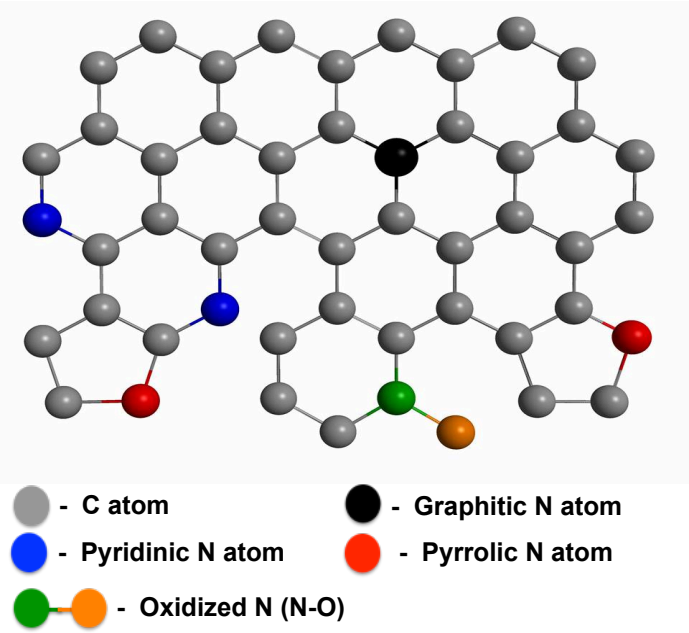

Scheme 1. Schematic structure of Nitrogen-doped Graphene.

The scalable synthesis of nitrogen-doped graphene with high atomic percentage of nitrogen enriched with high ratio of pyridinic N and graphitic N is crucial for revealing the best performance. The types and amounts of the different nitrogen bonding configurations in an N-doped graphene sample largely depend on the nitrogen source as well as the synthesis method. Nitrogen has been incorporated into the graphitic lattice from sources like acetonitrile,[52] pyridine[53] and ammonia[54, 55] via chemical vapor deposition (CVD) or high-temperature treatment, and the resulting materials have been applied in lithium batteries,[52-55] field effect transistors,[53] and as catalysts for oxygen reduction.[54] However, it is difficult to obtain materials with high levels of atomic nitrogen doping, and on a large scale, *via* CVD using gaseous or liquid sources of nitrogen, and the method also suffers from practical limitations due to possible contamination from the metal deposition catalyst as well as the toxicity of the precursors. On the other hand, the co-pyrolysis of graphene or a graphene precursor with a solid source of nitrogen, such as melamine[55] or cyanamide,[56] has produced NG with high levels

of nitrogen (~9 at%). Co-pyrolysis methods are attractive because they can be scaled up without any catalyst.[57] However, the NG synthesized from melamine had a low surface area; whereas cyanamide, on the other hand, required a surfactant to bind to the graphene surface.[56] Moreover, the NG synthesized from cyanamide did not contain pyrrolic nitrogen,[56] which plays an important role in enhancing capacitance.[37] In addition to melamine and cyanamide, urea has been employed as a solid source of nitrogen in the synthesis of N-doped graphene, however both the capacitance and electrocatalytic properties in the material were not investigated.[57-59] In order to show both high capacitance and electrocatalytic activity, an NG sample must contain sufficient percentages of pyridinic, pyrrolic, and graphitic nitrogen atoms, and have large surface area and high pore volume.

The improvement of the electrochemical properties of graphene via heteroatom doping can be suffered due to the assembling nature of graphene driven by the van der Waals interactions between neighboring sheets and results in a loss of effective surface area during the device fabrication for high amount of mass loading on the current collector. The use of nanoparticles or carbon nanostructure as spacer between the graphene layers can be an excellent option to overcome this limitation. [60-61] The restacking of graphene layers is the major limitation which prevent the permeation of electrolyte between the layers and reduce the surface area causing the decrease of capacitance and electrochemical properties.[62] Tremendous efforts are going on to improve the capacitance properties of graphene by modifying the structural effect. [63-66] Alternatively, graphene based nanocomposites with other carbonaceous nanomaterials, conductive polymer and metallic nanoparticles have gained a lot of attractions by enhancing the excellent electrical conductivity with high surface area of graphene *via* the different structural effect to prevent the restacking of the layers with the aid of conjugated nanomaterials. [67-69] Among the metallic nanoparticles except noble metal nanoparticles, transition metal nanoparticles are showing superior electrocatalytical activity and their low cost production is suitable for device fabrication as well as commercial applications. [67] The insertion of transition metal nanoparticles between the nitrogen-doped graphene layers not only increase the electrochemically active surface area but also enhance the electrocatalytic activity *via* the synergistic effect of both the materials. The insertion of nanoparticles inside the graphene layers helps to develop a three dimensional structure, however it is hard to develop a regular structure with strong attachment of nanoparticles with the graphene surface as there are no chemical

bonding. The conjugation of one-dimensional carbon nanotubes (CNTs) with two-dimensional graphene nanosheets can be an alternate option by utilizing the carbon-carbon strong bond which not only provide a three-dimensional lamellar structure for better electrolyte penetration but also develop a strong electromechanical properties for better stability during the cycle test and stress in energy storage and conversion devices. [70-73] The nitrogen-doped three-dimensional building block nanocarbon structure can provide the space for permeation of ions for increasing the capacitance properties and metal ion storage properties for metal-ion batteries as well as improve the electrocatalytical activity for oxygen reduction reaction and oxygen evolution reaction.[33, 74] To further improve the electrochemical properties, the transitional metal nanoparticles embedded three-dimensional nitrogen-doped graphene/ carbon nanotube lamellar structure can be the promising electrode material for their rigid structure, better conductivity due to carbon/ metal network, large electrocatalytic surface area and stability for fabricating advanced energy storage and conversion devices for commercial applications.

Here, in this thesis, we have synthesized nitrogen-doped graphene with high atomic percentage of nitrogen enriched with high ratio of pyridinic N and graphitic N in a facile synthesis method of thermal annealing of graphene oxide with uric acid as a solid nitrogen precursor. The resultant material shows excellent capacitance properties and electrocatalytical activity of oxygen reduction reaction and oxygen evolution reaction and discussed in details in chapter 3. The electrocatalytical properties of the material has been improved by inserting transition metal nanoparticle (nickel) inside the graphene layers by single pot synthesis, which not only provide better ion permeation by forming a three dimensional structure but also enhance the electrochemical activity by incorporating the superior electrocatalytical properties of nickel nanoparticles. The resultant nickel embedded nitrogen-doped graphene material shows synergistic electrocatalytic activity as a quadrafunctional electrocatalyst for oxygen reduction reaction, oxygen evolution reaction, hydrogen evolution reaction and hydrogen peroxide oxidation reaction (Chapter 4). To improve the energy storage properties for supercapacitors and metal-ion battery application, a three-dimensional lamellar-architectured nitrogen-doped graphene/ carbon nanotube composite has been synthesized and that composite shows superior gravimetric and volumetric capacitance properties as electrode for solid state supercapacitors due to the better electrochemical surface area and high rate capability and stability as anode for lithium-ion battery. The high atomic percentage of nitrogen doping and three-dimensional

structure also lead to investigate the electrocatalytical activity and the composite and the electrode shows superior bifunctional electrocatalytical activity of oxygen reduction reaction and oxygen evolution reaction comparable with the state of the art noble metal electrocatalyst as a promising electrode material for metal-air batteries (Chapter 5). Following the similar facile one pot procedure of nitrogen-doped graphene/ carbon nanotube composite, copper nanoparticle confined nitrogen doped graphene/ carbon nanotube composite has been synthesized. The resultant composite possess higher conductivity due to the presence of highly conductive copper nanoparticles inside the graphene/ carbon nanotube layers and exhibits superior electrode as anode for lithium-ion battery than the nitrogen-doped graphene/ carbon nanotube discussed in chapter 6. This composite shows promising material for fabricating hybrid supercapacitor, metal-ion and metal-air batteries. The synthesized procedure can be applied to develop different nanostructured composites by inserting different metal nanoparticles inside the graphene/carbon nanotube network to explore the electrochemical energy storage and elecrocatalytical properties to develop advanced energy storage and hybrid devices, metal air batteries and rechargeable fuel cells.

References:

1. Winter, M., Brodd, R. J. What are Batteries, Fuel Cells and Supercapacitors. *Chem. Rev.* **2004,** *104,* 4245–4269.

2. Liu, C., Li, F., Ma, L. –P. Cheng, H. -M. Advanced Materials for Energy Storage. *Adv. Mater.* **2010,** *22,* E28–E62.

3. Arico, A. S., Bruce, P., Scrosati, B., Tarascon, J. M., Schalkwijk, W. V. Nanostructured Materials for Advanced Energy Conversion and Storage Devices. *Nat. Mater.* **2005,** *4,* 366–377.

4. Wang, Y.; Wei, H.; Lu, Y.; Wei, S.; Wujcik, E. K.; Guo, Z. Multifunctional Carbon Nanostructures for Advanced Energy Storage Applications. *Nanomaterials* **2015,** *5,* 755-777.

5. Chen, Z.; Higgins, D.; Yu, A.; Zhang, J. A Review on Non-Precious Metal Electrocatalysts for PEM Fuel Cells. *Energy. Environ. Sci.* **2011***, 4,* 3167-3192.

6. Manthiram, A.; Murugan, A. V.; Sarkar, A.; Muraliganth, T. Nanostructured Electrode Materials for Electrochemical Energy Storage and Conversion. *Energy Environ. Sci.* **2008,** *1,* 621-638.

7. Jaouen, F., Proietti, E., Lefèvre, M., Chenitz, R., Dodelet, J. –P., Wu, G., Chung, H. T., Johnston, C. M., Zelenay, P. Recent Advances in Non-Precious Metal Catalysis for Oxygen Reduction Reaction in Polymer Electrolyte Fuel Cells. *Energy Environ. Sci.* **2011,** *4,* 114–130.

8. Choi, H. –J., Jung, S. -M. Seo, J. M., Chang, D. W., Dai, L., Baek, J. –B. Graphene for Energy Conversion and Storage in Fuel Cells and Supercapacitors. *Nano Energy* **2012,** *1,* 534–551.

9. Zhang, X., Wang, B., Sunarso, J., Liu, S., Zhi, L. Graphene Nanostructures toward Clean Energy Technology Applications. *WIREs Energy Environ.* **2012,** *1,* 317–336.

10. Sun, Y., Wu, Q., Shi, G. Graphene based New Energy Materials. *Energy Environ. Sci.* **2011,** *4,* 1113-1132.

11. Ramuz, M. P., Vosgueritchian, M., Wei, P., Wang, C., Gao, Y., Wu, Y. Chen, Y., Bao, Z. Evaluation of Solution-Processable Carbon-based Electrodes for all-Carbon Solar Cells. *ACS Nano* **2012,** *6,* 10384–10395.

12. Simon, P., Gogotsi, Y. Materials for Electrochemical Capacitors. *Nat. Mater.* **2008,** *7,* 845–854.

13. Zhu, Y., Murali, S., Stoller, M. D., Ganesh, K. J., Cai, W., Ferreira, P. J., Pirkle, A., Wallace, R. M., Cychosz, K. A., Thommes, M., Su, D., Stach, E. A., Ruoff, R. S. Carbon-based Supercapacitors Produced by Activation of Graphene. *Science* **2011,** *332,* 1537-1541.

14. Shao, Y., Liu, J., Wang, Y. Lin, Y. Novel Catalyst Support Materials for PEM Fuel Cells: Current Status and Future Prospects. *J. Mater. Chem.* **2009,** *19,* 46–59.

15. Zheng, Y. Jiao, Y., Jaroniec, M., Jin, Y., Qiao, S. Z. Nanostructured Metal-Free Electrochemical Catalysts for Highly Efficient Oxygen Reduction. *Small* **2012,** *8,* 3550–3566.

16. Geim, A. K., K. S. K. S. The Rise of Graphene. *Nat. Mater.* **2007,** *6,* 183–191.

17. Liu, H., Liu, Y., Zhu, D. Chemical Doping of Graphene. *J. Mater. Chem.* **2011,** *21,* 3335–3345.

18. Guo, B., Fang, L., Zhang, B., Gong, J. R. Graphene Doping: A Review. *Insci. J.* **2011,** *1,* 80–89.

19. Lv, R., Terrones, M. Towards New Graphene Materials: Doped Graphene Sheets and Nanoribbons. *Mater. Lett.* **2012,** *78,* 209–218.

20. Han, J., Zhang, L. L., Lee, S., Oh, J., Lee, K. –S., Potts, J. R., Ji, J., Zhao, X., Ruoff, R. S., Park, S. Generation of B-doped Graphene Nanoplatelets using a Solution Process and their Supercapacitor Applications. *ACS Nano* **2013,** *7,*19–26.

21. Wu, Z. –S., Winter, A., Chen, L., Sun, Y., Turchanin, A., Feng, X., Müllen, K. Three-dimensional Nitrogen and Boron Co-doped Graphene for High-Performance All-Solid-State Supercapacitors. *Adv. Mater.* **2012,** *24,* 5130–5135.

22. Yang, Z., Yao, Z., Li, G., Fang, G., Nie, H., Liu, Z., Zhou, X., Chen, X., Huang, S. Sulfur-doped Graphene as an Efficient Metal-free Cathode Catalyst for Oxygen Reduction. *ACS Nano* **2012**, *6,* 205–211.

23. Sheng, Z. –H., Gao, H. –L., Bao, W. –J., Wang, F. –B., Xia, X. –H. Synthesis of Boron-doped Graphene for Oxygen Reduction Reaction in Fuel Cells. *J. Mater. Chem.* **2012,** *22,* 390–395.

24. Yang, S., Zhi, L., Tang, K., Fang, X., Maier, J., Müllen, K. Efficient Synthesis of Heteroatom (N or S) –doped Graphene based on Ultrathin Graphene Oxide-porous Silica Sheets for Oxygen Reduction Reactions. *Adv. Funct. Mater.* **2012,** *22,* 3634–3640.

25. Guo, H. –L., Su, P., Kang, X., Ning, S. –K., Synthesis and Characterization of Nitrogen-doped Graphene Hydrogels by Hydrothermal Route with Urea as Reducing-doping Agent. *J. Mater. Chem. A* **2013**, *1,* 2248-2255.

26. Qiu, Y., Zhang, X., Yang, S. High Performance Supercapacitors based on Highly Conductive Nitrogen-doped Graphene Sheets. *Phys. Chem. Chem. Phys.* **2011,** *13,* 12552-12558.

27. Sun, L. Wang, L., Tian, C., Tan, T., Xie, Y., Shi, K., Li, M., Fu, H. Nitrogen-doped Graphene with High Nitrogen Level via a One-step Hydrothermal Reaction of Graphene Oxide with Urea for Superior Capacitive Energy Storage. *RSC Adv.* **2012,** *2,* 4498–4506.

28. Wen, Z., Wang, X., Mao, S., Bo, Z., Kim, H., Cui, S., Lu, G., Feng, X., Chen, J. Crumpled Nitrogen-doped Graphene Nanosheets with Ultrahigh Pore Volume for High-performance Supercapacitor. *Adv. Mater.* **2012,** *24,* 5610–5616.

29. Haque, E.; Islam, M. M.; Pourazadi, E.; Hasan, M.; Faisal, S. N.; Roy, A. K.; Konstantinov, K.; Harris, A. T.; Minett, A. I.; Gomes, V. G. Nitrogen-doped Graphene via Thermal Treatment of Composite Solid Precursors as a High Performance Supercapacitor. *RSC Adv.* **2015,** *5,* 30679–30686.

30. Lai, L., Potts, J. R., Zhan, D., Wang, L., Poh, C. K., Tang, C., Gong, H., Shen, Z., Lin, J., Ruoff, R. S. Exploration of the Active Center Structure of Nitrogen-doped Graphene-

based Catalysts for Oxygen Reduction Reaction. *Energy Environ. Sci.* **2012,** *5,* 7936–7942.

31. Qu, L., Liu, Y., Baek, J. –B., Dai, L. Nitrogen-doped Graphene as Efficient Metal-free Electrocatalyst for Oxygen Reduction in Fuel Cells. *ACS Nano* **2010**, *4,* 1321–1326.

32. Lin, Z.; Waller, G. H.; Liu, Y.; Liu, M.; Wong, C. –P. Simple Preparation of Nanoporous Few-layer Nitrogen-doped Graphene for use as an Efficient Electrocatalyst for Oxygen Reduction and Evolution Reactions. *Carbon* **2013,** *53,* 130–136.

33. Tian, G. –L.; Zhao, M. –Q.; Yu, D.; Kong, X. –Y.; Huang, J. –Q.; Zhang, Q. Wei, F. Nitrogen-Doped Graphene/Carbon nanotube Hybrids: In Situ formation of bifunctional Catalysts and Their Superior Electrocatalytic Activity for Oxygen Evolution/ Reduction Reaction. *Small* **2014,** *10*, 2251–2259.

34. Wang, H., Maiyalagan, T., Wang, X. Review on Recent Progress in Nitrogen-doped Graphene: Synthesis, Characterization and its Potential Applications. *ACS Catal.* **2012,** *2*, 781–794.

35. Shao, Y., Sui, J., Yin, G., Gao, Y. Nitrogen-doped Carbon Nanostructures and their Composites as Catalytic Materials for Proton Exchange Membrane Fuel Cell. *Appl. Catal. B* **2008,** *79,* 89–99.

36. Thorum, M. S. Hankett, J. M., Gewirth, A. A. Poisoning the Oxygen Reduction Reaction on Carbon-supported Fe and Cu Electrocatalysis: Evidence for Metal-centered Activity. *J. Phys. Chem. Lett.* **2011,** *2,* 295–298.

37. Jeong, H. M., Lee, J. W., Shin, W. H., Choi, Y. J., Shi, J. H., Kang, J. K., J. W. Choi, J. W. Nitrogen-doped Graphene for High Performance Ultracapacitors and the Importance of Nitrogen-doped Sites at Basal Planes. *Nano Lett.* **2011,** *11*, 2472-2477.

38. Zhang, L. L., Zhao, X., Ji, H., Stoller, M. D., Lai, L., Murali, S., Mcdonnell, S., Cleveger, B., Wallace, R. M., Ruoff, R. S. Nitrogen doping of Graphene and its Effect on Quantum Capacitance, and a New Insight on the Enhanced Capacitance of N-doped Carbon. *Energy Environ. Sci.* **2012,** *5,* 9618–9625.

39. Ikeda, T., Boero, M., Huang, S. –F., Terakura, K., Oshima, M., Ozaki, J. Carbon Alloy Catalysts: Active Sites for Oxygen Reduction Reaction. *J. Phys. Chem. C* **2008,** *112,* 14706–14709.

40. Yang, S., Feng, X. Wang, X., Müllen, K. Graphene-based Carbon Nitride Nanosheets as Efficient Metal-free Electrocatalysts for Oxygen Reduction Reactions. *Angew. Chem. Int. Ed.* **2011,** *50,* 5339-5343.

41. Reddy, A. L. M., Srivastava, A., Gowda, S. R., Gullapalli, H., Dubey, M., Ajayan, P. M. Synthesis of Nitrogen-doped Graphene Films for Lithium Battery Application. *ACS Nano* **2010,** *4,* 6337-6342.

42. Biddinger, E. J.; Ozkan, U. S. Role of Graphitic Edge Plane Exposure in Carbon Nanostructures for Oxygen Reduction Reaction. *J Phys. Chem. C* **2010**, *114,* 15306–15314.

43. Xing, T,; Zheng, Y.; Li. L. H.; Cowie, B. C. C.; Gunzelmann, D.; Qiao, S. Z.; Huang, S.; Chen, Y. Observation of Active Sites for Oxygen Reduction Reaction on Nitrogen-doped Multilayer Graphene. *ACS Nano* **2014,** *8,* 6856–6862.

44. Wu, J.; Ma, L.; Yadav, R. M.; Yang, Y.; Zhang, X.; Vajtai, R.; Lou, J.; Ajayan, P. M. Nitrogen-Doped Graphene with Pyridinic Dominance as a Highly Active and Stable Electrocatalyst for Oxygen Reduction, *ACS Appl. Mater. Interfaces* **2015**, *7,* 14763–14769.

45. Peng, Z.; Freunberger, S. A.; Chen, Y. ; Bruce, P. G. A Reversible and Higher-rate Li-O_2 Battery. *Science* **2012**, *337,* 563–566.

46. Park, M.; Sun, H.; Lee, H.; Lee, J. Cho, J. Lithium-Air Batteries: Survey on the Current Status and Perspectives towards Automotive Applications from a Battery Industry Standpoint. *Adv. Energy Mater.* **2012,** *2,* 780–800.

47. Kraytsberg, A.; Ein-Eli, Y. The Impact of Nano-Scaled Materials on Advanced Metal-Air Battery Systems. *Nano Energy* **2013,** *2,* 468–480.

48. Tian, G. -L.; Zhang, T. Q.; Zhang, B.; Jin, Y. -G.; Huang, J. -Q.; Su, D. S.; Wei, F. Toward Full Exposure of "Active Sites": Nanocarbon Electrocatalyst with Surface Enriched Nitrogen for Superior Oxygen Reduction and Evolution Reactivity. *Adv. Funct. Mater.* **2014,** *24,* 5956–5961.

49. Yadav, R. M.; Wu, J.; Kochandra, R.; Ma, L. Tiwari, C. S.; Ge, L.; Ye, G.; Vajtai, R.; Lou, J.; Ajayan, P. M. Carbon Nitrogen Nanotubes as Efficient Bifunctional Electrocatalysts for Oxygen reduction and Evolution Reactions. *ACS Appl. Mater. Interfaces* **2015,** *7,* 11991–2000.

50. Zhang, J.; Zhao, Z.; Xia, Z.; Dai, L. A Metal-free Bifunctional Electrocatalyst for Oxygen Reduction and Oxygen Evolution Reactions. *Nat. Nanotechnol.* **2015,** *10,* 444–452.

51. Li, R.; Wei, Z.; Gou, X. Nitrogen and Phosphorus Dual-doped Graphene/Carbon Nanosheets as bifunctional Electrocatalysts for Oxygen Reduction and Evolution. *ACS Catal.* **2015,** *5,* 4133–4142.

52. Jin, Z., Yao, J., Kittrell, C., Tour, J. M., Large-scale Growth and Characterizations of Nitrogen-doped Monolayer Graphene Sheets. *ACS Nano* **2011,** *5,* 4112–4117.

53. Geng, D., Chen, Y., Chen, Y., Li, Y., Li, R., Sun, X., Ye, S. Knights, S. High Oxygen-Reduction Activity and Durability of Nitrogen-doped Graphene. *Energy Environ. Sci.* **2011,** *4*, 760-764.

54. Sheng, Z. –H., Shao, L., Chen, J. –J., Bao, W. –J., Wang, F. –B., Xia, X. –H. Catalyst-free Synthesis of Nitrogen-doped Graphene via Thermal Annealing Graphite Oxide with Melamine and its Excellent Electrocatalysis. *ACS Nano* **2011,** *5,* 4350–4358.

55. Wang, H., Zhang, C., Liu, Z., Wang, L., Han, P., Xu, H., Dong, S., Yao, J., Cui, G. Nitrogen-doped Graphene Nanosheets with Excellent Lithium Storage Properties. *J. Mater. Chem.* **2011,** *21,* 5430–5434.

56. Parvez, K., Yang, S., Hernandez, Y., Winter, A. Turchanin, A., Feng, X., Müllen, K. Nitrogen-doped Graphene and its Iron-based Composites as Efficient Electrocatalysis for Oxygen Reduction Reaction. *ACS Nano* **2012,** *6,* 9541–9550.

57. Lin, Z., Waller, G., Liu, Y., Liu, M., Wong, C. –P. Facile Synthesis of Nitrogen-doped Graphene via Pyrolysis of Graphene Oxide and Urea, and its Electrocatalytic Activity toward the Oxygen-Reduction Reaction. *Adv. Energy Mater.* **2012,** *2,* 884–888.

58. Lei, Z., Lu, L., Zhao, X. S. The Electrocapacitive Properties of Graphene Oxide reduced by Urea, *Energy Environ. Sci.* **2012,** *5,* 6391–6399.

59. Mou, Z., Chen, X., Du, Y., Wang, X., Yang, P., Wang, S. Forming Mechanism of Nitrogen doped Graphene Prepared by Thermal Solid-State Reaction of Graphite Oxide and Urea. *Appl. Surf. Sci.* **2011,** 258, 1704–1710.

60. Zhou, R.; Jaroniec, M.; Qiao, S. –Z. Nitrogen-Doped Carbon Electrocatalysis Decorated with Transition Metals for the Oxygen Reduction Reaction. *ChemCatChem,* **2015,** *7,* 3808-3817.

61. Du, J.; Cheng, F.; Wang, S.; Zhang, T.; Chen, J. M(Salen)-derived Nitrogen-doped M/C (M = Fe, Co, Ni) Porous Nanocomposites for Electrocatalytic Oxygen Reduction. *Sci. Reports* **2014,** *4,* 4386-4393.

62. Li, D.; Muller, M. B.; Gilje, S.; Kaner, R. B.; Wallace, G. G. Processable Aqueous Dispersions of Graphene Nanosheets. *Nat. Nanotechnol.* **2008,** *3,* 101-105.

63. Zhao, Y.; Liu, J.; Hu, Y.; Cheng, H.; Hu, C.; Jiang, C.; Jiang, L.; Cao, A.; Qu, L. Highly Compression-Tolerant Supercapacitor Based on Polypyrrole-mediated Graphene Foam Electrodes. *Adv. Mater.* **2013,** *25,* 591-595.

64. Xu, Y.; Sheng, K.; Li, C.; Shi, G. Self-Assembled Graphene Hydrogel via a One-Step Hydrothermal Process. *ACS Nano* **2010**, *4,* 4324-4330.

65. Luo, J.; Hang, H. D.; Huang, J. Effect of Sheet Morphology on the Scalability of Graphene-Based Ultracapacitors. **ACS Nano 2013***, 7,* 1464-1471.

66. Zhu,Y.; Murali, S.; Stoller, M. D.; Ganesh, K. J.; Cai, W.; Ferreira, P. J.; Pirkle, A.; Wallace, R. M.; Cychosz, K. A.; Thommes, M.; Su, D.; Stach, E. A.; Ruoff, R. S. Carbon-Based Supercapacitors Produced by Activation of Graphene. *Science* **2011,** *332,* 1537-1541.

67. Choi, H. J.; Jung, S. M.; Seo, J. M.; Chang, D. W.; Dai, L.; Baek, J. B. Graphene for Energy Conversion and Storage in Fuel Cells and Supercapacitors. *Nano Energy* **2012,** *1,* 534-551.

68. Sun, Y.; Wu, Q.; Shi, G. Graphene based New Energy Materials. *Energy Environ. Sci.* **2011,** *4,* 1113-1132.

69. Huang, X.; Qi, X.; Boey, F.; Zhang, H. Graphene-Based Composites. *Chem. Soc. Rev.* **2012,** *41,* 666-686.

70. Wang, Y.; Wu, Y.; Huang, Y.; Zhang, F.; Yang, F.; Ma, Y.; Chen, Y. Preventing Graphene Sheets from Restacking for High-Capacitance Performance. *J. Phys. Chem. C* **2011,** *115,* 23192-23197.

71. Du, F.; Yu, D.; Dai, L.; Ganguli, S.; Varshney, V.; Roy, A. K. Preparation of Tunable 3D Pillared Carbon Nanotube-Graphene networks for High-Performance Capacitance. *Chem. Mater.* **2011,** *23,* 4810-4816.

72. Zhao, M. Q.; Zhang, Q.; Huang, J. Q.; Tian, G. L.; Chen, T. C.; Qian, W. Z.; Wei, F. Towards high Purity Graphene/single-walled carbon Nanotube Hybrids with Improved Electrochemical capacitive Performance. *Carbon* **2013,** *54,* 403-411.

73. Xue, Y.; Ding, Y.; Niu, J.; Xia, Z.; Roy, A.; Chen, H.; Qu, J.; Wang, Z. L.; Dai, L. Rationally designed graphene-nanotube 3D architectures with a seamless nodal junction for efficient energy conversion and storage. *Sci. Adv.* **2015,** *1*, 1400198-1400207.

74. Chabi, S.; Peng, C.; Hu, D. Zhu, Y. Ideal Three-Dimensional Electrode Structures for Electrochemical Energy Storage. *Adv. Mater.* **2014,** *26,* 2440-2445.

Chapter 2:
LITERATURE REVIEW

2.1 LITERATURE REVIEW

This section is about the discussion of related published articles firstly on graphene and graphene-nanoparticles hybrid material synthesis and their applications in energy storage and conversion. Later, a brief discussion on the synthesis of nitrogen doped graphene and their hybrid composite with nanomaterials has been presented. From the literature review, the literature gap in this field is addressed and the research was carried out based on the literature gap.

2.1.1 Synthesis of Graphene

Graphene is a two-dimensional material of *sp2*-hybridized carbon with honeycomb network. The long-range π-conjugation in graphene is contributed its extraordinary thermal, mechanical and electrical properties, which are highly crucial for the development of next generation energy storage and conversion devices. Alternatively, the ambipolar field effect, quantum hall effect at room temperature and high carrier mobility generated huge interest in the possible implementation of graphene in a myriad of devices. These include future generations of high-speed and radio frequency logic devices, thermally and electrically conductive reinforced composites, sensors, and transparent electrodes for displays and solar cells. [1,2] The first isolation of single layer graphene sheet from the bulk graphite via micromechanical scotch tape exfoliation method has been widely credited for the tremendous growth of interest in graphene. [1] However this method suffered from large-scale synthesis of graphene for practical applications, so the development the methods for graphene synthesis techniques that have shown promise for circumventing the aforementioned limitations are crucial. Chemical Vapor Deposition (CVD) technique allows to synthesis graphene of single layer or few-layer from carbon containing gases on catalytic metal surfaces and/or by surface segregation of carbon dissolved in the bulk of such metals. The metal surfaces can be varied like Pt, Pd, Fe, Ni, Co metals. [3] As example, the graphitization of Ni in a CH_4-H mixture at ≥1000 ^{O}C, where the production of carbon species at the Ni surface by the decomposition of CH_4 creates a concentration gradients between the surfaces and bulk causing carbon atoms to diffuse into the metal and form a solid solution. After saturation, graphite forms on the surface. Upon cooling,

C atoms dissolved in the metal at high temperature precipitate out and segregate at the metal surface, forming more layers of graphene. [4] It is possible to grow a large film of single layer graphene via CVD, however it is difficult to scalable production of graphene by this method and it also suffers for metallic impurity presence in the graphene sheets. [5] To overcome the limitation of CVD and to produce large-scale graphene (gram scale), solution based process is an alternate option. In 2006, Ruoff's group was the first to demonstrate a solution-based process for producing single-layer graphene. [6] The method based on chemical modification of graphite to produce a water dispersible intermediary, graphite oxide (GO). After oxidation by Hummers' method, GO is a layered stack of puckered sheets with AB stacking, which completely exfoliates upon the addition of mechanical energy. This is due to the strength of interactions between water and the oxygen-containing (epoxide and hydroxyl) functionalities introduced into the basal plane during oxidation. The hydrophilicity leads water to readily intercalate between the sheets and disperse them as individuals. Although GO itself is nonconducting, the graphitic network can be substantially restored through treatment with chemical reducing agents or by thermal treatment. [2, 6] The reduction of graphene oxide by chemical reducing agents in at moderate temperature has gained huge attention to synthesis graphene for electrochemical energy and sensing related applications. However, the use of toxic chemical like hydrazine limited the scalable production for commercial application. [7] Various non-toxic and green reducing agents like ascorbic acid, glucose, thiourea, green tea and similar compounds have been reported till now, which are good alternatives for avoiding toxic chemicals like hydrazine. [8] Even though the reduction with reducing agents at moderate temperature can synthesis few layer reduced graphene oxide, but this technique cannot remove the oxygenated groups on the graphene surface properly and creates defects on the surfaces containing high ratio of carbon and oxygen. The microwave and hydrothermal assisted reduction with reducing agent can overcome the limitation of oxygenated groups but the change of structure and morphology of graphene happened due to microwave heating or hydrothermal reaction. [9] Thermal annealing in inert gas at high temperature around 600-900 ºC is an excellent option to reduce graphene oxide without any reducing agent for scalable production. [9, 10] This low-cost procedure produced graphene with low percentage of oxygen and also beneficial for heteroatom doping as well as manipulating the properties by forming pores and defects for the application of electrochemical energy storage and conversion. [11, 12] Another solution based approach for large-scale synthesis is exfoliation of graphene in

solvent containing surfactant or stabilizing agent by shear mixing. [13] This method is highly attractive for solution-based production of graphene (in liter scale), however the complete removal of the surfactant or stabilizing agent from the graphene solution is very difficult and that may hamper the actual properties of graphene for device fabrication.

2.1.2 Synthesis of Graphene/Metal nanoparticle Hybrid

2.1.2.1 Ex situ Hybridization

In the *ex situ* hybridization, the graphene sheets are mixed with pre-synthesized nanoparticles in solution either through covalent or through noncovalent interactions (electrostatic, π-π stacking, hydrogen bonding or van der Waals interactions) by functionalizing the surface via linking agents. Covalent bonding occurs majorly with GO rather than RGO due to its large amount of oxygen containing group, which help to link with the other functional groups. The functionalized gold nanoparticle can be immobilized on GO surface by covalent bonding through simple amidation reaction using 4-aminothiophenol.[14] In noncovalent bonding, the simple electrostatic interactions occur due to the negative charge on the surface of graphene or RGO where the positively charged nanoparticles can be interacted via electrostatic force. As example, The positively charged alloy of Pt/Ag coated on gold nanorod was self-assembled on negatively charged graphene nanosheets by electrostatic bond and that composite was successfully applied for methanol electro-oxidation in Direct methanol fuel cell (DMFC).[15] But in some cases the negative charged of graphene is often too weak to assemble nanoparticle directly. For such cases the graphene need to be functionalized with a linking agent like 1-pyrene butyric acid which was used to anchor positively charged gold nanoparticle on graphene sheet for developing uric acid sensor.[16] For the case of negatively charged noble metal nanoparticles, the surface of graphene/RGO need to be converted to positively charged via functionalizing with cationic polyelectrolytes generally. The deposition of gold nanoparticles on graphene via poly(diallyldimethyl ammonium chloride) (PDDA) for applying the composite for hydrogen peroxide sensing [17] and depositing Pt nanoparticle on graphene linked by polyallylamine (PAA) for methanol oxidation are the examples of this method. [18] The aromatic compounds containing thiol, amine or acidic group can functionalize the noble metal nanoparticles and attach them with the graphene via π-π stacking. The development of immunosensor for detecting

toxoplasma gondii-specific IgM (Tg-IgM) is constructed by the gold nanoparticles attached with the graphene sheet through poly-thionine film by π-π interactions. [19] The interaction of GNP with sulfonated graphene sheet for making two dimensional (2D) heterostructure has shown promising enzyme less sensing platform for detecting hydrogen peroxide. [20]

Besides the aromatic compounds and cationic polyelectrolytes, biopolymers and proteins are also applied intensively to anchor the nanoparticles on graphene sheet. The attachment of negatively charged gold nanoparticles (GNPs) were done by positively charged chitosan/TiO_2-Gr composite film through electrostatic adsorption and applied as a label free amperometric immunosensing platform. [21] The GNPs are also distributed uniformly on the graphene sheet by using anti IgG (Immunoglobin G) as probe protein which covalently bonded to GNPs and anchored noncovalently to graphene sheet in a FET biosensor. [22] Utilizing the amphiphilic protein, bovine serum albumin it is possible to not only assemble the nanoparticles on graphene sheet but also control the density of those by changing the concentration of BSA during the assembly process. [23] Alternatively, DNA molecules can be applied for anchoring nanoparticles with graphene surface by the adsorption methods where the adsorption on GNPs occurs via chemical interactions but the adsorption on GO occurs via aromatic stacking or hydrophobic interactions. [24] The Pyrene labeled single stranded DNAs used to immobilize on graphene surface and make hybridization with the complementary DNA labeled gold nanoparticles is also reported. [25] Beside these methods, Layer by Layer (LBL) self-assembly is becoming an excellent synthesis method for fabricating nanocomposite films by blending two components through the electrostatic layers of opposite charges which provide better electrochemical properties with increasing surface area. As example, The 3D electrocatalytic multilayer thin film formed by integrating positively charged 4-dimethylaminopyridine (DMP) coated gold nanoparticles on GO surface has been applied to methanol oxidation. The number of bilayers has played a critical role for achieving the maximum current density. The diffusion of methanol into the electrode and the electron and mass transfer are also crucial for better catalytic activities of this type of catalysts in direct methanol fuel cell. [26]

2.1.2.2 In situ Crystallization

The *In situ* crystallization provides the growth of nanoparticles by controlling the nucleation sites on graphene sheet via surface functionalization. It is possible to reduce the excess surfactant or

linker molecules as well as enhance the functions of nanoparticle through this method. Different chemical and physical techniques like reduction and precipitation in solutions, *in situ* deposition by electrochemical method, electroless techniques, thermal deposition, hydrothermal, microwave assisted deposition as well as other reduction methods like photochemical and sonication have been applied intensively in *in situ* methods.

In preparation of graphene metal nanocomposites, Chemical reduction by a reducing agent in the solution of metal precursors and GO or rGO solution is the most popular method. The preparation of graphene-silver nanocomposite for designing actuators has been reported by using hydrazine as reducing agent. On that work, the GO suspension was mixed with $Ag(NH_3)_2OH$ solution where the positively charged $Ag(NH_3)_2^+$ easily absorbed on the GO surface and after reduction by hydrazine that became deposited as Ag np on GO surfaces. The GO was further treated thermally to convert in rGO. [27] Others reducing agents like sodium borohydrate, ascorbic acid, silver nitrate and ethylene glycol have been reported for preparing graphene noble metal nanocomposites. [28-31] The polyelectrolyte (PDDA) can also be act as reducing agent as well as stabilizer by supporting the growth of Pt nanoparticle on graphene surface. This nanocomposites could be achieved from exfoliated Graphite oxide in a green and facile synthetic route and applied for formic acid oxidation. [32] The tuning of the shape of nanoparticles from the sphericals to nanorods or nanowires can be achieved by the solution based *in situ* technique. Different dimensional nanostructures are also possible to achieve by manipulating the structure of metallic nanoparticles. The direct growth of gold nanorods on graphene film could be obtained by seed mediated method or seedless method using CTAB as surfactant and ascorbic acid as reducing agent. [33] One-dimensional Au nanowire could be obtained by heating gold salt with 1-amino-9-octadecene in the presence of GO sheet at 55ºC for 36 hours which manipulates the shape of gold nanoparticle in chain structure by making [(1-amino-9-octadecene) AuCl] complex. [34] The process of preparing the growth of nanoclusters of gold or other noble metal (Pd, Pt) on graphene surface were reported by H. Yin *et al*. This surfactant free gold nanoclusters were occurred by sonicating, washing and freeze-drying of the rGO solution with gold solution, which showed excellent catalytic activity towards oxygen reduction reaction. [35] The incorporation of two noble metals to make bimetallic three dimensional nanodendrite hybrids with PVP functionalized graphene nanosheets by wet chemical approach provides excellent nano-electrocatalytic activity towards methanol oxidation. [36] The alloy of noble

metals with graphene had also demonstrated as highly efficient anode material for direct formic acid fuel cell. The synthesis was conducted by reflux method followed by heat treatment with the presence of ethylene glycol, worked as a reducing agent. [37] Among the *in situ* based deposition techniques, electrochemical depositions are based on the reduction of metal salts from the electrolyte solution containing metallic precursor and deposition on Graphene coated electrode upon applied potential. This green process is an excellent one-stop technique for preparing noble metal-graphene nanocomposites by controlling the size, shape and density of nanoparticles by manipulating the potential, time and concentration of solution of metal precursor. The synthesis of graphene-nanogold composites through electrodeposition had shown significant improvement for biosensing applications. Here the graphene oxide was reduced first by applying potential of -0.8V for 10 minutes and then the electrodeposition of gold nanoparticles at -0.5V for 100s. [38, 39] The nanocomposite of highly dispersed and small sized Pt with graphene, synthesized by simultaneously reduction of Pt and GrO had been shown excellent catalytic activity as anode materials for direct methanol fuel cell [40]

The mechanism of electroless deposition is based on the reduction capability of substrate to make metal nanoparticles from metal ions by acting as electron donating source utilizing the differences of redox potential between the substrate and metal ions. This surfactant free, clean deposition method had been employed to disperse Pd nanoparticles on graphene oxide using the difference of the reduction potential of $PdCl_4^{2-}$ (+0.83 V vs SCE) and the oxidation potential of GrO (+0.48 V vs SCE). [41] As the reduction potentials of noble metal salts are generally higher than the oxidation potential of RGO (+0.38V vs SCE), It is a preferable technique for preparing graphene-noble metal nanocomposites. [42] Thermal treatment is an alternative way to deposit metal nanoparticles on the basal plane of graphene directly without any functionalization. Utilizing the thermal evaporation techniques by annealing at 1260 ºC for 30 sec it the deposition of gold nanoparticles on graphene were observed where the density and size of the nanoparticles were related to the numbers of layers of graphene. [43] The deposition of different transition metals including Pt, Pd, Rh, Co and Au were analyzed using Ultra high vacuum (UHV) system by annealing from 600K to 1100K for 10 minute which showed the formation of finely dispersed small clusters of of Pt and Rh, large clusters of Pd and Co and single layer of Au film on the substrate of Graphene/Ru(0001). [44] For higher deposition rate and controllable composition can be achieved by applying chemical vapor deposition process. The growth of CNT on

graphene nanosheets and anchoring the metal nanoparticles is a promising way to enhance the catalytic property of the materials. The composite of Pt nanoparticle on MWNT wrapped graphene showed excellent oxygen reduction reaction in proton exchange membrane. [45]

Incorporating high pressure with high temperature in the solution of graphene oxide and metal salts in autoclave, is one of the *in situ* processes to make nanocomposites known as hydrothermal process. Here reducing agent can be added for complete the reduction. The synthesis of silver graphene nanocomposite in ionic liquid solution with the addition of ascorbic acid in an autoclave at 160ºC for 4 hour is a prominent way to make composite for SERS based applications. [46] Beside these direct thermal methods, microwave energy assisted deposition is frequently used due to its uniform and rapid heating properties. The rapid synthesis of different noble metals-graphene nanocomposite by microwave irradiation using hydrazine or oleylamine as reducing agent was demonstrated.[47] Here the gold, silver and copper salts were mixed with GO in oleylamin (70%) solution and kept in the microwave oven for 1-2 minutes for preparing the nanocomposites.[47] Using foaming agent, azodicarbonamide (ADC) with mild oxidizer, worm like structure of graphene can be achievable by microwave which can be decorated by metal nanoparticles using metal precursors. The nanocomposites of Pd and Pt showed excellent electrocatalytic activity and glucose biosensing properties respectively. Surfactant free ultrafine Pt nanoparticle deposition was also reported using ethylene glycol as reducing agent in microwave. [48, 49] Alternatively bare surfaced gold-graphene nanocomposites were prepared without any reducing agent by incubating the GO sheets in gold salt solution for 24 hours after keeping 2 minutes in microwave irradiation. [50]

Photochemical reduction is a solution-based process, which provides a uniform reducing environment in solution by photo irradiation. The mechanism is based on the removal of oxygen functional group of GO as well as making nanostructure of metal precursor via photo reduction. The synthesis and self-assemble of the chain of gold nanodots on reduced graphene oxide nanosheets with the presence of octadecanthiol was reported by Huang et al. [51] The formation of nanocomposites of graphene with noble metals could be possible without reducing agent in aqueous solution by irradiating by white light using ionic surfactants. [52] The one pot synthesis of ultrathin gold nanocrystal deposited graphene nanosheets was also demonstrated using light emitting diode in absence of any reducing agent and surfactants which showed high

electrocatalytic activity and stability for methanol oxidation. [53] Another solution based technique utilizing the ultrasonic frequency named Sonochemical methods are also proposed to make nanocomposites by forming highly reactive free radicals from homolysis of water due to high temperature condition. As example, the formation of graphene-gold nanocomposite by applying high frequency ultrasound of 211 kHz was reported by Vinodgopal *et al*., where the high frequency formed the free radicals which were scavenged by the alcohol group of polyethylene glycol to create the organic radicals for reducing the mixture of GO and gold ions. [54] The preparation of two dimensional catalyst surface by graphene-Pt composite using duel frequency was also demonstrated by the same group. [55]

2.1.2.3 Energy Storage Application

Supercapacitors are energy storage devices based on electrochemical double layer capacitance, which become an emerging candidate for smart and portable energy storage devices due to its high power density with fast charge/discharge rate and long cycle efficiency. [56-59] Among the different carbon based materials and composites, Graphene-inorganic oxides and hydroxides nanocomposites become the emerging materials for supercapacitors by limiting the agglomeration of graphene layers and thus enhance the effective high surface area and additional pseudocapacitance from the nanoparticles. [60, 61] Alternatively noble metal nanocomposites are recently explored as promising materials for supercapacitor due to their excellent electroactive properties . As example, Utilizing the capacitance like redox response of Pd nanoparticle situated on defect engineered three dimensional graphene carbon nanotube structure, specific capacitance around 700 F/g had been achieved at a scan rate of 100 mV/s. Here the graphene sheets were first irradiated by microwave in the presence of ionic liquid and metal salt palladium acetate and the Pd ions were reduced by the ionic liquid and deposited on the sheets as Pd nanoparticles. Further irradiation decomposed the imidazolium component of the ionic liquid that produced carbonaceous gases, which captured by the Pd nanoparticles and subsequently transform into nanotube following the mechanism of tip-growth dissolution. [62] γ-ray induced graphene-Pt nanocomposite had also reported as supercapacitor materials where the capacitance properties of graphene were enhanced by the accelerating electron transfer properties of platinum

nanoparticles, which also aided to increase the electrochemical active surface area of graphene. [63] Besides the noble metals, highly conductive and chemically stable noble metal oxides are also playing excellent roles to increase the capacitance properties. The nanocrystaline RuO dispersed on few layer graphene nanoflake synthesized by microwave plasma chemical vapor deposition had been influenced to achieve the capacitance property of 648 F/g. [64]

2.1.2.4 Electrocatlytic Application

Fuel cell is an excellent sustainable energy source but still suffers for the expensive cathode materials, especially noble metals. The use of graphene noble metal nanocomposites can be an alternative way to replace the cathode, which not only minimize the cost but also provide efficiency utilizing the high surface area and electrical conductivity of graphene as well as tolerability of fuel crossover. [65] Among the supporting noble nanoparticles with graphene, Platinum nanoparticles were used most widely due to its excellent electrocatalytical activity. [66-69] Different modifications on structure and nanoparticle depositions were carried out to achieve high performance. As example, electrodeposition of Pt on 3D graphene foam had shown better result for oxidation of methanol in acidic media than Pt/C fiber. [70] The composite of Pt-dispersed graphene-wrapped multi walled carbon nanotube prepared by CVD method was also shown higher power density than the pure-catalyst-support based fuel cells. [71] The impregnation of graphene supported Pt nanoparticles in ionic liquid not only enhanced the ORR activity but also provided excellent methanol tolerance. Here the ionic liquid of [MTBD][bmsi] was chosen due to its hydrophobic, high oxygen solubility and less methanol-philic nature. Due to the large polarity difference of the ionic liquid and methanol than between methanol and water, methanol cannot diffuse to ionic liquid from water. Additionally the ionic liquid can conduct proton by the lone electron pairs of nitrogen and perfluorinated side chains attract the oxygen. [72] The bi-metallic composites like Pd or Au with Pt were reported as promising electrocatalyst for fuel cells. [73] Composites of Pt-Ru nanoparticles also become a good choice for enhanced methanol oxidation in direct methanol fuel cell. [74-76] The PdAg nanorings supported on graphene nanosheets had been approached as Pt free composites fabricated galvanic displacement reaction. This composite contained of high surface area utilizing the exterior and interior surface as well as high electrocatalytic nature from the synergistic effect of noble metal alloys. It also showed high tolerability of methanol crossover. [77] The metal alloy nanoparticles

of Pt-Co supported on N-doped graphene had shown four times higher power density in proton exchange membrane fuel cells over commercial Pt/C catalyst. In this work, the polypyrolle had been used as a precursor of nitrogen for synthesizing N-doped hydrogen exfoliated graphene sheets via pyrolysis and the nanoparticles were deposited by polyol reduction method. [78]

2.1.3 Synthesis of Nitrogen-doped Graphene

Chemical doping is an effective approach to tailor the property of graphene, which has been proved effective in the doping of carbon nanotubes and greatly. [79, 80] Usually there are two means of chemically doped graphene: 1) the adsorption of gas, metal or organic molecules to the graphene surface and 2) substitutional doping, which introduces heteroatoms, such as nitrogen atoms, sulfur atoms, phosphorous atoms and boron atoms into the carbon lattice of graphene. Both of these methods can modulate the electronic properties of graphene, however substitutional doping found more effective to tailor the properties for electrochemical energy storage and conversion based applications. [80, 81] Among the different heteroatoms such as nitrogen (N), sulphur (S), phosphorous (P) and boron (B); substitutional doping of nitrogen (N) shows enhance electrochemical properties both for the energy storage and electrocatalysis influencing the spin density and charge distribution of the neighboring carbon atoms and thus induce the "activation region" on the graphene surface. Usually three common bonding configurations are observed within the carbon lattice, including graphitic N, pyridinic N and pyrrolic N. Because of the similar bond lengths of C–N (1.41 Å) and C–C (1.42 Å), pyridinic and graphitic N exert a marginal influence on the graphene structure. In contrast, *sp3*-bonded pyrrolic N disrupts the planar structure of graphene. Pyridinic N bonding configuration is the most stable in the presence of monovacancy, while pyridinic and graphitic N dominate in the presence of Stone–Wales and divacancy defects. The larger electronegativity of N (3.04 on the Pauling scale) than that of C (2.55 on the Pauling scale) creates polarization in the carbon network, thereby influencing the electronic, magnetic and optical properties of graphene. N-doping opens a bandgap near the Dirac point by suppressing the nearby density of states (DOS), thereby conferring graphene with semiconducting properties. [81]

The roles of the differently configured nitrogen atoms in enhancing capacitance or generating catalytically active sites are still controversial,[82, 83] but both quantum mechanical

calculations[84-86] and experimental[87] investigations indicate that graphitic, pyridinic, and pyrrolic N can enhance the capacitance, whereas pyridinic N and graphitic N can be essential to catalyzing oxygen reduction reaction by enhancing the adsorption of O_2 on the adjacent carbon atoms and thus promotes the four-electron pathway.[88-91] Besides the capacitance and oxygen reduction reaction, oxygen evolution reaction has gained a considerable attention due to the promising future of rechargeable metal-air batteries.[92-94] N-doped graphene,[95] NG/CNT composites,[96] N-doped coaxial carbon nanotube,[97] carbon nitrogen nanotubes[98] and nitrogen and phosphorous co-doped nanocarbons[99, 100] have shown to be promising alternatives to noble and transition metal based OER catalysts.

The enhanced supercapacitative and electrocatalytic properties are highly dependent on the type and amount of nitrogen present. To obtain both the capacitance and electrocatalytic properties, high atomic concentrations of pyridinic, pyrrolic and graphitic nitrogen are required. The types and amounts of the different nitrogen bonding configurations in an N-doped graphene sample depend on the nitrogen source as well as the synthesis method. Nitrogen has been incorporated into the graphitic lattice from sources like acetonitrile,[101] pyridine[102] and ammonia[102, 104] via chemical vapor deposition (CVD) or high-temperature treatment, and the resulting materials have been applied in lithium batteries,[101, 104] field effect transistors,[102] and as catalysts for oxygen reduction.[103] However, it is difficult to obtain materials with high levels of atomic nitrogen doping, and on a large scale, *via* CVD using gaseous or liquid sources of nitrogen, and the method also suffers from practical limitations due to possible contamination from the metal deposition catalyst as well as the toxicity of the precursors. On the other hand, the co-pyrolysis of graphene or a graphene precursor with a solid source of nitrogen, such as melamine[103] or cyanamide,[105] has produced NG with high levels of nitrogen (~9 at%). Co-pyrolysis methods are attractive because they can be scaled up without any catalyst.[106] However, the NG synthesized from melamine had a low surface area;[103] whereas cyanamide, on the other hand, required a surfactant to bind to the graphene surface.[105] Moreover, the NG synthesized from cyanamide did not contain pyrrolic nitrogen,[105] which plays an important role in enhancing capacitance.[84] In addition to melamine and cyanamide, urea has been employed as a solid source of nitrogen in the synthesis of N-doped graphene, however both the capacitance and electrocatalytic properties in the material were not investigated.[106-108] In order to show both high capacitance and electrocatalytic activity, an NG sample must contain

sufficient percentages of pyridinic, pyrrolic, and graphitic nitrogen atoms, and have large surface area and high pore volume.

2.1.4 Synthesis of Nitrogen-doped Graphene/Nanomaterial Composites

The modification of nitrogen-doped graphene by incorporating metal nanoparticles can enhance the electrocatalytical performance of the ORR, HER and OER comparable with the noble metal electrodes. [109-111] Platinum (Pt) nanoparticle based composite materials have been widely used as active ORR catalysts because of their low overpotential and fast kinetics for ORR. However, the high cost, low durability and poor toxicity tolerance of Pt impede their widespread application in viable commercial progress. [110] Therefore, it is highly desirable to develop alternative non-precious metal catalysts with high oxygen reduction reaction, oxygen evolution reaction and hydrogen evolution reaction activity. Various promising alternative ORR catalysts, including transition metal nanoparticle, metal oxides, transition metal nitrides/carbides and transition metal oxynitrides, have been explored. [109] Among them metal nanoparticles decorated nitrogen-doped graphene shows excellent electrocatalytical activity via single atom catalysis of metal doped nitrogen-doped graphene. [111] The cobalt decorated nitrogen graphene film shows excellent hydrogen evolution reaction by doped inside the carbon lattice of graphene as single atom catalysis.[111] Alternatively cobalt embedded porous carbon/ nitrogen doped graphene hybrid showed superior oxygen reduction reaction and oxygen evolution reaction compare to Pt/C. [112] Like cobalt nanoparticles, other transition metal nanoparticles/nitrogen doped graphene hybrids are also shown enhance electrocatalytical activity both in acidic and alkaline media. [109] Among them, nickel nanoparticle confined nitrogen-doped graphene has exhibited remarkable electrocatalytical activity of oxygen evolution reaction as well as hydrogen evolution reaction, which are highly important for water splitting on the both side. [113, 114] The single pot synthesized iron-decorated nitrogen-doped graphene by thermal annealing also showed enhanced oxygen reduction reaction via four-electron pathway. [115] Beside the metal nanoparticles, metal oxides and metal chalcogenides decorated nitrogen-doped graphene also exhibit promising electrocatalytical activity. [116] Beside the nitrogen-doped graphene/metal nanoparticle hybrid materials, conjugation of one-dimensional carbon nanotubes (CNTs) with two-dimensional graphene nanosheets showed formation of three-dimensional composites materials for energy storage by the intercalation of carbon nanotubes in the graphene layers

prevent the aggregation of graphene sheets. [117-120] The specific three-dimensional structure is highly important to get the best electrochemical performance including high gravimetric and volumetric capacitance as well as efficient electrocatalysis, if not the composites can be suffered for the agglomeration of carbon nanotubes as well restacking of graphene layers that reduce the energy storage efficiency and the low capacitance properties of CNTs can also decrease the average capacitance value of the composites. [121, 122] This limitation has a big impact on getting high performance as well as the commercialization of graphene/carbon nanotube based supercapacitors.

To obtain a proper structure for the better penetration of electrolyte as well prevention of restacking of graphene layers, the catalytic growth of carbon nanotube on the graphene layer via chemical vapor deposition (CVD) has been shown as promising pathway and possess good electrochemical and electromechanical properties for energy storage and electrocatalysis. [123-126] However, due to the limitation of the CVD process it is hard to scalable and the presence of metal catalyst in the process can cause detrimental effect. Alternatively, formation of chemical bonding between graphene oxide and carbon nanotube via thermal annealing can be superior way to build a three-dimensional structure for better ion permeation. [127-128] The composites of reduced graphene oxides with multiwalled carbon nanotubes bonded by the *p*-phenyldiamine showed good capacitive behavior, however the presence of organic compound between the layers might hinder the electrochemical properties as well as the structure of the hybrid materials suffered from the proper insertion of carbon nanotubes inside the graphene layers.[127] The carbon nanotube-bridged graphene 3D building blocks using electrostatic self-assembled CTAB showed excellent intercalation of CNTs inside the graphene layers but the capacitance property was not high enough as the capacitance of reduced graphene oxide is low. [128] The chemically bonded graphene/carbon nanotube utilization of amidation reaction between amine-functionalized CNTs with NHS-activated graphene oxides nanosheets and further reduction with hydrazine and ammonia by the microwave hydrothermal showed not only good gravimetric capacitance but also large volumetric capacitance due to the spacing of CNTs in graphene layers but still limited for the large scale synthesis of the composites due to the multiple synthesis steps as well as handling with highly toxic and dangerously unstable chemicals like hydrazine. [129] Besides the structural effects of graphene/CNT composites, the intrinsic capacitance and electrocatalysis properties and cycle efficiency can be improved by the nitrogen doping in

graphene lattice, which can enhance the electronic properties based on the bond configurations of nitrogen atoms. [130-131] The formation of high pore volume and surface area due to the nitrogen doping favor the increment of capacitor behavior as well as the long cycling performance. The uniformly dispersed and covalently bonded molecular nitrogen groups on the graphene plane improve the psudocapacitance properties and the electrocatalysis activity *via* activation of the adjacent carbon atoms. [132, 133] The presence of nitrogen and the three-dimensional structure not only shows the electrocatalytical activity of oxygen reduction reactions (ORR) but also facilitate the oxygen evolution reactions (OER), which are highly important characteristic for developing metal-air batteries and rechargeable fuel cells. [126, 134] To obtained the best performance in energy storage and electrocatalysis, a single step scalable synthesis of three-dimensional graphene/carbon nanotube composite with high atomic percentage of nitrogen is highly desirable.

2.2 FINDINGS FROM THE LITERATURE REVIEW

From the literature review the following findings were observed and the research plan was carried based on these observations.

1. The chemically doped graphene, in particular nitrogen-doped graphene showed enhanced electrochemical energy storage and conversion properties compare to the graphene and heteroatom doped graphene.

2. Synthesis of Nitrogen-doped Graphene with high atomic percentage of nitrogen is highly crucial to enhance the electrochemical property and it is highly dependent on nitrogen enriched precursor and doping method.

3. Thermal Annealing of graphene oxide with a nitrogen precursor for synthesizing nitrogen-doped graphene has been found most suitable method for proper doping as well as a low cost, scalable production method.

4. A new solid nitrogen precursor is needed to get high atomic percentage of doping.

5. Nitrogen-doped graphene/nanoparticle hybrid showed superior electrochemical performance compare to graphene/ nanoparticle hybrids.

6. Single pot synthesis of nitrogen-doped graphene/ metal nanoparticle hybrid with high electrochemical properties will be attractive for scalable commercial application.

7. Fabrication of a three-dimensional nanostructure by intercalated or bonded carbon nanotube and metal nanoparticle between the carbon lattices of graphene would be an excellent method to utilize the electro active surface area of the composite for achieving high performance in electrochemical energy storage and conversion for future energy storage devices.

References:

1. Geim, A. K., K. S. K. S. The Rise of Graphene. *Nat. Mater.* **2007,** *6,* 183–191.

2. Allen, M. J.; Tung, V. C.; Kaner, R. B. Honeycomb Carbon: A Review of Graphene. *Chem. Rev.* **2010,** *110,* 132-145.

3. Avouris, P.; Dimitrakopoulos, C. Graphene: Synthesis and Applications, *Mater. Today,* **2012,** *15,* 86-97.

4. Zhang, Y.; Gomez, L.; Ishikawa, F. N.; Madaria, A.; Ryu, K.; Wang, C.; Badmaev, A.; Zhou, C. Comparison of Graphene Growth on Single-Crystalline and Polycrystalline Ni by Chemical Vapor Deposition. *J. Phys. Chem. Lett.* **2010,** *1,* 3101-3107.

5. Munoz, R.; Aleixandre, C. G. Review of CVD Synthesis of Graphene, *Chem. Vap. Deposition* **2013**, *19,* 297-322.

6. Stankovich, S.; Dikin, D. A.; Dommett, G. H. B.; Kohlhaas, K. M.; Zimney, E. J.; Stach, E. A.; Piner, R. D.; Nguyen, S. T.; Ruoff, R. S. Graphene-based Composite Materials, *Nature,* **2006**, *442,* 282-286.

7. Stankovich, S.; Dikin, D. A.; Piner, R. D.; Kohlhass, K. A.; Kleinhammes, A.; Jia, Y.; Wu, Y.; Nguyen, S. T.; Rouff, R. S. Synthesis of Graphene-Based Nanosheets via Chemical Reduction of Exfoliated Graphite Oxide, *Carbon,* **2007,** *45,* 1558-1565.

8. Chua, C. K.; Pumera, M. Chemical Reduction of Graphene Oxide: A Synthetic Chemistry Viewpoint, *Chem. Soc. Rev.,* **2014,** *43*, 291-312.

9. Mao, S.; Pu, H.; Chen, J. Graphene Oxide and Its Reduction: modeling and Experimental Progress. *RSC Advances*, **2012**, *2*, 2643-2662.

10. Kumar, P. V.; Bardhan, N. M.; Tongay, S.; Wu, J.; Belcher, A. M.; Grossman, J. C. Scalable Enhancment of Graphene Oxide Properties by Thermally Driven Phase Transformation. *Nat. Chem.* **2014**, *6,* 151-172.

11. Zhu, B. Y.; Murali, S.; Cai, W.; Li, X.; Suk, J. W.; Potts, J. R.; Rouff, R. S. Graphene and Graphene Oxide: Synthesis, Properties and Applications. *Adv. Mater.* **2010**, *22,* 3906-3924.

12. Choi, H. –J., Jung, S. -M. Seo, J. M., Chang, D. W., Dai, L., Baek, J. –B. Graphene for Energy Conversion and Storage in Fuel Cells and Supercapacitors. *Nano Energy* **2012**, *1*, 534–551.

13. Hernandez, Y., Nicolosi, V., Lotya, M., Blighe, F. M., Sun, Z., De, S., McGovern, I. T., Holland, B., Byrne, M., Gun'ko, Y. K., Boland, J. J., Niraj, P., Duesberg, G., Krishnamurthy, S., Goodhue, R., Hutchison, J., Scardaci, V., Ferrari, A. C., Coleman, J.

N. High-Yield Production of Graphene by Liquid-Phase Exfoliation of Graphite. *Nat. Nanotechnol*. **2008,** *3,* 563–568.

14. Pham, T. A.; Choi, B. C.; Lim K. T.; Jeong, Y. T. A Simple Approach for Immobilization of Gold Nanoparticles on Graphene Sheets by Covalent Bonding. *Appl.Surf. Sci*. **2011,** *257,* 3350-3357.

15. Feng, L.; Gao, G.; Huang, P.; Wang, X.; Zhang, C.; Zhang, J.; Guo S.; Cui, D. Preparation of Pt Ag Alloy Nanoisland/Graphene Hybrid Composites and Its High Stability and Catalytic Activity in Methanol Electro-Oxidation. *Nanoscale Res. Lett*. **2011,** *6,* 551-561.

16. Hong, W.; Bai, H.; Xu, Y.; Yao, Z. Gu, Z.; Shi, G. Preparation of Gold Nanoparticle/Graphene Composites with Controlled Weight Contents and Their Application in Biosensors. *J. Phys. Chem. C*, **2010,** *114(4),* 1822-1826.

17. Fang, Y.; Guo, S.; Zhou, C.; Zhai Y.; Wang, E. Self-Assembly of Cationic Polyelectrolyte-Functionalized Graphene Nanosheets and Gold Nanoparticles: A Two-Dimensional Heterostructure for Hydrogen Peroxide Sensing. *Langmuir,* **2010,** *26(13),* 11277-11282.

18. Hu, J.; He, B.; Lu, J.; Yuan, J. Song, J.; Niu, L. Facile Preparation of Pt/Polyallylamine/Reduced Graphene oxide Composites and Their Application in the Electrochemical Catalysis on Methanol Oxidation. *Int. J. Electrochem Sci*. **2012,** *7,* 10094-10107.

19. Jiang, S.; Hua, E.; Liang, M.; Liu B.; Xie, G. A Novel Immunosensor for Detecting Toxoplasma Gondii-specific IgM based Goldmag Nanoparticles and Graphene Sheets. *Colloids and Surf. B: Biointerfaces* **2013,** *101,* 481-486.

20. Li, S. J.; Shi, Y. F.; Liu, L.; Song, L. X.; Pang H.; Du, J. M. Electrostatic Self-Assembly for Preparation of Sulfonated Graphene/Gold Nanoparticle Hybrids and Their Application for Hydrogen Peroxide Sensing. *Electrochim. Acta* **2012,** *85,* 628-635.

21. Huang, K. J.; Li, J.; Wu, Y. Y.; Liu, Y. M. Amperometric Immunobiosensor for alpha-Fetoprotein using Ag Nanoparticles/Chitosan/TiO_2-Graphene Composite Based Platform. *Bioelectrochemistry* **2013,** *90,* 18-23.

22. Mao, S.; Lu, G.; Yu, K.; Bo Z.; Chen, J. Specific Protien Detection Using Thermally Reduced Graphene Oxide Sheet Decorated with Gold Nanoparticle-antibody Conjugates. *Adv. Mater*. **2010**, *22,* 3521-3526.

23. Liu, J.; Fu, S.; Yuan, B.; Li, Y.; Deng, Z. Toward a Universal "Adhesive Nanosheet" for the Assembly of Multiple Nanoparticles Based on A Protein-Induced Reduction/Decoration of Graphene Oxide. *J. Am. Chem. Soc*. **2010,** *132,* 7279-7281.

24. Liu, J. Adsorption of DNA onto Gold Nanoparticles and Graphene Oxide: Surface Science and Applications. *Phys. Chem. Chem. Phys.* **2012,** *14,* 10485-10496.

25. Liu, F.; Choi J. Y.; Seo, T. S. DNA Mediated Water-Dispersible Graphene Fabrication and Gold Nanoparticle-Graphene Hybrid. *Chem. Commun.* **2010,** *46,* 2844-2846.

26. Choi, Y.; Gu, M.; Park, J.; Song H. K.; Kim, B. S. Graphene Multilayer Supported Gold Nanoparticles for Efficient Electrocatalysts Toward Menthol Oxidation. *Adv. Enrgy Mate*r. **2012,** *2,* 1510-1518.

27. Lu, L.; Liu, J.; Hu, Y.; Zhang Y.; W. Chen, W. Graphene-Stabilized Silver Nanoparticle Electrochemical Electrode for Actuator Design. *Adv. Mater.* **2013,** *25,* 1270-1274.

28. Tien, H. W.; Huang, Y. L.; Yang, S. Y.; Wang, J. Y.; Ma, C. C. M. Using Self-Assembly to prepare a Graphene-Silver Nanowire Hybrid Film That is Transparent and Electrically Conductive. *Carbon* **2013,** *58,* 198-207..

29. Kim, S. H.; Jeong, G. H.; Choi, D.; Yoon, S.; Jeon, H. B.; Lee S. M.; S. Kim, S. W. Synthesis of Noble Metal/Graphene Nanocomposites without Surfactants by One-Step Reduction of Metal Salt and Graphene Oxide. *J. Colloid Interface Sci.* **2013,** *389,* 85-90.

30. Liu, X.; Yi, L.; Wang, X.; Su, J.; Song Y.; Liu, J. Graphene Supported Platinum Nanoparticles as Anode Electrocatalyst for Direct Borohydride Fuel Cell. *Int. J. Hydrogen Energy,* **2012,** *37,* 17984-17991.

31. He Y.; Cui, H. Synthesis of Highly Chemiluminescent Graphene Oxide/Silver Nanoparticle Nano-Composites and Their Analytical Applications. *J. Mat. Chem.* **2012,** *22,* 9086-9091.

32. Zhang, S.; Shao, Y.; Liao, H.; Engelhard, M. H.; Yin G.; and Lin, Y. Polyelectrolyte-Induced Reduction of Exfloited Graphite Oxide: A Facile Route to Synthesis of Soluble Graphene nanosheets. *ACS Nano* **2011**, *5 (3),* 1785-1791.

33. Kim, Y. K.; Na, H. K.; Lee, Y. W.; Jang, H.; Han S. W.; Min, D. H. The Direct Growth of Gold Rods on Graphene Thin Films. *Chem. Commun.* **2010,** *46,* 3185-3187.

34. Huang, X.; Li, S.; Wu, S.; Huang, Y.; Boey, F.; Gan C. L.; Zhang, H. Graphene Oxide-Templated Synthesis of Ultrathin or Tadpole-Shaped Au Nanowires with Alternating hcc and fcc Domains. *Adv. Mater.* **2012,** *24,* 979-983.

35. Yin, H.; Tang, H.; Wang, D.; Gao Y.; and Tang, Z. Facile Synthesis of Surfactant-Free Au Cluster/Graphene Hybrids for High-Performance Oxygen Reduction Reaction. *ACS Nano*, **2012,** *6 (9),* 8288-8297.

36. Guo, S.; Dong, S.; Wang, E. Three-Dimensional Pt on Pd Bimetallic Nanodendrites Supported on Graphene Nanosheet: Facile Synthesis and Used as An Advanced Nanoelectrocatalyst for Methanol Oxidation. *ACS Nano* **2010,** *4 (1),* 547-555.

37. Rao, C. V.; Cabrera C. R.; Ishikawa, Y. Graphene-Supported Pt-Au Alloy Nanoparticles: A Highly Efficient Anode for Direct Formic Acid Fuel Cells. *J. Phy. Chem. C,* **2011**, *115*, 21963-21970.

38. Liu, C.; Wang, K.; Luo, S.; Tang Y.; Chen, L. Direct Electrodeposition of Graphene Enabling the One-Step Synthesis of Graphene-Metal Nanocomposite Films. *Small* **2011**, *7 (9),* 1203-1206.

39. Li, S. J.; Deng, D. H.; Shi Q.; Liu, S. R. Electrochemical Synthesis of a Graphene Sheet and Gold Nanoparticle-based nanocomposte and Its Application to Amperometric Sensing of Dopamine. *Microchim Acta* **2012,** *177,* 325-331.

40. Zhou, Y. G.; Chen, J. J.; Wang, F.; Sheng, Z. H.; Xia, X. H. A Facile Approach to the Synthesis of Highly Electroactive Pt Nanoparticles on Graphene as an Anode Catalyst for Direct Methanol Fuel Cells. *Chem Commun,* **2010,** *46,* 5951-5953.

41. Chen, X.; Wu, G.; Chen, J.; Chen, X.; Xie Z.; Wang, X. Synthesis of "Clean" and Well-Despersive Pd Nanoparticles with Excellent Electrocatalytic Property on Graphene Oxide. *J. Am. Chem. Soc***. 2011,** *133,* 3693-3695.

42. Liu, X. W.; Mao, J. J.; Liu, P. D.; Wei, X. W. Fabrication of Metal-Graphene Hybrid Materials by Electroless Deposition. *Carbon*, **2011**, *49,* 477-483.

43. Zhou, H.; Qiu, C.; Liu, Z.; Yang, H.; Hu, L.; Liu, J.; Yang, H.; Gu C. Sun, L. Thicknes-Dependent Morphologies of Gold on N-Layer Graphenes. *J. Am. Chem. Soc.,* **2010***, 132,* 944-946.

44. Zhou, Z.; Gao F.; Goodman, D. W. Deostion of Metal Clusters on Single-Layer Graphene/Ru (0001): Factors that Govern Cluster Growth. *Surface Science,* **2010,** *604,* L31-L38.

45. Jyothirmayee S. S.; Ramaprabhu, S. Pt Nanoparticle-Dispersed Graphene-Wrapped MWNT Composites as Oxygen Reduction Reaction Electrocatalyst in Proton Exchange Membrane Fuel Cell. *ACS Appl. Mater. Interfaces*, **2012**, *4*, 3805-3810.

46. Shen, J.; Shi, M.; Yan, B.; Ma, H.; Li, N.; Ye, M. One-Pot Hydrothermal Synthesis of Ag-Reduced Graphene Oxide Composite with Ionic Liquid. *J. Mater. Chem.* **2011,** *21,* 7795-7801.

47. Hassan, H. M. A.; Abdelsayed, V.; Khder, A. E. R. S.; AbouZied, K. M.; Terner, J.; El-Shall, M. S.; Al-Resayes S. I.; El-Azhary, A. A. Microwave Synthesis of Graphene

Sheets Supporting Metal Nanocrystals in Aqueous and Organic Media. *J. Mater. Chem.* **2009,** *19*, 3832-3837.

48. Vadahanambi,S.; Jung J. H.; Oh, I. K. Electro-active Graphene-Nafion Actuators. *Carbon* **2011,** *49,* 4449-4457.

49. Kundu, P.; Nethravathi, C.; Deshpande, P. A.; Rajamathi, M.; Madras G.; Ravishankar, N. Ultrafast Microwave-assisted route to Surfactant-Free Ultrafine Pt Nanoparticles on Graphene: Synergistic Co-reduction Mechanism and High catalytic Activity. *Chem. Mater.* **2011,** *23,* 2772-2780.

50. Jasuja, K.; Linn, J.; Melton S.; V. Berry, V. Microwave-reduced Uncapped Metal nanoparticles on Graphene: Tuning Catalytic, Electrical and Raman Properties. *J. Phys. Chem. Lett.* **2010,** *1,* 1853-1860.

51. Huang, X.; Zhou, X.; Wu, S.; Wei, Y.; Qi, X.; Zhang, J.; Boey F.; Zhang, H. Reduced Graphene Oxide-templeted Photochemecal Synthesis and in situ Asembly of Au nanodots to Orderly Patterned Au Nanodot Chains. *Small,* **2010,** *6,* 513-514.

52. Jeong, G. H.; Kim, S. H.; Kim, M.; Choi, D.; Lee, J. H.; Kim, J. H.; and Kim, S. W. Direct Synthesis of Noble-Metal/Graphene Nanocomposites from Graphite in Water: Photo-Synthesis. *Chem. Commun.* **2011,** *47,* 12236-12238.

53. Chen, J.; Cui, X.; Wang, Q.; Wang, H.; Zheng, X.; Liu, C.; Xue, T.; Wang, S.; Zheng, W. One-Pot Photochemical Synthesis of Ultrathin Au Nanocrystals on Co-Reduced Graphene Oxide and Its Application. *J. Colloid and Interfac. Sci.* **2012,** *383,* 140-147.

54. Vinodgopal, K.; Neppolian, B.; Lightcap, I. V.; Grieser, F.; Ashokkumar, M.; Kamat, P. V. Sonolytic Design of Graphene-Au nanocomposites, simultaneous and Sequential Reduction of Graphene Oxide and Au (III). *J. Phys. Chem. Lett.* **2010,** *1,* 1987-1993.

55. Vinodgopal, K.; Neppolian, B.; Salleh, N.; Lightcap, I. V.; Grieser, F.; Ashokkumar, M.; Ding T. T.; Kamat, P. V. Dual-Frequency Ultrasound for Designing Two-Dimensional Catalyst: Reduced Graphene Oxide-Pt Composite. *Colloids and Surfaces A: Physicochem. Eng. Aspects* **2012,** *409,* 81-87.

56. Simon, P., Gogotsi, Y. Materials for Electrochemical Capacitors. *Nat. Mater.* **2008,** *7,* 845–854.

57. Liu, C.; Li, F.; Ma, L. P.; Cheng, H. M. Advanced Materials for Energy Storage. *Adv. Mater.* **2010**, *22,* 28-62.

58. Zhu, Y., Murali, S., Stoller, M. D., Ganesh, K. J., Cai, W., Ferreira, P. J., Pirkle, A., Wallace, R. M., Cychosz, K. A., Thommes, M., Su, D., Stach, E. A., Ruoff, R. S.

Carbon-based Supercapacitors Produced by Activation of Graphene. *Science* **2011,** *332,* 1537-1541.

59. Stoller M. D.; Rouff, R. S. Best Practice Methods for Determining an Electrode Material's Performance for Ultracapacitors. *Energy Environ. Sci.* **2010,** *3,* 1294-1301.

60. Zhi, M.; Xiang, C.; Li, J.; Li, M.; Wu, N. Nanostructured Carbon-Metal oxide Composite Electrode for Supercapacitors: A Review. *Nanoscale* **2013,** *5,* 72-88.

61. Huang, Y.; Liang J.; Chen, Y. An Overview of the Applications of Graphene-based Materials in Supercapacitors. *Small,* **2012,** *8(12),* 1805-1834.

62. Sridhar, V.; Kim, H. J.; Jung, J. H.; Lee, C.; Park S.; Oh, I. K. Defect-Engineered Three-Dimensional Graphene-Nanotube-Palladium Nanostructures with Ultrahigh capacitance. *ACS Nano* **2012,** *6(12)* 10562-10570.

63. Zhang, Q.; Zhang, Y.; Gao, Z.; Ma, H. L.; Wang, S.; Peng, J.; Li, J.; Zhai, M. A Facile Synthesis of Platinum nanoparticle Decorated Graphene by One-Step ϒ-ray Induced Reduction for High Rate Supercapacitors. *J. Mater. Chem. C,* **2013,** *1,* 321-328.

64. Soin, N.; Roy, S. S.; Mitra, S. K.; Thundat, T.; McLaughlin, J. A. Nanocrystalline Ruthenium Oxide Dispersed Few Layered Graphene (FLG) Nanoflakes as Supercapacitor Electrodes. *J. Mater. Chem.* **2012**, *22,* 14944-14950.

65. Hur S. H.; Park, J. N. Graphene and Its Application in Fuel Cell Catalysis: A Review. *Asia-Pac. J. Chem. Eng.* **2013,** *8,* 218-233.

66. Vinayan, B. P.; Nagar R.; Ramaprabhu, S. Synthesis and Investigation of Mechanism of Platinum-Graphene Electrocatalytsts by Novel Co-Reduction Techniques for Proton Exchange Fuel Cell Applications. *J. Mater. Chem.* **2012,** *22,* 25325-25334.

67. Nam, K. W.; Song, J.; Oh, K. H.; Choo, M. J.; Park, H. A.; Park J. K.; Choi, J. W. Perfluorosulfonic Acid Functionalized Pt-Graphene as a High Performance Oxygen Reduction Catalyst for Proton Exchange Membrane Fuel Cells. *J. Solid State Electrochem,* **2013,** *17,* 767-774.

68. Wang, Q.; Song, M.; Chen, C.; Hu W.; Wang, X. Plasma Synthesis of Surface-Functionalized Graphene-Based Platinum Nanoparticles: Highly Active Electrocatalysts as Electrodes for Direct Methanol Fuel Cells. *ChemPlusChem* **2012**, *77,* 432-436.

69. Zhao, J.; Zhang, L.; Chen, T.; Yu, H.; Zhang, L.; Xue H.; Hu, H. Supercritical Carbon-Dioxide –Assisted Deposition of Pt Nanoparticles on Graphene Sheets and Their Application as an Electrocatalyst for Direct Methanol Fuel Cells. *J. Phys. Chem. C* **2012,** *116,* 21374-21381.

70. Maiyalagan, T.; Dong, X.; Chen P.; Wang, X. Electrodeposited Pt on three-dimensional Interconnected Graphene as A Free-Standing Electrode for Fuel Cell Application. *J. Mater. Chem.* **2012,** *22,* 5286-5290.

71. Aravind S. S. J.; Ramaprabhu, S. Pt Nanoparticle-Dispersed Graphene-Wrapped MWNT Composites As Oxygen Reduction Reaction Electrocatalyst in proton Exchange Membrane Fuel Cell. *ACS Appl. Mater. Interfaces*, **2012,** *4,* 3805-3810.

72. Tan, Y.; Xu, C.; Chen, G.; Zheng N.; Xie, Q. A Graphene-Platinum nanoparticles-Ionic Liquid Composite catalyst for Methanol-Tolerant Oxygen Reduction Reaction. *Energy, Environ. Sci.* **2012,** *5,* 6923-6927.

73. Rao, C. V.; Cabrera C. R.; Ishikawa, Y. Graphene-Supported Pt-Au Alloy Nanoparticles: A Highly Efficient Anode for Direct Formic Acid Fuel Cells. *J. Phy. Chem. C,* **2011**, *115*, 21963-21970.

74. Galal, A.; Atta N. F.; Hassan, H. K. Electropolymerization of Aniline Over Chemically Converted Graphene-Systematic Study and Effect of Dopant. *Int. J. Electrochem. Sci.* **2012,** *7,* 768-784.

75. Zhao, J.; Zhang, L.; Xue, H.; Wang Z.; Hu, H. Methanol Electrocatalytic Oxidation on Highly Dispersed Platinum-Ruthenium/Graphene Catalysts Prepared in Supercritical Carbon Dioxide-Methanol Solution. *RSC Adv.* **2012**, *2,* 9651-9659.

76. Cong, H. P.; Ren X. C.; Yu, S. H. Controlled Synthesis of PtRu/Graphene Nanocatalysts with Enhanced Methanol Oxidation Activity for Fuel Cells. *ChemCatChem,* **2012,** *4,* 1555-1559.

77. Liu, M.; Lu Y.; Chen, W. PdAg Nanorings Supported on Graphene Nanosheets: Highly Methanol-Tolerant Cathode Electrocatalyst for Alkaline Fuel Cells. *Adv. Func. Mater.*, **2013,** *23*, 1289-1296.

78. Vinayan, B. P.; Nagar, R.; Rajalakshmi N.; Ramaprabhu, S. Novel Platinum-Cobalt Alloy Nanoparticles Dispersed on Nitrogen-Doped Graphene as a Cathode Electrocatalyst for PEMFC Application. *Adv. Func. Mater.* **2012,** *22,* 3519-3520.

79. Liu, H., Liu, Y.; Zhu, D. Chemical Doping of Graphene, *J. Mater. Chem.,* **2011,** *21,* 3335-3345.

80. Wang, H.; Maiyalagan, T.; Wang, X. Review on Recent Progress in Nitrogen-Doped Graphene: Synthesis, Characterization and Its Potential Applications, *ACS Catal.* **2012,** *2,* 781-794.

81. Wang, X.; Sun, G.; Routh, P.; Kim, D. H.; Huang, W.; Chen, P. Heteroatom-doped Graphene Materials: Syntheses, Properties and Applications. *Chem Soc. Rev.*, **2014,** *43,* 7067-7080.

82. Shao, Y., Sui, J., Yin, G., Gao, Y. Nitrogen-doped Carbon Nanostructures and their Composites as Catalytic Materials for Proton Exchange Membrane Fuel Cell. *Appl. Catal. B* **2008,** *79,* 89–99.

83. Thorum, M. S. Hankett, J. M., Gewirth, A. A. Poisoning the Oxygen Reduction Reaction on Carbon-supported Fe and Cu Electrocatalysis: Evidence for Metal-centered Activity. *J. Phys. Chem. Lett.* **2011,** *2,* 295–298.

84. Jeong, H. M., Lee, J. W., Shin, W. H., Choi, Y. J., Shi, J. H., Kang, J. K., J. W. Choi, J. W. Nitrogen-doped Graphene for High Performance Ultracapacitors and the Importance of Nitrogen-doped Sites at Basal Planes. *Nano Lett.* **2011**, *11,* 2472-2477.

85. Zhang, L. L., Zhao, X., Ji, H., Stoller, M. D., Lai, L., Murali, S., Mcdonnell, S., Cleveger, B., Wallace, R. M., Ruoff, R. S. Nitrogen doping of Graphene and its Effect on Quantum Capacitance, and a New Insight on the Enhanced Capacitance of N-doped Carbon. *Energy Environ. Sci.* **2012**, *5,* 9618–9625.

86. Ikeda, T., Boero, M., Huang, S. –F., Terakura, K., Oshima, M., Ozaki, J. Carbon Alloy Catalysts: Active Sites for Oxygen Reduction Reaction. *J. Phys. Chem. C* **2008**, *112,* 14706–14709.

87. Yang, S., Feng, X. Wang, X., Müllen, K. Graphene-based Carbon Nitride Nanosheets as Efficient Metal-free Electrocatalysts for Oxygen Reduction Reactions. *Angew. Chem. Int. Ed.* **2011**, *50,* 5339-5343.

88. Reddy, A. L. M., Srivastava, A., Gowda, S. R., Gullapalli, H., Dubey, M., Ajayan, P. M. Synthesis of Nitrogen-doped Graphene Films for Lithium Battery Application. *ACS Nano* **2010**, *4,* 6337-6342.

89. Biddinger, E. J.; Ozkan, U. S. Role of Graphitic Edge Plane Exposure in Carbon Nanostructures for Oxygen Reduction Reaction. *J Phys. Chem. C* **2010,** *114,* 15306–15314.

90. Xing, T.; Zheng, Y.; Li. L. H.; Cowie, B. C. C.; Gunzelmann, D.; Qiao, S. Z.; Huang, S.; Chen, Y. Observation of Active Sites for Oxygen Reduction Reaction on Nitrogen-doped Multilayer Graphene. *ACS Nano* **2014,** *8,* 6856–6862.

91. Wu, J.; Ma, L.; Yadav, R. M.; Yang, Y.; Zhang, X.; Vajtai, R.; Lou, J.; Ajayan, P. M. Nitrogen-Doped Graphene with Pyridinic Dominance as a Highly Active and Stable Electrocatalyst for Oxygen Reduction, *ACS Appl. Mater. Interfaces* **2015,** *7,* 14763–14769.

92. Peng, Z.; Freunberger, S. A.; Chen, Y. ; Bruce, P. G. A Reversible and Higher-rate Li-O_2 Battery. *Science* **2012,** *337,* 563–566.

93. Park, M.; Sun, H.; Lee, H.; Lee, J. Cho, J. Lithium-Air Batteries: Survey on the Current Status and Perspectives towards Automotive Applications from a Battery Industry Standpoint. *Adv. Energy Mater.* **2012,** *2,* 780–800.

94. Kraytsberg, A.; Ein-Eli, Y. The Impact of Nano-Scaled Materials on Advanced Metal-Air Battery Systems. *Nano Energy* **2013,** *2,* 468–480.

95. Lin, Z.; Waller, G. H.; Liu, Y.; Liu, M.; Wong, C. –P. Simple Preparation of Nanoporous Few-layer Nitrogen-doped Graphene for use as an Efficient Electrocatalyst for Oxygen Reduction and Evolution Reactions. *Carbon* **2013,** *53,* 130–136.

96. Tian, G. –L.; Zhao, M. –Q.; Yu, D.; Kong, X. –Y.; Huang, J. –Q.; Zhang, Q. Wei, F. Nitrogen-Doped Graphene/Carbon nanotube Hybrids: In Situ formation of bifunctional Catalysts and Their Superior Electrocatalytic Activity for Oxygen Evolution/ Reduction Reaction. *Small* **2014,** *10,* 2251–2259.

97. Tian, G. -L.; Zhang, T. Q.; Zhang, B.; Jin, Y. -G.; Huang, J. -Q.; Su, D. S.; Wei, F. Toward Full Exposure of "Active Sites": Nanocarbon Electrocatalyst with Surface Enriched Nitrogen for Superior Oxygen Reduction and Evolution Reactivity. *Adv. Funct. Mater.* **2014,** *24,* 5956–5961.

98. Yadav, R. M.; Wu, J.; Kochandra, R.; Ma, L. Tiwari, C. S.; Ge, L.; Ye, G.; Vajtai, R.; Lou, J.; Ajayan, P. M. Carbon Nitrogen Nanotubes as Efficient Bifunctional Electrocatalysts for Oxygen reduction and Evolution Reactions. *ACS Appl. Mater. Interfaces* **2015,** *7,* 11991–2000.

99. Zhang, J.; Zhao, Z.; Xia, Z.; Dai, L. A Metal-free Bifunctional Electrocatalyst for Oxygen Reduction and Oxygen Evolution Reactions. *Nat. Nanotechnol.* **2015,** *10,* 444–452.

100. Li, R.; Wei, Z.; Gou, X. Nitrogen and Phosphorus Dual-doped Graphene/Carbon Nanosheets as bifunctional Electrocatalysts for Oxygen Reduction and Evolution. *ACS Catal.* **2015,** *5,* 4133–4142.

101. Jin, Z., Yao, J., Kittrell, C., Tour, J. M., Large-scale Growth and Characterizations of Nitrogen-doped Monolayer Graphene Sheets. *ACS Nano* **2011,** *5,* 4112–4117.

102. Geng, D., Chen, Y., Chen, Y., Li, Y., Li, R., Sun, X., Ye, S. Knights, S. High Oxygen-Reduction Activity and Durability of Nitrogen-doped Graphene. *Energy Environ. Sci.* **2011,** *4,* 760-764.

103. Sheng, Z. –H., Shao, L., Chen, J. –J., Bao, W. –J., Wang, F. –B., Xia, X. –H. Catalyst-free Synthesis of Nitrogen-doped Graphene via Thermal Annealing Graphite Oxide with Melamine and its Excellent Electrocatalysis. *ACS Nano* **2011**, *5,* 4350–4358.

104. Wang, H., Zhang, C., Liu, Z., Wang, L., Han, P., Xu, H., Dong, S., Yao, J., Cui, G. Nitrogen-doped Graphene Nanosheets with Excellent Lithium Storage Properties. *J. Mater. Chem.* **2011,** *21,*5430–5434.

105. Parvez, K., Yang, S., Hernandez, Y., Winter, A. Turchanin, A., Feng, X., Müllen, K. Nitrogen-doped Graphene and its Iron-based Composites as Efficient Electrocatalysis for Oxygen Reduction Reaction. *ACS Nano* **2012**, *6,* 9541–9550.

106. Lin, Z., Waller, G., Liu, Y., Liu, M., Wong, C. –P. Facile Synthesis of Nitrogen-doped Graphene via Pyrolysis of Graphene Oxide and Urea, and its Electrocatalytic Activity toward the Oxygen-Reduction Reaction. *Adv. Energy Mater.* **2012**, *2,* 884–888.

107. Lei, Z., Lu, L., Zhao, X. S. The Electrocapacitive Properties of Graphene Oxide reduced by Urea, *Energy Environ. Sci.* **2012,** *5,* 6391–6399.

108. Mou, Z., Chen, X., Du, Y., Wang, X., Yang, P., Wang, S. Forming Mechanism of Nitrogen doped Graphene Prepared by Thermal Solid-State Reaction of Graphite Oxide and Urea. *Appl. Surf. Sci.* **2011,** *258,* 1704–1710.

109. Zhou, R.; Jaroniec, M.; Qiao, S. Z. Nitrogen-doped Carbon Electrocatalysis Decorated with Transition Metals for the Oxygen Reduction Reaction. *ChemCatChem*, **2015,** *7*, 3808-3817.

110. Wu, G.; More, K. L.; Johnston, C. M.; Zelenay, P. High Performance Electrocatalysis for Oxygen Reduction Derived from Polyaniline, Iron and Cobalt, *Science* **2011,** *332*, 443-447.

111. Fei, H.; Dong, J.; Jimenez, M. J. A.; Ye, G.; Kim, N. D.; Samuel, E. L. G.; Peng, Z.; Zhu, Z.; Qin, F.; Bao, J.; Yacaman, M. J.; Ajayan, P. M.; Chen, D.; Tour, J. M. Atomic Cobalt on Nitrogen-doped Graphene for Hydrogen Generation. *Nat. Commun.* **2015,** *6,* 86668-86676.

112. Hou, Y.; Wen, Z.; Cui, S.; Ci, S.; Mao, S.; Chen, J. An Advanced Nitrogen-doped Graphene/Cobalt-embedded Porous Carbon Polyhedron Hybrid for Efficient Catalysis of Oxygen Reduction and Water Splitting. *Adv. Funct. Mater.* **2015**, *25,* 872-882.

113. Chen, S.; Duan, J.; Ran, J.; Jaroniec, M.; Qiao, S. Z. N-doped Graphene Film-Confined Nickel Nanoparticles as a Highly Efficient Three-Dimensional Oxygen Evolution Electrocatalyst. *Energy. Environ. Sci.* **2013,** *6,* 3693-3700.

114. Liu, X.; Liu, W.; Ko, M. Park, M. Kim, M. G.; Oh, P.; Chae, S.; Park, S.; Casimir, A.; Wu, G.; Cho, J. Metal (Ni, Co)-Metal Oxides/ Graphene Nanocomposites as Multifunctional Electrocatalysts. *Adv. Func. Mater.* **2015,** *25,* 5799-5808.

115. Parvez, K., Yang, S., Hernandez, Y., Winter, A. Turchanin, A., Feng, X., Müllen, K. Nitrogen-doped Graphene and its Iron-based Composites as Efficient Electrocatalysis for Oxygen Reduction Reaction. *ACS Nano* **2012**, *6,* 9541–9550.

116. Xia, B. Y.; Yan, Y.; Wang, X.; Lou, W. X. Recent Progress on Graphene-based Hybrid Electrocatalysts. *Mater. Horiz.* **2014,** *1,* 379.

117. Wang, Y.; Wu, Y.; Huang, Y.; Zhang, F.; Yang, F.; Ma, Y.; Chen, Y. Preventing Graphene Sheets from Restacking for High-Capacitance Performance. *J. Phys. Chem. C* **2011,** *115,* 23192-23197.

118. Du, F.; Yu, D.; Dai, L.; Ganguli, S.; Varshney, V.; Roy, A. K. Preparation of Tunable 3D Pillared Carbon Nanotube-Graphene networks for High-Performance Capacitance. *Chem. Mater.* **2011,** *23,* 4810-4816.

119. Zhao, M. Q.; Zhang, Q.; Huang, J. Q.; Tian, G. L.; Chen, T. C.; Qian, W. Z.; Wei, F. Towards high Purity Graphene/single-walled carbon Nanotube Hybrids with Improved Electrochemical capacitive Performance. *Carbon* **2013,** *54,* 403-411.

120. Xue, Y.; Ding, Y.; Niu, J.; Xia, Z.; Roy, A.; Chen, H.; Qu, J.; Wang, Z. L.; Dai, L. Rationally designed graphene-nanotube 3D architectures with a seamless nodal junction for efficient energy conversion and storage. *Sci. Adv.* **2015,** *1*, 1400198-1400207.

121. Buglione, L.; Pumera, M. Graphene/Carbon nanotube Composites Not Exhibiting Synergic Effect for Supercapacitors: The Resulting Capacitance Being Average of Capacitance of Individual Components, *Electrochem. Commun.* **2012**, *17(1),* 45-47.

122. Gogotsi, Y. What Nano Can Do for Energy Storage. *ACS Nano* **2014,** *8 (6),* 5369-5371.

123. Kholmanov, I. N.; Magnuson, C. W.; Piner, R.; Kim, J. –Y.; Aliev, A. E.; Tan, C.; Kim, T. Y.; Zakhidov, A. A.; Sberveglieri, G.; Baughman, R. H.; Rouff, R. S. Optical, Electrical and Electromechanical properties of Hybrid Graphene/Carbon nanotube Films. *Adv. Mater.* **2015,** *27,* 3053-3059.

124. Tang, C.; Zhang, Q.; Zhao, M. –Q.; Huang, J. –Q.; Cheng, X. –B.; Tan, G. –L.; Peng, H. –J.; Wei, F. Nitrogen-doped Aligned Carbon Nanotube/Graphene Sandwiches: Facile Catalytic Growth on Bifunctional Natural Catalysts and Their Applications as Scaffolds for High-Rate Lithium-Sulfur Batteries. *Adv. Mater.* **2014**, *26,* 6100-6105.

125. Zhu, Y.; Li, L.; Zhang, C.; Casillas, G.; Sun, Z.; Yan, Z.; Ruan, G.; Peng, Z.; Raji, A. –R.; Kittrell, C.; Hague, R. H.; Tour, J. M. A seamless three-dimensional carbon nanotube graphene hybrid material. *Nat. Commun.* **2012,** *3,* 1225.

126. Tian, G. L.; Zhao, M. –Q.; Yu, D.; Kong, X. –Y.; Huang, J. –Q.; Zhang, Q.; Wei, F. Nitrogen-doped Graphene/Carbon nanotube Hybrids: In Situ Formation on

Bifunctional Catalysts and Their Superior Electrocatalytic Activity for Oxygen Evolution/ Reduction Reaction. *Small* **2014,** *10(11),* 2251-2259.

127. Kotal, M.; Bhowmick, A. K. Multifunctional Hybrid materials based on Carbon nanotube Chemically Bonded to Reduced Graphene Oxide. *J. Phys. Chem. C*, **2013**, *117,* 25865-25875.

128. D. T. Pham, T. H. Lee, D. h. Luong, F. Yao, A. Ghosh, V. T. Le, T. h. Kim, B. li, J. Chang and Y. H. Lee, Carbon Nanotube-Bridged graphene 3D Building Blocks for Ultrafast Compact Supercapacitors. *ACS Nano* **2015**, *9 (2),* 2018-2027.

129. Jung, N.; Kwon, S.; Lee, D.; Yoon, D.; Park, Y. M.; Benayad, A.; Choi, J.; Park J. S. Synthesis of Chemically Bonded Graphene/Carbon Nanotube Composites and their Application in Large Volumetric Capacitance Supercapacitors. *Adv. Mater.* **2013**, *25,* 6854-6858.

130. Liu, H.; Liu, Y.; Zhu, D. Chemical Doping of Graphene. *J. Mater. Chem.* **2011**, *21*, 3335-3345.

131. Guo, B.; Fang, L.; Zhang, B.; Gong, J. R.; Graphene Doping: A Review. *Insciences J.* **2011**, *1*, 80-89.

132. Wang, H.; Maiyalagan, T.; Wang, X. Review on Recent Progress in Nitrogen-Doped Graphene: Synthesis, Characterization, and Its Potential Applications. *ACS Catal.* **2012**, *2*, 781-794.

133. Wen, Z.; Wang, X.; Mao, S.; Bo, Z.; Kim, H.; Cui, S.; Lu, G.; Feng, X.; Chen, J. Crumpled Nitrogen-Doped Graphene nanosheets with Ultrahigh Pore Volume for High-Performance Supercapacitor. *Adv. Mater.* **2012,** *24,* 5610-5616.

134. Shui, J.; Du, F.; Xue, C.; Li, Q.; Dai, L. Vertically Aligned N-Doped Coral-like Carbon Fiber Arrays as Efficient Air Electrodes for High-Performance Nonaqueous Li-O_2 Batteries. *ACS Nano* **2014,** *8,* 3015-3022.

Chapter 3:
N-Doped Graphene with High Atomic Percentages of Pyridinic N and Graphitic N as Electrode for High-Performance Supercapacitor and Metal-Free Bifunctional Electrocatalyst for ORR and OER

3. N-Doped Graphene with High Atomic Percentages of Pyridinic N and Graphitic N as Electrode for High-Performance Supercapacitor and Metal-Free Bifunctional Electrocatalyst for ORR and OER

ABSTRACT: A facile synthesis method to produce nitrogen-doped graphene containing high atomic percentage of pyridinic N and graphitic N *via* the thermal annealing of graphene oxide and uric acid is reported. The method yielded N-doped graphene nanosheets that had high surface areas and that contained 9.22 at% nitrogen, which was present in four bonding configurations with high ratio of pyridinic N and graphitic N. The synthesized N-doped graphene showed excellent capacitance properties, which led to fabricate a stacked electrode supercapacitor cell of 2-electrode configuration with a specific capacitance of 230 F g^{-1} at a current density of 1 A g^{-1} and with remarkably high energy density of 62.6 Wh kg^{-1} in aqueous electrolyte. Additionally, this material showed superior properties as an electrocatalyst for both the oxygen-reduction reaction (ORR) and oxygen evolution reaction (OER), producing high current density primarily via the four-electron pathway for ORR at a current density of -4.3 mA cm^{-2} and OER activity of generating current density of 10 mA cm^{-2} at 1.74 V *vs*. RHE in alkaline media. Hence, this dual-natured N-doped graphene could provide a platform for developing nanostructured graphene-based advanced energy storage and conversion devices.

3.1. INTRODUCTION

Carbon-based materials for clean and renewable energy are becoming promising candidates to help meet the global demand for sustainable energy development. In particular, nanostructured materials for efficient energy storage and conversion devices have been reported for a wide range of applications including as solar cells,[1] fuel cells, lithium-ion batteries and electrochemical double-layer capacitors.[2-4] Among these energy storage devices, supercapacitors have gained attention due to their orders-of-magnitude-higher power density, cycle efficiency and charge/discharge rates than batteries.[5, 6] Besides energy storage, energy conversion is also crucial to meeting global energy demands. Fuel cells are among the promising methods of delivering energy in the future, but their widespread implementation is hindered by the expense

of the cathode material (platinum), as well as by their deactivation by the by-products of fuel decomposition (the fuel crossover effect), making the development of alternative, precious-metal-free electrode materials essential.[7-9] Graphene, composed of a one-atom-thick honeycomb lattice of sp^2-hybridized carbons, has shown great potential as an electrode material in energy storage and conversion due to its excellent electrical conductivity and high specific surface area.[10-13]

Chemical dopants can alter the electronic properties of graphene.[14] The introduction of dopants, either by the adsorption of molecules on the graphene surface or by the substitution of dopant atoms into the carbon lattice, can produce a band gap in graphene, and this strategy has led to the development of high-performance energy storage and conversion devices.[15, 16] Various heteroatoms, including N, B, and S, have imparted excellent electrochemical properties,[17-21] and N-doped graphene in particular has shown capacitance suitable for high-performance supercapacitor applications,[22-26] excellent electrocatalytic activity for oxygen reduction in fuel cells[27, 28] and oxygen evolution reaction for rechargeable metal-air batteries.[29, 30] The properties of nitrogen-doped graphene (NG) are conferred by nitrogen atoms within the carbon lattice, where they can exist as pyridinic, pyrrolic, graphitic, and oxidized N.[31]

The roles of the differently configured nitrogen atoms in enhancing capacitance or generating catalytically active sites are still controversial,[32, 33] but both quantum mechanical calculations[34-36] and experimental[24, 37] investigations indicate that graphitic, pyridinic, and pyrrolic N can enhance the capacitance, whereas pyridinic N and graphitic N can be essential to catalyzing oxygen reduction reaction by enhancing the adsorption of O_2 on the adjacent carbon atoms and thus promotes the four-electron pathway.[38-41] Besides the capacitance and oxygen reduction reaction, oxygen evolution reaction has gained a considerable attention due to the promising future of rechargeable metal-air batteries.[42-44] N-doped graphene,[29] NG/CNT composites,[30] N-doped coaxial carbon nanotube,[45] carbon nitrogen nanotubes[46] and nitrogen and phosphorous co-doped nanocarbons[47, 48] have shown to be promising alternatives to noble and transition metal based OER catalysts.

The enhanced supercapacitative and electrocatalytic properties are highly dependent on the type and amount of nitrogen present. To obtain both the capacitance and electrocatalytic properties,

high atomic concentrations of pyridinic, pyrrolic and graphitic nitrogen are required. The types and amounts of the different nitrogen bonding configurations in an N-doped graphene sample depend on the nitrogen source as well as the synthesis method. Nitrogen has been incorporated into the graphitic lattice from sources like acetonitrile,[49] pyridine[50] and ammonia[51, 52] via chemical vapor deposition (CVD) or high-temperature treatment, and the resulting materials have been applied in lithium batteries,[49, 52] field effect transistors,[50] and as catalysts for oxygen reduction.[51] However, it is difficult to obtain materials with high levels of atomic nitrogen doping, and on a large scale, *via* CVD using gaseous or liquid sources of nitrogen, and the method also suffers from practical limitations due to possible contamination from the metal deposition catalyst as well as the toxicity of the precursors. On the other hand, the co-pyrolysis of graphene or a graphene precursor with a solid source of nitrogen, such as melamine[51] or cyanamide,[53] has produced NG with high levels of nitrogen (~9 at%). Co-pyrolysis methods are attractive because they can be scaled up without any catalyst.[54] However, the NG synthesized from melamine had a low surface area;[51] whereas cyanamide, on the other hand, required a surfactant to bind to the graphene surface.[53] Moreover, the NG synthesized from cyanamide did not contain pyrrolic nitrogen,[53] which plays an important role in enhancing capacitance.[34] In addition to melamine and cyanamide, urea has been employed as a solid source of nitrogen in the synthesis of N-doped graphene, however both the capacitance and electrocatalytic properties in the material were not investigated.[54-56] In order to show both high capacitance and electrocatalytic activity, an NG sample must contain sufficient percentages of pyridinic, pyrrolic, and graphitic nitrogen atoms, and have large surface area and high pore volume.

Herein, we report the synthesis of NG via the thermal annealing of graphene oxide (GO) with uric acid at 800 °C under an argon atmosphere. This is, to the best of our knowledge, the first use of uric acid as a solid source of nitrogen in the synthesis of nitrogen-doped graphene. Uric acid has a high nitrogen content (~33 wt%), and its crystals can adhere to surfaces bearing various organic functionalities, and via multiple types of forces (electrostatic interactions, hydrogen bonding and/or van der Waals interactions), without the aid of surfactants.[57] These properties allowed the co-pyrolysis of graphene oxide and uric acid to produce a nitrogen-doped reduced graphene oxide (rGO) with nitrogen atoms in all of the possible configurations in the graphitic

lattice, a high total nitrogen content with a high ratio of pyridinic N and graphitic N and a high surface area after pyrolysis. As a result, the N-doped graphene had both high capacitance and high bifunctional electrocatalytic activity towards oxygen reduction and evolution.

3.2. EXPERIMENTAL SECTION

Synthesis of nitrogen-doped graphene

GO was prepared from naturally expanded graphite (Ashbury Carbons, Grade-3772) using a reported procedure for the generation of ultra-large GO sheets. [58] The GO sheets (approx. 20 mg) were dispersed in water by ultrasonication for 30 min at a frequency of 50 Hz, then mixed with uric acid in a ratio of 1:1, 1:5 or 1:10 by mass. The mixtures were then stirred continuously and heated at 80 ºC for 10–12 h to remove the water. The resulting solids were transferred to a tubular furnace and heated in an argon atmosphere at 5 °C min^{-1} to 800 ºC, then annealed for 1 h. The synthesized nitrogen-doped graphenes produced with 1:1, 1:5 and 1:10 ratios of graphene oxide and uric acid were named NG1, NG5 and NG10, respectively. Pure GO was also thermally annealed to yield reduced graphene oxide (rGO) under the same conditions, and used as reference.

Characterization

The microstructures and morphology of the synthesized samples were investigated by Field Emission Scanning Electron Microscopy (FESEM, Zeiss ULTRA *plus*) and High Resolution Transmission Electron Microscopy (HRTEM, JEOL 2200FS) with an acceleration voltage of 200 kV. Thermogravimetric Analysis (TGA, TA Q500) was performed under Ar and at a heating rate of 5 °C min^{-1}. X-ray Diffractometry (XRD) was performed on a Shimadzu S6000 equipped with Cu Kα radiation (λ = 0.154 nm) with a resolution of 0.02°. Raman spectra were collected with Renishaw inVia Raman Spectrometer with laser wavelength of 514 nm. Nitrogen adsorption/desorption isotherms and Brunauer–Emmett–Teller (BET) surface areas were measured over P/P_0 = 0.05–0.3 at 77 K on an Autosorb iQ (Quantachrome, USA). X-ray photoelectron spectroscopy (XPS) analyses were performed by ESCALAB250Xi (Thermo Scientific, UK) with a monochromated Al Kα (energy 1486.68 eV) operating at 150 W (13 kV ×

12 mA) under a vacuum of 2×10^{-9} mbar. The analysis spot was 500 μm in diameter. The binding energies were referenced to the adventitious hydrocarbon C 1*s* signal at 284.9 eV.

Electrochemical measurement:

For electrochemical characterization and measurement, the nitrogen-doped graphenes were deposited from a 1-mg/mL mixture, prepared by sonicating in degassed isopropanol, on a glassy-carbon electrode. The glassy-carbon working electrode was polished mechanically with a slurry of 0.05-μm alumina particles to obtain a mirror-like surface, washed with Milli-Q water and acetone, and allowed to dry. It was then tested in a three-electrode cell, using platinum wire as the counter electrode and a Ag/AgCl, KCl (3 M) electrode as the reference electrode. Measurements were taken using a Bio-logic SP300 potentiostat. The binding agents were 10 wt% PTFE for capacitance measurements and 5 wt% Nafion for electrocatalytic measurements. Capacitance was determined using a T-cell device in a two-electrode cell configuration, as described previously.[59, 60] The device was fabricated using a Swaglok system with two stainless steel current collector. The PVDF separator was placed between the current collectors where the material to be studied was pressing together at high pressure. 0.5-M H_2SO_4 was used as the electrolyte and the cell was airtight. 0.5 mg active materials were deposited on the diameter of an 8-mm stainless steel electrode surface using a 10-wt% PTFE binder. The gravimetric capacitance from galvanostatic charge/discharge was calculated using Eq. 1.[6]

$$C = \frac{4I}{m\frac{dv}{dt}} \qquad (1)$$

Where C is specific capacitance (F g^{-1}), I is the charge/discharge current density (A g^{-1}), m is the total mass of materials deposited on the electrodes and dV/dt was calculated from the slope of the discharge curve. The energy density (E) and power density (P) were calculated using Eqs. 2 and 3, respectively.[60, 61]

$$E = \frac{1}{2} \times C(\Delta V)^2 \qquad (2)$$

$$P = E/t \quad (3)$$

Where C is the specific capacitance of the device, ΔV is the potential range and t is the time to discharge. The electrocatalytic properties were evaluated by rotating disk electrode (RDE) experiments in an O_2-saturated 0.1-M KOH solution. First, the oxygen-reduction capability was assessed by comparing cyclic voltammetric curves measured in argon- and oxygen-saturated electrolytes. Linear sweep voltammetry curves were recorded over the potential range of 0 to 1 V versus reversible hydrogen electrode (RHE) at a scan rate of 10 mV/s at ambient temperature and at rotation speeds of 100–1600 rpm. The effects of different mass loading on the glassy carbon electrode in electrocatalysis were evaluated by depositing 4, 8, 12, 16 and 20 μg of NG10. OER activity was measured by linear sweep voltammetry in the potential window ranging from 1.0 to 2.0 V versus reversible hydrogen electrode (RHE) scale by adding a value of 0.964 V. The commercial Pt/C (20 wt %) and Ru/C (20 wt %) into nafion solution with same loading amount were taken for comparison.

3.3. RESULTS AND DISCUSSION

In the synthesis of NG (Scheme 1), graphene oxide and uric acid were mixed together in water (in ratios of 1:1, 1:5 or 1:10 by mass in mg scale for NG1, NG5 and NG10, respectively), and then stirred continuously at 80 °C to remove the water. We expect that the uric acid molecules adsorbed on the graphene oxide surface during this time. The solid mixtures were then heated in a tubular furnace at a rate of 5 °C min^{-1} to 800 °C in an argon environment. The formation of N-doped graphenes from the pyrolysis of GO with melamine [51] and cyanamide [53] had been proposed to proceed in two steps via formation of carbon nitride first, which forms from the pyrolysis of cyanamide.[62] For the present case, from the thermogravimetric-analysis curves examined under argon in a thermogravimetric analyser (TGA) (Figure 1), it is observed that the rapid weight losses started from 400 °C due to the decomposition of uric acid and the complete decomposition of the GO/uric acid mixture occurred around 750 °C.

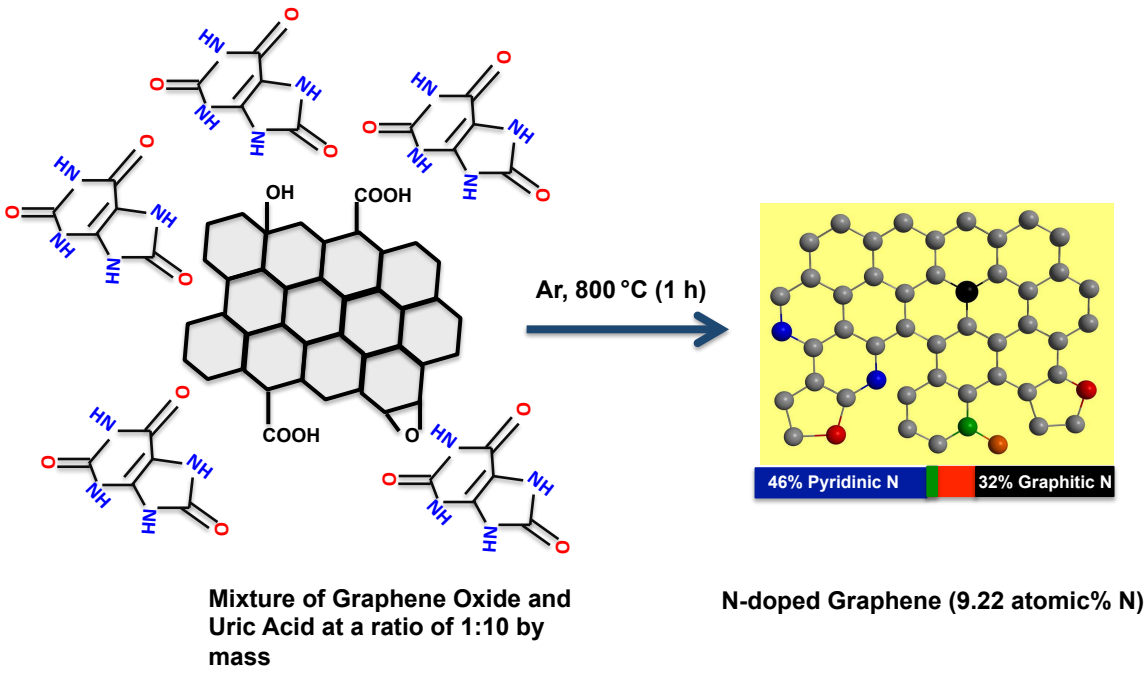

Scheme 1. Schematic diagram of the formation of NG via the thermal annealing of graphene oxide with uric acid.

The thermogravemetric analysis of uric acid has also been performed to measure the possible amount of hard carbon transformed from the uric acid after carbonization. The TGA curve of uric acid showed the almost complete decomposition from 650 °C and only 0.38 % of the initial mass of uric acid remained after the complete carbonization. This behavior supports the mechanism of interaction of heterocyclic -NH groups of uric acid with the functional groups of GO, contributing to the incorporation of N into the graphene lattice rather than *via* formation of carbon nitride.[53] Due to organic in nature and high surface attachment ability,[57] uric acid can be attached on the graphene surface better than the inorganic solid precursor urea and thus higher atomic percentage of nitrogen with four possible bonding configurations has been achieved.

The morphology, structure, and graphitic layers of the obtained NGs were characterized by scanning electron microscopy (SEM) and transmission electron microscopy (TEM). The SEM images of NG10 showed a laminar morphology (Figure 2a), and its low-resolution TEM image showed transparent stacked graphene sheets. The high-resolution transmission electron micrograph (HRTEM) and selected area electron diffraction (SAED) pattern revealed the highly crystalline nature of NG10 (Figure 2b). The well-defined diffraction spots and rings in the SAED pattern confirmed that the sample was comprised of the hexagonal carbon lattice typical of

graphene-like materials.[63] The XRD patterns of NG1, NG5 and NG10 (Figure 2c) showed broad peaks at around 26.0°, which corresponded to an interlayer spacing of 0.342 nm.

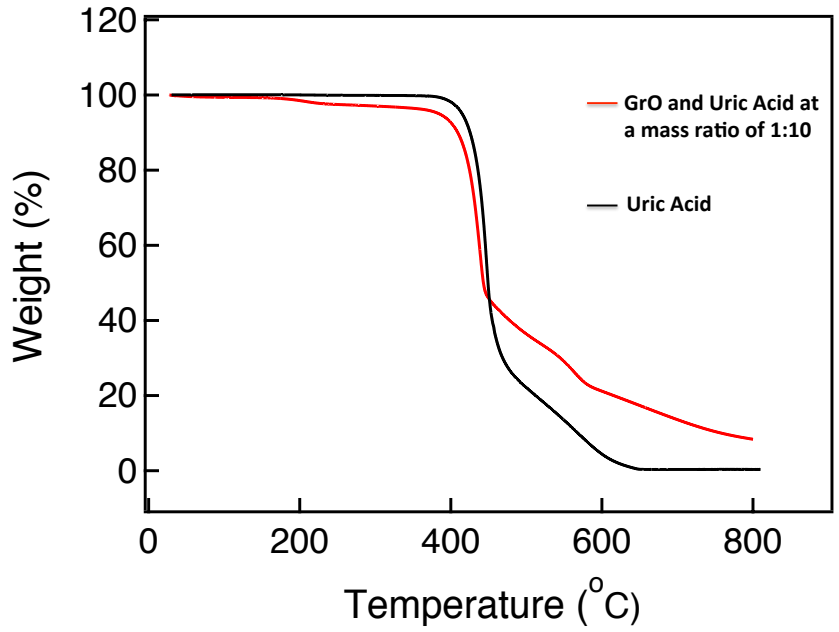

Figure 1. Thermogravimetric analysis of an as-prepared GO–uric acid composite at a ratio of 1:10 by mass and uric acid only. The composites were heated at 5 ºC min^{-1} under flowing argon.

GO, rGO, and the N-doped materials NG1, NG5 and NG10, were characterized by Raman spectroscopy at an excitation wavelength of 514 nm under ambient conditions. As shown in Figure 2d and Table 1, the G peaks of the GO, rGO, NG1, NG5 and NG10 occurred between 1582 and 1598 cm^{-1}. The G peaks shifted to lower energy from GO to NG10, indicating that a conjugated sp^2 structure was restored during pyrolysis.[53] The I_D/I_G ratios of GO, rGO, NG1, NG5 and NG10 (Table 1) were used to evaluate the defects or in-plane crystallite size after pyrolysis, and the crystallite sizes, L_a, were calculated according to the Tuinstra–Koenig (TK) relation, Eq. 4.[38, 64]

$$L_a = (2.4\times10^{-10})\lambda^4(I_D/I_G)^{-1} \quad (4)$$

Where λ is the Raman excitation wavelength (514 nm). The crystallite sizes of rGO, NG1, NG5 and NG10 were smaller than that of GO (Table 1), indicating that the crystallite sizes decreased upon thermal annealing.

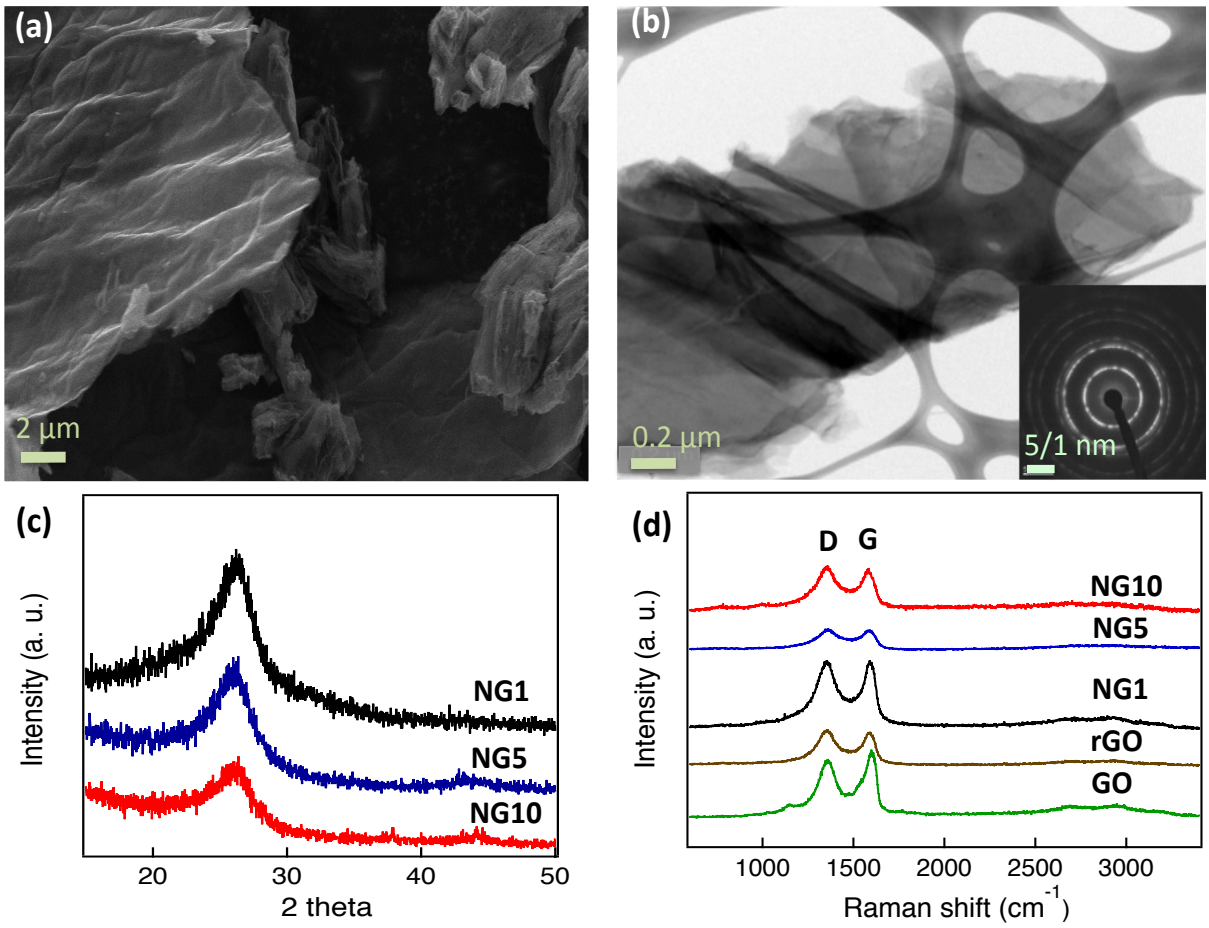

Figure 2. (a) SEM image of NG10, (b) TEM image and selected area electron diffraction (SAED) pattern (inset) of NG10, (c) XRD pattern of NG1 (black), NG5 (blue) and NG10 (red), (d) Raman spectra of NG10 (red), NG5 (blue), NG1 (black), reduced graphene oxide (brown) and graphene oxide (green).

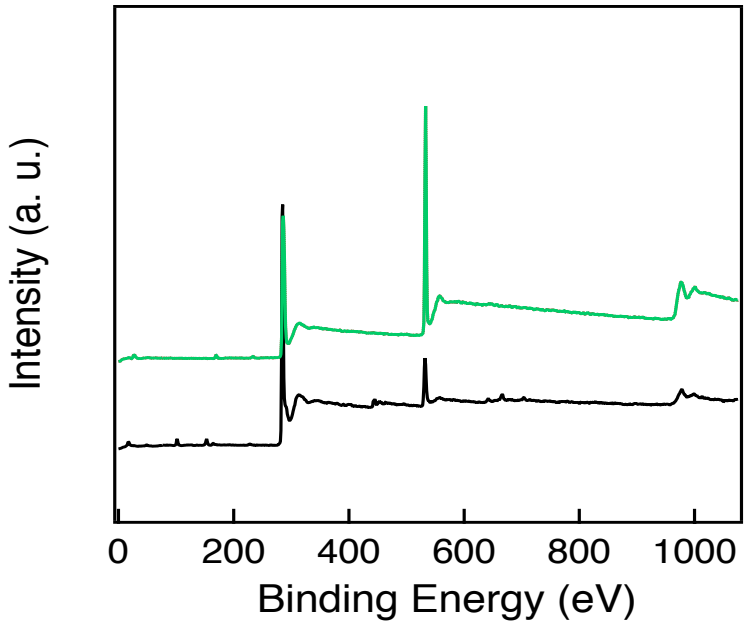

Figure 3. XPS spectra of GO (green) and rGO (black).

To characterize the elemental composition and nitrogen content in the NGs, X-ray photoelectron spectra (XPS) of the materials were measured. A comparison of the spectra of GO and rGO showed a decrease in oxygen content in rGO; neither spectrum showed obvious N 1*s* peaks (Figure 3). As shown in Figure 4a, the survey spectra of NG samples revealed the presence of C, O and N. In NG1, NG5 and NG10, the high-resolution C 1*s* peak was centered at 284.4 eV and tailed at higher binding energies, indicating the connection of carbon atoms with N and O atoms. Though NG10 (Figure 2b), NG5 (Figure 5) and NG1 (Figure 4c) showed significant amounts of graphite-like C (284.40 eV),[65] quantitative analysis of the C 1s region of the spectrum was impossible due to the likely presence of adventitious carbon in the samples. The deconvolutions of the N 1*s* peaks (Figures 4d, 6 and 7, Table 1) showed the presence of four nitrogen configurations. All the NG1, NG5 and NG10 contained primarily (>40%) pyridinic nitrogen and minor amounts (<10%) of N-oxides, but they differed in that NG1 contained much more pyrrolic N, whereas NG5 and NG10 was richer in graphitic N. Moreover, NG10 and NG5 had a much greater total nitrogen content (9.22 at% for NG10 and 6.75 at% for NG5, Table 1) and higher Brunauer–Emmett–Teller (BET) surface area (197.8 $m^2 g^{-1}$ measured over P/P_0 = 0.05–0.30 for NG10 and 164.04 $m^2 g^{-1}$ measured over P/P_0 = 0.05–0.30 for NG5, Figure 8, 9 and Table 1) than did NG1 (1.52 at% N, Table 1; S_{BET} = 96.06 $m^2 g^{-1}$ measured over P/P_0 = 0.05–0.30, Figure 10

and Table 1); the NG materials had greater surface area than rGO (75.68 m^2 g^{-1} measured over P/P_0 = 0.05–0.30, Figure S10 and Table 1). NG10 also displayed high pore volume of 0.8 cm^3 g^{-1} (as defined at P/P_0 = 0.995), whereas the pore volumes of NG5, NG1 and rGO were 0.68, 0.2 and 0.07 cm^3 g^{-1} (as defined at P/P_0 = 0.995), respectively. Based on the above results, it is evident that the inclusion of N from uric acid contributed to raise the surface areas and pore volumes of the pyrolyzed N-doped graphene materials.

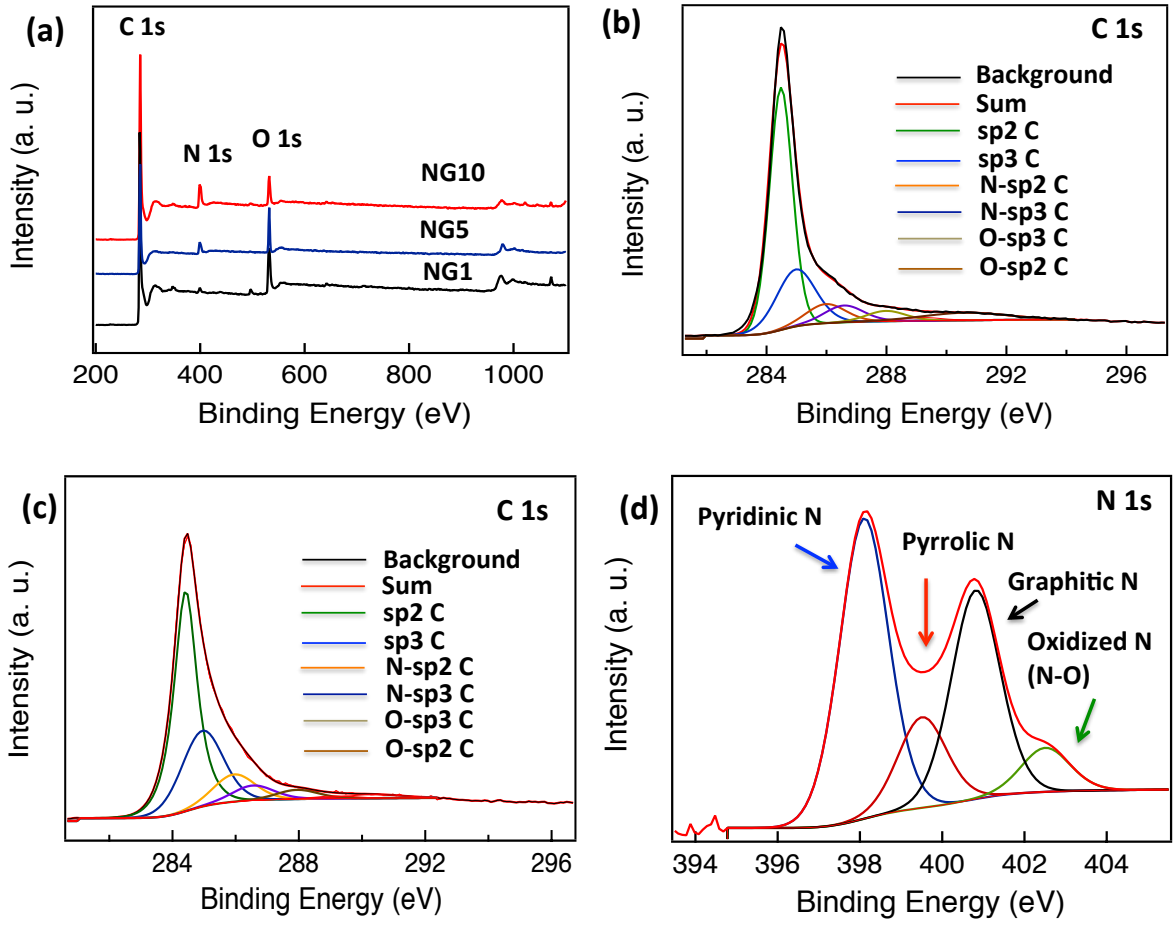

Figure 4. (a) XPS spectra of NG10 (red), NG5 (blue) and NG1 (black), (b) High-resolution C 1*s* spectrum of NG10, (c) High-resolution C 1*s* spectrum of NG1, (d) N 1*s* spectrum of NG10.

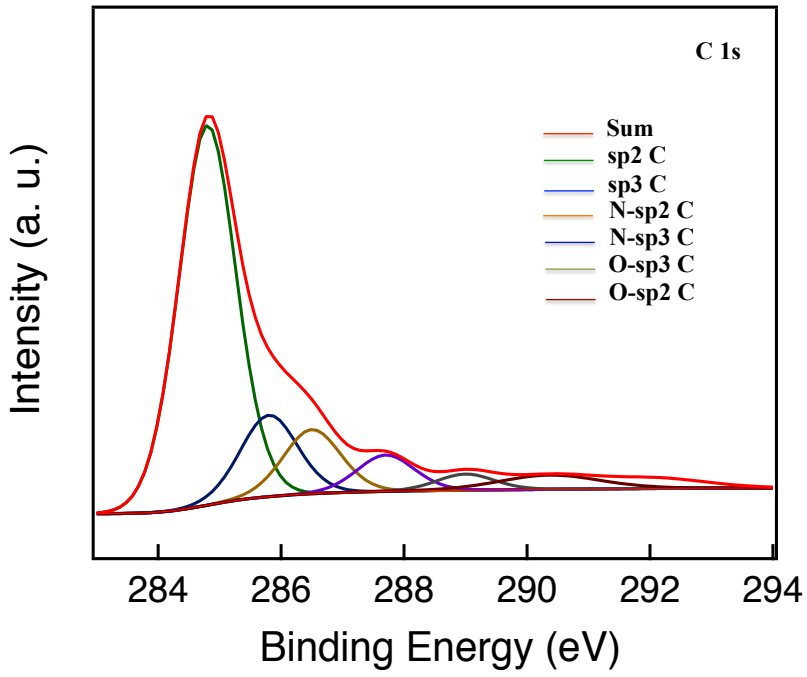

Figure 5. High-resolution C1*s* XPS spectra of NG5.

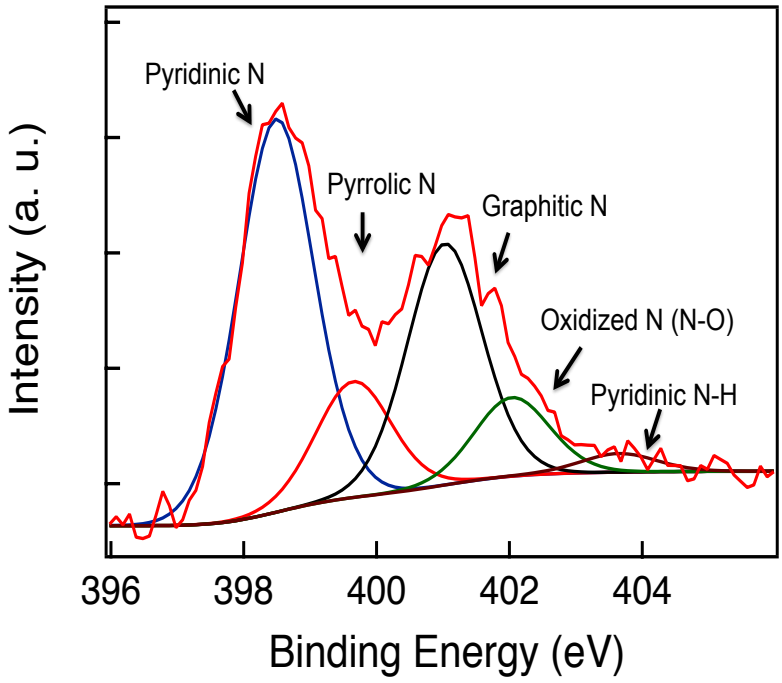

Figure 6. High-resolution N1*s* XPS spectra of NG5.

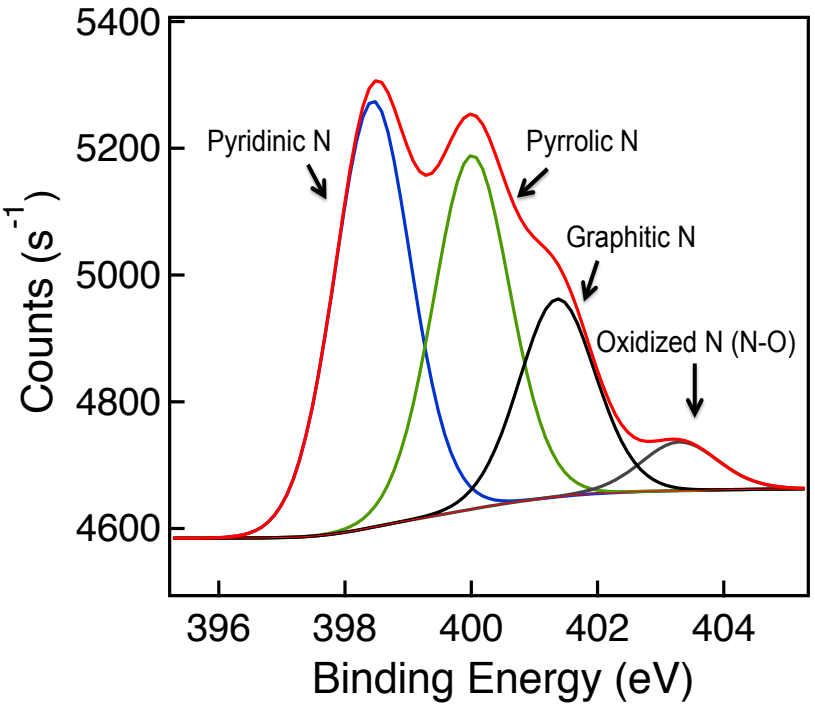

Figure 7. High-resolution N1*s* XPS spectra of NG1.

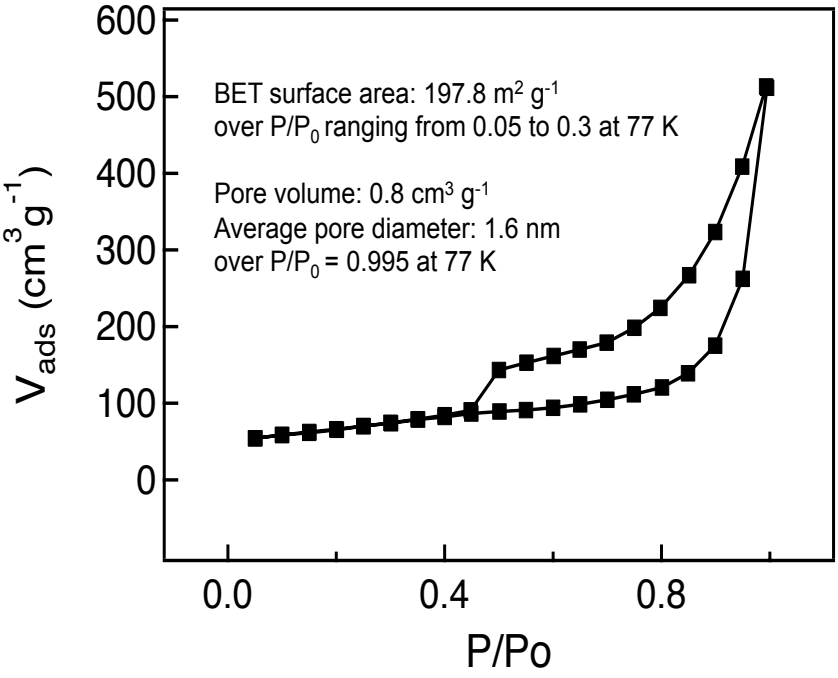

Figure 8. Nitrogen adsorption/desorption isotherm of NG10.

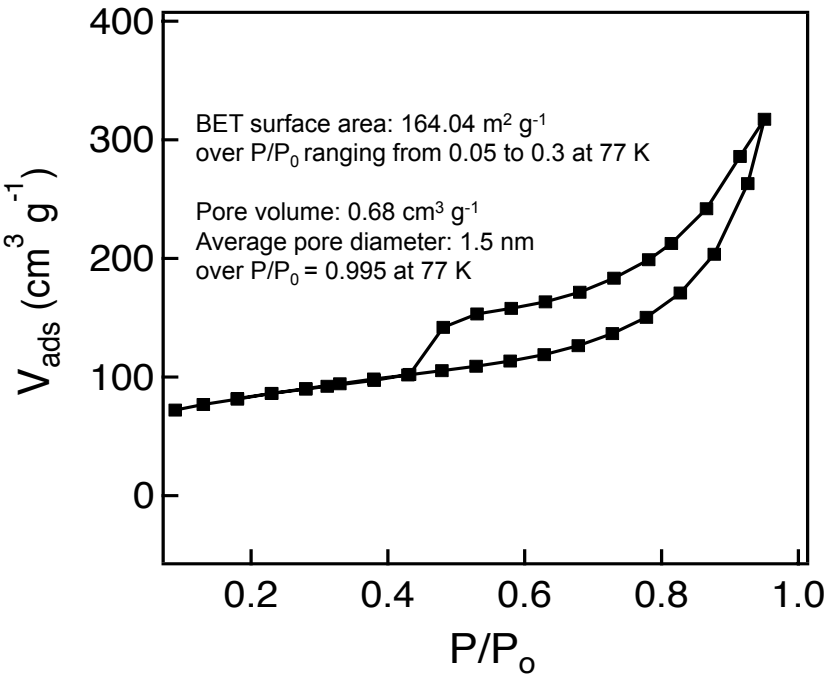

Figure 9. Nitrogen adsorption/desorption isotherm of NG5.

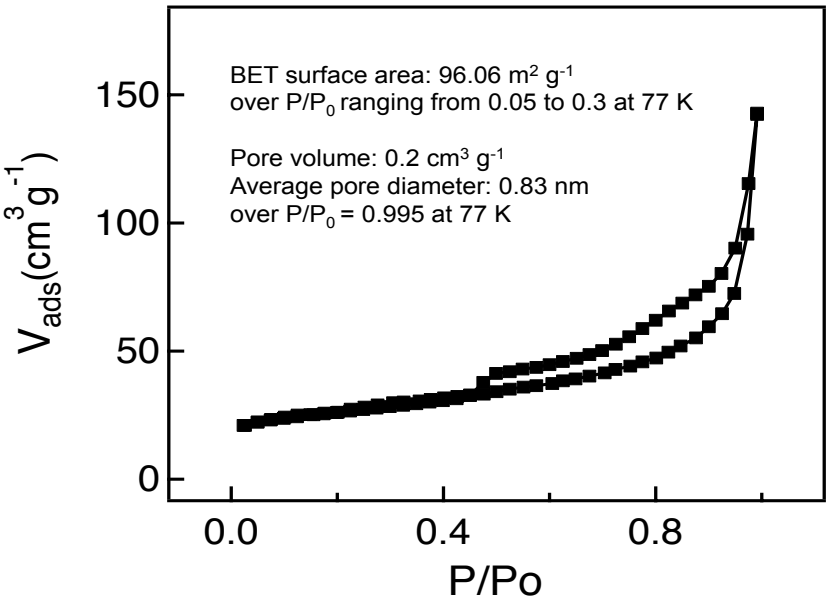

Figure 10 Nitrogen adsorption/desorption isotherms of NG1.

Cyclic voltammetry (CV) was used to investigate the electrochemical behavior of rGO, NG1, NG5 and NG10 in 0.5-M aqueous H_2SO_4 electrolyte deposited on a glassy carbon electrode at potential limits of 1.2 to – 0.2 V *vs*. Ag/AgCl electrode in a three-electrode system at a scan rate

of 100 mV s^{-1} (Figure 11a), with 10 wt% PTFE in isopropanol being used as a binder. A comparison of the CVs for rGO, NG1, NG5 and NG10 revealed that the capacitive response became larger with a highly rectangular nature with increasing nitrogen content, and the higher doping percentage resulted in an enhancement of the double layer capacitance, indicating the more effective contribution of electrochemical double layer capacitance with pseudocapacitance for the sample with higher nitrogen content, NG10. Thus the electrochemical activity and reversibility of the capacitance of NG10 were recorded at different scan rates and the capacitance increased at greater scan rates.

Table 1. Characterization data for GO, rGO, NG1, NG5 and NG10.

	$\nu(G)$[a]	I_D/I_G[a]	L_a[b]	S_{BET}[c]	V_{total}[d]	N Sites[e]				Total N[e]
	(cm^{-1})	(–)	(nm)	($m^2\ g^{-1}$)	($cm^3\ g^{-1}$)	(% of total N)				(at%)
						Pyridinic	Pyrrolic	Graphitic	Oxide	
GO	1598	0.87	19	–[f]	–[f]	–[f]	–[f]	–[f]	–[f]	–[f]
rGO	1594	1.03	16.3	75.68	0.07	–[f]	–[f]	–[f]	–[f]	–[f]
NG1	1592	0.99	16.8	96.06	0.20	41.4	34.9	19.1	4.61	1.52
NG5	1582	1.03	16.2	164.04	0.68	46.3	13.6	28.4	9.33	6.75
NG10	1582	1.03	16.2	197.80	0.80	46.6	14.1	32.4	6.83	9.22

[a] Position of the *G* peak ($\nu(G)$) and ratio of D and G peak intensities (I_D/I_G) determined from Raman spectroscopy using $\lambda_{excitation}$ = 514 nm. [b] Crystallite size (L_a) calculated from Raman data according to the Tuinstra–Koenig relation.[64] [c] BET surface area calculated over P/P_0 = 0.05–0.30 from N_2 adsorption at 77 K. [d] Total Pore volume calculated from P/P_0 = 0.995 from N_2 adsorption at 77 K. [e] Calculated from X-ray photoelectron spectroscopy. Total nitrogen was calculated from detection-sensitivity-adjusted peak areas. [f] Not determined.

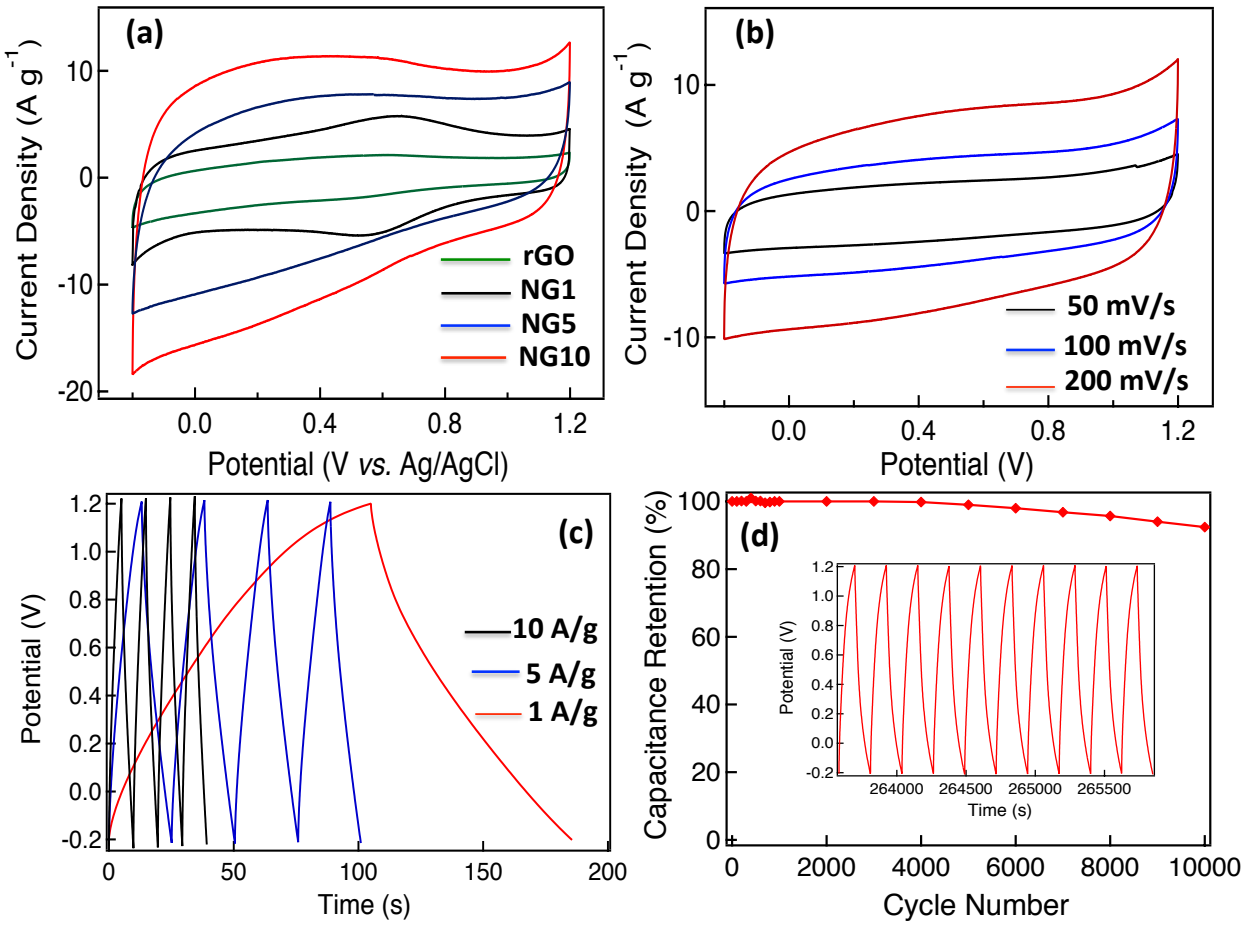

Figure 11. (a) Cyclic voltammograms of rGO, NG1, NG5 1 and NG10 using a three-electrode cell at a scan rate of 100 mV s^{-1} in 0.5-M H_2SO_4 solution, (b) Cyclic voltammograms of NG10 at different scan rates (50, 100 and 200 mV s^{-1}) in a two-electrode T-cell system, (c) Galvanostatic charge/discharge curves for NG10 in a two-electrode T-cell system tested at current density of 1–10 A g^{-1}, (d) Cycling stability of NG10 measured at 5 A g^{-1} over the potential range of 1.2 to –0.2 V. The inset shows the charge–discharge curves over the last ten cycles.

A T-Cell device consisting of stainless steel electrodes with a Teflon cover was used to investigate the capacitive properties of NG10 for practical application (Figure 12).[60] The active material was deposited on the electrodes with a PTFE binder and dried in an oven at 110 °C for 1 h. A PVDF membrane separator was inserted between the two electrodes, which were then pressed under high pressure. The H_2SO_4 electrolyte was poured from the top to completely fill the device before it was sealed air-tight.

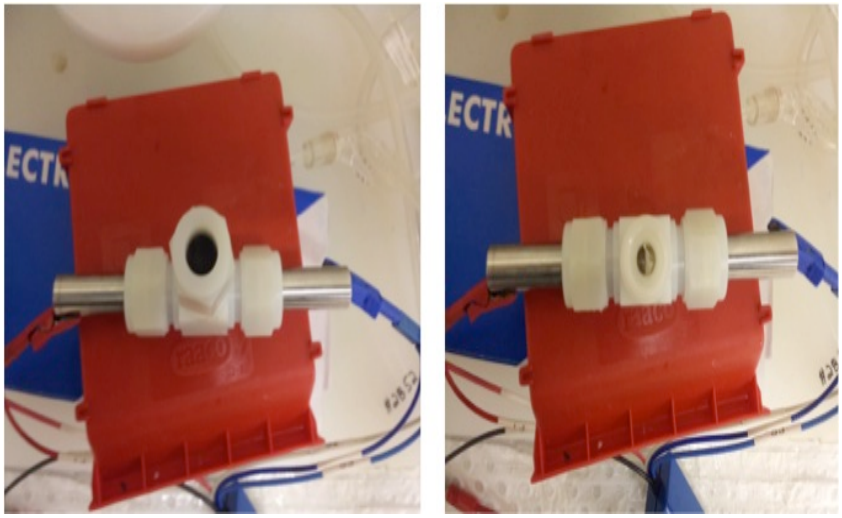

Figure 12. Optical images of stacked electrodes supercapacitor (T-cell).

CVs recorded in the T-Cell at different scan rates (50, 100 and 200 mV s^{-1}) showed near-ideal rectangular voltammetric responses (Figure 11b). The specific capacitance (*Csp*) of the NG10 electrode material was calculated from the galvanostatic discharge curves (Figure 11c) to be 230 F g^{-1} in 0.5-M H_2SO_4 at a current density of 1 A g^{-1}. At a high current density of 10 A g^{-1}, the specific capacitance value remained as high as 137 F g^{-1}. The RC constants at 1 and 10 A g^{-1} were 40.25 and 2.39 s, respectively. The energy density and power density of the device were calculated based on the discharge rates and plotted on a Ragone plot (Figure 13). The highest energy density, 62.61 Wh kg^{-1} was achieved at the power density of 2.79 kW kg^{-1}, and an energy density of 37.29 Wh kg^{-1} was retained even at a high power density of 28.08 kW kg^{-1}; this was superior than the values reported for chemical-doped graphene-based materials. (Table 2).

Besides the gravimetric capacitance, volumetric capacitance is also very important for fabricating devices for practical applications. The average density of the active material on the electrodes was calculated based on the thickness measured by SEM to be 0.5 g cm^{-3}, meaning that the volumetric capacitance was 115 F cm^{-3}, which is higher than that of nanostructured graphene-based supercapacitor materials such as activated graphene,[6] graphene foam,[66] graphene hydrogel[67] and laser-scribed graphene.[68]

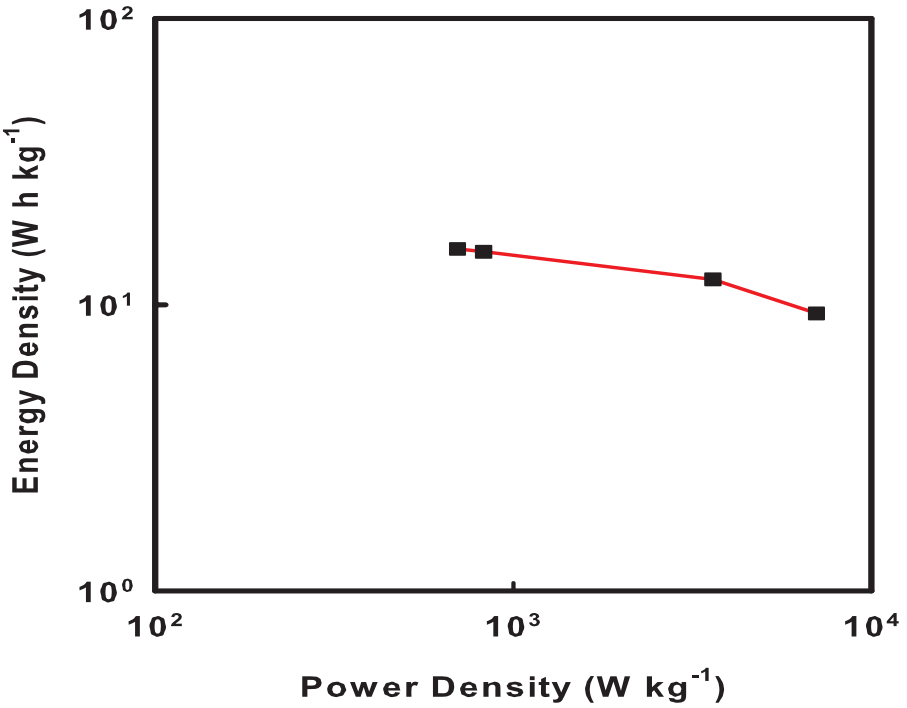

Figure 13. Ragone plot of the T-cell device based on two-electrode mass of active materials.

The superior performance of NG10 could be attributed to its high contents of pyridinic, pyrrolic and graphitic N, as well as to its high surface area with large pore volume, which provided excellent electrical conductivity and pseudocapacitance with favorable electrolyte penetration. The stability of the device was also investigated over 10000 cycles between 1.2 and –0.2 V at a high current density of 5 A g^{-1} (Figure 11d). The material maintained almost 100% of its initial specific capacitance upto 4000 cycles and then gradually started decreasing and kept 92.4% of its initial specific capacitance after 10000 cycles. The charge/discharge curves for the last ten cycles demonstrate the stability of the device (inset of Figure 11d).

NG10 was also tested as an electrocatalyst for the oxygen-reduction reaction (ORR) under alkaline conditions. Thus, NG10 was deposited on a glassy carbon electrode and its cyclic voltammetry was measured in both argon- and oxygen-saturated 0.1-M KOH(*aq*) at a scan rate of 50 mV s^{-1}.

Material	Doping agent	Capacitance, C_g (F g^{-1})	Electrolyte	Energy density (Wh kg^{-1})	Ref.
Crumpled N-doped Graphene nanosheets	Cyanamide (NH_2CN)	245.9 F g^{-1} at 1 A g^{-1}	$[Bu_4N]BF_4$ acetonitrile	-	25
3D Nitrogen-doped Graphene-CNT	Pyrrole	180 F g^{-1} at 0.5 A g^{-1}	6 M KOH	-	71
Reduced Graphene Oxide	Urea	255 Fg^{-1} at 0.5 Ag^{-1}	6 M KOH	-	55
Nitrogen-doped Graphene	Urea	326 F g^{-1} at 0.2 A g^{-1}	6 M KOH	25.02	24
3D N and B co-doped Graphene	Ammonia borontriflouride	239 F g^{-1} at 1 mV s^{-1}	1 M H_2SO_4	8.7	18
Boron-doped graphene nanoplatelets	Borane-tetrahydrofuran	160 F g^{-1} at 1 A g^{-1}	6 M KOH	-	17
Nitrogen-doped Graphene	phenylenediamine	301 F g^{-1} at 0.1 A g^{-1}	6 M KOH	-	72
Nitrogenenriched nonporous carbon	Ammonia	198 F g^{-1} at 0.05 A g^{-1}	6 M KOH	-	73
Nitrogen-enriched carbon nanotube	Melamine	167 F g^{-1} at 1 V s-^{1}	1 M H_2SO_4	-	74
Nitrogen-doped porous carbon nanofiber	Polypyrrole	202 F g^{-1} at 1 A g^{-1}	6 M KOH	7.1	75
N-doped porous carbon	Pyrrole	240 F g^{-1} at 0.1 A g^{-1}	1 M H_2SO_4	19.5	76
Nitrogen-doped carbon foam	Melamine	203 F g^{-1} at 0.5 A g^{-1}	6 M KOH	47.8	77
Graphitic Carbon nitride	Melamine	264 at F g^{-1} 0.4 A g^{-1}	0.1 M $LiClO_4$	30	78
Nitrogen-doped Graphene	Hexamethylenetetramine	270 F g^{-1} at 1 A g^{-1}	1 M H_2SO_4	-	79
Nitrogen-doped Graphene	Aminoterphthalic acid	210 F g^{-1} at 1 A g^{-1}	0.5 M H_2SO_4	-	26
N-doped Graphene	**Uric Acid**	**230 Fg^{-1} at 1Ag^{-1}**	**0.5M H_2SO_4**	**62.6**	**This work**

Table 2. Comparison of the gravimetric performance for the as-prepared NG10 with previously reported nitorgen-doped and boron-doped nanocarbon materials.

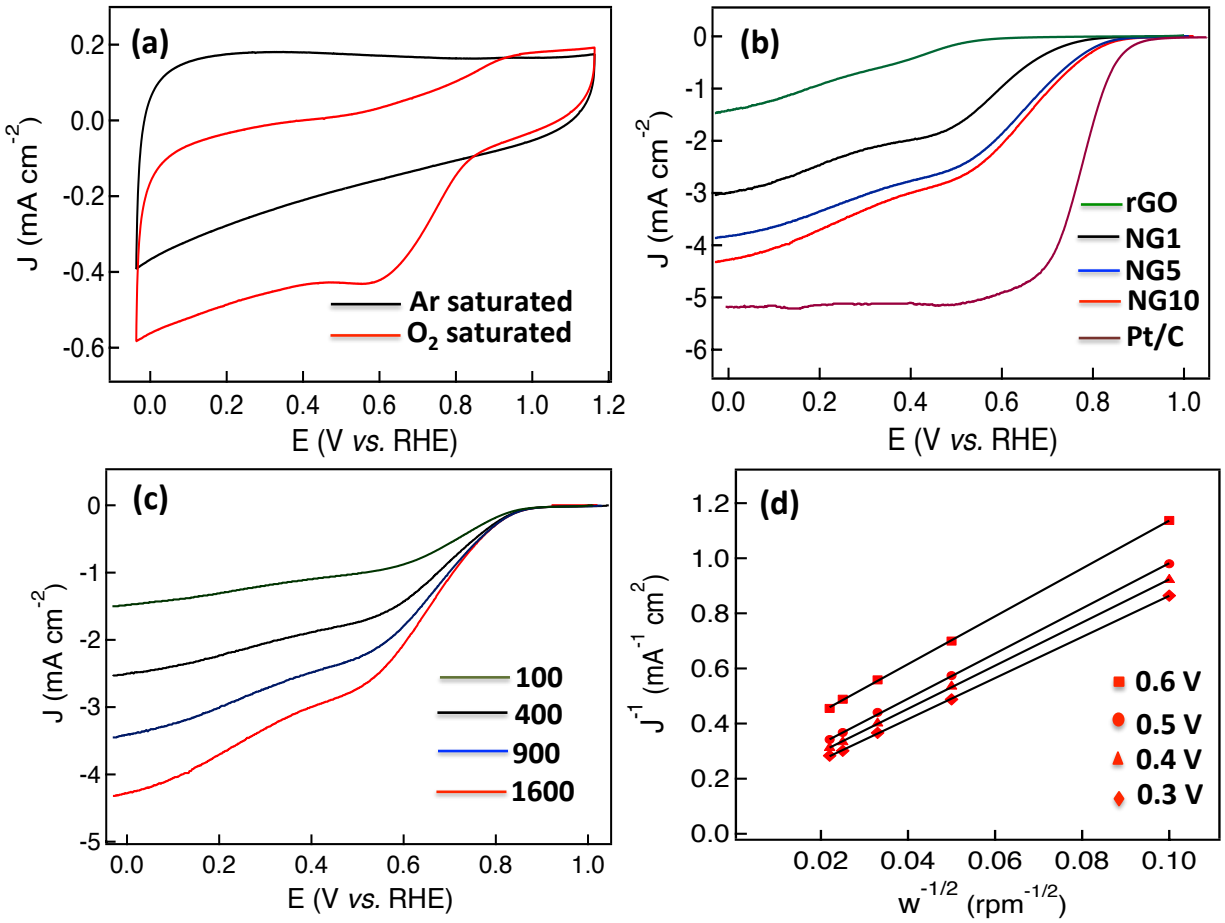

Figure 14. (a) Cyclic voltammograms of NG10 at a scan rate of 50 mV/s in Ar-saturated (black) and O_2-saturated (red) 0.1-M KOH(*aq*) solution, (b) Linear sweep voltammograms (LSV) of rGO, NG1, NG5, NG10 and Pt/C at 1600 rpm and a scan rate of 10 mV/s in O_2-saturated 0.1-M KOH(*aq*), (c) RDE measurements of NG10 in O_2-saturated 0.1-M KOH(*aq*) at scan rates of 10 mV/s, and (d) Koutecky–Levich plots of NG10 at electrode potentials of 0.6, 0.5, 0.4 and 0.3 V.

As shown in Figure 14a, a clean capacitive CV background was observed within a potential range of 1.0 to –0.05 V in the argon-saturated electrolyte. In contrast, in the oxygen-saturated electrolyte, a well-defined cathodic current was detected, and peaked at ≈+0.6 V. This indicated that NG10 was an active catalyst for O_2 reduction. The electrocatalytic activities of NG10 and the related materials rGO, NG1 and NG5 were further investigated using rotating disk electrodes (RDE). Figure 14b shows the linear sweep voltammograms of rGO, NG1, NG5 and NG10, all measured at a scan rate of 10 mV/s and rotation frequency of 1600 rpm in oxygen-saturated 0.1-M KOH(*aq*). To reveal the best performance in electrocatalysis, the effect of mass loading of the

active material on the glassy carbon electrode has been investigated (Figure 15). Different masses of NG10 (4, 8, 12, 16 and 20 µg) have been deposited on a glassy carbon electrode having an area of 0.197 cm^2. From the linear sweep voltammograms curves at 1600 rpm with the presence of oxygen, it was observed that the current density was increasing with the mass loading from 4 to 12 µg due to the increment of density of the active material (NG10). However, the current density was started to decrease even with the increasing mass loading from 16 to 20 µg. The possible reason for this behavior is due to the restacking of graphene layers after covering the whole surface area which hamper the permeation of electrolyte between the graphene layers causing less current density.[61] The electrochemical impedance spectroscopy (EIS) study (Figure 16) also showed the highest conductivity as well as very small inherent resistance from 4 to 12 µg mass loading and a formation of semi Nyquist plot for 20 µg mass loading indicated higher charge transfer resistance compared to the rest of the plots in higher frequencies. Moreover, all the spectra in low frequencies exhibit a Warburg angle higher than 45° indicating the electrodes were highly controlled by ion diffusion/transport process.

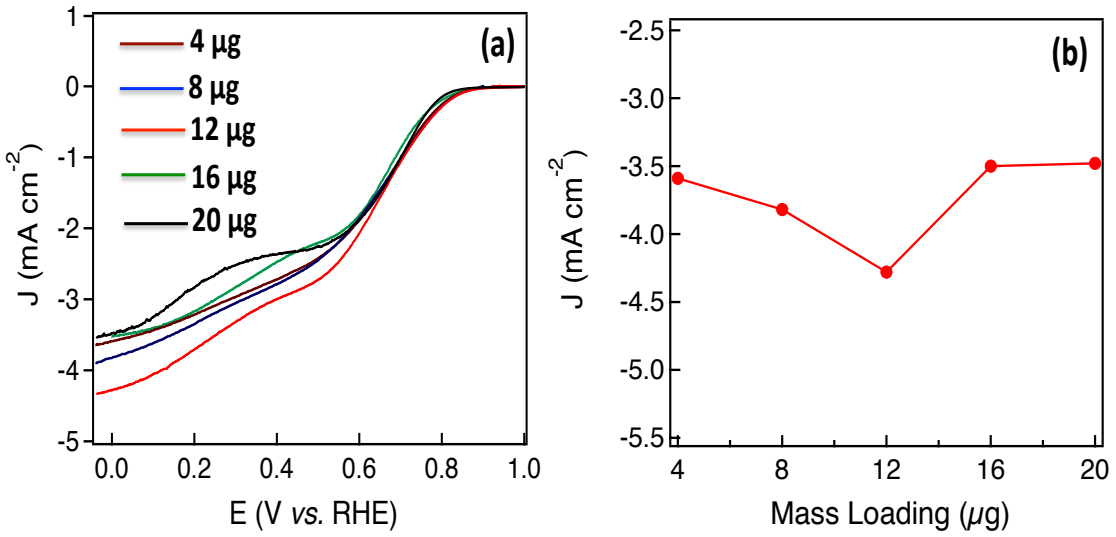

Figure 15. (a) LSV curves at 1600 rpm with the presence of oxygen for different mass loading of NG10 for ORR. (b) Comparison of current density with mass loading of active material.

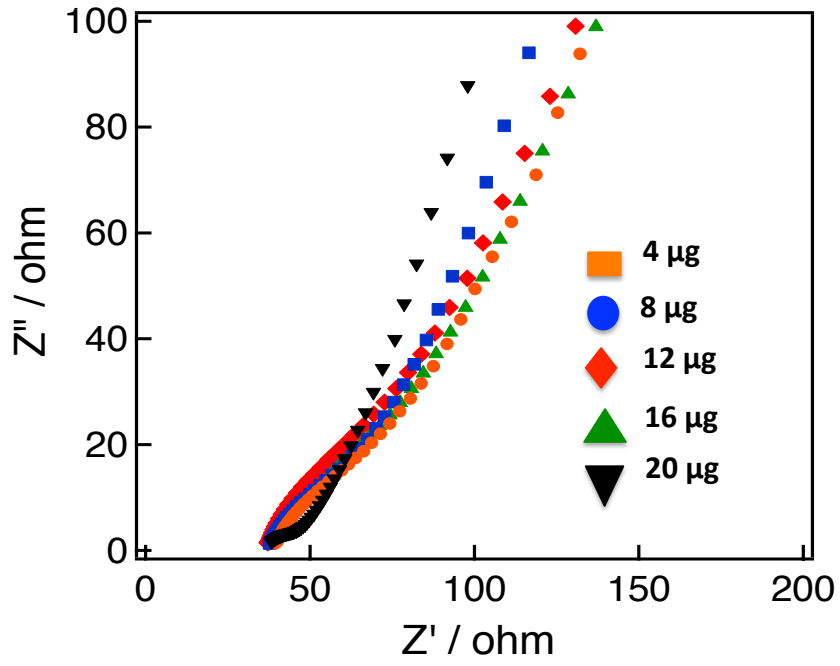

Figure 16. EIS curves for different mass loading of NG10.

The NG10 produced the most positive onset potential of +0.75 V and highest current density of –4.3 mA cm^{-2}, and further RDE measurements (Figure 14c) were thus used to calculate, via the Koutecky–Levich equation (Eq. 5),[28] the number of electrons transferred to an oxygen molecule by the NG10 electrode.

$$\frac{1}{J} = \frac{v^{1/6}}{0.2nFC_oD_o^{2/3}\omega^{1/2}} + \frac{1}{J_K} \quad \frac{1}{J} = \frac{\nu^{1/6}}{0.2nFC_oD_o^{2/3}\omega^{1/2}} + \frac{1}{J_K} \tag{5}$$

In the Koutecky–Levich equation, J, J_L, J_K are the measured current density, the diffusion-limiting current density and the kinetic-limiting current density, respectively; ω is the angular velocity of the disc, n is the overall number of electrons transferred in the oxygen reduction, F is the Faraday constant (96485 C mol^{-1}), C_o is the bulk concentration of oxygen (1.2×10^{-6} mol cm^{-3}), D_o is the diffusion coefficient of oxygen in 0.1-M KOH(aq) (1.9×10^{-5} cm^2 s^{-1}), v is the kinetic viscosity (0.01 cm^2/s) and 0.2 is a constant that is valid when the rotation speed is expressed in rpm. The Koutecky–Levich plot of J^{-1} *vs* $\omega^{-1/2}$ at a potential of 0.6 V on the NG10

electrode (Figure 14d) exhibited good linearity (R^2 = 0.998). The average electron transfer number was 3.82 at different potentials of 0.6, 0.5, 0.4 and 0.3 V, which indicated that a four-electron process, with water as the product, was the preferred pathway. In addition, efficient electrocatalytic activity was observed from the cyclic voltammetry in the presence of 3 M methanol (Figure 17), indicating the stability of NG10 to the fuel crossover effect.[54]

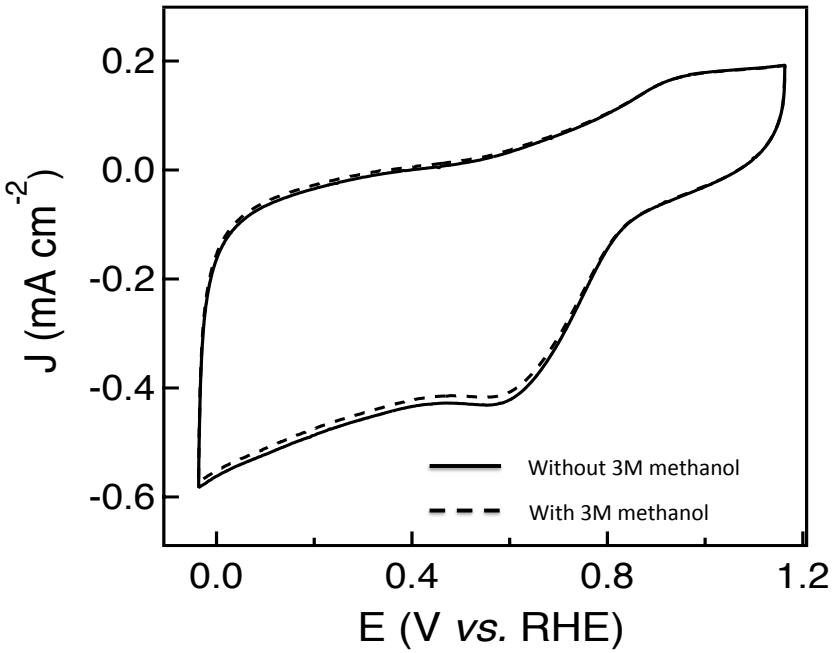

Figure 17. Cyclic voltammograms of NG10 at a scan rate of 50 mV s^{-1} in O_2-saturated 0.1-M KOH solution and O_2-saturated 0.1-M KOH solution containing 3 M methanol.

To further investigate the potential application of NG10 enriched with pyridinic N and graphitic N, OER activity was assessed by sweeping the RDE potential from 1.0 to 2.0 V. From the LSV curves of NG10, NG5, NG1, Ru/C and Pt/C plotted in Figure 18a, the onset potentials were measured 1.52, 1.56, 1.72, 1.46, and 1.68 V respectively. The onset potential is the potential when oxidative current start to increase from the background current in LSV. The rGO did not show any significant response towards OER activity. The potentials for a current density of 10 mA cm^{-2} for NG10, NG5, Ru/C and Pt/C were evaluated at 1.74, 1.76, 1.64 and 1.88 V respectively as the required potential to oxidize water at the current density of 10 mA cm^{-2} is used to judge the OER activity. Therefore, NG10 exhibited the lowest onset potential and large

current density among the studied catalysts of NG5 and Pt/C as well as close to Ru/C (one of the best electrocatalysts for OER at present). The effect of mass loading was also investigated for OER activity and the similar behavior was obtained showing 12 μg mass loading as the optimum amount for achieving the best electrocatalytic performance (Figure 19).

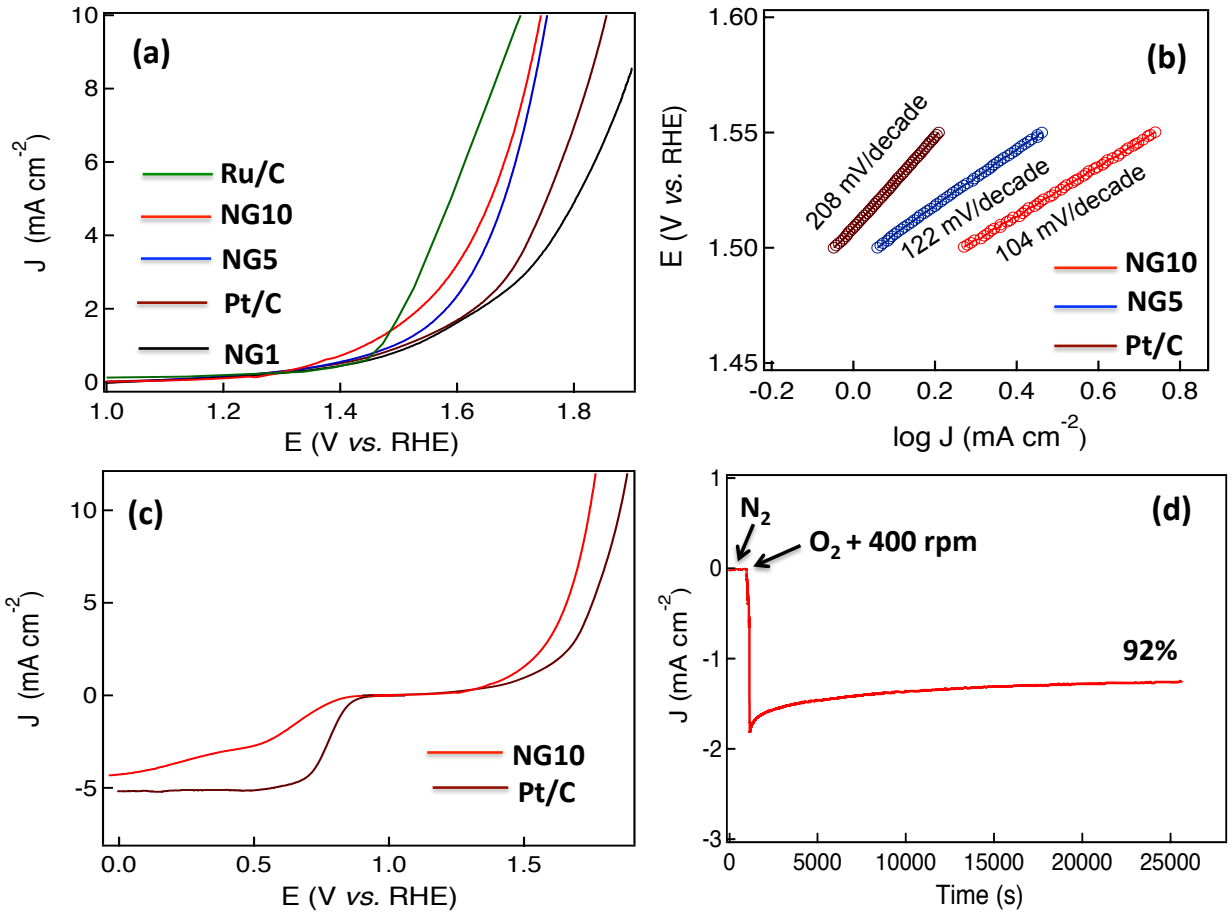

Figure 18. (a) Linear sweep voltammograms (LSV) of Ru/C, NG10, NG5, Pt/C and NG1 at a scan rate of 10 mV/s in 0.1-M KOH(*aq*); the inset in (a) shows the tafel plots for Pt/C, NG5 and NG10 and (b) LSV curves of NG10 and Pt/C on an RDE (1600 rpm) in O_2-saturated 0.1-M KOH(*aq*) at scan rates of 10 mV/s showing the electrocatalytic activities towards both ORR and OER.

The Tafel slope for the NG10 and NG5 were about 104 and 122 mV/decade respectively, much smaller than the Pt/C (208 mV/decade), which indicated the better OER activity of NG10 (Figure

18b). The OER performance of NG10 was found to be superior to the commercial Pt/C as well as similar to transition metal oxides supported by carbon materials.[45, 69. 60] Even though the exhibition of OER activities in metal-free nitrogen-doped few layers graphene is highly rare,[30, 47] the possible reason of the attribution of OER activity in NG10 even in two-dimensional nanostructure is due to the presence of high atomic percentages of N including high level of pyridinic N and graphitic N as well as the large surface area with high pore volume.

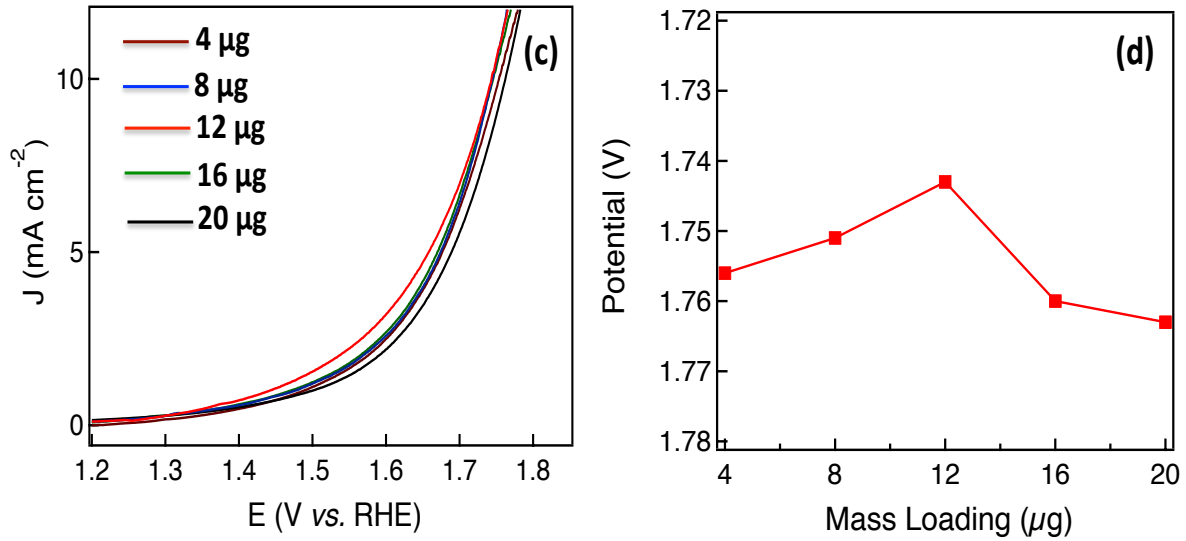

Figure 19. (a) LSV curves for different mass loading of NG10 for OER. (b) Comparison of Potentials at a current density of 10 mA cm^{-2} with the different mass loadings of active material.

The high percentage of pyridinic N and graphitic N on the edge of the surface creates the active sites for efficient bi-catalysis reaction towards oxygen reduction and evolution. The comparison of bifunctional electrocatalysis with Pt/C measuring by LSV plots at 1600 rpm in oxygen-saturated 0.1 M KOH, (Figure 18c) the comparable ORR with four electrons transfer pathway and better OER activity of NG10 were observed. In ORR the onset potential and current density of NG10 were lower than the commercial Pt/C as it is the state-of-the-art ORR electrode, however in OER the good catalytic activity of NG10 was reflected for its lower onset potential and higher current density than the Pt/C. Even though the OER activity of Ru/C is better than NG10; however, the ORR activity of Ru/C is poor compared to Pt/C and nitrogen-doped carbons,[48] thus not suitable as a bifunctional electrocatalyst. The electrocatalytical stability of NG10 was also investigated by continuous chronoamperometric measurement at a constant potential of +0.6 V (Figure 18d). The sharp increment of current density was observed after

adding oxygen to the solution as well as keeping the rotation speed at 400 rpm. A nearly constant current density curve after stabilization was observed for a long cycle time and even at 25000 s around 92% of its initial current density had been retained. Thus this active material can be a potential platform for developing bifunctional electrocatalyst for metal-air batteries and rechargeable fuel cells as well as further modification of structure and/or incorporation of nanomaterials can enhance the electrocatalytical activity superior than the commercial noble metal based catalysts.

3.4. CONCLUSIONS

In conclusion, we report a facile synthesis of N-doped graphenes with high surface areas as well as nitrogen atoms in all of the reported nitrogen configurations, using uric acid as a solid source of nitrogen. The synthesized material NG10, produced from the co-pyrolysis of graphene oxide and uric acid in a 1:10 mass ratio, showed excellent capacitive properties in acidic media and efficient catalytic activity for oxygen reduction and evolution reaction in an alkaline solution, and could therefore be applied as a promising material in devices for energy storage and conversion. The superb stability and efficient bifunctional electrocatalytic activity could make this material an ideal candidate not only in the field of supercapacitors, fuel cell and metal-air battery electrodes, but also in the area of sensors and transistors. The incorporation of nanoparticles, polymers and other carbon-based nanostructures could further enhance the electrochemical properties for a broader range of applications.

REFERENCES

1. Ramuz, M. P., Vosgueritchian, M., Wei, P., Wang, C., Gao, Y., Wu, Y. Chen, Y., Bao, Z. Evaluation of Solution-Processable Carbon-based Electrodes for all-Carbon Solar Cells. *ACS Nano* **2012,** *6,* 10384–10395.

2. Winter, M., Brodd, R. J. What are Batteries, Fuel Cells and Supercapacitors. *Chem. Rev.* **2004,** *104,* 4245–4269.

3. Liu, C., Li, F., Ma, L. –P. Cheng, H. -M. Advanced Materials for Energy Storage. *Adv. Mater.* **2010,** *22,* E28–E62.

4. Arico, A. S., Bruce, P., Scrosati, B., Tarascon, J. M., Schalkwijk, W. V. Nanostructured Materials for Advanced Energy Conversion and Storage Devices. *Nat. Mater.* **2005,** *4,* 366–377.

5. Simon, P., Gogotsi, Y. Materials for Electrochemical Capacitors. *Nat. Mater.* **2008,** *7,* 845–854.

6. Zhu, Y., Murali, S., Stoller, M. D., Ganesh, K. J., Cai, W., Ferreira, P. J., Pirkle, A., Wallace, R. M., Cychosz, K. A., Thommes, M., Su, D., Stach, E. A., Ruoff, R. S. Carbon-based Supercapacitors Produced by Activation of Graphene. *Science* **2011,** *332,* 1537-1541.

7. Shao, Y., Liu, J., Wang, Y. Lin, Y. Novel Catalyst Support Materials for PEM Fuel Cells: Current Status and Future Prospects. *J. Mater. Chem.* **2009,** *19,* 46–59.

8. Jaouen, F., Proietti, E., Lefèvre, M., Chenitz, R., Dodelet, J. –P., Wu, G., Chung, H. T., Johnston, C. M., Zelenay, P. Recent Advances in Non-Precious Metal Catalysis for Oxygen Reduction Reaction in Polymer Electrolyte Fuel Cells. *Energy Environ. Sci.* **2011,** ***4,*** 114–130.

9. Zheng, Y. Jiao, Y., Jaroniec, M., Jin, Y., Qiao, S. Z. Nanostructured Metal-Free Electrochemical Catalysts for Highly Efficient Oxygen Reduction. *Small* **2012,** *8,* 3550–3566.

10. Geim, A. K., K. S. K. S. The Rise of Graphene. *Nat. Mater.* **2007,** *6,* 183–191.

11. Choi, H. –J., Jung, S. -M. Seo, J. M., Chang, D. W., Dai, L., Baek, J. –B. Graphene for Energy Conversion and Storage in Fuel Cells and Supercapacitors. *Nano Energy* **2012,** *1,* 534–551.

12. Zhang, X., Wang, B., Sunarso, J., Liu, S., Zhi, L. Graphene Nanostructures toward Clean Energy Technology Applications. *WIREs Energy Environ.* **2012,** *1,* 317–336.

13. Sun, Y., Wu, Q., Shi, G. Graphene based New Energy Materials. *Energy Environ. Sci.* **2011**, *4,* 1113-1132.

14. Liu, H., Liu, Y., Zhu, D. Chemical Doping of Graphene. *J. Mater. Chem.* **2011**, *21,* 3335–3345.

15. Guo, B., Fang, L., Zhang, B., Gong, J. R. Graphene Doping: A Review. *Insci. J.* **2011**, *1,* 80–89.

16. Lv, R., Terrones, M. Towards New Graphene Materials: Doped Graphene Sheets and Nanoribbons. *Mater. Lett.* **2012**, *78,* 209–218.

17. Han, J., Zhang, L. L., Lee, S., Oh, J., Lee, K. –S., Potts, J. R., Ji, J., Zhao, X., Ruoff, R. S., Park, S. Generation of B-doped Graphene Nanoplatelets using a Solution Process and their Supercapacitor Applications. *ACS Nano* **2013,** *7,*19–26.

18. Wu, Z. –S., Winter, A., Chen, L., Sun, Y., Turchanin, A., Feng, X., Müllen, K. Three-dimensional Nitrogen and Boron Co-doped Graphene for High-Performance All-Solid-State Supercapacitors. *Adv. Mater.* **2012**, *24,* 5130–5135.

19. Yang, Z., Yao, Z., Li, G., Fang, G., Nie, H., Liu, Z., Zhou, X., Chen, X., Huang, S. Sulfur-doped Graphene as an Efficient Metal-free Cathode Catalyst for Oxygen Reduction. *ACS Nano* **2012,** 6, 205–211.

20. Sheng, Z. –H., Gao, H. –L., Bao, W. –J., Wang, F. –B., Xia, X. –H. Synthesis of Boron-doped Graphene for Oxygen Reduction Reaction in Fuel Cells. *J. Mater. Chem.* **2012**, *22,* 390–395.

21. Yang, S., Zhi, L., Tang, K., Fang, X., Maier, J., Müllen, K. Efficient Synthesis of Heteroatom (N or S) –doped Graphene based on Ultrathin Graphene Oxide-porous Silica Sheets for Oxygen Reduction Reactions. *Adv. Funct. Mater.* **2012**, *22,* 3634–3640.

22. Guo, H. –L., Su, P., Kang, X., Ning, S. –K., Synthesis and Characterization of Nitrogen-doped Graphene Hydrogels by Hydrothermal Route with Urea as Reducing-doping Agent. *J. Mater. Chem. A* **2013,** *1,* 2248-2255.

23. Qiu, Y., Zhang, X., Yang, S. High Performance Supercapacitors based on Highly Conductive Nitrogen-doped Graphene Sheets. *Phys. Chem. Chem. Phys.* **2011**, *13,* 12552-12558.

24. Sun, L. Wang, L., Tian, C., Tan, T., Xie, Y., Shi, K., Li, M., Fu, H. Nitrogen-doped Graphene with High Nitrogen Level via a One-step Hydrothermal Reaction of Graphene Oxide with Urea for Superior Capacitive Energy Storage. *RSC Adv.* **2012**, *2,* 4498–4506.

25. Wen, Z., Wang, X., Mao, S., Bo, Z., Kim, H., Cui, S., Lu, G., Feng, X., Chen, J. Crumpled Nitrogen-doped Graphene Nanosheets with Ultrahigh Pore Volume for High-performance Supercapacitor. *Adv. Mater.* **2012,** *24,* 5610–5616.

26. Haque, E.; Islam, M. M.; Pourazadi, E.; Hasan, M.; Faisal, S. N.; Roy, A. K.; Konstantinov, K.; Harris, A. T.; Minett, A. I.; Gomes, V. G. Nitrogen-doped Graphene via Thermal Treatment of Composite Solid Precursors as a High Performance Supercapacitor. *RSC Adv.* **2015,** *5,* 30679–30686.

27. Lai, L., Potts, J. R., Zhan, D., Wang, L., Poh, C. K., Tang, C., Gong, H., Shen, Z., Lin, J., Ruoff, R. S. Exploration of the Active Center Structure of Nitrogen-doped Graphene-based Catalysts for Oxygen Reduction Reaction. *Energy Environ. Sci.* **2012**, *5,* 7936–7942.

28. Qu, L., Liu, Y., Baek, J. –B., Dai, L. Nitrogen-doped Graphene as Efficient Metal-free Electrocatalyst for Oxygen Reduction in Fuel Cells. *ACS Nano* **2010**, *4,* 1321–1326.

29. Lin, Z.; Waller, G. H.; Liu, Y.; Liu, M.; Wong, C. –P. Simple Preparation of Nanoporous Few-layer Nitrogen-doped Graphene for use as an Efficient Electrocatalyst for Oxygen Reduction and Evolution Reactions. Carbon **2013,** *53,* 130–136.

30. Tian, G. –L.; Zhao, M. –Q.; Yu, D.; Kong, X. –Y.; Huang, J. –Q.; Zhang, Q. Wei, F. Nitrogen-Doped Graphene/Carbon nanotube Hybrids: In Situ formation of bifunctional Catalysts and Their Superior Electrocatalytic Activity for Oxygen Evolution/ Reduction Reaction. *Small* **2014,** *10,* 2251–2259.

31. Wang, H., Maiyalagan, T., Wang, X. Review on Recent Progress in Nitrogen-doped Graphene: Synthesis, Characterization and its Potential Applications. *ACS Catal*. **2012**, *2,* 781–794.

32. Shao, Y., Sui, J., Yin, G., Gao, Y. Nitrogen-doped Carbon Nanostructures and their Composites as Catalytic Materials for Proton Exchange Membrane Fuel Cell. *Appl. Catal. B* **2008,** *79,* 89–99.

33. Thorum, M. S. Hankett, J. M., Gewirth, A. A. Poisoning the Oxygen Reduction Reaction on Carbon-supported Fe and Cu Electrocatalysis: Evidence for Metal-centered Activity. *J. Phys. Chem. Lett*. **2011,** *2,* 295–298.

34. Jeong, H. M., Lee, J. W., Shin, W. H., Choi, Y. J., Shi, J. H., Kang, J. K., J. W. Choi, J. W. Nitrogen-doped Graphene for High Performance Ultracapacitors and the Importance of Nitrogen-doped Sites at Basal Planes. *Nano Lett*. **2011**, *11,* 2472-2477.

35. Zhang, L. L., Zhao, X., Ji, H., Stoller, M. D., Lai, L., Murali, S., Mcdonnell, S., Cleveger, B., Wallace, R. M., Ruoff, R. S. Nitrogen doping of Graphene and its Effect on Quantum Capacitance, and a New Insight on the Enhanced Capacitance of N-doped Carbon. *Energy Environ. Sci*. **2012**, *5,* 9618–9625.

36. Ikeda, T., Boero, M., Huang, S. –F., Terakura, K., Oshima, M., Ozaki, J. Carbon Alloy Catalysts: Active Sites for Oxygen Reduction Reaction. *J. Phys. Chem. C* **2008**, *112,* 14706–14709

37. Yang, S., Feng, X. Wang, X., Müllen, K. Graphene-based Carbon Nitride Nanosheets as Efficient Metal-free Electrocatalysts for Oxygen Reduction Reactions. *Angew. Chem. Int. Ed*. **2011**, *50,* 5339-5343.

38. Reddy, A. L. M., Srivastava, A., Gowda, S. R., Gullapalli, H., Dubey, M., Ajayan, P. M. Synthesis of Nitrogen-doped Graphene Films for Lithium Battery Application. *ACS Nano* **2010**, *4,* 6337-6342.

39. Biddinger, E. J.; Ozkan, U. S. Role of Graphitic Edge Plane Exposure in Carbon Nanostructures for Oxygen Reduction Reaction. *J Phys. Chem. C* **2010,** *114,* 15306–15314.

40. Xing, T.,; Zheng, Y.; Li. L. H.; Cowie, B. C. C.; Gunzelmann, D.; Qiao, S. Z.; Huang, S.; Chen, Y. Observation of Active Sites for Oxygen Reduction Reaction on Nitrogen-doped Multilayer Graphene. *ACS Nano* **2014,** *8,* 6856–6862.

41. Wu, J.; Ma, L.; Yadav, R. M.; Yang, Y.; Zhang, X.; Vajtai, R.; Lou, J.; Ajayan, P. M. Nitrogen-Doped Graphene with Pyridinic Dominance as a Highly Active and Stable Electrocatalyst for Oxygen Reduction, *ACS Appl. Mater. Interfaces* **2015,** *7,* 14763–14769.

42. Peng, Z.; Freunberger, S. A.; Chen, Y. ; Bruce, P. G. A Reversible and Higher-rate Li-O_2 Battery. *Science* **2012,** *337,* 563–566.

43. Park, M.; Sun, H.; Lee, H.; Lee, J. Cho, J. Lithium-Air Batteries: Survey on the Current Status and Perspectives towards Automotive Applications from a Battery Industry Standpoint. *Adv. Energy Mater.* **2012,** *2,* 780–800.

44. Kraytsberg, A.; Ein-Eli, Y. The Impact of Nano-Scaled Materials on Advanced Metal-Air Battery Systems. *Nano Energy* **2013,** *2,* 468–480.

45. Tian, G. -L.; Zhang, T. Q.; Zhang, B.; Jin, Y. -G.; Huang, J. -Q.; Su, D. S.; Wei, F. Toward Full Exposure of "Active Sites": Nanocarbon Electrocatalyst with Surface Enriched Nitrogen for Superior Oxygen Reduction and Evolution Reactivity. *Adv. Funct. Mater.* **2014,** *24,* 5956–5961.

46. Yadav, R. M.; Wu, J.; Kochandra, R.; Ma, L. Tiwari, C. S.; Ge, L.; Ye, G.; Vajtai, R.; Lou, J.; Ajayan, P. M. Carbon Nitrogen Nanotubes as Efficient Bifunctional Electrocatalysts for Oxygen reduction and Evolution Reactions. *ACS Appl. Mater. Interfaces* **2015,** *7,* 11991–2000.

47. Zhang, J.; Zhao, Z.; Xia, Z.; Dai, L. A Metal-free Bifunctional Electrocatalyst for Oxygen Reduction and Oxygen Evolution Reactions. *Nat. Nanotechnol.* **2015,** *10,* 444–452.

48. Li, R.; Wei, Z.; Gou, X. Nitrogen and Phosphorus Dual-doped Graphene/Carbon Nanosheets as bifunctional Electrocatalysts for Oxygen Reduction and Evolution. *ACS Catal.* **2015,** *5,* 4133–4142.

49. Jin, Z., Yao, J., Kittrell, C., Tour, J. M., Large-scale Growth and Characterizations of Nitrogen-doped Monolayer Graphene Sheets. *ACS Nano* **2011,** *5,* 4112–4117.

50. Geng, D., Chen, Y., Chen, Y., Li, Y., Li, R., Sun, X., Ye, S. Knights, S. High Oxygen-Reduction Activity and Durability of Nitrogen-doped Graphene. *Energy Environ. Sci.* **2011,** *4,* 760-764.

51. Sheng, Z. –H., Shao, L., Chen, J. –J., Bao, W. –J., Wang, F. –B., Xia, X. –H. Catalyst-free Synthesis of Nitrogen-doped Graphene via Thermal Annealing Graphite Oxide with Melamine and its Excellent Electrocatalysis. *ACS Nano* **2011**, *5,* 4350–4358.

52. Wang, H., Zhang, C., Liu, Z., Wang, L., Han, P., Xu, H., Dong, S., Yao, J., Cui, G. Nitrogen-doped Graphene Nanosheets with Excellent Lithium Storage Properties. *J. Mater. Chem.* **2011,** *21,*5430–5434.

53. Parvez, K., Yang, S., Hernandez, Y., Winter, A. Turchanin, A., Feng, X., Müllen, K. Nitrogen-doped Graphene and its Iron-based Composites as Efficient Electrocatalysis for Oxygen Reduction Reaction. *ACS Nano* **2012**, *6,* 9541–9550.

54. Lin, Z., Waller, G., Liu, Y., Liu, M., Wong, C. –P. Facile Synthesis of Nitrogen-doped Graphene via Pyrolysis of Graphene Oxide and Urea, and its Electrocatalytic Activity toward the Oxygen-Reduction Reaction. *Adv. Energy Mater.* **2012**, *2,* 884–888.

55. Lei, Z., Lu, L., Zhao, X. S. The Electrocapacitive Properties of Graphene Oxide reduced by Urea, *Energy Environ. Sci.* **2012,** *5,* 6391–6399.

56. Mou, Z., Chen, X., Du, Y., Wang, X., Yang, P., Wang, S. Forming Mechanism of Nitrogen doped Graphene Prepared by Thermal Solid-State Reaction of Graphite Oxide and Urea. *Appl. Surf. Sci.* **2011,** *258,* 1704–1710.

57. Presores, J. B., Swift, J. A. Adhesion Properties of Uric Acid Crystal Surfaces. *Langmuir*, **2012**, *28,* 7401–7406.

58. Jalili, R., Aboutalebi, S. H., Esrafilzadeh, D., Shepherd, R. L., Chen, J., Yamini, S. A., Konstantinov, K., Minett, A. I., Razal, J. M., Wallace, G. G. Scalable One-step Wet-spinning of Graphene Fibers and Yarns from Liquid Crystalline Dispersions of Graphene Oxide: Towards Multifunctional Textiles. *Adv. Funct. Mater.* **2013**, *23,* 5345–5355.

59. Romano, M. S., Li, N., Antiohos, D., Razal, J. M., Nattestad, A., Beirne, S., Fang, S., Chen, Y., Jalili, R., Wallace, G. G., Baughman, R., Chen, J. Carbon nanotube-reduced Graphene oxide Composites for Thermal Energy Harvesting Applications. *Adv. Mater.* **2013**, *25,* 6602–6606.

60. Antiohos, D., Romano, M. S., Razal, J. M., Beirne, S., Aitchison, P., Minett, A. I., Wallace, G. G., Chen, J. Performance Enhancement of Single-walled Nanotube-Microwave Exfoliated Graphene Oxide Composite Electrodes using a Stacked Electrode Configuration. *J. Mater. Chem. A* **2014,** *2,*14835–14843.

61. Jung, N., Kwon, S., Lee, D., Yoon, D., Park, Y. M., Benayad, A., Choi, J., Park, J. S. Synthesis of Chemically bonded Graphene/Carbon nanotube Composites and their Application in Large Volumetric Capacitance. *Adv. Mater.* **2013,** *25,* 6854–6859.

62. Wang, X., Maeda, K., Thomas, A., Takanabe, K., Xin, G., Carlsson, J. M., Domen, K., Antonietti, M. A Metal-Free Polymeric Photocatalyst for Hydrogen Production from Water under Visible Light. *Nat. Mater.* **2009,** *8,* 76–80.

63. Hernandez, Y., Nicolosi, V., Lotya, M., Blighe, F. M., Sun, Z., De, S., McGovern, I. T., Holland, B., Byrne, M., Gun'ko, Y. K., Boland, J. J., Niraj, P., Duesberg, G., Krishnamurthy, S., Goodhue, R., Hutchison, J., Scardaci, V., Ferrari, A. C., Coleman, J. N. High-Yield Production of Graphene by Liquid-Phase Exfoliation of Graphite. *Nat. Nanotechnol.* **2008,** *3,* 563–568.

64. Tuinstra, F., Koenig, J. L. Raman Spectrum of Graphite. *J. Chem. Phys.* **1970,** 53,1126–1130.

65. Powell, C. J. Recommended Augur parameters for 42 elemental solids. *J. Electron Spectrosc. Relat. Phenom.* **2012,** *185,* 1–3.

66. Zhao, Y., Liu, J., Hu, Y., Cheng, H., Hu, C., Jiang, C., Jiang, L., Cao, A., Qu, L. Highly Compression-Tolerant Supercapacitor based on Polypyrrole-Mediated Graphene Foam Electrodes. *Adv. Mater.* **2013**, 25, 591–596.

67. Xu, Y., Sheng, K., Li, C., Shi, G. Self-assembled Graphene Hydrogel via a One Step Hydrothermal Process. *ACS Nano* **2010**, *4,* 4324–4330.

68. Kady, M. F., Strong, V., Dubin, S., Kaner, R. B. Laser scribing of High-Performance and Flexible Graphene-based Electrochemical Capacitors. *Science* **2012**, *335,* 1326–1330.

69. Gorlin, Y.; Jaramillo, T. F. A Bifunctional Nonprecious Metal Catalyst for Oxygen Reduction and Water Oxidation. *J. Am. Chem. Soc.* **2010,** *132,* 13612–13614.

70. Wang, Y.; Ding, W.; Chen, S.; Nie, Y.; Xiong, K.; Wei, Z. Cobalt Carbonate Hydroxide/C: An Efficient Dual Electrocatalyst for Oxygen Reduction/Evolution Reactions. *Chem. Commun.* **2014,** *50,* 15529–15532.

71. You, B.; Wang, L.; Yao, L.; Yang, J. Three dimensional N-doped Graphene-CNT Networks for Supercapacitor. *Chem. Commun.* **2013,** *49,* 5016–5018.

72. Lu, Y.; Zhang, F.; Zhang, T.; Leng, K.; Zhang, L.; Yang, X.; Ma, Y.; Huang, Y.; Zhang, M.; Chen, Y. Synthesis and Supercapacitor Performance Studies of N-doped Graphene Materials using *o*-phenylenediamine as the Double-N Precursor. *Carbon* **2013,** *63,* 508–516.

73. Hulicova-Jurcakova, D.; Kodama, M.; Shiraishi, S.; Hatori, H.; Zhu, Z. H.; Lu, G. Q. Nitrogen-Enriched Nonporous Carbon Electrodes with Extraordinary Supercapacitance. *Adv. Funct. Mater.* **2009,** *19,* 1800–1809.

74. Lota, G.; Lota, K.; Frackowiak, E. Nanotubes based composites rich in nitrogen for supercapacitor application. *Electrochem. Commun.* **2007,** *9,* 1828–1832.

75. Chen, J. –F.; Zhang, X. –D.; Liang, H. –W.; Kong, M.; Guan, Q. –F.; Chen, P.; Wu, Z. –Y.; Yu, S. –H. Synthesis of Nitrogen-Doped Porous Carbon Nanofibers as an Efficient Electrode Material for Supercapacitors. *ACS Nano* **2012,** *6,* 7092–7102.

76. Ferrero, G. A.; Fuertes, A. B.; Seyilla, M. N-doped Porous Carbon Capsules with Tunable Porosity for High-Performance Supercapacitors. *J. Mater. Chem. A* **2015,** *3,* 2914–2923.

77. Wang, J.; Shen, L.; Nie, P.; Yun, X.; Xu, Y.; Dou, H.; Zhang, X. N-doped Carbon Foam based Three-dimensional Electrode Architectures and Asymmetric Supercapacitors. *J Mater. Chem. A* **2015,** *3,* 2853–2860.

78. Chen, Q.; Zhao, Y.; Huang, X.; Chen, N.; Qu, L. Three-dimensional Graphitic Carbon Nitride Functionalized Graphene-based High-Performance Supercapacitors. *J. Mater Chem A* **2015,** *3,* 6761–6766.

79. Zou, Y.; Kinloch, I. A.; Dryfe, R. A. W. Nitrogen-Doped and Crumpled Graphene Sheets with Improved Supercapacitance. *J. Mater. Chem. A* **2014,** *2,* 19495-19499.

*THIS CHAPTER IS A PART OF A PATENT APPLICATION AND PUBLISHED AS A FULL PAPER IN THE FOLLOWING JOURNAL;

1. 1. Electrocatalysis and Electrochemical cell. M. Arab, A. I. Minett, T. L. Church, L. Xiaobo, T. Maschmeyer, N. Noorbehesht, A. T. Harris, **S. N. Faisal**, A. Hussain, Patent Number- WO/2016/141414, Patent Application number-PCT/AU2016/000081.

2. Pyridinic and Graphitic Nitrogen-rich Graphene for High-Performance Supercapacitors and Metal-Free Bifunctional Electrocatalysts for ORR and OER**. S. N. Faisal***, E. Haque, N. Noorbehesht, W. Zhang, A. T. Harris, T. L. Church and A. I. Minett*, *RSC Advances* 2017, 7(29), 17950-17958.

Chapter 4:
Nickel Embedded N-Doped Graphene as Quadrafunctional Electrocatalyst for ORR, OER, HER and HPOR

4. Nickel Embedded N-Doped Graphene as Quadrafunctional Electrocatalyst for ORR, OER, HER and HPOR

ABSTRACT: The synthesized nitrogen-doped graphene shows efficient energy storage and electrocatalytical activity. To further improve the electrocatalytical activity to compete the noble-metal electrocatalysts, a single pot synthesis of nitrogen-doped graphene/ nickel nanoparticle hybrid is reported. The method yielded N-doped graphene nanosheets with high atomic percentage of nitrogen (8.1 at%) and embedded with highly distributed nickel nanoparticles inside the graphene layers, The resultant composite demonstrates excellent electrocatalytic activities utilizing the superior electrocatalytical properties of nickel nanoparticle with nitrogen-doped graphene. The hybrid exhibits efficient oxygen reduction reaction (ORR) properties comparable with state of the art electrode Pt/C with four-electron transfer pathway and superior oxygen evolution reaction (OER) compare to the state of the art electrode for OER, Ru/C. Alternatively, this composite acts as an excellent electrode material for hydrogen evolution reaction (HER) both in the acidic and alkaline media. Nevertheless, this composite demonstrates hydrogen peroxide oxidation reaction (HPOR), which is crucial for developing rechargeable fuel cell and fuel cell with liquid oxidant.

4.1. INTRODUCTION

The development of sustainable energy storage and conversion devices for the next generation electronics are highly crucial due to the rapid growth of technology. [1-3] The metal-air batteries, rechargeable fuel cells, flexible supercapacitors and hybrid energy storage devices can be the strong candidates to meet the future global energy demand, however the performance and commercialization of these devices are limited due to the highly expensive electrode materials like platinum and ruthenium oxide. [2] These materials are not only scarce and expensive but also easy to get poisoning and do not possess the similar performance for both the oxygen reduction and oxygen evaluation reactions. [2,4,5] The demand of alternative multifunctional nonprecious electrode materials with multiple electrocatalysis properties is highly essential to overcome these limitations. [5,6] Chemically doped carbon nanostructured materials have been

demonstrated remarkable electrocatalytical properties as a promising alternate to noble metals. [2, 7-9, 10] Among the different types of chemically doped carbon, the two-dimensional carbon material, in particular chemically doped graphene has gained a wide attention due to its extraordinary electrochemical properties by introducing an active site for electrocatalysis. [9] Different heteroatoms (N, B, P, S) have been utilized for doping in the carbon lattice and among them nitrogen doped carbon and graphene showed superior performance both for the ORR and OER. [7, 9, 11] The further modification of nitrogen-doped graphene by dual doping or incorporating non-precious metal nanoparticles can enhance the performance of the ORR and OER comparable to the noble metal electrodes. [12-15] Among the dual doping, N and P has gained a lot of interest recently for their enhance bifunctional metal-free electrocatalytical activity by increasing active sites with surface area.[14, 15] However, the restacking nature of graphene can reduce the active electrochemical surface area and thus hinder the properties for practical applications. [16] The decoration of nonprecious metal catalyst in the graphene layers can provide a three-dimensional structure with high electroactive surface area as well as synergistic electrocatalysis activity with the conjugation of metal catalyst. [12, 13, 17] Transition metal nanoparticles, in particular, nickel and cobalt have demonstrates efficient electrocatalytical activity towards ORR, OER and HER, however pure cobalt, nickel and nickel oxides generally show insufficient electrical conductivity and limited kinetics for electrocatalysis of ORR, OER and HER. [6, 17-19] The combination of N-Gr with transition metal nanoparticle can be an effective way to improve the active electrochemical properties and the atomic percentage of doping of the metal on the graphene lattice can play the role of single atom catalysis. [17, 20-22] Even though, the hybrid of cobalt nanoparticle with nitrogen-doped graphene has demonstrated superior ORR and HER, [20, 21] the combination of nickel nanoparticle with nitrogen doped graphene can improve the electrocatalytical activity of composite for OER, HER and hydrogen oxidation reaction (HOR) due to the high affinity towards hydrogen adsorption of nickel and active side for OER. [23-27] The nickel confined N-Gr has shown superior OER properties, however the synthesis procedures require several steps and ORR property was not mentioned. [27] Alternatively, the hybrid of Ni/NiO with N-Gr demonstrates efficient OER and HER, however the ORR of the composite was poor. [20]

Herein we are reporting a single-step synthesis of nickel nanoparticle incorporated nitrogen doped graphene with multifunctional electrocatalytic properties via thermal annealing. The

synthesis procedures is performed by thermal annealing of the mixture of graphene oxide, nickel nitrate and uric acid as a solid precursor of nitrogen at 800 °C under an argon atmosphere. Uric acid has a high nitrogen content (~33 wt%), and its crystals can adhere to surfaces bearing various organic functionalities, and via multiple types of forces (electrostatic interactions, hydrogen bonding and/or van der Waals interactions), without the aid of surfactants.[28] These properties allowed the co-pyrolysis of graphene oxide and uric acid with reducing the nickel nitrate to nickel nanoparticles to produce a nickel embedded nitrogen-doped reduced graphene oxide (Ni/NGr) nanocomposite with nitrogen atoms in all of the possible configurations in the graphitic lattice, a high total nitrogen content, and a high surface area with three dimensional structure for insertion of nickel nanoparticles all over the graphene lattice at different dimensions. As a result, the N-doped graphene/ nickel nanocomposite had high electrocatalytic active sites due to the synergistic effects as well as three-dimensional structure for remarkable electrocatalytical activity for ORR, OER, HER and HPOR.

4.2. EXPERIMENTAL SECTION

Synthesis of Ni/N-doped graphene

GO was prepared from naturally expanded graphite (Ashbury Carbons, Grade-3772) using a reported procedure for the generation of ultra-large GO sheets.[28] The GO sheets (approx. 20 mg) were dispersed in water by ultrasonication for 30 min at a frequency of 50 Hz, then mixed with uric acid and nickel nitrate in a ratio of 1:5:0.2 by mass. The mixtures were then stirred continuously and heated at 80 °C for 10–12 h to remove the water. The resulting solids were transferred to a tubular furnace and heated in an argon atmosphere at 5 °C min^{-1} to 800 °C, then annealed for 1 h. The synthesized nitrogen-doped graphenes with nickel nanoparticle was named Ni/NGr. GO mixed with uric acid at a same ratio (1:5) without nickel nitrate was also thermally annealed to yield nitrogen-doped graphene named NGr under the same conditions, and used as reference. [28]

Characterization

The microstructures and morphology of the synthesized samples were investigated by Field Emission Scanning Electron Microscopy (FESEM, Zeiss ULTRA *plus*) and High Resolution

Transmission Electron Microscopy (HRTEM, JEOL 2200FS) with an acceleration voltage of 200 kV. X-ray Diffractometry (XRD) was performed on a Shimadzu S6000 equipped with Cu Kα radiation (λ = 0.154 nm) with a resolution of 0.02°. Raman spectra were collected with Renishaw inVia Raman Spectrometer with laser wavelength of 514 nm. X-ray photoelectron specstroscopy (XPS) analyses were performed by ESCALAB250Xi (Thermo Scientific, UK) with a monochromated Al Kα (energy 1486.68 eV) operating at 150 W (13 kV × 12 mA) under a vacuum of 2×10^{-9} mbar. The analysis spot was 500 μm in diameter. The binding energies were referenced to the adventitious hydrocarbon C 1*s* signal at 284.9 eV.

Electrochemical measurement:

For electrochemical characterization and measurement, the Ni/NGr and NGr were deposited from a 1-mg/mL mixture, prepared by sonicating in degassed isopropanol, on a glassy-carbon electrode. The glassy-carbon working electrode was polished mechanically with a slurry of 0.05-μm alumina particles to obtain a mirror-like surface, washed with Milli-Q water and acetone, and allowed to dry. It was then tested in a three-electrode cell, using platinum wire as the counter electrode and a Ag/AgCl, KCl (3 M) electrode as the reference electrode. Measurements were taken using a Bio-logic SP300 potentiostat. The binding agents was 0.5 wt% Nafion for electrocatalytic measurements.

The electrocatalytic properties were evaluated by rotating disk electrode (RDE) experiments in an O_2-saturated 0.1-M KOH solution. First, the oxygen-reduction capability was assessed by comparing cyclic voltammetric curves measured in argon- and oxygen-saturated electrolytes. Linear sweep voltammetry curves were recorded over the potential range of 0.0 to –0.8 V at a scan rate of 10 mV s^{-1} at ambient temperature and at rotation speeds of 100–2000 rpm. OER activity was measured by linear sweep voltammetry in the potential window ranging from 1.0 to 1.8 V versus reversible hydrogen electrode (RHE) scale by adding a value of 0.964 V. The HER activity was carried out in 0.1 M KOH and 0.1 M H_2SO_4 solution and the HPOR property was evaluated in 0.1 M NaOH electrolyte. The commercial Pt/C (20 wt %) into nafion solution with same loading amount was taken for comparison.

4.3. RESULTS AND DISCUSSION

In the single pot synthesis of nickel nanoparticles embedded in nitrogen-doped graphene (Scheme 1), graphene oxide, uric acid and Nickel nitrate were mixed together in water (in ratio of 1:5:0.2 by mass in mg scale for NG1 and NG10, respectively), then stirred continuously at 80 °C to remove the water. The nickel nitrate salt and uric acid dispersed and adsorbed on the graphene oxide surface during the mixing. The semi-solid mixture was then heated in a tubular furnace at a rate of 5 °C min^{-1} to 800 °C in an argon environment. Uric acid has been reported as a solid nitrogen precursor which can be doped in graphene lattice with high atomic percentage of N in all the possible configuration. [28] The nickel salt reduced at high temperature to form nickel nanoparticles on the graphene surface and hence forming a three dimensional structure by intercalated in the graphene layers and performs as bifunctional electrocatalyst.

The morphology, structure and graphitic layers of the obtained Ni/NGr were characterized by scanning electron microscopy (SEM) and transmission electron microscopy (TEM). The SEM images of Ni/NG showed laminar morphology of graphene and the nanoparticles of nickel of approximately 50 nm are easily visible situated on the edge as well as inside the graphene layers (Figure 1a). The low-resolution TEM image showed highly distributed nickel nanoparticles embedded in the transparent stacked graphene sheets from a range of 5 to 50 nm (Figure 1b). To investigate the proper distribution of nickel nanoparticle on the graphene sheet, high-angle annular dark field (HAADF) STEM was applied. The bright-field STEM image shows the distribution of nickel nanoparticles on the graphene sheet from 5 – 50 nm ranges and the small particles are embedded into the graphene layers (Figure 1c). The corresponding HAADF image (Figure 1d) clearly shows the bright spots of nanoparticles well dispersed in the carbon matrix. The high-resolution transmission electron micrograph (HRTEM) combined with STEM-EDS clearly verifies the formation of nanoparticles onto graphene sheets (Figure 1e). The lattice fringes with widths of 2.12 and 2.05 Å are assigned to (200) and (111) crystal planes of fcc structures of pure Ni, respectively. The selected area electron diffraction (SAED) pattern revealed the highly crystalline nature of the composite (Figure 1f). The well-defined diffraction

spots and rings in the SAED pattern confirmed that the sample was comprised of the hexagonal carbon lattice typical of graphene-like materials and the comparatively bigger spot of nickel were clearly identified adjacent to the hexagonal carbon lattice. The STEM-EDS mapping provided further confirmation and elemental distribution of Ni/NGr (Figure 2). The distribution of carbon, nitrogen and nickel (Figure 2b, 2c and 2d) demonstrated the dominant metallic Ni with nitrogen on the carbon. Based on the STEM images, the regular distribution of embedded nickel nanoparticle on nitrogen-doped graphene layers was clearly visible.

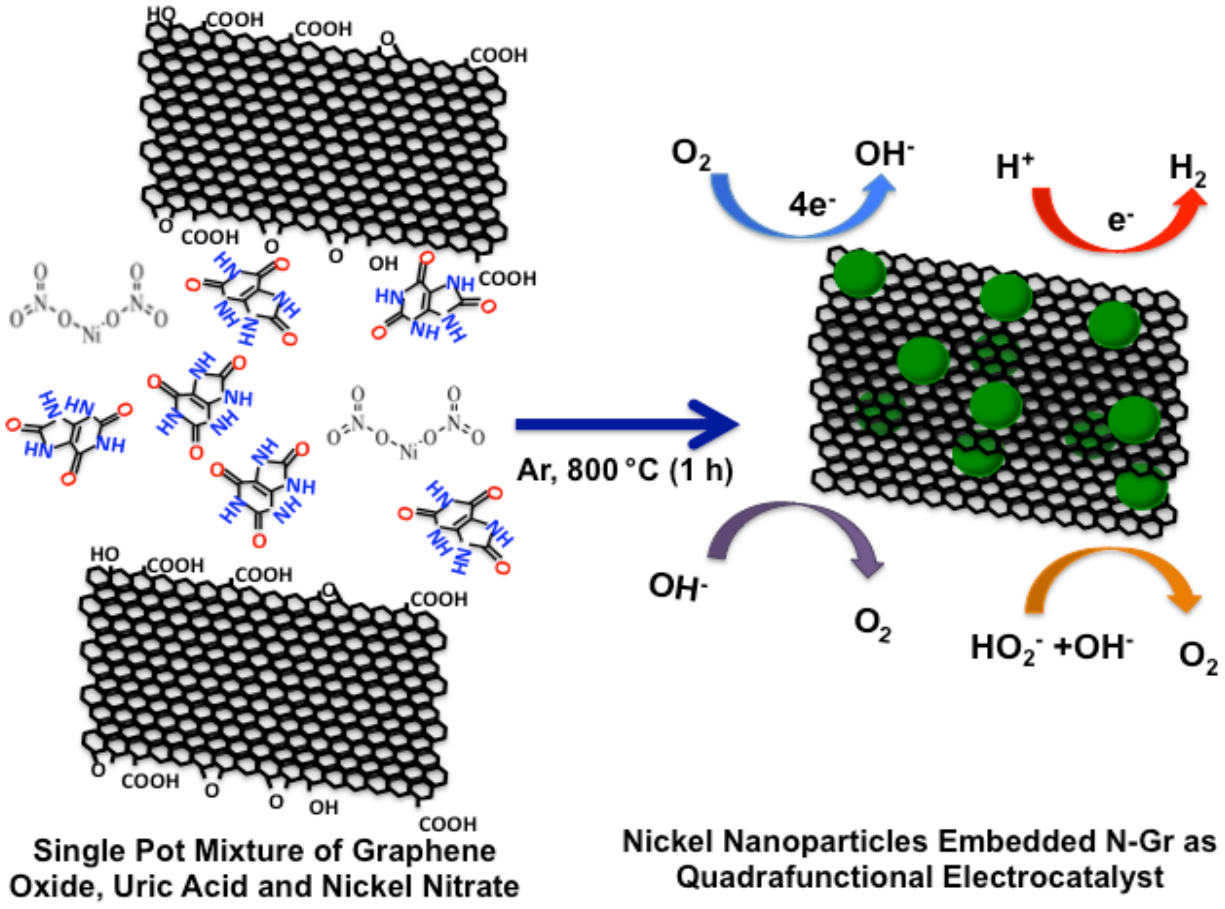

Scheme 1. Schematic diagram of the formation of Ni/NGr via the thermal annealing of graphene oxide with uric acid and nickel nitrate.

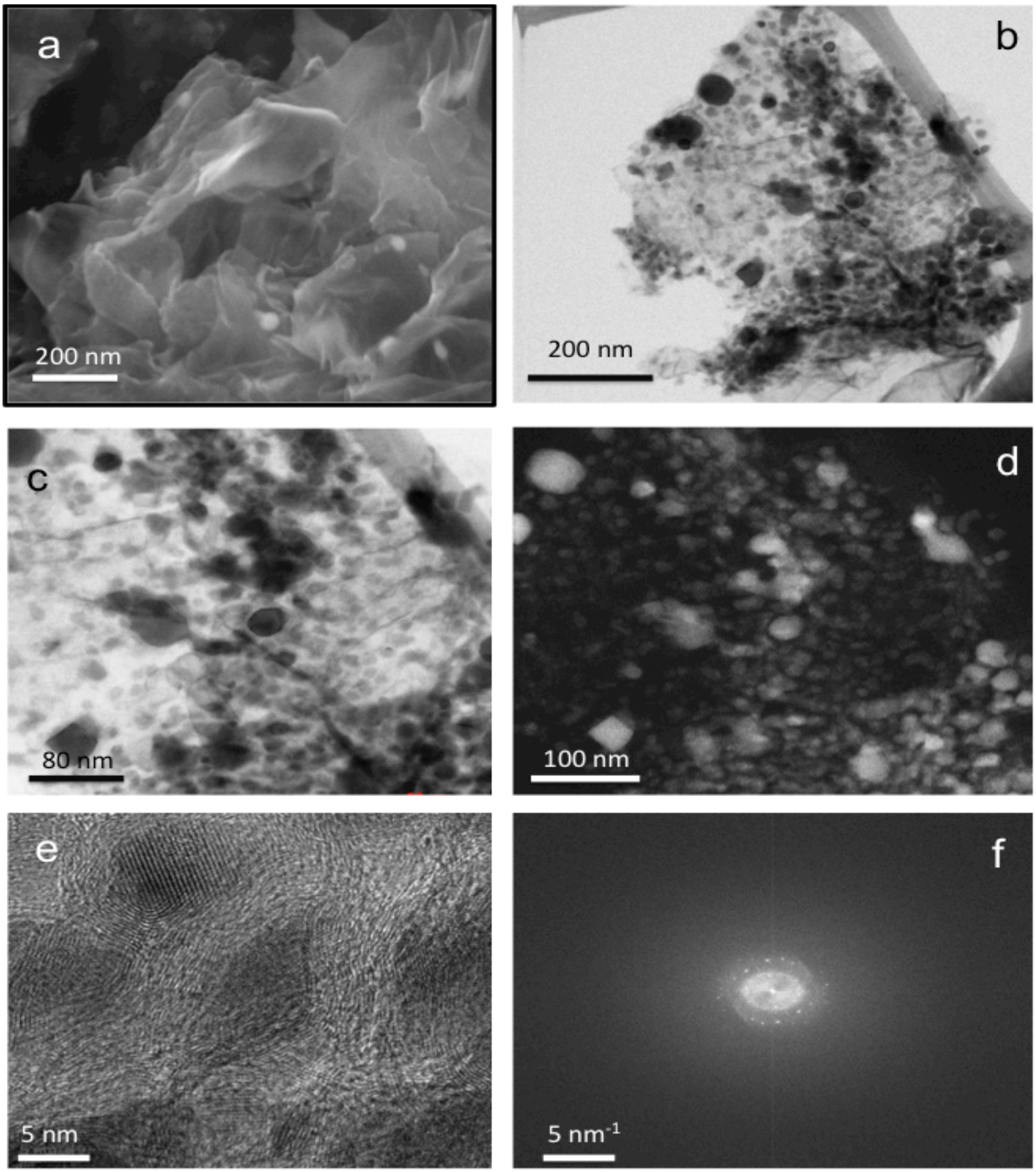

Figure 1. (a) SEM image of Ni/NGr, (b) TEM image of Ni/NGr, (c) Bright field STEM image of Ni/NG, (d) HAADF-STEM image showing highly distributed nickel nanoparticles on graphene, (e) HRTEM image showing lattices of embedded nickel into graphene lattice and (f) selected area electron diffraction (SAED) pattern (inset) of Ni/NGr showing adjacent nickel atoms with hexagonal graphene pattern.

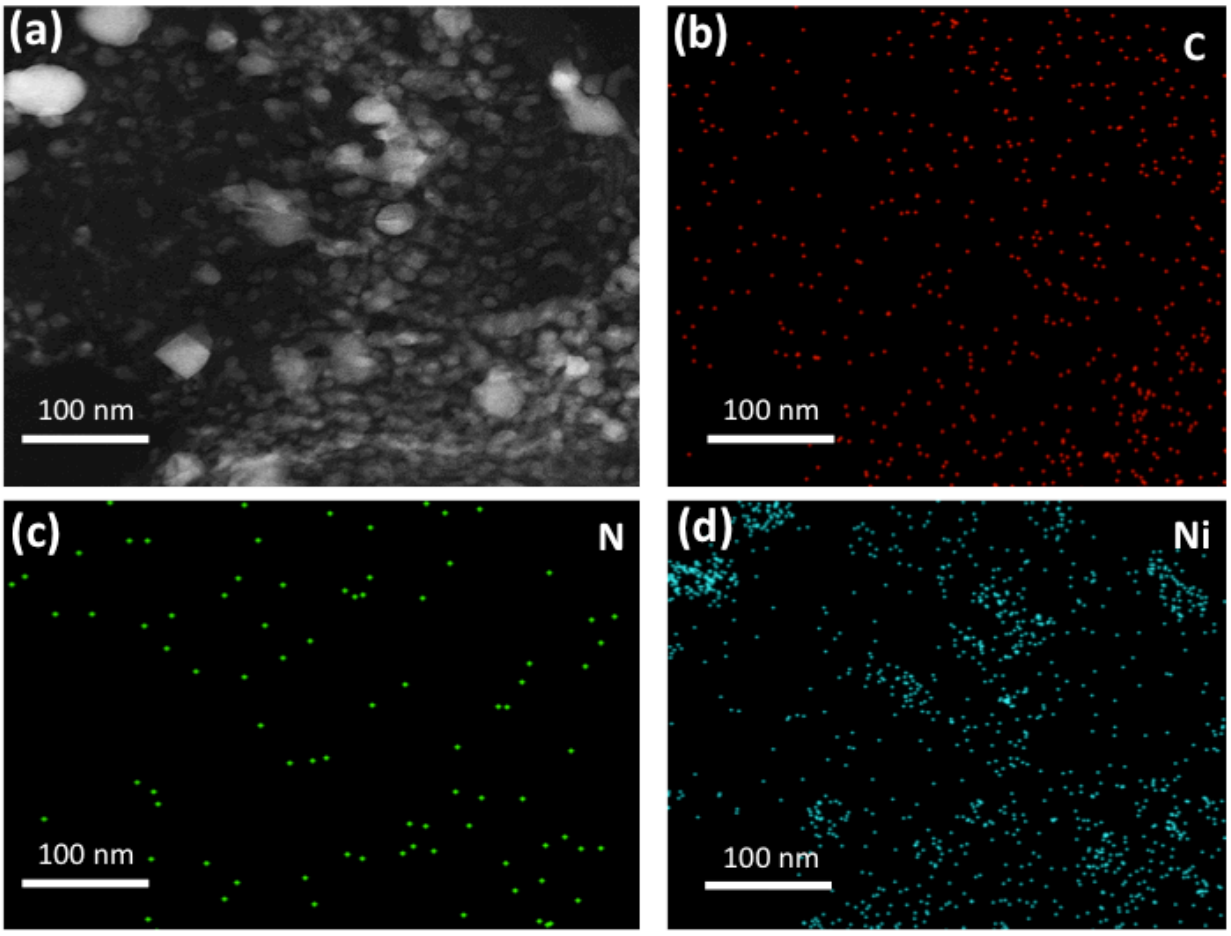

Figure 2. (a) Enlarge selected area for STEM-EDS Mapping, (b) STEM-EDS mapping of C, (c) STEM-EDS mapping of N, (d) STEM-EDS mapping of Ni.

The XRD patterns of Ni/NGr and NGr (Figure 3a) indicated the slight shifting of graphene peak corresponded to Ni/NGr around 25.0° from the graphene peak of NGr at 26.0°, which corresponded to an interlayer spacing of 0.362 nm larger than the usual interlayer spacing of NGr (0.322 nm) calculated at 26.0° probably due to the insertion of nickel nanoparticles inside the graphene layers. The peak of Ni/NGr at 38.4, 44.5 and 51.8° belong to fcc NiO (110), fcc Ni (111) and fcc Ni (200) respectively, which were absent for NGr. The presence of NiO nanoparticles in lesser extent with Ni nanoparticles in the composite was confirmed from the XRD pattern. The Ni/NGr and NGr were further characterized by Raman spectroscopy at an excitation wavelength of 514 nm under ambient conditions. As shown in Figure 4 the G peaks of

the Ni/NGr and NGr occurred between 1582 and 1598 cm^{-1} indicating the defect formed due to the nitrogen doping as well as thermal treatment.

To characterize the elemental composition and nitrogen content in the Ni/NGr and NGr, X-ray photoelectron spectra (XPS) of the materials were measured. A comparison of the spectra of Ni/NGr and NGr showed a increase in nitrogen content in Ni/NGr due to contribution of nitrogen in the nickel salt and an obvious Ni2p peaks for nickel (Figure 3b). The deconvolutions of the N 1*s* peaks (Figures 3c) showed the presence of five nitrogen configurations. Both N/NGr and NGr contained primarily (>40%) pyridinic nitrogen, ~15% pyrrolic N, 35% graphitic N and minor amounts (<10%) of N-oxides and pyridinic N-H. The total nitrogen contain in Ni/NGr was 8.1 at.% and in NGr was 7.6 at.%. The efficient doping of nickel (0.56 at.%) was also observed which might contribute to enhance electrocatalytical properties. (Figure 3d)

The electrocatalytical activity of Ni/NGr is evaluated as an electrocatalyst for the oxygen-reduction reaction (ORR) first under alkaline conditions. The electrocatalytic activities are investigated using rotating disk electrodes (RDE). Figure 4a shows the linear sweep voltammograms of Ni/NGr in different rotation frequency, all measured at a scan rate of 10 mV s^{-1} in oxygen- saturated 0.1-M KOH(*aq*). Ni/NGr produced the positive onset potential of +0.82 V and highest current density of −5.0 mA cm^{-2} at a rotation frequency of 2000 rpm. Further RDE measurements (Figure 6b) were thus used to calculate, via the Koutecky–Levich equation (Eq. 1), [20] the number of electrons transferred to an oxygen molecule by the Ni/NGr electrode.

$$\frac{1}{J} = \frac{v^{1/6}}{0.2nFC_oD_o^{2/3}\omega^{1/2}} + \frac{1}{J_K} \qquad (1)$$

In the Koutecky–Levich equation, J, J_L, J_K are the measured current density, the diffusion-limiting current density and the kinetic-limiting current density, respectively; ω is the angular velocity of the disc, n is the overall number of electrons transferred in the oxygen reduction, F is the Faraday constant (96485 C mol^{-1}), C_o is the bulk concentration of oxygen (1.2×10^{-6} mol cm^{-3}), D_o is the diffusion coefficient of oxygen in 0.1-M KOH(*aq*) (1.9×10^{-5} cm^2 s^{-1}), v is the kinetic viscosity (0.01 $cm^2 s^{-1}$) and 0.2 is a constant that is valid when the rotation speed is expressed in rpm.

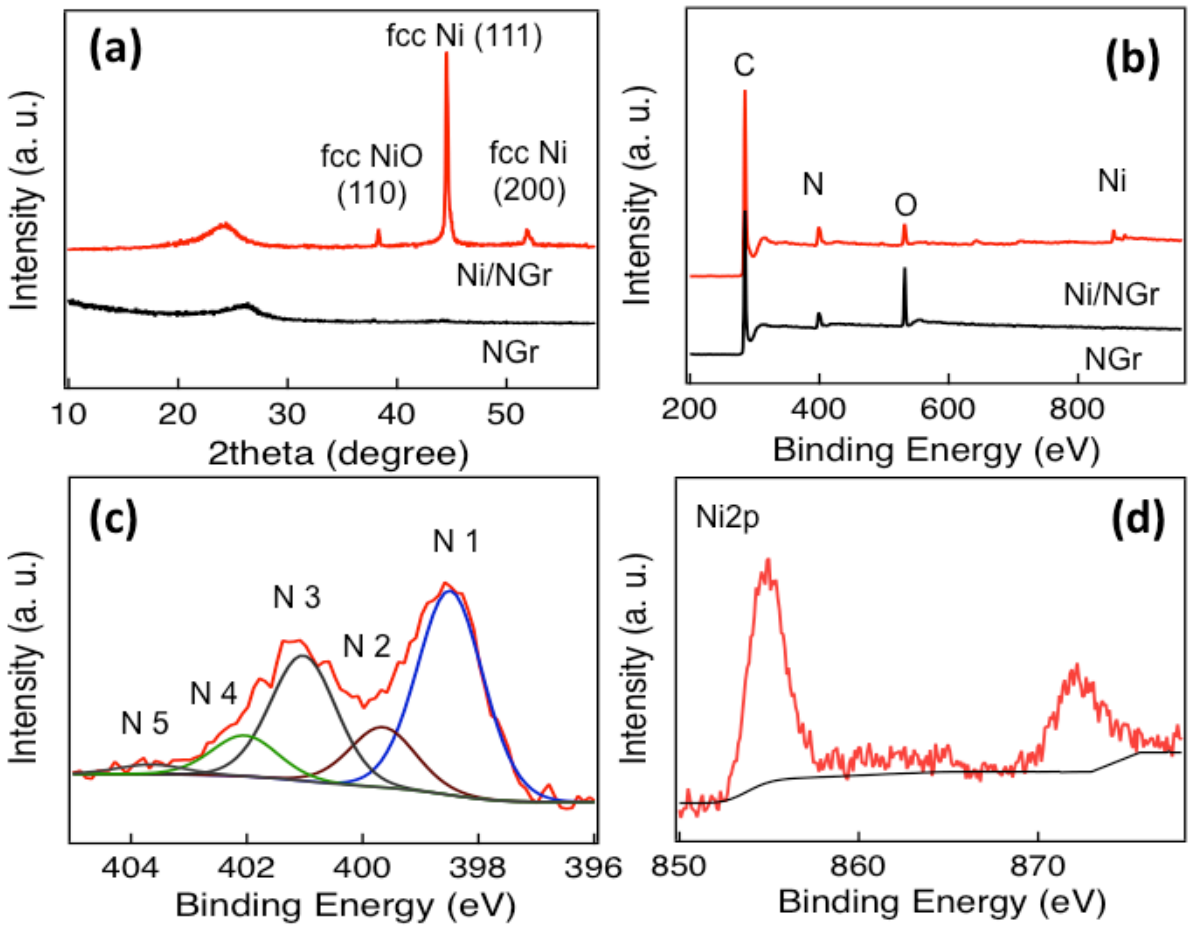

Figure 3. (a) XRD patterns of Ni/NGr and NGr, (b) XPS survey of Ni/NGr and NGr, (c) N 1s XPS peak of Ni/NGr (d) Ni2p XPS peaks of Ni/NGr.

The Koutecky–Levich plot of J^{-1} *vs* $\omega^{-1/2}$ at a potential of +0.3, +0.4 and +0.5 V on the Ni/NGr electrode (Figure 4b) exhibited good linearity (R^2 = 0.998). The electron transfer number was 3.7-3.9 at potential of 0.3 to 0.5 V, which indicated that a four-electron process, with OH^- as the product, was the preferred pathway. The comparison of LSV curves of Ni/NGr with NGr and PT/C (Figure 4c) shows the enhanced onset potential and current density of Ni/NGr compared to NGr due to the interaction of graphene with nickel nanoparticles, which plays role to form a three-dimensional structure, and thus increase the current density, even though nickel nanoparticles have poor ORR activity.[20] The onset potential and current density of Ni/NGr is slightly lower than the Pt/C, state of the art electrode for ORR, which is obvious. In addition, The electrocatalytical stability of Ni/NGr was also investigated by continuous

chronoamperometric measurement at a constant potential of +0.6 V (Figure 4d). The sharp increment of current density was observed after adding oxygen to the solution as well as keeping the rotation speed at 200 rpm. A nearly constant current density curve after stabilization was observed for a long cycle time and even at 25000 s around 91% of its initial current density had been retained.

Based on the efficient electrocatalytical OER activity of nickel nanoparticle [26] and nitrogen-doped graphene [11, 28], the OER properties of the hybrid electrode material of Ni/NGr is investigated by sweeping the RDE potential from 1.0 to 2.0 V. From the LSV curves of Ni/NGr, Ru/C, NGr and Pt/C plotted in Figure 5a, the onset potentials were measured 1.48, 1.46, 1.56, and 1.68 V respectively. The potentials for a current density of 10 mA cm^{-2} for Ni/NGr, Ru/C, NGr and Pt/C were evaluated at 1.62, 1.64, 1.76 and 1.88 V respectively as the required potential to oxidize water at the current density of 10 mA cm^{-2} is used to judge the OER acitivity. Therefore, Ni/NGr exhibited almost similar onset potential and lower potential to oxidize water at the current density of 10 mA cm^{-2} compare to Ru/C (one of the best electrocatalysts for OER at present) and superior to Pt/C. The Tafel slope for the Ni/NGr, Ru/C and Pt/C were about 98, 109 and 238 mV/decade respectively indicating the better OER activity of Ni/NGr (Figure 7b). The highly distribution of nickel nanoparticles along with high atomic percentage of nitrogen including high percentage of pyridinic N and graphitic N on the edge of the surface creates the active sites for efficient bi-catalysis reaction towards oxygen reduction and evolution. The comparison of bifunctional electrocatalysis with Pt/C measuring by LSV plots at 1600 rpm in oxygen-saturated 0.1 M KOH, (Figure 5c) the comparable ORR with four electrons transfer pathway and better OER activity of Ni/NGr were observed. In ORR the onset potential and current density of Ni/NGr were lower than the commercial Pt/C as it is the state-of-the-art ORR electrode, however in OER the good catalytic activity of Ni/NGr was reflected for its lower onset potential and higher current density than the Pt/C.

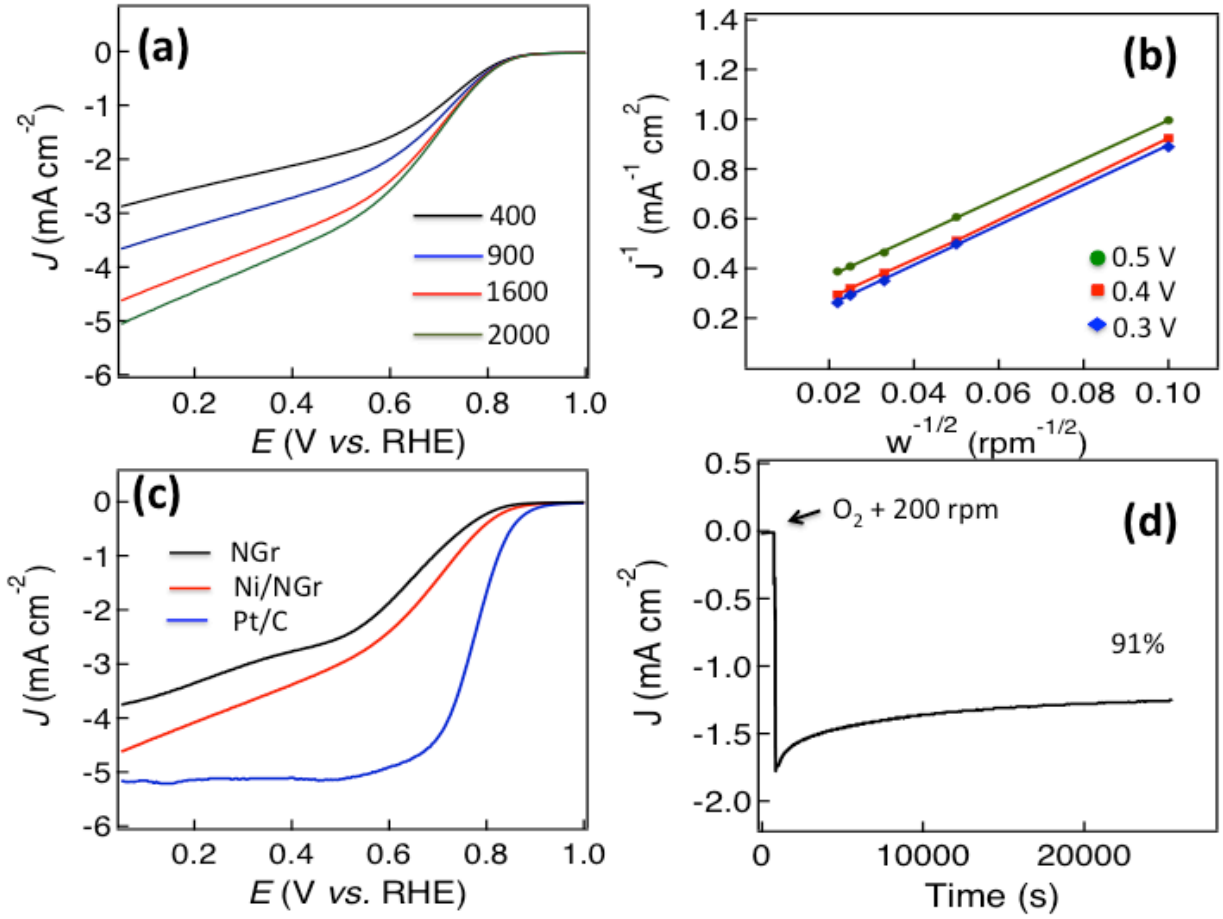

Figure 4. (a) Linear sweep voltammograms (LSV) of Ni/NGr at different rpm at a scan rate of 10 mV s^{-1} in O_2-saturated 0.1-M KOH(*aq*), (b) Koutecky–Levich plot of Ni/NGr at an electrode potential of 0.3, 0.4 and 0.5 V vs. RHE. (c) Comparison of LSV plots at 1600 rpm of NGr, Ni/NGr and Pt/C. (d) Stability test of Ni/NGr in chronoamperometry for 25000 s.

The OER and ORR activity of Ni/NGr is also superior to Ru/C, as the ORR activity of Ru/C is poor compared to Pt/C and nitrogen-doped carbons. [15] The electrocatalytical stability of the Ni/NGr for OER is also evaluated and after almost similar properties is observed after 1000 cycles (Figure 5d). Thus this active material can be a potential platform for developing bifunctional electrocatalyst for rechargeable metal-air batteries and fuel cells.

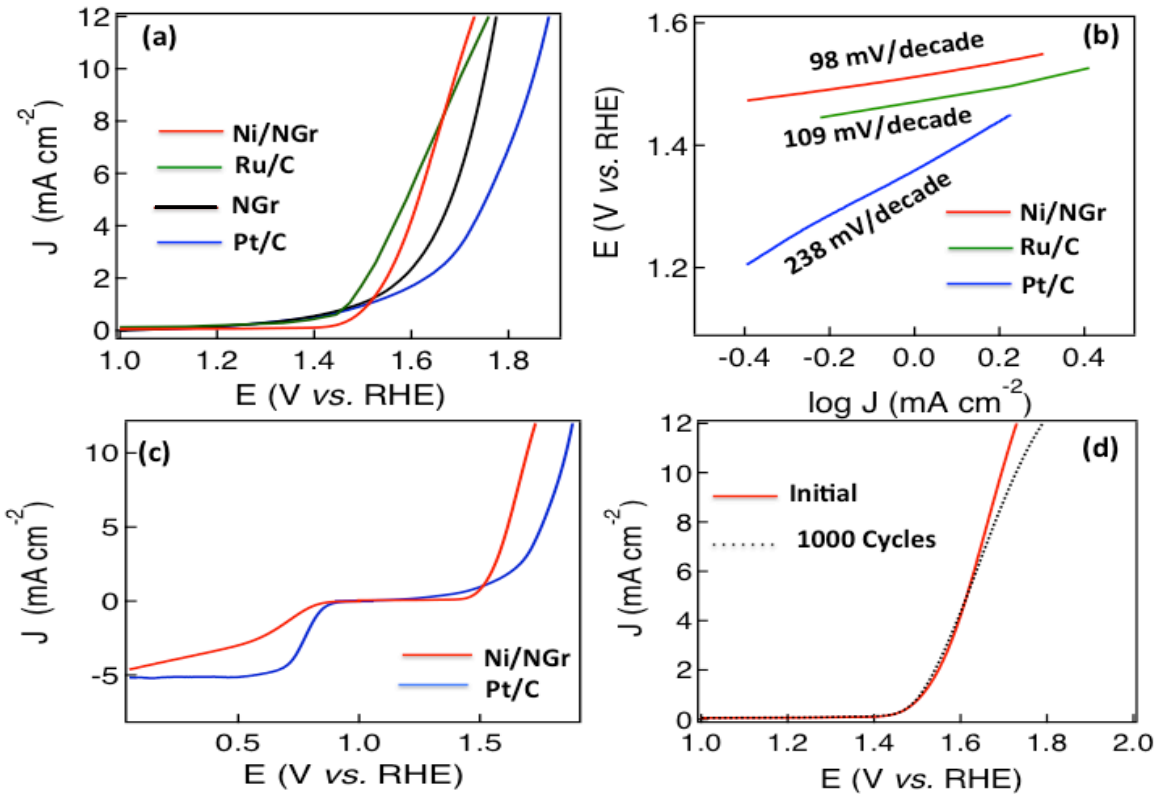

Figure 5. (a) Linear sweep voltammograms (LSV) of Ni/NGr, Ru/C, NGr and Pt/C at a scan rate of 10 mV/s in 0.1-M KOH(*aq*), (b) shows the tafel plots for Ni/NGr, Ru/C and Pt/C (c) LSV curves of Ni/NGr and Pt/C on an RDE (1600 rpm) in O_2-saturated 0.1-M KOH(*aq*) at scan rates of 10 mV/s showing the electrocatalytic activities towards both ORR and OER. (d) Comparison of LSV curves of Ni/NGr at initial and after 1000 cycles for OER.

After observing the efficient ORR and OER electrocatalytical properties of Ni/NGr, the electrodes were assessed in nitrogen-saturated 0.1 M KOH electrolyte using a typical three-electrode cell at room temperature. NGr and Pt/C catalyst loading the same mass on glassy carbon electrode were examined for comparison. The linear sweep voltammetry curves of the Ni/NGr, NGr and Pt/C (Figure 6a) at a scan rate of 5 mV s^{-1} in 0.1 M KOH solution demonstrated electrocatalytical activity towards HER.

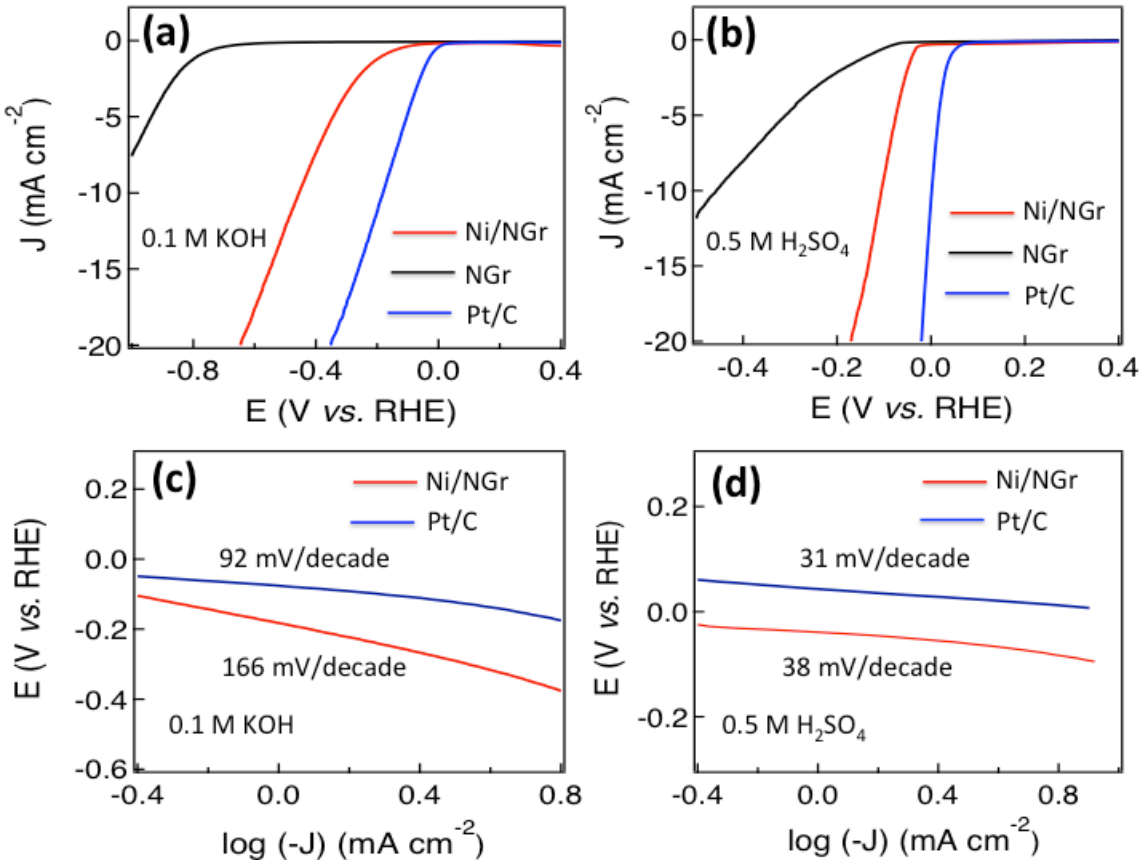

Figure 6. (a) Linear sweep voltammograms (LSV) of Ni/NGr, NGr and Pt/C at a scan rate of 5 mV/s in argon-saturated 0.1-M KOH(*aq*), (b) LSV curves of Ni/NGr, NGr and Pt/C at a scan rate of 5 mV/s in argon-saturated 0.1-M H_2SO_4 (*aq*), (c) shows the tafel plots for Ni/NGr and Pt/C in 0.1 M KOH(*aq*), (d) shows the tafel plots for Ni/NGr and Pt/C in 0.1 M H_2SO_4 (*aq*).

The commercial Pt/C shows best HER activity and Ni/NGr shows comparable HER activity close to Pt/C and the NGr shows the poor activity toward HER. The superior activities of Ni/NGr indicating the active sites in Ni/NGr are associated with the Ni and N. The HER activity of the electrodes are also investigated in acidic electrolyte of 0.1 M H_2SO_4 (Figure 6b) and the electrodes found more active in acidic media. The potential for generating current density of -20 mA cm^{-2} for Ni/NGr is -0.18 V vs. RHE which is superior than the reported Co-NG. [17] The tafel plots in alkali medium show 166 mV/decade for NI/NGr and 92 mV/decade for Pt/C (Figure 6c) but in the acidic medium the tafel plot of Ni/NGr is 38 mV/decade close to Pt/C (32mV/decade) (Figure 6d). The small tafel slope of Ni/NGr showed its efficiency of hydrogen evolution in acidic media by the active electrocatalytical nano-interface of metal/nitrogen-doped

graphene. The interaction of nitrogen with nickel and the presence of small amount of nickel oxide, the N-Gr/Ni/NiO nano-interface might be the synergistically active sites for HER catalysis for both in the acidic and alkaline media. In alkaline media, the HER pathway could be through the Volmer-Heyrovsky process or Volmer-Tafel pathways. [24]

$H_2O + e^- \longrightarrow H_{ads} + OH^-$ (Volmer) and

$H_{ads} + H_{ads} \longrightarrow H_2$ (Tafel) (2)

$H_2O + e^- \longrightarrow H_{ads} + OH^-$ (Volmer) and

$H_2O + H_{ads} + e^- \longrightarrow H_2 + OH^-$ (Heyrovsky) (3)

Both pathways involve the adsorption of H_2O molecule, electrochemical reduction of adsorbed H_2O into adsorbed OH^- and H atom, desorption of OH^- to refresh the surface and formation of H adsorbed intermediate for H_2 generation. The H atom binding energy of Ni metal is close to Pt, however the HER catalytic activity is worse compared with Pt. [26] The exact nature of HER of nickel/ nitrogen-doped graphene is still unknown. Therefore, we assume that the nature would be similar to the proposed mechanism for heterostructured NiO/Ni hybrid as OH^- generated by H_2O splitting could preferentially attach to the nitrogen-doped graphene/NiO site at the interface duo to strong electrostatic affinity to the locally positive charged Ni^{2+} species and more unfilled d orbitals in Ni^{2+} than Ni metal, while a nearby Ni site would facilitate H adsorption and thus the Volmer process, imparting synergistic HER catalytic activity of Ni/NGr. [24]

The recent attention to develop hydrogen peroxide fuel cell, hydroxide exchange membrane fuel cell and fuel cell for outer space and under water, efficient noble metal free electrodes for hydrogen oxidation reaction (HOR) and hydrogen per oxide oxidation reaction (HPOR) are highly crucial. [29-30] Due to the multifunctional roles of hydrogen peroxide in fuel cell

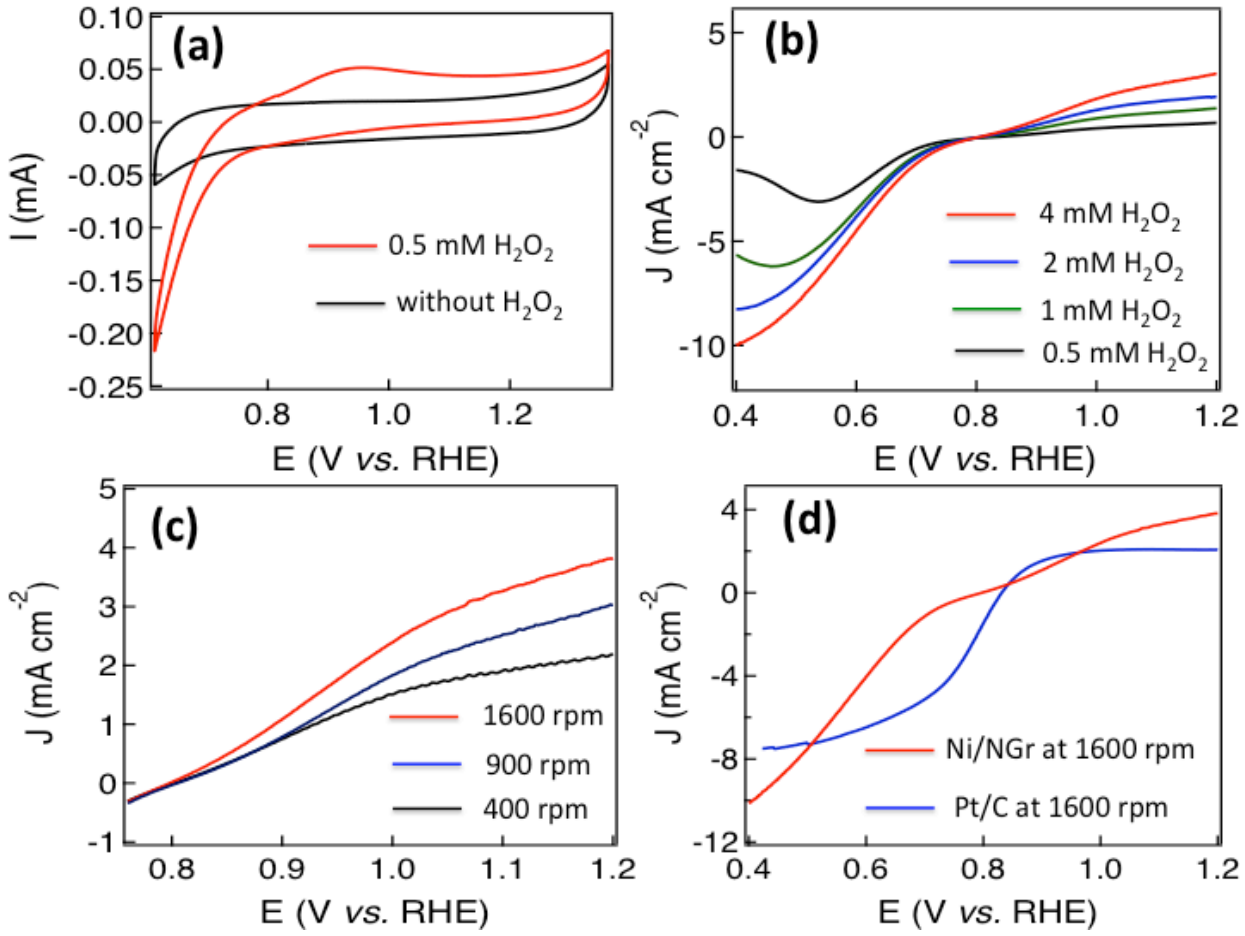

Figure 7. (a) Cyclic voltammograms (CV) of Ni/NGr in argon-saturated 0.1 M NaOH (*aq*) in the absence and presence of H_2O_2, (b) LSV curves of Ni/NGr at a scan rate of 5 mV/s in argon-saturated 0.1-M NaOH (*aq*) with different concentrations of H_2O_2, (c) shows the LSV curves of Ni/NGr at different rpm at a scan rate of 5 mV/s in argon-saturated 0.1-M NaOH (*aq*) with 4 mM of H_2O_2, (d)) LSV curves of Ni/NGr and Pt/C on an RDE (1600 rpm) in argon-saturated 0.1-M NaOH(*aq*) with 4 mM of H_2O_2 at scan rates of 5 mV/s showing the electrocatalytic activities towards both HPOR and ORR .

applications as liquid oxidant, fuel for one-compartment or membrane less fuel cell, source of oxygen in air-free environment and to avoid the water flooding, the importance of use of hydrogen per oxide for developing advanced fuel cell is highly crucial, thus the development of efficient noble-metal free electrocatalysts. [30-32] Nickel supported nitrogen-doped carbon nanotube and nickel deposited carbon fibre had been demonstrated the promising

electrocatalytical properties for HOR and HPOR activity respectively. [30, 33] Observing the HPOR activity of nickel depoited carbon material, the HPOR activity of synthesized Ni/NGr is also explored. The cyclic voltammograms of Ni/NGr in argon saturated 0.1 M NaOH solution without adding any hydrogen peroxide showed linear voltammogram without oxidation or reduction peak and a broad electrooxidation peak of hydrogen peroxide around 0.96 V associated with small hydrogen peroxide reduction peak at 0.85 V were observed after adding 0.5 mM solution of hydrogen peroxide (Figure 8a). The linear sweep voltammetry was applied to investigate the effects of current density with the raising of concentrations at a rotation frequency of 1600 rpm and the increment of currents for HPOR as well as associated oxygen reduction reaction (ORR) for the generation of oxygen in the solution on the process of HPOR were observed for the increasing concentrations. The increments of current were also observed with the increments of rotation frequency in the solution of 0.1 M NaOH with 4 mM H_2O_2. In alkaline media, HPOR take place to form oxygen, water and electrons according to following mechanism, [30]

$$HO_2^- + OH^- \longrightarrow O_2 + H_2O + 2e^- \quad (4)$$

In addition, the ORR takes place in alkaline media according to

$$O_2 + 2H_2O + 4e^- \longrightarrow 4\ OH^- \quad (5)$$

The comparison of Ni/NGr with Pt/C for HPOR and associate ORR indicates the superior current density of Ni/NGr than the Pt/C at rotation frequency of 1600 rpm in argon saturated 0.1 M NaOH solution with 4 mM of H_2O_2. Thus the hybrid shows remarkable electrocatalytic activity for HPOR and can be a promising electrode for the development of one compartment hydrogen peroxide based fuel cells.

4.4. CONCLUSIONS

In conclusion, we report a single pot synthesis of nickel embedded N-doped graphenes (Ni/NGr) with high electrocatalytical activity. The superior electrochemical activities for ORR, OER, HER and HPOR are attributed to the synergistic effect of the high atomic percentage of nitrogen including edge N atom and Ni. The efficient atomic percentage of nickel doping (0.56 at.%) on the carbon lattice of graphene may contribute the single atom catalysis. The quadrafunctional electrocatalytical activity of the composite can make it a promising electrode material for rechargeable fuel cell, metal-air battery, hybrid energy device, complete water splitting and hydrogen peroxide based one compartment fuel cell.

REFERENCES

1. Arico, A. S., Bruce, P., Scrosati, B., Tarascon, J. M., Schalkwijk, W. V. Nanostructured Materials for Advanced Energy Conversion and Storage Devices. *Nat. Mater.* **2005,** *4,* 366–377.

2. Zhang, J.; Xia, Z.; Dai, L. Carbon-based Electrocataysts for Advanced Energy Conversion and Storage. *Sci. Adv.* **2015,** *1,* 1500564-1500583.

3. Zhai, S.; Karahan, H. E.; Wei, L.; Qian, Q.; Harris, A. T.; Minett, A. I.; Ramakrishna, S.; Ng, A. K.; Chen, Y. Textile Energy Storage: Structural Design Concepts, material Selection and Future Perspectives. *Energy Storage Mater.* **2016,** *3,* 123-129.

4. Joo, S. H.; Choi, S. J.; Oh, I. Kwak, J.; Liu, Z.; Terasaki, O.; Ryoo, R. Ordered Nanoporous Arrays of Carbon Supporting High Dispersions of Platinum Nanoparticles. *Nature* **2001,** *412,* 169-172.

5. Kamat, P. V. The Magic of Electrocatalysts. *J. Phys. Chem. Lett.* **2012,** *3*, 3404-3404.

6. Hou, Y.; Wen, Z.; Cui, S.; Ci, S.; Mao, S. Chen, J. An Advanced Nitorgen Doped Graphene/Cobalt-Embedded Porous Carbon Polyhedron Hybrid for Efficient Catalysis of Oxygen Reduction and Water Splitting. *Adv. Funct. Mater.* **2015,** *25,* 872-882.

7. Liu, H.; Liu, Y.; Zhu, D. Chemical Doping of Graphene. *J. Mater. Chem.* **2011**, *21*, 3335-3345.

8. Candelaria, S. L.; Shao, Y.; Zhou, W. Li, W.; Li, X.; Xiao, J.; Zhang, J. –G.; Wang, Y.; Liu, J.; Li, J.; Cao, G. Nanostructured carbon for Energy Storage and Conversion. *Nano Energy* **2012,** *1,* 195-220.

9. Wang, H.; Maiyalagan, T.; Wang, X. Review on Recent Progress in Nitrogen-Doped Graphene: Synthesis, Characterization, and Its Potential Applications. *ACS Catal*. **2012**, *2*, 781-794.

10. Zhao, Y.; Nakamura, R.; Kamiya, K.; Nakanishi, S.; Hashimoto, K. Nitorgen-doped Carbon Nanomaterials as Non-Metal Electrocatalysts for Water Oxidation. *Nat*. *Commun*. **2013,** *4,* 2391-2398.

11. Lin, Z.; Waller, G. H.; Liu, Y.; Liu, M.; Wong, C. –P. Simple Preparation of Nanoporous Few-layer Nitrogen-doped Graphene for use as an Efficient Electrocatalyst for Oxygen Reduction and Evolution Reactions. Carbon **2013,** *53,* 130–136.

12. Zhou, R.; Jaroniec, M.; Qiao, S. Z. Nitrogen-doped Carbon Electrocatalysts Decorated with Transition Metals for the Oxygen Reduction Reaction. *ChemCatChem,* **2015,** *7,* 3808-3817.

13. Xia, B. Y.; Yan, Y.; Wang, X.; Lou, X. W. Recent Progress on Graphene-based Hybrid Electrocatalysts. *Mater*. *Horiz*. **2014,** *1*, 379-399.

14. Zhang, J.; Zhao, Z.; Xia, Z.; Dai, L. A Metal-free Bifunctional Electrocatalyst for Oxygen Reduction and Oxygen Evolution Reactions. *Nat*. *Nanotechnol*. **2015,** *10,* 444–452.

15. Li, R.; Wei, Z.; Gou, X. Nitrogen and Phosphorus Dual-doped Graphene/Carbon Nanosheets as bifunctional Electrocatalysts for Oxygen Reduction and Evolution. *ACS Catal*. **2015,** *5,* 4133–4142.

16. Li, D.; Muller, M. B.; Gilje, S.; Kaner, R. B.; Wallace, G. G. Processable Aqueous Dispersions of Graphene Nanosheets. *Nature Nanotechnol*. **2008,** *3,* 101-105.

17. Fei, H.; Dong, J.; Jimenez, M. J. A.; Ye, G.; Kim, N. D.; Samuel, E. L. G.; Peng, Z.; Zhu, Z.; Qin, F.; Bao, J.; Yacaman, M. J.; Ajayan, P. M.; Chen, D.; Tour, J. M. Atomic Cobalt on Nitrogen-doped Graphene for Hydrogen Generation. *Nat*. *Commun*. **2015**, *6,* 8668-8676.

18. Guo, S.; Zhang, S.; Wu, L.; Sun, S. Co/CoO Nanoparticles Assembled on Graphene for Electrochemical Reduction of Oxygen. *Angew*. *Chem*. *Int*. *Ed*. **2012**, *51,* 11770-11773.

19. Quaino, P.; Juarez, F.; Santos, E. and Schmickler, W. Volcano Plots in Hydrogen Electrocatalysis-Uses and Abuses. *Beilstein J*. *Nanotechnol*. **2014,** *5,* 846-854.

20. Liu, X.; Liu, W.; Ko, M.; Park, M.; Kim, M. G.; Oh, P.; Chae, S.; Park, S.; Casimir, A.; Wu, G.; Cho, J. Metal (Ni, Co)-Metal Oxides/Graphene Nanocomposites as Multifunctional Electrocatalysts. *Adv. Funct. Mater.* **2015,** *25,* 5799-5808.

21. Du, J.; Cheng, F.; Wang, S.; Zhang, T.; Chen, J. M (Salen)-Derived Nitrogen-doped M/C (M = Fe, Co, Ni) Porous Nanocomposites for Electrocatalytic Oxygen Reduction. *Sci. Reports* **2014,** *4,* 4386-4392.

22. Gracia-Espano, E.; Jia, X.; Wagberg, T. Improved Oxygen Reduction Performance of Pt-Ni Nanoparticles Adhesion on Nitrogen-Doped Graphene. *J. Phys. Chem. C* **2014**, *118,* 2804-2811.

23. Zhuang, Z.; Giles, S. A.; Zheng, J.; Jenness, G. R.; Caratzoulas, S.; Vlachos, D. G. and Yan, Y. Nickel Supported on Nitrogen-Doped Carbon nanotubes as Hydrogen Oxidation Reaction Catalyst in Alkaline Electrolyte. *Nat. Commun.* **2016,** *7,* 10141-10148.

24. Gong, M.; Zhou, W.; Tsai, M. –C.; Zhou, J.; Guan, M.; Lin, M.; Zhang, Bo.; Hu, Y.; Wang, D.-Y.; Yang, J.; Pennycook, S. J.; Hwang, B. –J.; Dai, H. Nanoscale Nickel Oxide/ Nickel Heterostructure for Active Hydrogen Evolution Electrocatalysis. *Nat. Commun.* **2014,** *5,* 4695-4701.

25. Ren, J.; Antonietti, M.; Fellinger, T. –P. Efficient Water Splitting Using a Simple Ni/N/C Paper Electrocatalyst. *Adv. Energy. Mater.* **2015,** *5,* 1401660-1401666.

26. Sheng, W.; Myint, M.; Chen, J. G.; Yan, Y. Correlating the Hydrogen Evolution Reaction Activity in Alkaline Electrolytes with The Hydrogen Binding Energy on Monometallic Surfaces. *Energy Environ. Sci.* **2013**, *6,* 1509-1512.

27. Chen, S.; Duan, J.; Ran, J.; Jaroniec, M.; Qiao, S. Z. N-Doped Graphene Film-Confined Nickel Nanoparticles as A Highly Effiecient Three-Dimensional Oxygen Evolution Electrocatalyst. *Energy Environ. Sci.* **2013,** *6,* 3693-3699.

28. Faisal, S. N.; Haque, E.; Noorbehesht, N.; Zhang, W.; Harris, A. T.; Church, T. L.; Minett, A. I. N-Doped Graphene with High Atomic Percentages of Pyridinic N and Graphitic N as Electrode for High-Performance Supercapacitor and Efficient Bifunctional Electrocatalyst for ORR and OER**.** *Carbon*, **2016** (under review).

29. Zhuang, Z.; Giles, S. A.; Zheng, J.; Jenness, G. R.; Caratzoulas, S.; Vlachos, D. G.; Yan, Y. Nickel Supported on Nitrogen-doped Carbon Nanotubes as Hydrogen Oxidation Reaction Catalyst in Alkaline Electrolyte. *Nat. Commun.* **2016,** *7,* 10141-10148.

30. An, L.; Zhao, T.; Yan, X.; Zhou, Z.; Tan, P. The Dual Role of Hydrogen Peroxide in Fuel Cells. *Sci. Bull.* **2015,** *60,* 55-64.

31. Yamada, Y.; Yoneda, M.; Fukuzumi, S. High and Robust Performance of H_2O_2 Fuel Cells in The Presence of Scandium Ion. *Energy Environ. Sci.* **2015,** *8,* 1698-1701.

32. Sanli, A. E. A Possible Future Fuel Cell: The Peroxide/Peroxide Fuel Cell. *Intl. J. Energy Res*. **2013,** *7,* 1488-1497.

33. Aytac, A.; Gurbuz, M.; A. E. Sanli, Electrooxidation of hydrogen Peroxide and Sodium Borohydride on Ni Deposited Carbon Fiber Electrode for Alkaline Fuel Cells. *Int. J. Hedrogen Energy,* **2011,** *36,* 1013-10021.

* THIS CHAPTER HAS BEEN SUBMITTED AS A FULL PAPER IN THE FOLLOWING JOURNAL;

Nickel Embedded Nitrogen-Doped Graphene as Quadrafunctional Electrocatalyst for ORR, OER, HER and HPOR**. S. N. Faisal**, N. Noorbehesht, L. Shabnam, A. K. Roy, E. Pourazadi, E. Haque, M. S. Islam, A. T. Harris and A. I. Minett, , *Nano Energy,* 2017 (Submitted).

Chapter: 5

3D Nanostructured N-Doped Graphene/Carbon Nanotube Composites for Large Volumetric Solid State Supercapacitor, Highly Stable Anode for Li-Ion Battery and Metal-Free Bifunctional Electrocatalyst

3D Nanostructured N-Doped Graphene/Carbon Nanotube Composites for Large Volumetric Solid State Supercapacitor, Highly Stable Anode for Li-Ion Battery and Metal-Free Bifunctional Electrocatalyst

ABSTRACT: A three-dimensional nanostructured nitrogen-doped graphene/carbon nanotube composite has been synthesized utilizing the adhesive properties of uric acid (solid nitrogen precursor). In the synthesis procedures, uric acid attached on the graphene oxide surfaces and with the oxidized multiwalled carbon nanotubes via hydrogen and electrostatic force in the solution and upon thermal annealing form a lameller nanostructured by the proper insertion of carbon nanotubes in graphene layer with nitrogen doping. The resultant composite having very high atomic percentage of nitrogen 11.2 (at.%) shows enhanced electrochemical energy storage and conversion properties than the synthesized nitrogen-doped graphene. The composite exhibits high gravimetric and volumetric capacitance (324 F/g at a current density of 1 A/g) as electrode in solid-state supercapacitor, high rate capable anode in lithium-ion battery (1150 mAh g^{-1} at 0.1 A g^{-1}) with high cycling stability. In addition, the composite demonstrates efficient metal-free bifunctional electrocatalysis comparable with the commercial electrocatalyst.

5.1 INTRODUCTION

The demand of high performance energy devices such as supercapacitors, metal-ion batteries, metal-air batteries and fuel cells are growing rapidly due to the recent advancement of electric vehicles, high power consuming portable electronics as well as a source of renewable energy. [1-2] Carbon nanomaterials have attracted great attention as potential electroactive materials for electrode fabrication of high performance energy devices. High native electrical conductivity, charge storage ability, electrochemical stability, and low cost of environment friendly carbon-based nanomaterials have inspired researchers to dense improvement of its real world application as an electroactive material. [3-5] However, most of the forms of carbon used commercially are limited to low capacitance, conductivity and porosity. [5, 6] Among the different forms of carbon, hexagonal graphitic carbon structures such as graphene and carbon nanotubes (CNTs) contain tremendous mechanical properties along with very high theoretical electroactive surface area,

which can provide promising electrochemical response towards electrode materials of power devices. [7-10] However the strong van-der-waals interaction form restacking of graphene layers which reduce the specific surface area of active materials to access by the electrolyte ions as well as represents inferior electrochemical response compare to the theoretical value. [11] Tremendous efforts are going on to improve the practical surface area capacity of graphene by mimicking this two-dimensional (2D) material to three-dimensional (3D) structure as well as the enhancement of electroactivity of individual layers by chemical modification. [12-15] Alternatively, graphene based nanocomposites with different carbon nanomaterials, conductive polymers (CPs) and metallic nanoparticles have provided huge attractions by enhancing the electrical conductivity along with surface area by preventing the restacking of graphene sheets with the aid of conjugated nanomaterials. [16-18] Among these different nanostructured formation, combination of one-dimensional (1D) carbon nanotubes (CNTs) with 2D graphene sheets showed development of 3D composites materials where CNTs can easily be intercalated in-between the graphene layers.[19-22] Natural insertion and homogeneous distribution of nanotubes in 3D structure of graphene create highly porous composite with very effective continuous ion conductive network to access by the electrolyte ions completely and results excellent electrochemical characteristics such as high gravimetric, volumetric capacitance and efficient electrocatalytic activity. [11, 23, 24]

To obtain such multidimensional graphitic architecture with hollow space for smooth penetration of electrolyte ions, the catalytic growth of CNTs on individual graphene layers via chemical vapor deposition (CVD) method has been explored and reveal good electrochemical behavior as promising electroactive carbon nanocomposite materials for energy devices as well as experience electrocatalytic activity with the insertion of metal center. [25-28] However, due to the complicacy of the CVD process it is hard to scale-up for large-scale production and the presence of metal catalyst in the process can cause detrimental effect. Alternatively, formation of chemical bonding between graphene and carbon nanotube via thermal annealing can be superior way to build a three-dimensional structure for better ion interactions. [29-30] The composites of reduced graphene oxides with multiwalled carbon nanotubes (MWCNTs) bonded by the *p*-phenyldiamine showed good capacitive behavior, however the presence of organic compound between the layers might hinder the electrochemical properties as well as the structure of the hybrid materials suffered from the proper insertion of carbon nanotubes inside the graphene layers.[29] The

carbon nanotube-bridged graphene 3D building blocks using electrostatic self-assembled CTAB showed excellent intercalation of CNTs inside the graphene layers but the capacitance was not high enough as the charge storage ability of reduced graphene oxide is low. [30] The chemically bonded graphene/CNTs obtained by amidation reaction of amine-functionalized CNTs with NHS-activated GO nanosheets followed by microwave hydrothermal reduction with hydrazine-ammonia showed not only good gravimetric as well as volumetric capacitance as an effect of the interlayer space created by graphene. Perhaps, multi-step synthesis approaches along with highly toxic and dangerously unstable chemicals such as hydrazine arise the issue of large-scale preparation of such composite materials. [31]

Besides the structural effects of graphene/CNT composites, the intrinsic capacitance, electrocatalytic responses and continuous electrochemical stability can be improved by the nitrogen doping in graphene lattice, which can enhance the electronic properties based on the bonding configurations of nitrogen atoms with adjacent carbon atoms. [32-33] Besides the modulation of planer electron spin density of native carbon lattice, the formation of high pore volume and surface area from high temperature nitrogen doping favor the increment of electrochemical behavior as well as the long cycling stability as electrode materials for supercapacitor and Li-ion battery. [54] The uniformly dispersed and covalently bonded molecular nitrogen groups on the graphene plane not only tailored the native electric double layer capacitance (EDLC) of graphene with generating pseudocapacitive nature on the edge but also provide active cites for electrocatalysis activity such as oxygen reduction reactions (ORR) *via* activation of the adjacent carbon atoms. [26, 34, 35] Additionally, the electron dense active cites on graphene surface able to facilitate the oxygen evolution reactions (OER), which are highly important characteristic for developing metal-air batteries and rechargeable fuel cells. [3,28, 36] To obtain the best performance in energy storage and electrocatalysis, a single step scalable synthesis of three-dimensional graphene/carbon nanotube composite with high atomic percentage of nitrogen doping is highly desirable for real world energy device electrode fabrication.

In this study, we have developed scalable single step synthesis approach for nitrogen-doped graphene/carbon nanotube (N-Gr/CNT) composite material in noble lamellar architecture. A simple thermal treatment at 800 °C of graphene oxide, oxidized carbon nanotubes with the

combination of solid doping precursor uric acid (UA) results high atomic percentage of nitrogen (11.2%) in the graphitic carbon network under an argon atmosphere. During the thermal treatment process at lower temperature the doping agent UA able to form electrostatic and hydrogen bonding with the carboxylic groups of GO and oxidized multiwalled carbon nanotubes (o-MWCNT) surface by the existing amino functional group of it, which promote to form a lamellar-structured 3D building block architecture. At higher temperature treatment the solid doping precursor breaks into highly active nitrogen species to successfully insert in the hexagonal carbon lattice of graphene and CNT homogeneously. The appropriate intercalation of CNT network in-between graphene layers prevents self-agglomeration towards increase the mass densities as well as volumetric charge storage ability. On the other hand, the nitrogen doped large number of active sites of the 3D network should promote the material for high performance metal-free electrocatalysis activity. The N-Gr/CNT performed as an electrode material for solid-state supercapacitor and Li-ion battery. Besides that the bifunctional ORR and OER electrocatalytic performance of the materials have also been explored to define the efficient metal-free electrocatalytic property comparable to noble metal catalyst for the application of metal-air battery and rechargeable fuel cells.

5.2 EXPERIMENTAL SECTION

Synthesis of N-doped graphene:

The graphene oxide was prepared from naturally expanded graphite (Ashbury Carbons, Grade-3772) using a procedure previously reported in the literature for the generation of ultra-large GO sheets. [37] The graphene oxide sheets were dispersed in water by ultrasonication. Graphene oxide and uric acid were mixed at a ratio of 1:5. The uric acid attached strongly on the surfaces of graphene oxide due to its high adhesion properties towards organic functional groups. The mixtures were then stirred continuously and heated at 80ºC for 10-12 h to remove the water. The resulting solid powders were annealed at 800^0C at a rate of 5ºC/min for 1 h in an argon atmosphere in a tubular furnace. [38]

Synthesis of N-doped carbon nanotube:

The oxidized multiwalled carbon nanotube (oMWCNT) was produced by simple gas-solid route reported previously.[39] The nitrogen doping was carried out by the similar way using uric acid at a ratio of (1:3) via thermal annealing at 800ºC for one hour. [38]

Synthesis of N-doped graphene/carbon nanotube composites:

The synthesis of N-doped graphene/carbon nanotube composites followed by the similar way stated above for N-doped graphene synthesis. The graphene oxide, multiwalled oxidized carbon nanotube (oCNT) and uric acid were mixed at a ratio of 1:3:10 respectively in the isopropanol solution. The mixtures were then stirred continuously and heated at 80ºC for 6-8 h to remove the isopropanol. The resulting solid powders were then annealed at 800^0C at a rate of 5ºC/min for 1 h in an argon atmosphere in a tubular furnace. The synthesized nitrogen doped reduced graphene oxides and carbon nanotubes composite was named N-Gr/CNT. Physically mixed nitrogen doped graphene and nitrogen doped carbon nanotube PM-[NGr/NCNT] was prepared by the physical mixing of NG and NCNT at a ratio of 1:3.

Characterization:

The microstructures and morphology of the synthesized samples were investigated by FESEM (Zeiss ULTRA *plus*), HRTEM (JEOL 2200FS) and XRD (Shimadzu S6000). Raman spectra were collected with Renishaw inVia Raman Spectrometer. X-ray photoelectron spectroscopy (XPS) analyses were performed by ESCALAB250Xi (Thermo Scientific, UK) with a monochromated Al K alpha (energy 1486.68 eV) operating at 150W (13 kV x 12 mA) under a vacuum of 2 x 10^{-9} mbar. The analysis spot size was 500 μm in diameter. The binding energies were referenced to the adventitious hydrocarbon C 1s signal at 284.9 eV.

Electrochemical measurement:

The electrochemical characterization and measurement of the nitrogen-doped graphene, nitrogen-doped carbon nanotube, PM-[NGr/NCNT] and N-Gr/CNT were evaluated by first depositing on an ITO-coated glass electrode in a three electrode cell using platinum wire as as counter electrode and an Ag/AgCl, KCl (3 M) electrode as reference electrode using a Bio-logic SP300 potentiostat. The Nitrogen doped graphene/carbon nanotube composites samples were prepared of 1 mg/ml mixture in isopropanol using sonication. For characterizing capacitance

properties 10 wt% PTFE were used as binding agents. For capacitance calculation, a two-electrode cell was developed using ITO-coated glass electrodes. The device was fabricated by depositing the active materials on the conductive side of the ITO-coated glasses and placing a PP separator (cellgard) between the coated electrodes and pressed together at high pressure. Before fabricating the device, the separator was soaked in electrolyte (1.0 M sulphuric acid) for 1 hour. 0.5 mg active materials were deposited on the area of 1.0 cm × 1.0 cm ITO-coated glass electrode surface using 10 wt% PTFE binder. The solid state device was fabricated using similar way replacing the separator with soaked electrolyte by gel electrolyte of poly(vinyl alcohol)/sulphuric acid. The preparation of gel electrolyte has been proceed by following the reported procedure. [22] 2.2 g of PVA powder was first added into 20 ml of water and after heating around 90 ^{O}C with continuous stirring until the solution become clear. Later 2.2 g of sulphuric acid had been added and cool down the solution at room temperature to form the gel electrolyte. The solid state supercapacitor was fabricated by depositing the active material on both of the ITO-coated glass slide and put two glass spacers on both side to make a gap between the two electrodes. The gap was then filled up by the gel electrolyte. The gravimetric capacitance of the cell from galvanostatic charge/discharge was calculated using the following formula: [15, 48]

$$C = \frac{4I}{m\frac{dv}{dt}} \quad (1)$$

Where C is specific capacitance (F g^{-1}), I is the charge/discharge current density (A g^{-1}), m is the total mass of materials deposited on the electrodes and dV/dt was calculated from the slope of the discharge curve. The energy density (E) and power density (P) were calculated using Eqs. 2 and 3, respectively. [48]

$$E = \frac{1}{2} \times C(\Delta V)^2 \quad (2)$$

$$P = E/t \quad (3)$$

Where C is the specific capacitance of the device, ΔV is the potential range and t is the time to discharge.

The electrocatalytic properties were evaluated by rotating disk electrode (RDE) experiments in an O_2-saturated 0.1-M KOH solution. First, the oxygen-reduction capability was assessed by comparing cyclic voltammetric curves measured in argon- and oxygen-saturated electrolytes. Linear sweep voltammetry curves were recorded over the potential range of 0 to 1 V versus reversible hydrogen electrode (RHE) at a scan rate of 10 mV/s at ambient temperature and at rotation speeds of 100–1600 rpm. The mass loading of the active materials on the glassy carbon electrode in electrocatalysis were evaluated by depositing 12 μg. OER activity was measured by linear sweep voltammetry in the potential window ranging from 1.0 to 2.0 V versus reversible hydrogen electrode (RHE) scale by adding a value of 0.964 V. The commercial Pt/C (20 wt %) and Ru/C (20 wt %) into nafion solution with same loading amount were taken for comparison.

Fabrication of Li-ion Battery: The electrochemical characterization of N-Gr/CNT) composite was carried out using coin cells. The electrode was tape-casted over Cu foil by blending the active material, N-Gr/CNT, with Super P carbon black and polyvinylidenedifluoride (PVDF) binder, at a weight ratio of 8:1:1, respectively, using N-methyl-2-pyrrolidone (NMP) as the blending solvent and subsequently dried at 120°C for 12 h. The electrode was cut from the as-prepared electrode paper in which the mass loading of an electrode was controlled with ~ 1 mg cm^{-2}. CR 2032 coin-type cells were assembled in an Ar-filled glove box by using the as-prepared electrodes as the working electrode, with Li foil as the counter electrode and reference electrode, a porous polypropylene film as separator, and 1 M $LiPF_6$ in a 1: 1 (v/v) mixture of ethylene carbonate (EC) and diethyl carbonate (DEC) as the electrolyte. The cells were galvanostatically charged and discharged using an automatic battery tester system (Land®, China) at various current densities in the range of 0.002 - 3 V. Cyclic voltammetry and electrochemical impedance spectroscopy (EIS) measurements were performed using a Biologic Science Instruments (Model: VMP3; S/n: 0398) between 0.1 MHz to 10 mHz under AC stimuli with 5 mV of amplitude. The specific capacity of as tested Li-ion battery is solely based on the mass of active material, N-Gr/CNT) neglecting the effect of super P carbon black due to its low reversible capacity.

5.3 RESULTS AND DISCUSSION

The synthesis of N-Gr/CNT is illustrated in Figure 1, where the graphene oxide, oxidized carbon nanotubes and uric acid are mixed together in isopropanol at a ratio of 1:3:10 respectively and stirred continuously at a temperature of 80 ^{0}C until the complete evaporation of solvent. The uric acid molecules adsorbed strongly *via* hydrogen bonding with the carboxyl groups on the graphene oxide and oCNT surfaces and form a lamellar structure *via* intercalating the oCNTs in graphene layers. The solid mixtures were collected in powder form and then heated in a tubular furnace at 800^{0}C at a rate of 5^{0}C/min for 1 hour. Upon pyrolysis the inclusion of nitrogen atom in graphene lattice from the uric acid occurs [38] and a lamellar structure of nitrogen-doped graphene/ carbon nanotube composite containing high atomic percentage of nitrogen is formed. The attachments of the graphene oxide with the oxidized carbon nanotube was developed by the formation of hydrogen bonding between the carboxylic groups of GO and oCNT with the amino group of uric acid (UA). Uric acid having good adhesion properties can form hydrogen bonding with carboxyl groups at an adhesion force of 1.62 nN.[40] During the sonication and stirring at 80^{0}C, the uric acid due to its excellent surface attachment properties can be intercalated inside the graphene layer and interconnecting the graphene layers and oCNTs by forming the hydrogen bonding with the carboxyl groups.

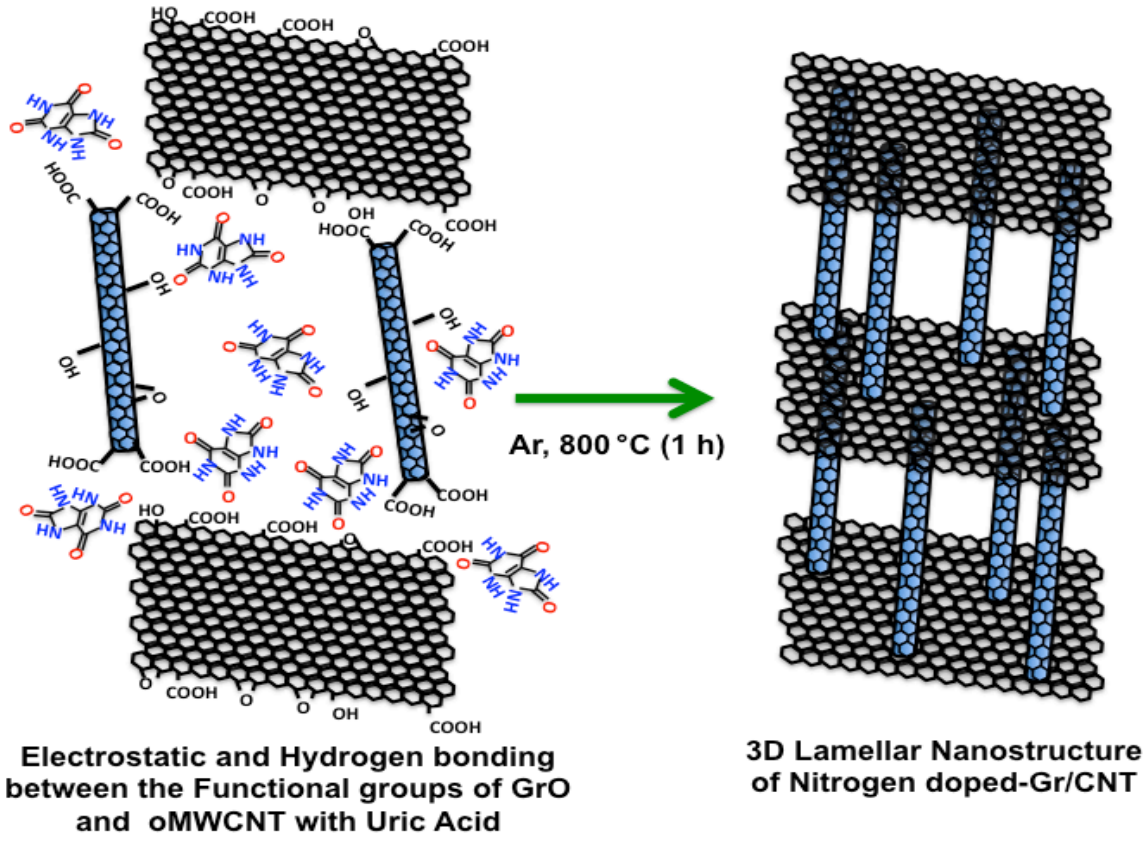

Figure 1: Schematic diagram of the formation of 3D nanostructured N-Gr/CNT via thermal annealing of graphene oxide and oxidized multiwalled carbon nanotubes with uric acid.

The FTIR spectra (Figure 2) present the comparison of the UA, mixture of graphene oxide and oxidized carbon nanotube (GO/oCNT) and the mixture of (GO/UA/oCNT). The (GO/UA/oCNT) mixture was being filtered and washed several times for removing the excess uric acid on the GO/oCNT surface. Uric acid shows the conformal FTIR spectrum. The absorption bands of GO/oCNT mixture appear at 3200-3600 (broad peak), 1726, 1640, 1582, 1226, 1160 and 1125 cm^{-1} for the corresponding —OH, C=O in carboxyl group, C=C aromatic ring, C—OH, C=O, C—O stretching vibrations. From the spectra of GO/UA/oCNT, the presence of uric acid was observed due to its strong signal towards IR region rather than the GO/CNT mixture. However small shifts toward left of C=O stretch (1658 cm^{-1}) and N-O stretch (1585 cm^{-1}) in GO/UA/oCNT from the C=O stretch (1664 cm^{-1}) and N-O stretch (1589 cm^{-1}) of uric acid indicated the formation of hydrogen bonding. [41]

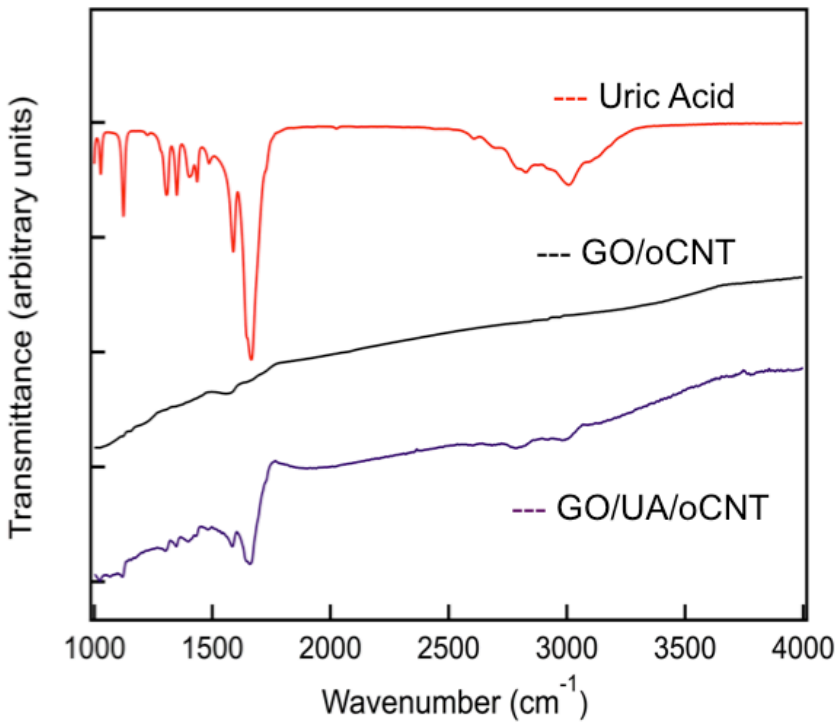

Figure 2: FTIR spectra of uric acid, mixture of graphene oxide with oxidized carbon nanotubes and the mixture of graphene oxide, oxidized carbon nanotube and uric acid.

The morphology and structure of the obtained composite after pyrolysis was characterized by scanning electron microscopy (SEM) and transmission electron microscopy (TEM). The SEM images of N-Gr/CNT revealed the intercalated CNT networks inside the graphene layers. (Figure 3a and Figure 4). The three-dimensional structure and the intercalation of carbon nanotubes inside the graphene layers were clearly visible. For further confirmation, low magnification TEM was used. The TEM image confirms the 3D structures of the composites by forming the CNT networks inside the graphene layers (Figure 3 (c)) whereas in PM-[NG/NCNT], CNTs are randomly placed on the graphene surface (Figure 3 (b)) and similar morphology was found in TEM image (Figure 3 (d)). High-resolution transmission electron micrograph (HRTEM) revealed the attachment of CNTs on the edge as well as basal plane of the graphene (Figure 5a).

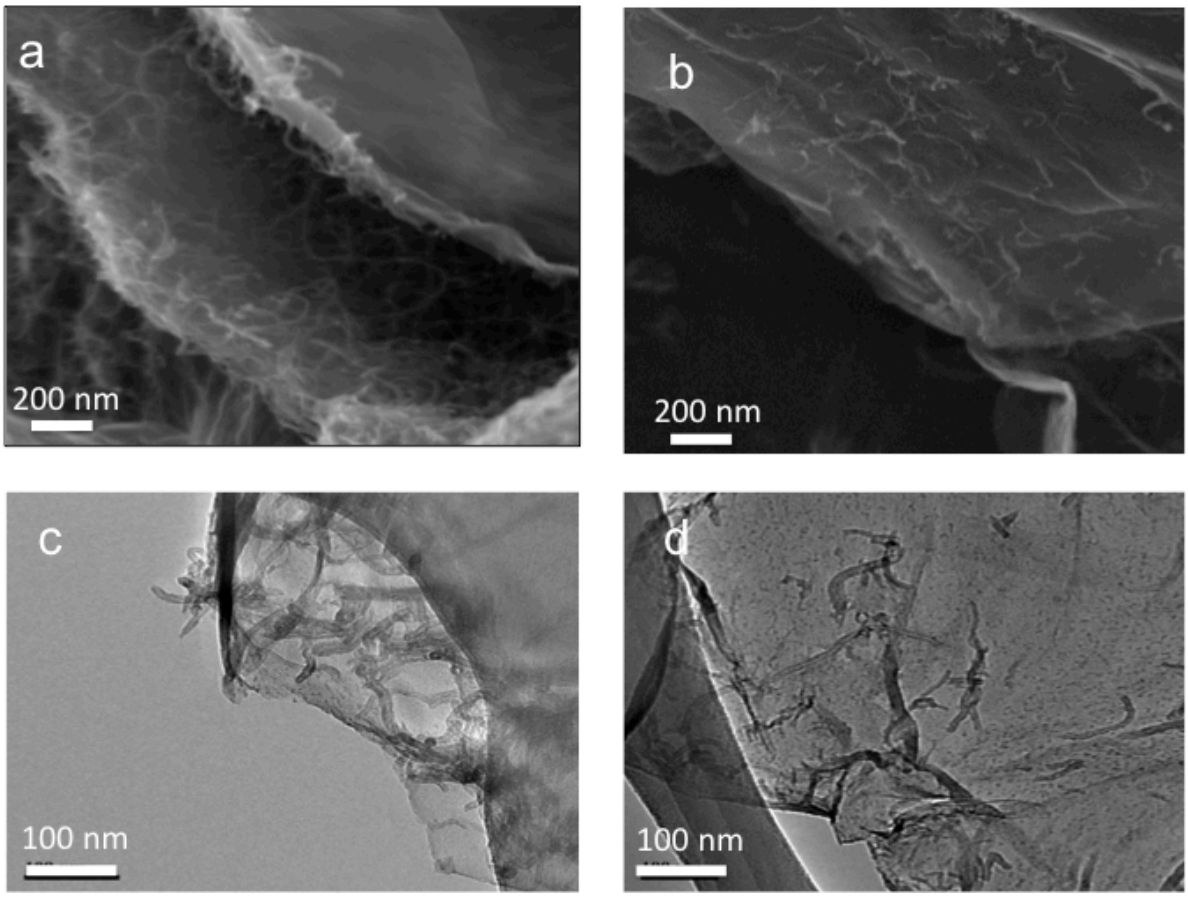

Figure 3: (a) SEM image of three-dimensional nanostructured N-Gr/CNT, (b) SEM image of PM-NG/NCNT (c) TEM image of N-Gr/CNT (d) TEM image of PM-NGr/NCNT.

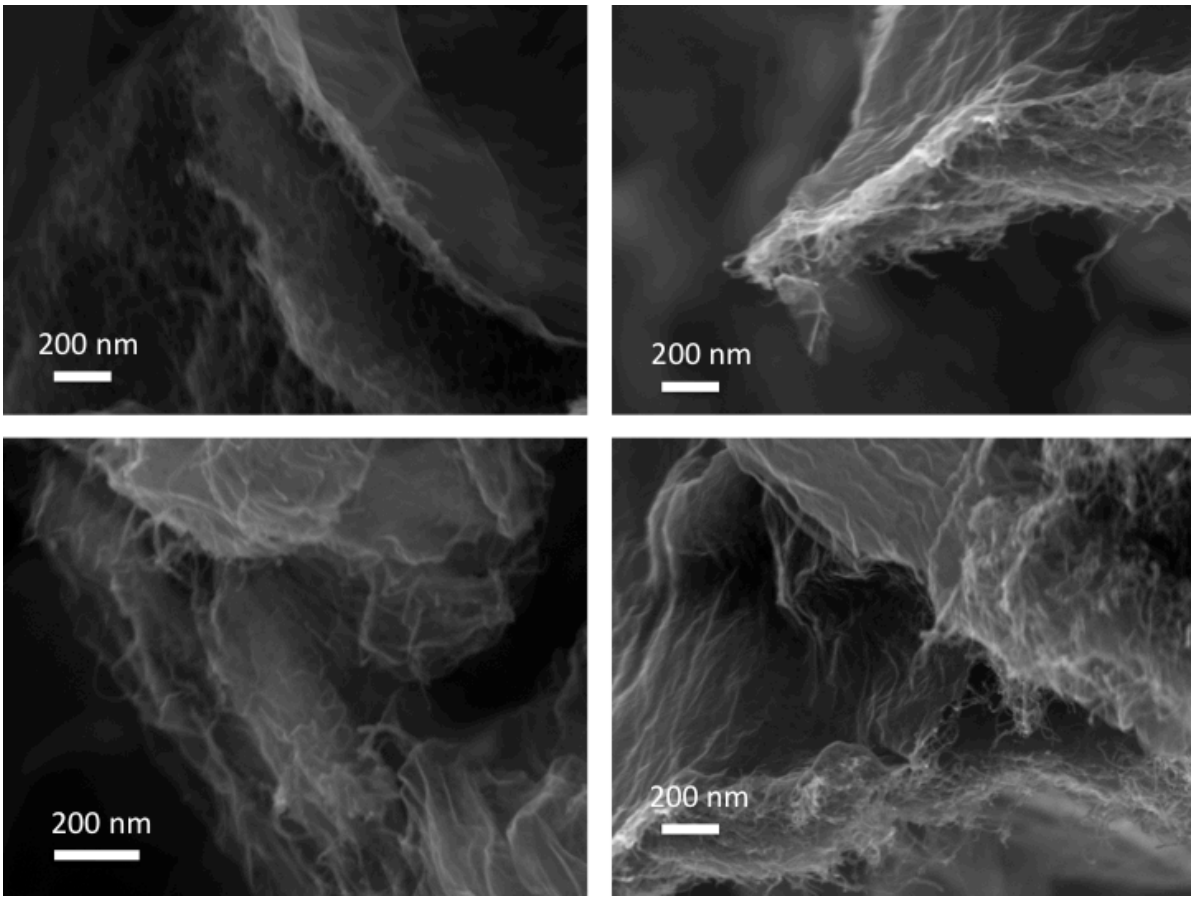

Figure 4: SEM images of NGr/CNT at different locations showing the three-dimensional nanostructured by the insertion of CNTs into the graphene layers.

The average d-spacing of the graphene layers of N-Gr/CNT from HR-TEM was found of 0.3946 nm, (Figure 5b) which is larger than the average layer-to-layer spacing of 0.352 nm observed in the thermally reduced graphene oxide film. [42] The increase of the distance of the graphene layers due to the presence of CNTs, which expected to prevent the restacking between the layers. The distance between the layers of graphene was also characterized with the XRD. (Figure 5c) The evaluation of the peak position indicated the slight shifting of the peaks of the composites than the peak for NG and NCNT. The calculated interlayer spacing found from the peak position was 0.38 nm, which is higher than the average layer-to-layer spacing of graphene and close to the value obtained from HR-TEM. The broader peak of N-Gr/CNT also indicated the intercalation of CNTs inside the graphene layers. [29]

The graphitic nature of both of composites of N-Gr/CNT and PM-NG/NCNT were characterized by Raman spectroscopy at an excitation wavelength of 514 nm under ambient conditions. As shown in Figure 5d, the G peaks of the N-Gr/CNT and PM-NG/NCNT were present at 1578 cm^{-1} and 1582 cm^{-1} respectively. The position of the G peak of N-Gr/CNT was shifted towards left as well as down than the G peak of PM-NG/NCNT indicated the presence of more defects due to the combined nitrogen doping rather than separated doping and physically mixing. [31] The distinguishable 2D peaks of N-Gr/CNT was observed at 2688 cm^{-1} 2722 cm^{-1} which confirmed the state of the composites as lamellar bilayers of few layers graphene flakes whereas the broad 2D peak of PM-NG/NCNT resembled the multilayered graphene like structure due to the random agglomeration of graphene sheets and carbon nanotubes. [43, 44]

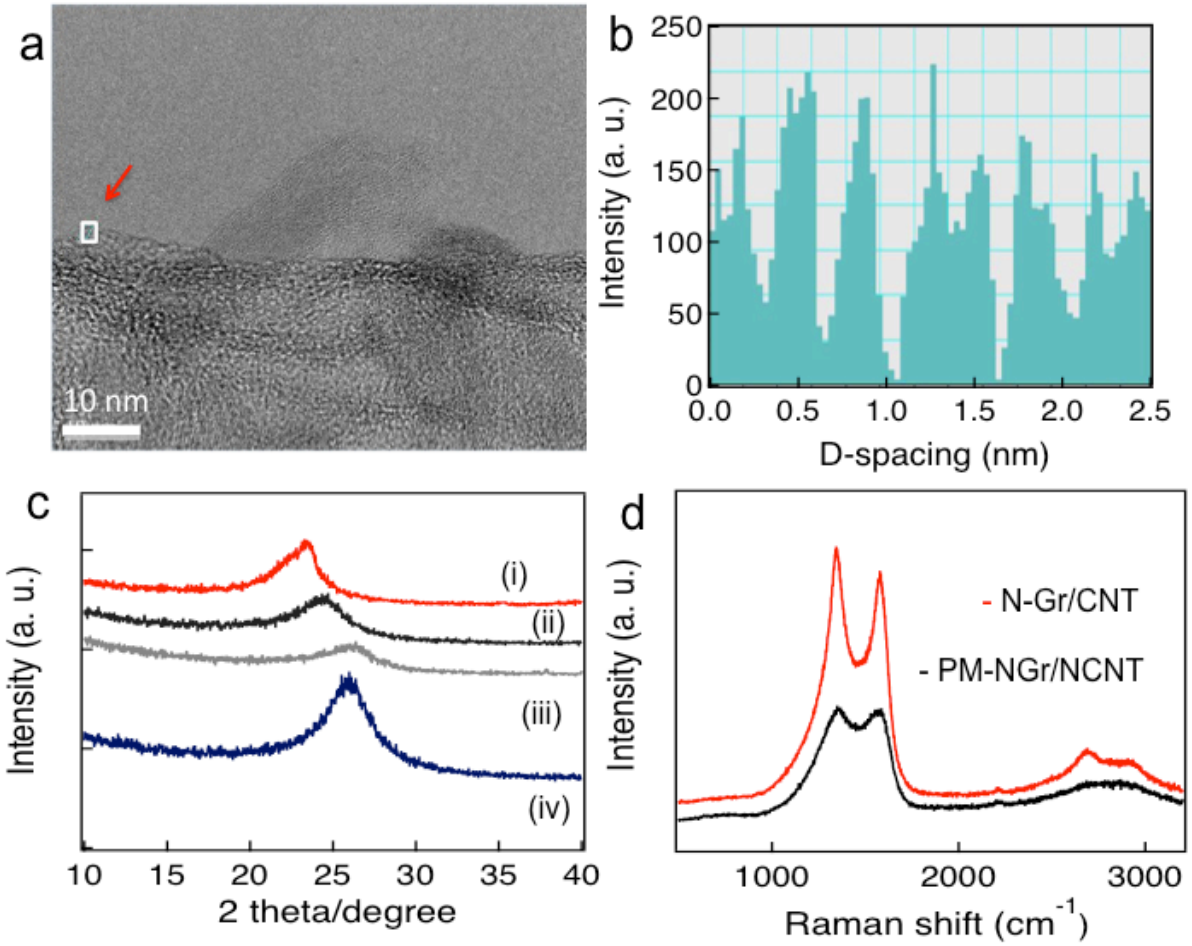

Figure 5: (a) HRTEM of N-Gr/CNT and selected area for calculating D-spacing, (b) D-spacing Calculation, (c) XRD patterns of N-Gr/CNT (i), PM-NGr/NCNT (ii), NGr (iii) and NCNT (iv), (d) Raman Spectra of N-Gr/CNT and PM-NGr/NCNT.

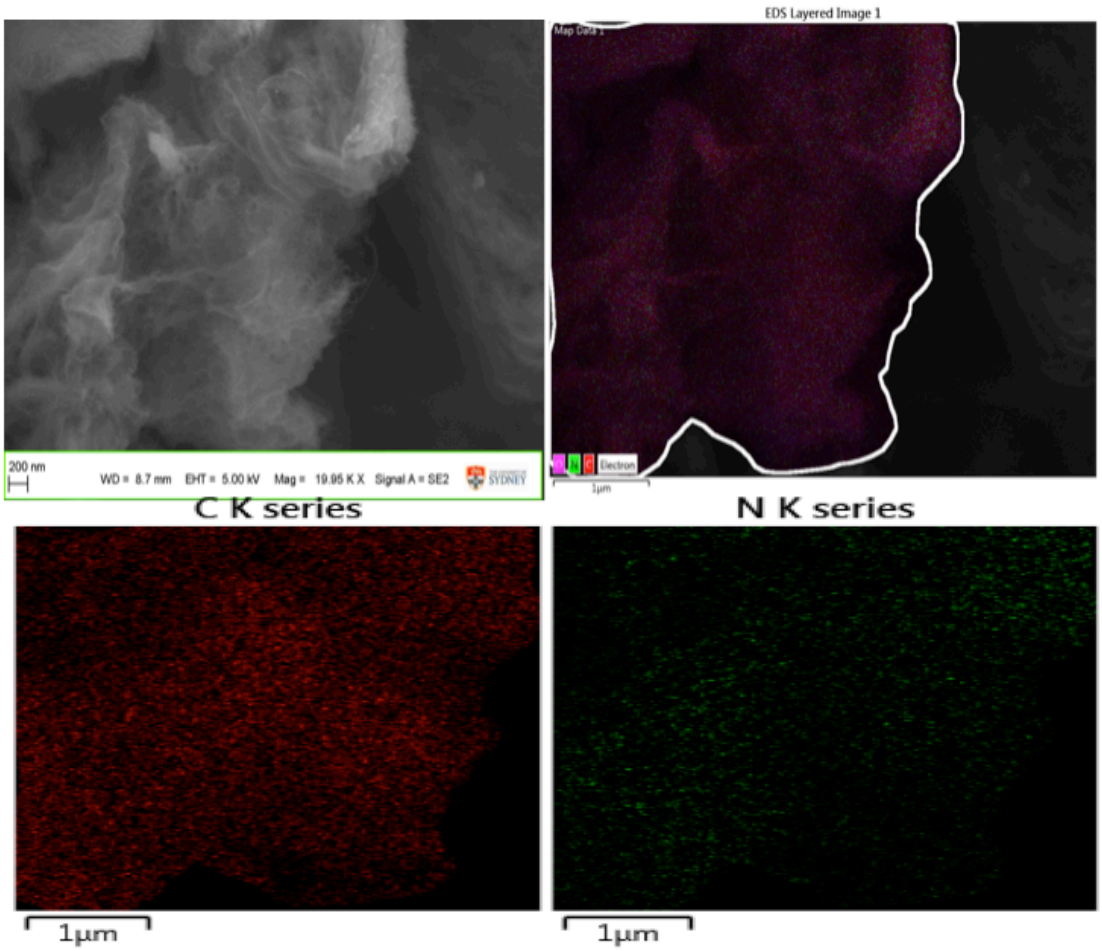

Figure 6: SEM-EDS mapping of N-Gr/CNT of elemental distribution of carbon and nitrogen.

SEM-EDS was applied to characterize the elemental distribution of carbon and nitrogen in the hybrid of N-Gr/CNT (Figure 6). From the EDS mapping, it is observed that the carbon and nitrogen atoms are distributed everywhere on the surface and the presence of high percentage of nitrogen all over the surface is found. To characterize the elemental composition and content of nitrogen in the composites, X-ray photoelectron spectroscopy (XPS) measurements were carried out on both of the composites. From the XPS measurements of N-Gr/CNT and PM-NG/NCNT, the survey spectra of both of the composites revealed the presence of C, O and N. (Figure 7a) In both of the composites, the high-resolution C1s peak was centered at 284.4 eV tailing at higher binding energies, indicating the connection of carbon atoms with N and O heteroatoms. The peak deconvolution of N1s showed (Figure 7b) five possible nitrogen configurations in N-Gr/CNT. These included 46.0% pyridinic N (N1, N in 6-member ring), 14.4% pyrrolic N (N2, N in 5-

member ring), 31.0% graphitic N (N3, N in graphene basal plane), 6.2% oxidized N (N4, N-O) and 2.4% protonated N (N5, N-H) in the total nitrogen content of 11.21%. The N1s peak deconvolution of PM-NG/NCNT showed 46.4% pyridinic N, 13.6% pyrrolic N, 28.5% graphitic N, 9.3% oxidized N and 2.2% protonated N (N5, N-H) (Figure S4) in total nitrogen content of 6.9%. The atomic percentage of Nitrogen found higher in N-Gr/CNT possibly due to the better interaction of the compounds with the dopant during the one pot mixing before pyrolysis. The Brunauer-Emmett-Teller (BET) surface are of both of the composites were measured and the higher surface area of N-Gr/CNT (293 m^2 g^{-1}) than the surface area of PM-NGr/NCNT (210 m^2 g^{-1}) were observed. The surface areas are higher than the surface area measured for NGr (198 m^2 g^{-1}) synthesized *via* similar method. [38] The total pore volume of N-Gr/CNT is found to be 0.55 cm^3 g^{-1}, the micropore volume 0.035 cm^3 g^{-1}, the average pore width 7.4 nm and the average pore diameter 3.8 nm. The formation of appropriate distribution of micropores and mesopores evaluated from the calculation using the conventional DFT method on the N_2 adsorbtion isotherm part ensures rapid ion diffusion.

Electrochemical Properties of N-Gr/CNT for Supercapacitors.

Cyclic voltammetry (CV) was used to investigate the electrochemical behavior of NG, NCNT, NGr/CNT and PM-NG/NCNT deposited on an ITO-coated glass electrode in 1.0 M aqueous H_2SO_4 electrolyte at potential limits of 1.1 to -0.2 V *vs*. Ag/AgCl electrode in a three-electrode system at a scan rate of 100 mV/s. (Figure 7c) 10 wt% PTFE solution was used as binder. From the CVs, it was observed that the CV of NCNT showed the lowest capacitive response due to the low capacitance property of multiwalled carbon nanotube. [45, 46] The NGr showed better capacitive behavior than the NCNT due to the contribution of electrochemical double layer capacitance and increased surface area for the nitrogen doping. [47] Interestingly, the capacitive response of PM-NG/CNT was slightly lower than the NG even though it has supposed to have some increment of capacitance due to have relatively higher surface area than NGr. The possible reason for this relatively low capacitance of PM-NG/NCNT is due to the lack of three-dimensional structure as well as low capacitive response of NCNT, which affects on the overall capacitance properties of the composite. [45]

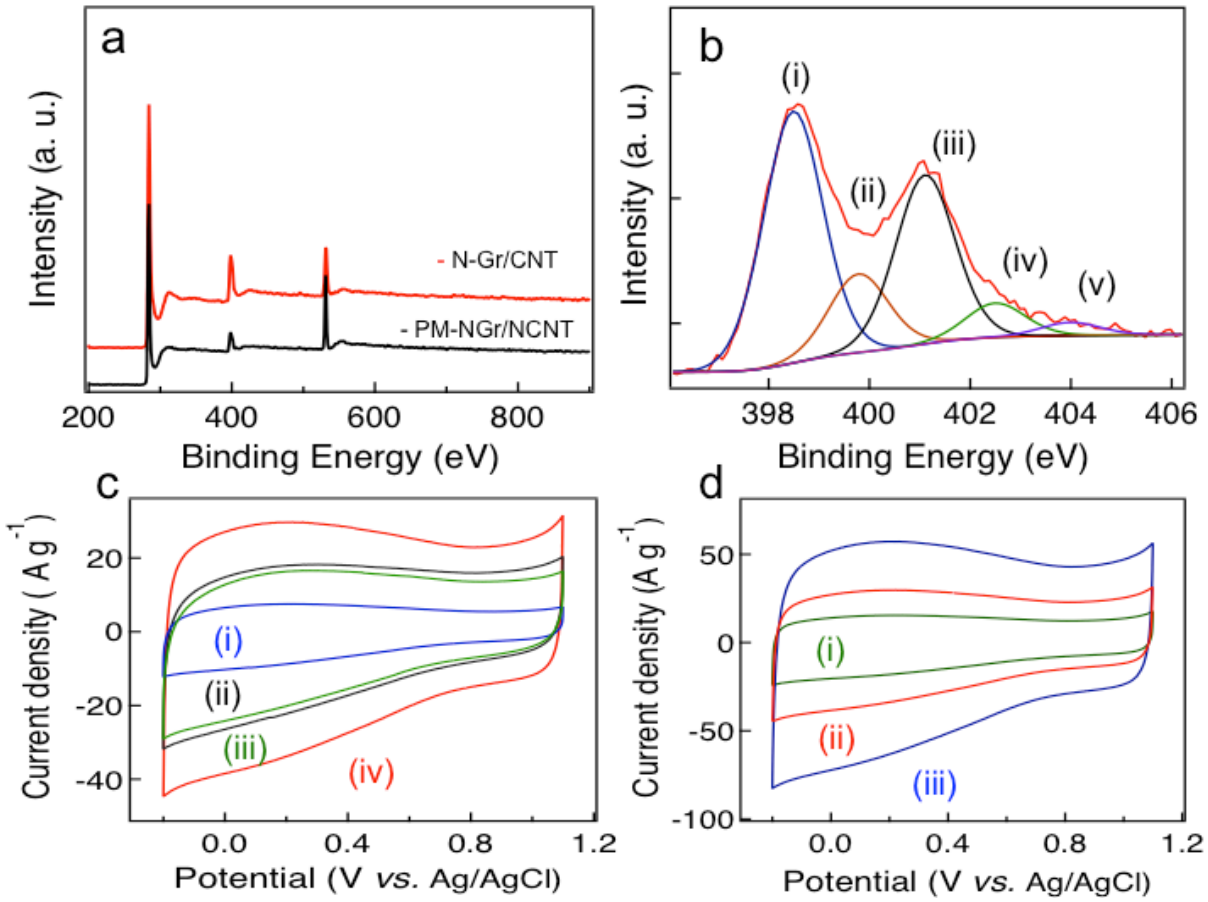

Figure 7: (a) XPS survey of N-Gr/CNT and PM-NGr/NCNT. (b) N 1s XPS peak of N-Gr/CNT. (c) Cyclic voltammograms of (i) NCNT, (ii) NGr, (iii) PM-NG/NCNT and (iv) N-Gr/CNT using a three-electrode cell at a scan rate of 100 mV s^{-1} in 0.5-M H_2SO_4 solution, (d) Cyclic voltammograms of N-Gr/CNT at different scan rates (i) 50, (ii) 100 and (iii) 200 mV s^{-1}.

The CV of N-Gr/CNT showed the highest capacitive response with electrochemical double layer capacitance indicated the better penetration of ions inside the lamellar structure of the composite. The spacing formed due to the intercalation of CNTs on the edges between the graphene layers provides the electrolyte to penetrate and get the maximum capacitive responses from both side of the graphene layer. The CV curves of N-Gr/CNT at different scan rates of 50, 100 and 200 mV/s showed increment of capacitive response with the scan rates. (Figure 7d)

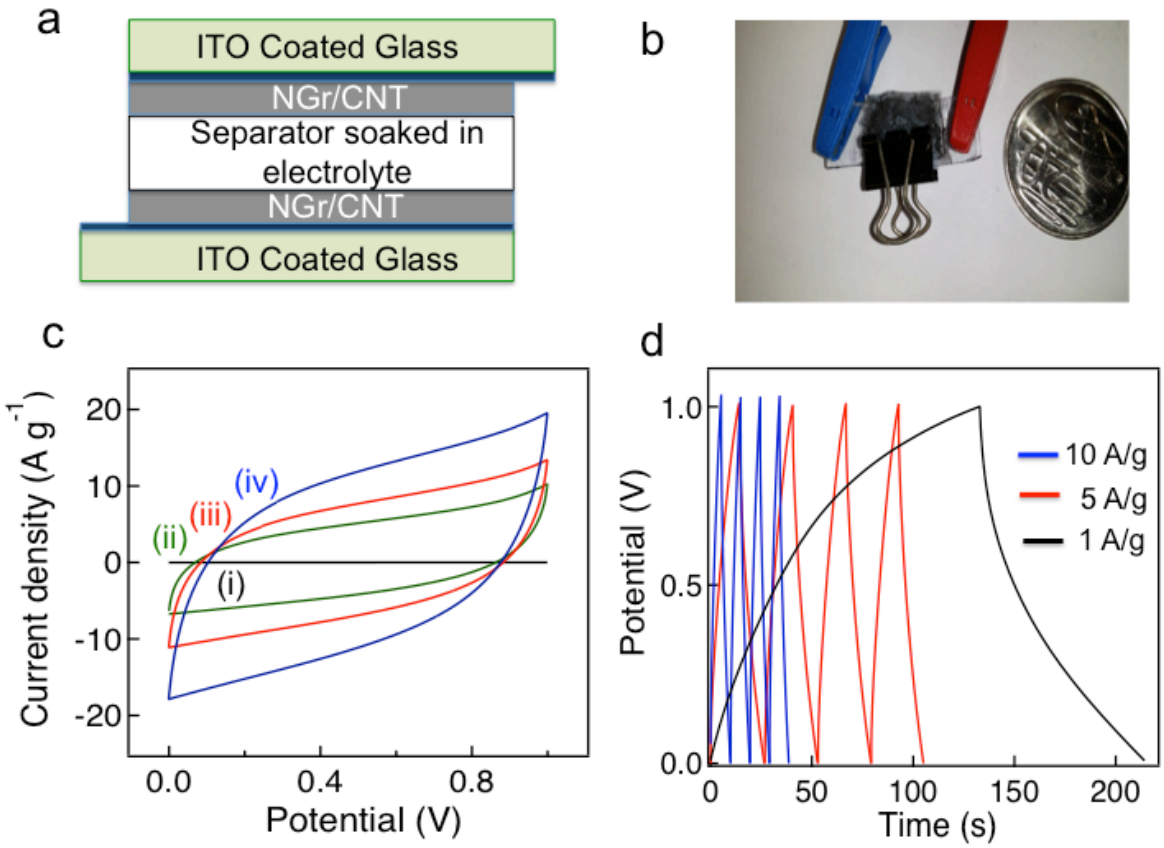

Figure 8: (a) Schematic diagram of 2-electrode solid-state supercapacitor using ITO-coated glass as current collector, (b) Optical image of the two-electrode cell, (c) Cyclic voltammograms of N-Gr/CNT and bare ITO-coated glass in two-electrode solid-state cell at different scan rates (i) bare ITO-coated glass, (ii) 50, (iii) 100 and (iv) 200 mV s^{-1}, (d) Galvanostatic charge/discharge curves for N-Gr/CNT in a two-electrode cell tested at current density of 1–10 A g^{-1}.

To reveal the capacitive properties of N-Gr/CNT for practical application, a two-electrode solid-state cell based on ITO-coated glass with an area of 1 cm^2 (1 cm x 1 cm) was constructed. (Figure 8a and 8b) The active material was drop casted on the conductive side of the electrodes by dispersing the composite material in isopropanol solution with a PTFE binder and dried in room temperature. The PP separator (Celgard) for aqueous electrolyte was soaked first in the electrolyte solution for 1 hour and then the two electrodes were sandwiched with a pressure inserting the separator between them. CV recorded in the cell at different scan rates (50, 100 and 200 mV/s) showed near ideal rectangular voltammetric responses (Figure 8c), The specific capacitance (*Csp*) of the electrode material was calculated from the galvanostatic discharge

curves (Figure 5d). The *Csp* value for N0Gr/CNT was found to be 324 F/g in 0.5 M H_2SO_4 at a current density of 1 A/g. At a high current density of 10 A/g, the specific capacitance value remained as high as 220 F/g. After achieving the high capacitance property in sandwiched based two-electrode device, a solid-state two-electrode device had been fabricated by gelifying the electrolyte replacing the separator soaked with electrolyte (Figure 9a and 9b). The fabrication of solid-state devices is highly important for future portable, wearable and flexible electronics. [48] The gelification of electrolyte was performed by the mixing of heated PVA solution with sulphuric acid following the reported procedure. [22] The solid-state device has been fabricated by putting a glass spacer between the active material deposited on the ITO-coated glass and the empty space between the two electrodes was filled up by the gel electrolyte. The electrochemical properties of solid-state device has been explored by the cyclic voltammetry and the CV curves (Figure 9c) at high scan rates (100, 200 and 500 mV s^{-1}) showed reversible electrochemical properties with high capacitance with slight resistivity, which is obvious for solid electrolytes. The galvanostatic charge-discharge curves showed distortion from the theoretical ideal charge discharge curve due to the contribution of pseudo capacitance and for device fabrication (Figure 9d). The specific capacitance was obtained from the discharge curve showing 312 F/g at a high current density of 1 A/g. The high capacitance behavior also remains to 220 F/g at high current density of 10 A/g. The specific capacitance of solid-state device is slightly lower than the specific capacitance of two-electrode device, which is due to formation of resistivity for gelifying. However, even the formation of resistivity hampers the capacitance properties, but the replacement of separator shorten the transport length of ions which contribute better ion diffusion on the electrode, hence indicating the slight decrease of capacitance properties. The comparison of CV curves and charge-discharge curve also showed the distortion for gel electrolyte in the solid-state device (Figure 10). The volumetric capacitance was calculated by multiplying the electrode mass density with the gravimetric capacitance. The mass density of N-Gr/CNT was calculated from the average thickness of mass loading on the electrode by cross sectional SEM. The value of mass density was found 0.97 g cm^{-3}, which is reasonable due to the high mass loading of the active material on the electrode. This value is also comparable with the reported three-dimensional composite of activated graphene/ single-walled carbon nanotube (1.06 g cm^{-3}). [30] The volumetric capacitance of 302 F cm^{-3} at a high current density of 1 A g^{-1} is the highest value among the reported values for capacitance related to graphene/crabon

nanotube based supercapacitors so far as well as comparable with the three-dimensional structured nanocarbon based supercapacitors [30].

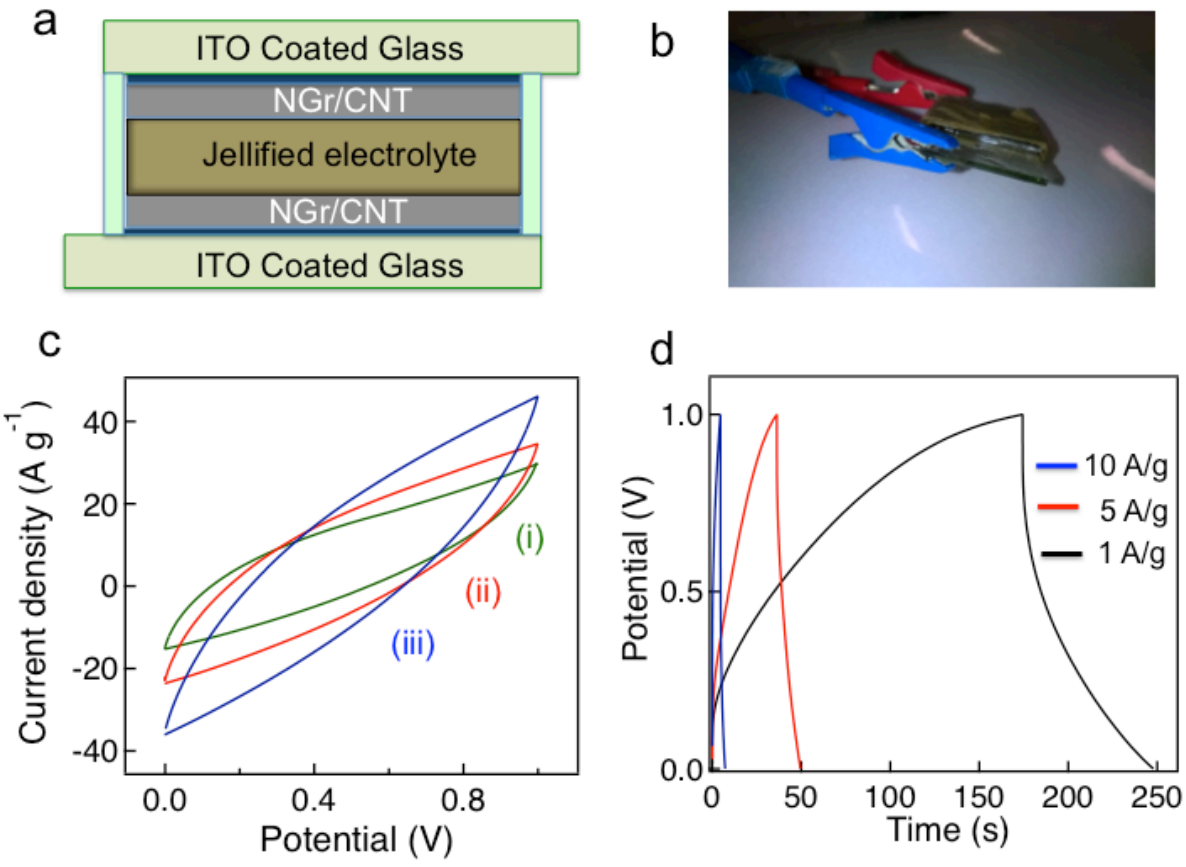

Figure 9: (a) Schematic diagram of 2-electrode solid-state supercapacitor using gellyfied electrolyte and ITO-coated glass as current collector, (b) Optical image of the two-electrode cell, (c) Cyclic voltammograms of N-Gr/CNT in two-electrode solid-state cell at different scan rates (i) 100 and (ii) 200 and (iii) 500 mV s^{-1}, (d) Galvanostatic charge/discharge curves for N-Gr/CNT in a two-electrode solid-state cell tested at current density of 1–10 A g^{-1}.

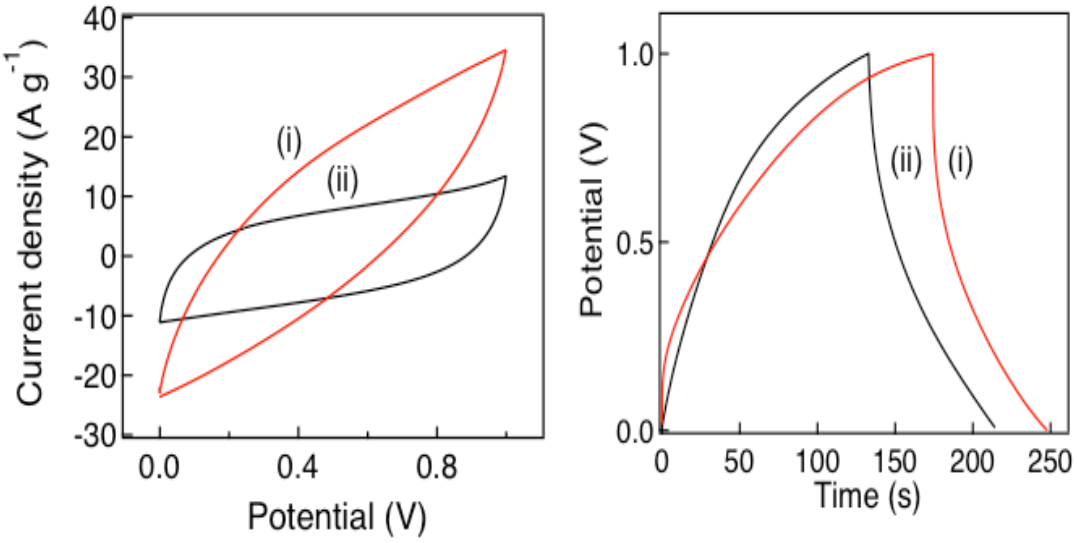

Figure 10: (a) Comparison of CVs of (i) Solid-state cell with gellyfied electrolyte and (ii) Solid-state cell with soaoked electrolyte membrane at a scan rate of 100 mV s^{-1}, (b) Comparison of charge-discharge curvess of (i) Solid-state cell with gellyfied electrolyte and (ii) Solid-state cell with soaoked electrolyte membrane at a current density of 1 A g^{-1}.

The energy density and the power density of the device were calculated based on the discharge rates. The highest energy density of 15.60 Wh/kg had been achieved at the power density of 702 W/kg and the energy density of 11 Wh/kg retained at a high power density of 6600 W/kg. The high capacitance performance of N-Gr/CNT could be attributed for the addition of pseudocapacitance with the electrochemical double-layer capacitance, due to the presence of high atomic percentage of nitrogen enriched with high ratio of pyrrolic N and graphitic N. [38, 47] The high surface area, pore volume and lamellar structure provided excellent electrical conductivity with favorable electrolyte penetration. The cycle stability of the device was also investigated at a high current density of 5 A/g for 2000 cycles between 1.0 and 0 V (Figure 11). To observe the life time of the solid-state cell, the cycling test was continuing upto 10000 cycles at high current density of 5 A/g and the cell exhibited the retention of 96% of its initial capacity after 2000 cycles, 82% after 5000 cycles and 46% after 10000 cycles, which indicates its stability at very high current density even in gellyfied electrolyte and laboratory grade manual fabrication (Figure 11a). The Nyquist plots before and after cycling confirmed the high electrochemical stability of the device (Figure 11b).

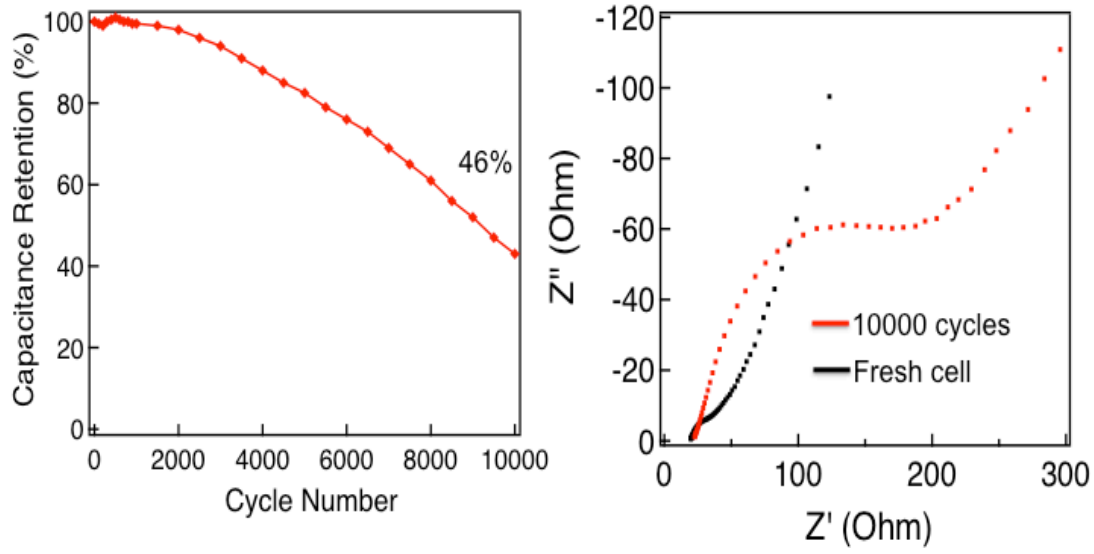

Figure 11: (a) Cycling test of Solid-state cell of gel electrolyte, (b) EIS of Solid-state cell with gel electrolyte at initial stage and after 10000 cycles.

Electrochemical Performance of N-Gr/CNT as Anode for Li-Ion Battery.

Three-dimensional porous carbon structure has been shown as excellent anode materials in metal-ion batteries. [6, 49-51] The incorporation of nitrogen doping in the three-dimensional structure can increase the Li-ion storage capacity, facilitate Li-ion adsorption, enhance ion diffusion through the structural defects and increase the stability. [26, 52-54] After observing the superior capacitance performance, the active material N-Gr/CNT has been utilized to explore the electrochemical properties as anode for Li-ion battery as this material enriched with lamellar structure with large surface area with efficient pore volume and high atomic percentage of nitrogen. The cyclic voltammograms profiles from 0 to 3 V exhibits the activity of the composite for lithium-ion batteries (Figure 12a). The CV curves were quite similar after the second cycle indicating a stable state. The capacity above 0.5 V is associated with defects, 3D architectures and layers, pores and Li binding with heteroatom [49, 55, 56] and from the CV curves the peak at 0.9 V indicates the binding of Li ions with heteroatom. During the Li-extraction process, the potential hysteresis showing the removal of inserted lithium ions at a wide potential of 0.1 to 3 V with the associated peaks of 0.1 and 1.2 V for lithium extraction from graphene layers and pore

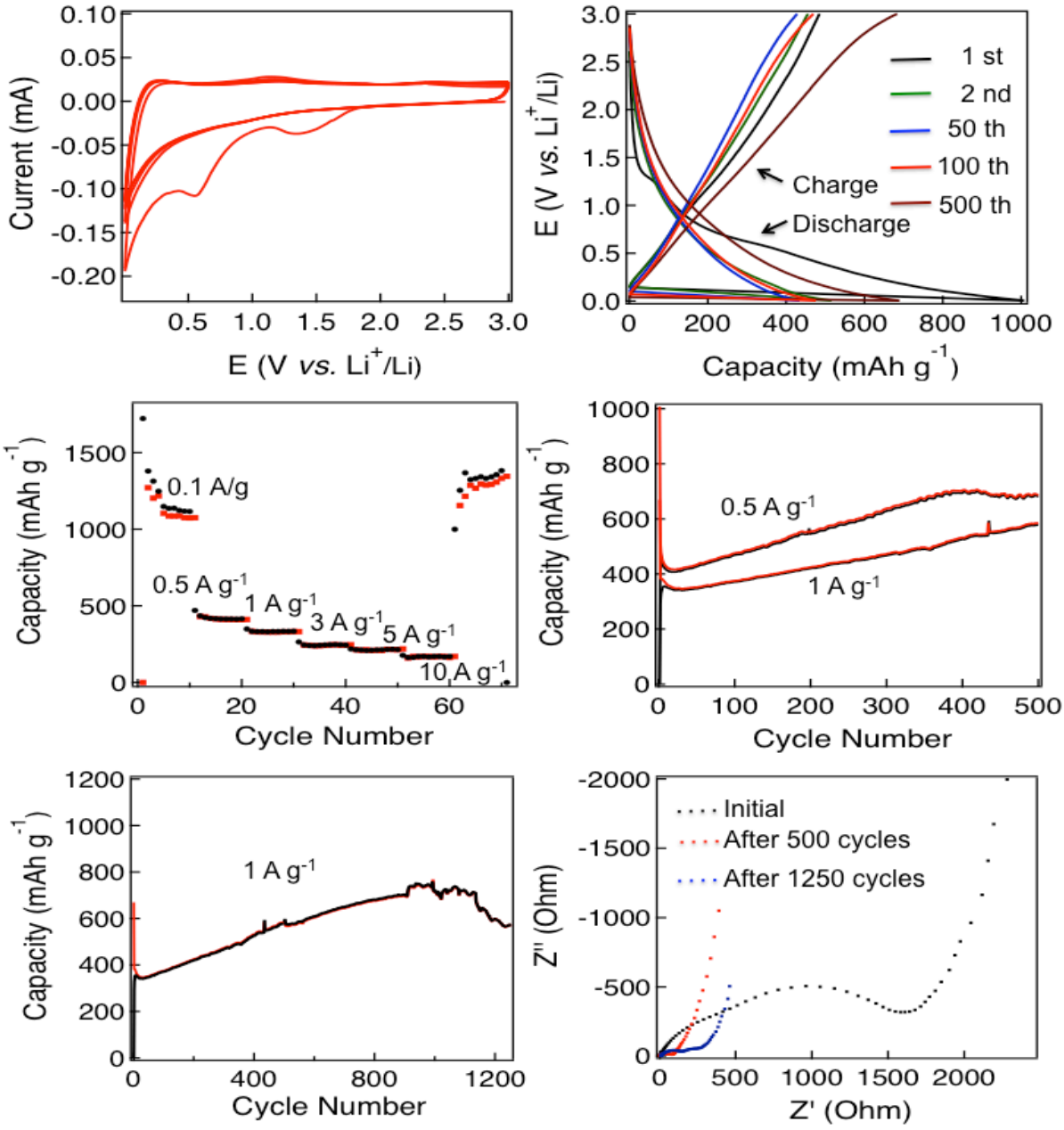

Figure 12: (a) CV curves (1st to 5th cycles) of N-Gr/CNT cell at a scan rate of 0.1 mV s^{-1}, (b) Discharge/charge curves from 1st, 2nd, 50th, 100th and 500th cycles, (c) Rate performance at various current densities, (d) High-rate cycling performance in the voltage range from 0.01 to 3.0 V at current densities of 0.5 A/ g and 1 A/g for 500 cycles, (e) High-rate cycling performance in the voltage range from 0.01 to 3.0 V at current densities of 1 A/g for 1250 cycles, (f) EIS of the cell at initial, after 500 cycles and after 1250 cycles.

structures or defects. [57, 58] The charge-discharge current densities from the capacity over cycling initiating from 0.1 to 10 A/g showing the reverible capacities of 1150, 500, 350, 300, 250 and 200 mA h/g at 0.1, 0.5, 1, 3, 5 and 10 A/g (60 cycle) (Figure 12b). After cycling at various rates, the specific capacity can still be recovered to 1150 mA h/g, implying high stability and reversibility. The specific capacitance of 1150 mA h/g obtained at 0.1 A/g is 3 times greater compared to the theoretical capacity of graphite (372 mA h/g) and is the highest capacity that has been reported so far for metal-free N-doped graphene and N-doped graphene/carbon nanotube based anode materials.[49] The cycling stability with reversible battery capacity were observed 1150, 400 and 350 mA h/g at current density of 0.1, 0.5 and 1 A/g in the first cycle (Figure 12c).The capacitance at low current density of 0.1 A/g remain constant after 500 cycles, interestingly rapid increment of capacitance were observed at high current density of 0.5 and 1 A/g (Figure 12d). The stability of the cell for long cycle life at high current density of 1 A/g was observed and the cell shows remarkable stability up to 1250 cycles with better retention of capacity than initial cell (Figure 12e). This behavior can be explained from the Nyquist plot of initial cell, after 500 cycles and after 1250 cycles (Figure 12f). At the initial the conductivity of the cell was poor but after cycling the electrolyte got better permeation in the three-dimensional nanostructured material and could store more charge, which led to enhance the conductivity and capacitance. The EIS after 500 cycles showed high conductivity of the composite and after 1250 cycles the conductivity decreased than the 500 cycles but still higher than the initial. The lamellar structure with high nitrogen doping active material ease the ion diffusion through its porous structures created by the defects and efficiently recovered the large initial loss of capacity and enhanced the lithium storage performance storage at high rates.

Electrocatalysis Activity of N-Gr/CNT as bifunctional Eletrocatalyst of ORR and OER.

N-Gr/CNT was also tested as bifunctional electrocatalyst for the oxygen-reduction reaction (ORR) and oxygen-evolution reaction (OER) under alkaline conditions. Thus, N-Gr/CNT was deposited on a glassy carbon electrode (~12 ug mass loading) and its electrocatalytic activities with the related materials of NGr, NCNT and PM-NGr/NCNT were investigated using rotating disk electrodes (RDE). Figure 13a shows the linear sweep voltammograms of NGr, NCNT, PM-NGr/NCNT, N-Gr/CNT and Pt/C, all measured at a scan rate of 10 mV/s and rotation frequency of 1600 rpm in oxygen-saturated 0.1-M KOH(*aq*). The N-Gr/CNT produced the most positive

onset potential of +0.8 V and highest current density of –4.7 mA cm^{-2} among the synthesized composites compared to NGr, NCNT and PM-NGr/NCNT and close to the Pt/C. Further RDE measurements (Figure 13b) were thus used to calculate, via the Koutecky–Levich equation (Eq. 5), the number of electrons transferred to an oxygen molecule by the N-Gr/CNT electrode.

$$\frac{1}{J} = \frac{v^{1/6}}{0.2nFC_o D_o^{2/3}\omega^{1/2}} + \frac{1}{J_K} \quad \frac{1}{J} = \frac{\nu^{1/6}}{0.2nFC_o D_o^{2/3}\omega^{1/2}} + \frac{1}{J_K} \tag{5}$$

In the Koutecky–Levich equation, J, J_L, J_K are the measured current density, the diffusion-limiting current density and the kinetic-limiting current density, respectively; ω is the angular velocity of the disc, n is the overall number of electrons transferred in the oxygen reduction, F is the Faraday constant (96485 C mol^{-1}), C_o is the bulk concentration of oxygen (1.2×10^{-6} mol cm^{-3}), D_o is the diffusion coefficient of oxygen in 0.1-M KOH(aq) (1.9×10^{-5} cm^2 s^{-1}), v is the kinetic viscosity (0.01 cm^2/s) and 0.2 is a constant that is valid when the rotation speed is expressed in rpm. The Koutecky–Levich plot of J^{-1} *vs* $\omega^{-1/2}$ at a potential of 0.6 V on the N-Gr/CNT electrode exhibited good linearity (R^2 = 0.998). The average electron transfer number was 3.94 at different potentials of 0.6, 0.5, 0.4 and 0.3 V, (Figure 14a) which indicated that a four-electron process, with OH^- as the product, was the preferred pathway.

To further investigate the potential application of three-dimensional metal-free nanostructured N-Gr/CNT, the electrocatalytical activity of OER was assessed by sweeping the RDE potential from 1.0 to 2.0 V. From the LSV curves of N-Gr/CNT, PM-NGr/NCNT, Ru/C and Pt/C plotted in Figure 13c, the onset potentials were measured 1.48, 1.50, 1.46, and 1.68 V respectively. The potentials for a current density of 10 mA cm^{-2} for N-Gr/CNT, PM-NGr/NCNT, Ru/C and Pt/C were evaluated at 1.65, 1.76, 1.64 and 1.88 V respectively as the required potential to oxidize water at the current density of 10 mA cm^{-2} is used to judge the OER activity. Therefore, N-Gr/CNT exhibited the lowest onset potential and large current density among the studied catalysts of PM-NGr/NCNT and Pt/C as well as almost similar to Ru/C (one of the best electrocatalysts for OER at present). [59] The Tafel slope for the N-Gr/CNT, Ru/C and Pt/C were about 126, 109 and 238 mV/decade respectively, much smaller than the Pt/C (238 mV/decade) and slightly larger than the Ru/C, which indicated the better OER activity of N-Gr/CNT (Figure 14b). The OER performance of N-Gr/CNT was found to be superior to the

commercial Pt/C as well as similar to transition metal oxides supported by carbon materials, [60, 61] metal-free three dimensional carbon nanostructures [28, 62] and dual doped carbon. [59, 63]

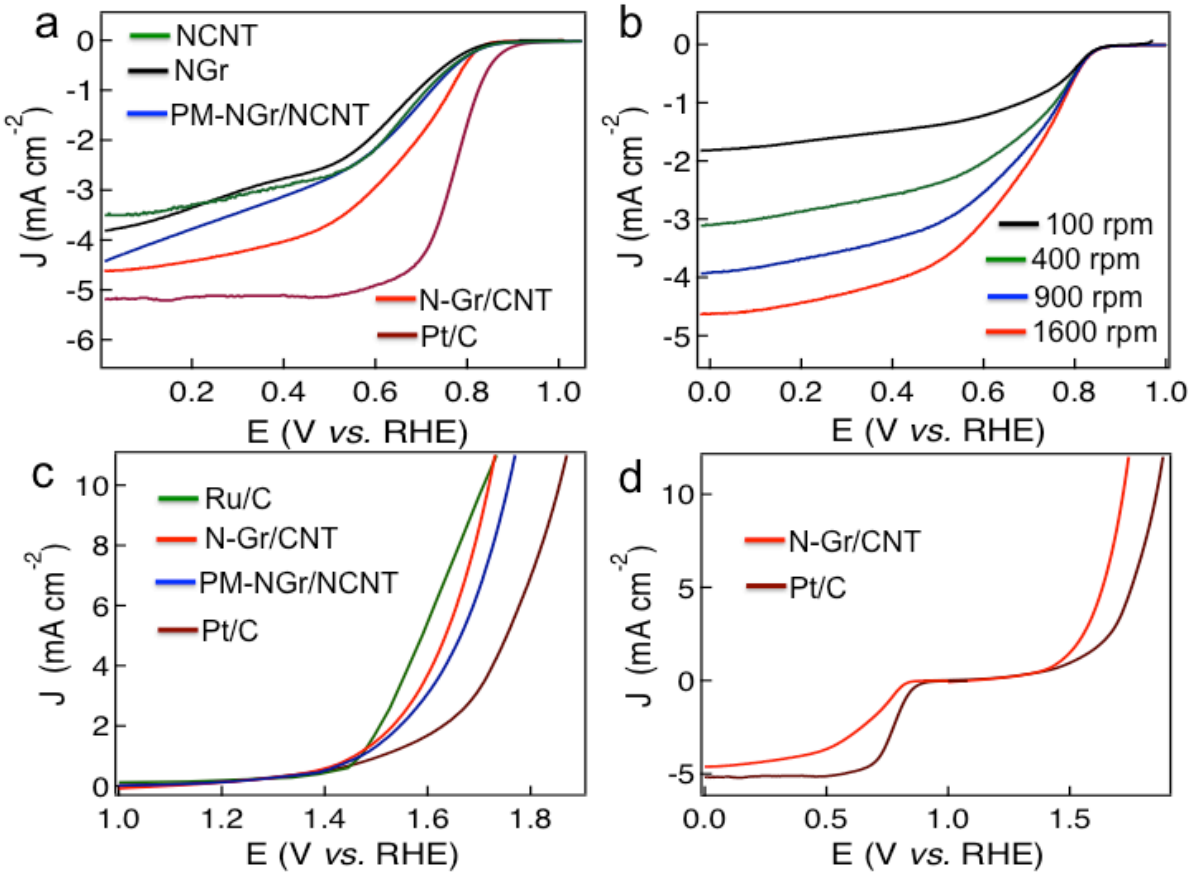

Figure 13: (a) Linear sweep voltammograms (LSV) of NCNT, NGr, PM-NGr/NCNT, N-Gr/CNT and Pt/C at 1600 rpm and a scan rate of 10 mV/s in O_2-saturated 0.1-M KOH(*aq*), (b) RDE measurements of N-Gr/CNT in O_2-saturated 0.1-M KOH(*aq*) at scan rates of 10 mV/s, (c) Linear sweep voltammograms (LSV) of N-Gr/CNT, PM-NGr/NCNT, Ru/C and Pt/C at a scan rate of 10 mV/s in 0.1-M KOH(*aq*), (d) LSV curves of N-Gr/CNT and Pt/C on an RDE (1600 rpm) in O_2-saturated 0.1-M KOH(*aq*) at scan rates of 10 mV/s showing the electrocatalytic activities towards both ORR and OER.

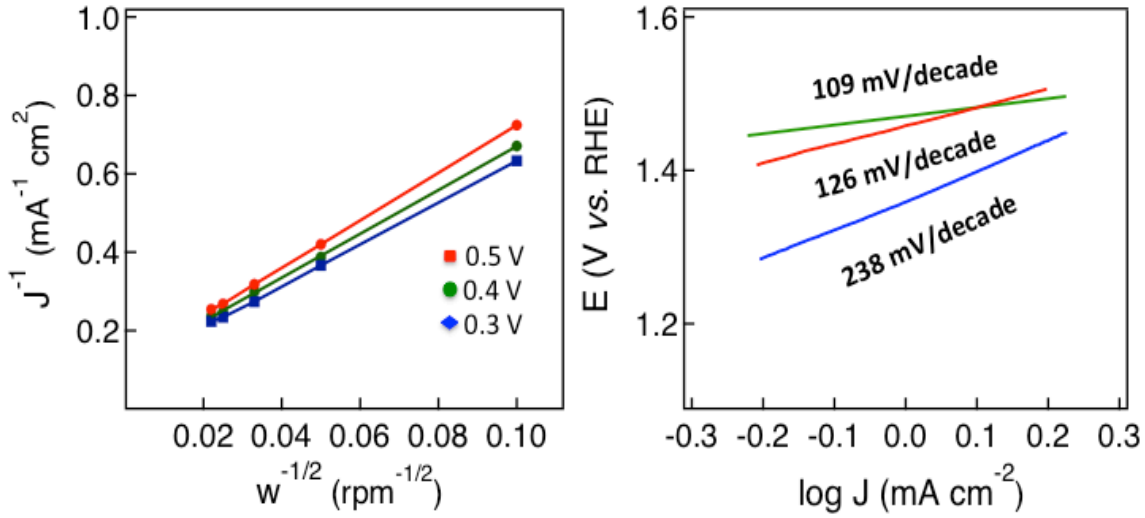

Figure 14. (a) Koutecky–Levich plot of N-Gr/CNT at an electrode potential of 0.3, 0.4 and 0.5 V vs. RHE. (b) shows the tafel plots for N-Gr/CNT (126 mV/decade), Ru/C (109 mV/decade) and Pt/C (238 mV/decade).

Even though the exhibition of OER activities in metal-free nitrogen-doped few layers graphene is highly rare, [59, 62-64] the possible reason of the attribution of OER activity in N-Gr/CNT due to its three-dimensional nanostructure as well as the presence of high atomic percentages of N including high level of pyridinic N and graphitic N with the large surface area with high pore volume. The three dimensional nanostructured with CNTs on the edge of graphene layers and high percentage of pyridinic N and graphitic N on the edge of the surface creates the active sites for efficient bi-catalysis reaction towards oxygen reduction and evolution. The comparison of bifunctional electrocatalysis with Pt/C measuring by LSV plots at 1600 rpm in oxygen-saturated 0.1 M KOH, (Figure 13d) the comparable ORR with four electrons transfer pathway and better OER activity of N-Gr/CNT were observed. In ORR the onset potential and current density of N-Gr/CNT were lower than the commercial Pt/C as it is the state-of-the-art ORR electrode, however in OER the good catalytic activity of N-Gr/CNT was reflected for its lower onset potential and higher current density than the Pt/C and similar to Ru/C. Thus this active material can be a potential platform for developing bifunctional electrocatalyst for metal-air batteries and rechargeable fuel cells with its remarkable capacitance properties for the charge storage both in the capacitors and batteries. These multifunctional electrochemical properties can of the

composite can led to fabricate hybrid devices like solid state metal ion supercapacitors, metal-air batteries and rechargeable fuel cells.

5.4. CONCLUSION

In conclusion, we report a facile synthesis method of three-dimensional lamellar structured nitrogen-doped graphene/ carbon nanotube hybrid containing high surface areas (~295m^2/g) as well as all high atomic percentage of nitrogen. The synthesized N-Gr/CNT showed excellent capacitive properties as fabricated in a solid state supercapacitor device, high rate capability anode in lithium-ion battery and metal-free bifunctional electrocatalyst of ORR and OER. These multifunctional properties could lead to fabricate a hybrid energy storage device, high performance metal-air batteries and rechargeable fuel cell. The superb stability and efficient electro-catalytic activity could make this material an ideal candidate not only in the field of supercapacitors, batteries and fuel cell electrodes but also in the area of hybrid solid state energy storage, hybrid solar cell with storage and transparent conductive displays. The incorporation of nanoparticles, polymers and other carbon-based nanostructures could further enhance the electrochemical properties for a broader range of applications.

REFERENCES

1. Winter, M.; Brodd, R. J. What Are Batteries, Fuel Cells, and Supercapacitors. *Chem. Rev.* **2004**, *104*, 4245-4269.

2. Liu, C.; Li, F.; Ma, L. P.; Cheng H. M. Advanced Materials for Energy Storage. *Adv. Mater.* **2010**, *22*, E28-E62.

3. Zhang, J.; Xia, Z.; Dai, L. Carbon-based Electrocataysts for Advanced Energy Conversion and Storage. *Sci. Adv.* **2015,** *1*, 1500564-1500583.

4. Candelaria, S. L.; Shao, Y.; Zhou, W. Li, W.; Li, X.; Xiao, J.; Zhang, J. –G.; Wang, Y.; Liu, J.; Li, J.; Cao, G. Nanostructured carbon for Energy Storage and Conversion. *Nano Energy* **2012,** *1,* 195-220.

5. Simon, P.; Gogotsi, Y. Materials for Electrochemical Capacitors. *Nature Mater.* **2008**, *7*, 845-854.

6. Kaskhedikar, N. A.; Maier, J. Lithium Storage in carbon nanostructures. *Adv. Mater.* **2009,** *21,* 2664-2680.

7. Novoselov, K. S.; Geim, A. K.; Morozov, S. V.; Jiang, D.; Zhang, Y.; Dubonos, S. V.; Grigorieva, I. V.; Firsov, A. A. *Science* **2004,** *306,* 666-669.

8. Nair, R. R.; Blake, P.; Grigorneko, A. N.; Novoselov, K. S.; Booth, T. J.; Stauber, T.; Peres N. M. R.; and Geim, A. K. *Science,* **2008,** *320,* 1308-1308.

9. Stoller, M. D.; Park, S.; Zhu, Y.; An J.; Ruoff, R. S.; *Nano Letter.* **2008,** *8,* 3498-3502.

10. Geim, A. K.; Novoselov, K. S. The Rise of Graphene. *Nature Mater.* **2007**, *6*, 183-191.

11. Li, D.; Muller, M. B.; Gilje, S.; Kaner, R. B.; Wallace, G. G. Processable Aqueous Dispersions of Graphene Nanosheets. *Nature Nanotechnol.* **2008,** *3,* 101-105.

12. Zhao, Y.; Liu, J.; Hu, Y.; Cheng, H.; Hu, C.; Jiang, C.; Jiang, L.; Cao, A.; Qu, L. Highly Compression-Tolerant Supercapacitor Based on Polypyrrole-mediated Graphene Foam Electrodes. *Adv. Mater.* **2013**, *25,* 591-595.

13. Xu, Y.; Sheng, K.; Li, C.; Shi, G. Self-Assembled Graphene Hydrogel *via* a One-Step Hydrothermal Process. *ACS Nano* **2010**, *4,* 4324-4330.

14. Luo, J.; Hang, H. D.; Huang, J. Effect of Sheet Morphology on the Scalability of Graphene-Based Ultracapacitors. *ACS Nano* **2013,** *7,* 1464-1471.

15. Zhu,Y.; Murali, S.; Stoller, M. D.; Ganesh, K. J.; Cai, W.; Ferreira, P. J.; Pirkle, A.; Wallace, R. M.; Cychosz, K. A.; Thommes, M.; Su, D.; Stach, E. A.; Ruoff, R. S. Carbon-Based Supercapacitors Produced by Activation of Graphene. *Science* **2011**, *332,* 1537-1541.

16. Choi, H. J.; Jung, S. M.; Seo, J. M.; Chang, D. W.; Dai, L.; Baek, J. B. Graphene for Energy Conversion and Storage in Fuel Cells and Supercapacitors. *Nano Energy* **2012**, *1*, 534-551.

17. Sun, Y.; Wu, Q.; Shi, G. Graphene based New Energy Materials. *Energy Environ. Sci.* **2011**, *4*, 1113-1132.

18. Huang, X.; Qi, X.; Boey, F.; Zhang, H. Graphene-Based Composites. *Chem. Soc. Rev.* **2012,** *41,* 666-686.

19. Wang, Y.; Wu, Y.; Huang, Y.; Zhang, F.; Yang, F.; Ma, Y.; Chen, Y. Preventing Graphene Sheets from Restacking for High-Capacitance Performance. *J. Phys. Chem. C* **2011,** *115,* 23192-23197.

20. Du, F.; Yu, D.; Dai, L.; Ganguli, S.; Varshney, V.; Roy, A. K. Preparation of Tunable 3D Pillared Carbon Nanotube-Graphene networks for High-Performance Capacitance. *Chem. Mater.* **2011,** *23,* 4810-4816.

21. Zhao, M. Q.; Zhang, Q.; Huang, J. Q.; Tian, G. L.; Chen, T. C.; Qian, W. Z.; Wei, F. Towards high Purity Graphene/single-walled carbon Nanotube Hybrids with Improved Electrochemical capacitive Performance. *Carbon* **2013,** *54,* 403-411.

22. Xue, Y.; Ding, Y.; Niu, J.; Xia, Z.; Roy, A.; Chen, H.; Qu, J.; Wang, Z. L.; Dai, L. Rationally designed graphene-nanotube 3D architectures with a seamless nodal junction for efficient energy conversion and storage. *Sci. Adv.* **2015,** *1,* 1400198-1400207.

23. Buglione, L.; Pumera, M. Graphene/Carbon nanotube Composites Not Exhibiting Synergic Effect for Supercapacitors: The Resulting Capacitance Being Average of Capacitance of Individual Components, *Electrochem. Commun.* **2012,** *17(1),* 45-47.

24. Gogotsi, Y. What Nano Can Do for Energy Storage. *ACS Nano* **2014,** *8(6),* 5369-5371.

25. Kholmanov, I. N.; Magnuson, C. W.; Piner, R.; Kim, J. –Y.; Aliev, A. E.; Tan, C.; Kim, T. Y.; Zakhidov, A. A.; Sberveglieri, G.; Baughman, R. H.; Rouff, R. S. Optical, Electrical and Electromechanical properties of Hybrid Graphene/Carbon nanotube Films. *Adv. Mater.* **2015**

26. Tang, C.; Zhang, Q.; Zhao, M. –Q.; Huang, J. –Q.; Cheng, X. –B.; Tan, G. –L.; Peng, H. –J.; Wei, F. Nitrogen-doped Aligned Carbon Nanotube/Graphene Sandwiches: Facile Catalytic Growth on Bifunctional Natural Catalysts and Their Applications as Scaffolds for High-Rate Lithium-Sulfur Batteries. *Adv. Mater.* **2014**, *26,* 6100-6105.

27. Zhu, Y.; Li, L.; Zhang, C.; Casillas, G.; Sun, Z.; Yan, Z.; Ruan, G.; Peng, Z.; Raji, A. –R.; Kittrell, C.; Hague, R. H.; Tour, J. M. A seamless three-dimensional carbon nanotube graphene hybrid material. *Nat. Commun.* **2012,** *3,* 1225-1232.

28. Tian, G. L.; Zhao, M. –Q.; Yu, D.; Kong, X. –Y.; Huang, J. –Q.; Zhang, Q.; Wei, F. Nitrogen-doped Graphene/Carbon nanotube Hybrids: In Situ Formation on Bifunctional Catalysts and Their Superior Electrocatalytic Activity for Oxygen Evolution/ Reduction Reaction. *Small* **2014,** *10(11),* 2251-2259.

29. Kotal, M.; Bhowmick, A. K. Multifunctional Hybrid materials based on Carbon nanotube Chemically Bonded to Reduced Graphene Oxide. *J. Phys. Chem. C,* **2013,** *117,* 25865-25875.

30. D. T. Pham, T. H. Lee, D. h. Luong, F. Yao, A. Ghosh, V. T. Le, T. h. Kim, B. li, J. Chang and Y. H. Lee, Carbon Nanotube-Bridged graphene 3D Building Blocks for Ultrafast Compact Supercapacitors. *ACS Nano,* **2015,** *9(2),* 2018-2027.

31. Jung, N.; Kwon, S.; Lee, D.; Yoon, D.; Park, Y. M.; Benayad, A.; Choi, J.; Park J. S. Synthesis of Chemically Bonded Graphene/Carbon Nanotube Composites and their Application in Large Volumetric Capacitance Supercapacitors. *Adv. Mater.* **2013**, *25,* 6854-6858.

32. Liu, H.; Liu, Y.; Zhu, D. Chemical Doping of Graphene. *J. Mater. Chem.* **2011**, *21*, 3335-3345.

33. Guo, B.; Fang, L.; Zhang, B.; Gong, J. R.; Graphene Doping: A Review. *Insciences J.* **2011**, *1*, 80-89.

34. Wang, H.; Maiyalagan, T.; Wang, X. Review on Recent Progress in Nitrogen-Doped Graphene: Synthesis, Characterization, and Its Potential Applications. *ACS Catal.* **2012**, *2*, 781-794.

35. Wen, Z.; Wang, X.; Mao, S.; Bo, Z.; Kim, H.; Cui, S.; Lu, G.; Feng, X.; Chen, J. Crumpled Nitrogen-Doped Graphene nanosheets with Ultrahigh Pore Volume for High-Performance Supercapacitor. *Adv. Mater.* **2012,** *24,* 5610-5616.

36. Shui, J.; Du, F.; Xue, C.; Li, Q.; Dai, L. Vertically Aligned N-Doped Coral-like Carbon Fiber Arrays as Efficient Air Electrodes for High-Performance Nonaqueous Li-O_2 Batteries. *ACS Nano* **2014,** *8,* 3015-3022.

37. Jalili, R.; Aboutalebi, S. H.; Esrafilzadeh, D.; Shepherd, R. L.; Chen, J.; Yamini, S. A.; Konstantinov, K.; Minett, A. I.; Razal, J. M.; Wallace, G. G. Sclable One-Step Wet-Spinning of Graphene Fibers and Yarns from Liquid Crystalline Dispersions of Graphene Oxide: Towards Multifunctional Textiles. *Adv. Func. Materials* **2013,** *23,* 5345-5354.

38. Faisal, S. N.; Haque, E.; Noorbehesht, N.; Zhang, W.; Harris, A. T.; Church, T. L.; Minett, A. I. N-Doped Graphene with High Atomic Percentages of Pyridinic N and Graphitic N as Electrode for High-Performance Supercapacitor and Efficient Bifunctional Electrocatalyst for ORR and OER**.** *Carbon*, **2016** (under review).

39. Variava, M. F.; Church, T. L.; Husin, A.; Harris, A. T.; Minett, A. I. A Simple Gas-Solid Route To Functionalize Ordered Carbon, *ACS Appl. Mater. Interfaces* **2014,** *6,* 2910-2916.

40. Presores, J. B.; Swift, J. A. Adhesion Properties of Uric Acid Crystal Surfaces. *Langmuir*, **2012**, *28*, 7401-7406.

41. H. Asami and H. Saigusa, Multiple Hydrogen-Bonding Interactions of Uric Acid/9-Methyluric Acid with Melamine Identified by Infrared Spectroscopy, *J. Phys. Chem. B* **2014,** *118,* 4851–4857.

42. N.-J. Song, C.-M. Chen, C. Lu, Z. Liu, Q.-Q. Kong and R. Cai, Thermally reduced graphene oxide films as flexible lateral heat spreaders, *J. Mater. Chem. A* **2014**, *2*, 16563–16568.

43. Y. Hernandez, V. Nicolosi, M. Lotya, F. M. Blighe, Z. Sun, S. De, I. T. McGovern, B. Holland, M. Byrne, Y. K. Gun'ko, J. J. Boland, P. Niraj, G. Duesberg, S. Krishnamurthy, R. Goodhue, J. Hutchison, V. Scardaci, A. C. Ferrari, J. N. Coleman, High-yield production of graphene by liquid-phase exfoliation of graphite. *Nat. Nanotechnol.* **2008,** *3,* 563-568.

44. C. Ferrari, D. M. Basko, Raman spectroscopy as a versatile tool for studying the properties of graphene, *Nat. Nanotechnol.* **2013,** *8,* 235–246.

45. L. Buglione and M. Pumera, Graphene/carbon nanotube composites not exhibiting synergic effect for supercapacitors: The resulting capacitance being average of capacitance of individual components, *Electrochem. Commun.* **2012,** *17(1),* 45–47.

46. Frackowiak, E.; Metenier, K.; Bertagna, V.; Beguin, F. Supercapacitor Electrodes from Multiwalled Carbon Nanotubes. *Appl. Phys. Lett.* **2000**, *77,* 2421-2423.

47. Wen, Z.; Wang, X.; Mao, S.; Bo, Z.; Kim, H.; Cui, S.; Lu, G.; Feng, X.; Chen, J. Crumpled Nitrogen-Doped Graphene nanosheets with Ultrahigh Pore Volume for High-Performance Supercapacitor. *Adv. Mater.* **2012,** *24,* 5610-5616.

48. Wang, P.; mai, W. Flexible solid-state electrochemical supercapacitors. *Nano Energy,* **2014**, *8,* 274-290.

49. Hou, J.; Cao, C.; Idrees, F. Ma, X. Hierarchical Porous Nitrogen-doped Carbon nanosheets Derived from Silk for Ultrahigh-capacity battery Anodes and Supercapacitors. *ACS Nano,* **2015,** *9,* 2556-2564.

50. Chen, Y.; Li, X.; Prak, K.; Song, J.; Hong, J.; Zhou, L.; Mai, Y. W.; Huang, H.; Goodenough, J. B. Hollow Carbon-Nanotube/Carbon-Nanofiber Hybrid Anodes for Li-Ion Batteries. *J. Am. Chem. Soc.* **2013,** *135,* 16280-16283.

51. Chabi, S.; Peng, C.; Hu, D.; Zhu, Y. Ideal Three-dimensional Electrode Structures for Electrochemical Energy Storage. *Adv. Mater.* **2014,** *26,* 2440-2445.

52. Lee, W. J.; Maiti, U. N.; Lee, J. M.; Lim, J.; Han, T. H.; Kim, S. O. Nitrogen-doped Carbon Nanotubes and Graphene Composites Structures for Energy and Catalytic Applications. *Chem. Commun.* **2014,** *50,* 6818-6830.

53. Wu, Z. S.; Ren, W. C.; Xu, L.; Li, F.; Cheng, H. M. Doped Graphene Sheets as Anode Materials with Superhigh Rate and Large Capacity for Lithium Ion Batteries. *ACS Nano* **2011,** *5,* 5463-5471.

54. Reddy, A. L. M.; Srivastava, A.; Gowda, S. R.; Gullapalli, H.; Dubey, M.; Ajayan, P. M. Synthesis of Nitrogen-Doped Graphene Films for Lithium Battery Application. *ACS Nano* **2010,** *4(11),* 6337-6342.

55. Xiao, Y.; Sun, P.; Cao, M. Core-Shell Bimetallic Carbide Nanoparticles Confined in a Three-Dimensional N-doped Carbon Conductive Network for Efficient Lithium Storage. *ACS Nano* **2014,** *8,* 7846-7857.

56. Mukherjee, R.; Thomas, A. V.; Datta, D.; Singh, E.; Li, J. W.; Eksik, O.; Shenoy, V. B.; Koratkar, N. Defect-Induced Plating of Lithium Metal within Porous Graphene Networks. *Nat. Commun.* **2014,** *5,* 3710-3719.

57. Guo, B.; Wang, X.; Fulvio P. F.; Chi, M.; Mahurin, S. M.; Sun, X.-G.; Dai, S.; Soft-Templated Mesoporous Carbon-Carbon Nanotube Composites for High Performance Lithium-ion Batteries. *Adv. Mater.* **2011,** *5,* 3710-3719.

58. Hu, C.; Wang, L.; Zhao, Y.; Ye, M.; Chen, Q.; Feng, Z.; Qu, L.; Designing Nitrogen-Enriched Echinus-like Carbon Capsules for Highly Efficient Oxygen Reduction Reaction and Lithium Ion Storage. *Nanoscale,* **2014,** *6*, 8002-8009.

59. Li, R.; Wei, Z.; Gou, X. Nitrogen and Phosphorus Dual-doped Graphene/Carbon Nanosheets as bifunctional Electrocatalysts for Oxygen Reduction and Evolution. *ACS Catal.* **2015,** *5,* 4133–4142.

60. Gorlin, Y.; Jaramillo, T. F. A Bifunctional Nonprecious Metal Catalyst for Oxygen Reduction and Water Oxidation. *J. Am. Chem. Soc.* **2010,** *132,* 13612–13614.

61. Wang, Y.; Ding, W.; Chen, S.; Nie, Y.; Xiong, K.; Wei, Z. Cobalt Carbonate Hydroxide/C: An Efficient Dual Electrocatalyst for Oxygen Reduction/Evolution Reactions. *Chem. Commun.* **2014,** *50,* 15529–15532.

62. Tian, G. -L.; Zhang, T. Q.; Zhang, B.; Jin, Y. -G.; Huang, J. -Q.; Su, D. S.; Wei, F. Toward Full Exposure of "Active Sites": Nanocarbon Electrocatalyst with Surface Enriched Nitrogen for Superior Oxygen Reduction and Evolution Reactivity. *Adv. Funct. Mater.* **2014,** *24,* 5956–5961.

63. Zhang, J.; Zhao, Z.; Xia, Z.; Dai, L. A Metal-free Bifunctional Electrocatalyst for Oxygen Reduction and Oxygen Evolution Reactions. *Nat. Nanotechnol.* **2015,** *10,* 444–452.

64. Lin, Z.; Waller, G. H.; Liu, Y.; Liu, M.; Wong, C. –P. Simple Preparation of Nanoporous Few-layer Nitrogen-doped Graphene for use as an Efficient Electrocatalyst for Oxygen Reduction and Evolution Reactions. Carbon **2013,** *53,* 130–136.

* THIS CHAPTER HAS BEEN SUBMITTED AS A FULL PAPER IN THE FOLLOWING JOURNAL;

3D Nanostructured Nitrogen-Doped Graphene/Carbon Nanotube Composites for Large Volumetric Solid State Supercapacitor, Highly Stable Anode for Li-Ion Battery and Metal-Free Bifunctional Electrocatalyst. **S. N. Faisal**, C. M. Subramaniyam, P. Newman, E. Haque, N. Noorbehesht, A. K. Roy, M. M. Islam, H. K. Liu, S. X. Dou, A. T. Harris and A. I. Minett, *ACS Nano*, 2017 (Under Review)

Chapter: 6

3D Copper-Confined N-Doped Graphene/Carbon Nanotube Composite for High Capacity Anode for Li-Ion Battery

6. 3D Copper-Confined N-Doped Graphene/Carbon Nanotube Composite for High Capacity Anode for Li-Ion Battery

ABSTRACT: Facile synthesis of copper nanoparticle confined nitrogen-doped graphene/carbon nanotube composite has been reported in a single pot process by reducing the copper salt to copper nanoparticle via thermal annealing in the process of nitrogen-doped graphene/ carbon nanotube synthesis. The presence of highly conductive copper nanoparticles in the lamellar structured nitrogen-doped graphene/ carbon nanotube composite can improve the conductivity as well as electrochemical properties. The composite containing 12 (at.%) of nitrogen doping exhibits enhanced rate performance (1250 mAh g^{-1} at 0.1 A g^{-1}) as anode in lithium-ion batteries and efficient cycling stability.

6.1 INTRODUCTION

Lithium-ion batteries (LIBs) are considered as potential energy storage device to alleviate the ever-growing demand for efficient energy storage. [1, 2] It is the widely used energy storage device for portable electronics, however to fulfill the ever growing energy demand not only for small portable electronics but also for large scale energy storage like hybrid electric vehicle, it has put forward the developments of LIBs with higher specific capacity and better cycle life. [3] The major limitation of the current LIBS is the most widely used commercial graphite as anode material, which suffers for low theoretical capacity (372 mAh g^{-1}). [4] Graphene, a single layer of graphite with two-dimensional structure, composed of a one-atom-thick honeycomb lattice of sp^2-hybridized carbons, has shown great potential as an electrode material in energy storage including as a promising anode material for LIBs due to its excellent electrical conductivity and high specific surface area. [4-7] However the strong van-der-Waals interaction form restacking of graphene layers which reduce the specific surface area of active materials to access by the electrolyte ions as well as represents inferior electrochemical response compare to the theoretical value. [8] The incorporation of metal nanoparticles including transitional and two-dimensional metals, carbon nanostructured like carbon nanotube, carbon nanofiber and porous carbon can overcome this limitation by preventing the restacking of graphene layers by forming a three-dimensional structure as well as increasing the surface area for better ion storage. [9-14] Alternatively, Chemically doped graphene, in particular nitrogen-doped graphene and its three-

dimensional structured composites formed by the incorporation of nanostructured materials have shown enhanced performance in LIBs by the improved electrochemical properties, surface area and the formation of nanopores for the substitutional doping of nitrogen on the carbon lattice of graphene. [15-18] The incorporation of metal nanoparticles on the nitrogen-doped graphene layers, can improve the performance of LIBs due to the high theoretical capacity and appropriate low discharge potential versus Li/Li^+. [14, 19-21] The transitional metal oxides, in particular copper oxide nanoparticles have gained a lot of attention due to their high theoretical capacity, abundance, low cost and high thermal and electrical conductivity. [22, 23] But the limitation of CuO for its low electrical conductivity, volumetric change during the insertion and extraction of Li ions and fast capacity decay hamper the implementation in LIBs. [22, 23] The implementation of pure copper nanoparticles incorporating with carbonaceous anode material can overcome this limitation by performing as current collector in LIBs and thus improve the charge-discharge properties, specific capacitance and cycling performance. [24, 25] Alternatively, the nanostructured composites coated with copper have shown superior capacitance performance due to the high electrical conductivity of copper. [26, 27] Based on the above observation, the insertion of copper nanoparticle inside a three dimensional nitrogen-doped graphene/ carbon nanotube network can be a new path to enhance the conductivity of the electrode and thus the performance of LIBs.

Here, we have developed a single step synthesis approach for copper-confined nitrogen-doped graphene/carbon nanotube (N-Gr/CNT) composite material. A simple thermal treatment at 800 °C of graphene oxide, oxidized carbon nanotubes with the combination of solid doping precursor uric acid (UA) and copper salt (copper chloride) results high atomic percentage of nitrogen (12.0%) in the graphitic carbon network under an argon atmosphere. During the thermal treatment process at lower temperature the doping agent UA able to form electrostatic and hydrogen bonding with the carboxylic groups of GO and oxidized multiwalled carbon nanotubes (o-MWCNT) surface by the existing amino functional group of it, which promote to form a lamellar-structured 3D building block architecture. At higher temperature treatment the solid doping precursor breaks into highly active nitrogen species to successfully insert in the hexagonal carbon lattice of graphene and CNT homogeneously and the copper salt get reduced to copper nanoparticles and deposited on the graphene surface. The appropriate intercalation of CNT and copper nanoparticles network in-between graphene layers prevents self-agglomeration

towards increase the mass densities as well as volumetric charge storage ability. On the other hand, the nitrogen doped large number of active sites of the 3D network along with the high conductive copper nanoparticles should promote the material for high performance energy storage. The presence of copper nanoparticles inside the graphene/carbon nanotube network can improve the electrochemical conductivity of the composite and thus the Cu-[N-Gr/CNT] exhibits superior capacitive performance as anode in Li-ion battery compared to metal-free N-Gr/CNT.

6.2 EXPERMENTAL SECTION

Synthesis of Cu-confined N-doped graphene/carbon nanotube composites:

The synthesis of Cu-confined N-doped graphene/carbon nanotube composites followed by the similar way stated above for N-doped graphene/ carbon nanotube synthesis. [28, 29 (Chapter 5)] The graphene oxide, multiwalled oxidized carbon nanotube (oCNT), uric acid and metal salt (copper chloride) were mixed at a ratio of 1:3:10:0.1 respectively in a isopropanol solution. The mixtures were then stirred continuously and heated at 80 ºC for 6-8 h to remove the isopropanol. The resulting solid powders were then annealed at 800 ºC at a rate of 5 ºC/min for 1 h in an argon atmosphere in a tubular furnace. The synthesized copper-confined nitrogen doped reduced graphene oxides and carbon nanotubes composite was named Cu-[N-Gr/CNT]. The metal-free nitrogen doped graphene and carbon nanotube composite named N-Gr/NCNT] was prepared for comparison.

Characterization:

The microstructures and morphology of the synthesized samples were investigated by FESEM (Zeiss ULTRA *plus*), HRTEM (JEOL 2200FS) and XRD (Shimadzu S6000). Raman spectra were collected with Renishaw inVia Raman Spectrometer. X-ray photoelectron spectroscopy (XPS) analyses were performed by ESCALAB250Xi (Thermo Scientific, UK) with a monochromated Al K alpha (energy 1486.68 eV) operating at 150W (13 kV x 12 mA) under a vacuum of 2 x 10^{-9} mbar. The analysis spot size was 500 μm in diameter. The binding energies were referenced to the adventitious hydrocarbon C 1s signal at 284.9 eV.

Electrochemical measurement:

The electrochemical characterization of Cu-[N-Gr/CNT] composite for lithium-ion batteries was carried out using coin cells. The electrode was tape-casted over Cu foil by blending the active material, Cu-[N-Gr/CNT], with Super P carbon black and polyvinylidenedifluoride (PVDF) binder, at a weight ratio of 8:1:1, respectively, using N-methyl-2-pyrrolidone (NMP) as the blending solvent and subsequently dried at 120°C for 12 h. The electrode was cut from the as-prepared electrode paper in which the mass loading of an electrode was controlled with ~ 1 mg cm^{-2}. CR 2032 coin-type cells were assembled in an Ar-filled glove box by using the as-prepared electrodes as the working electrode, with Li foil as the counter electrode and reference electrode, a porous polypropylene film as separator, and 1 M $LiPF_6$ in a 1: 1 (v/v) mixture of ethylene carbonate (EC) and diethyl carbonate (DEC) as the electrolyte. The cells were galvanostatically charged and discharged using an automatic battery tester system (Land®, China) at various current densities in the range of 0.002 - 3 V. Cyclic voltammetry and electrochemical impedance spectroscopy (EIS) measurements were performed using a Biologic Science Instruments (Model: VMP3; S/n: 0398) between 0.1 MHz to 10 mHz under AC stimuli with 5 mV of amplitude. The specific capacity of as tested Li-ion battery is solely based on the mass of active material, Cu-[N-Gr/CNT] neglecting the effect of super P carbon black due to its low reversible capacity.

6.3 RESULTS AND DISCUSSION

The synthesis of Cu-[N-Gr/CNT] is illustrated in Figure 1, where the graphene oxide, oxidized carbon nanotubes, uric acid and copper chloride are mixed together in isopropanol at a ratio of 1:3:10:0.1 respectively by mass and stirred continuously at a temperature of 80 ^{0}C until the complete evaporation of solvent. The uric acid molecules adsorbed strongly *via* hydrogen bonding with the carboxyl groups on the graphene oxide and oCNT surfaces and form a lamellar structure *via* interclating the oCNTs in graphene layers. The solid mixtures were collected in powder form and then heated in a tubular furnace at 800 ^{0}C at a rate of 5 ^{0}C/min for 1 hour. Upon pyrolysis the inclusion of nitrogen atom in graphene lattice from the uric acid occurs as well as the copper ion reduced to copper nanoparticles [28, 30] and a three-dimensional structure of

copper nanoparticles decorated nitrogen-doped graphene/ carbon nanotube composite containing high atomic percentage of nitrogen is formed.

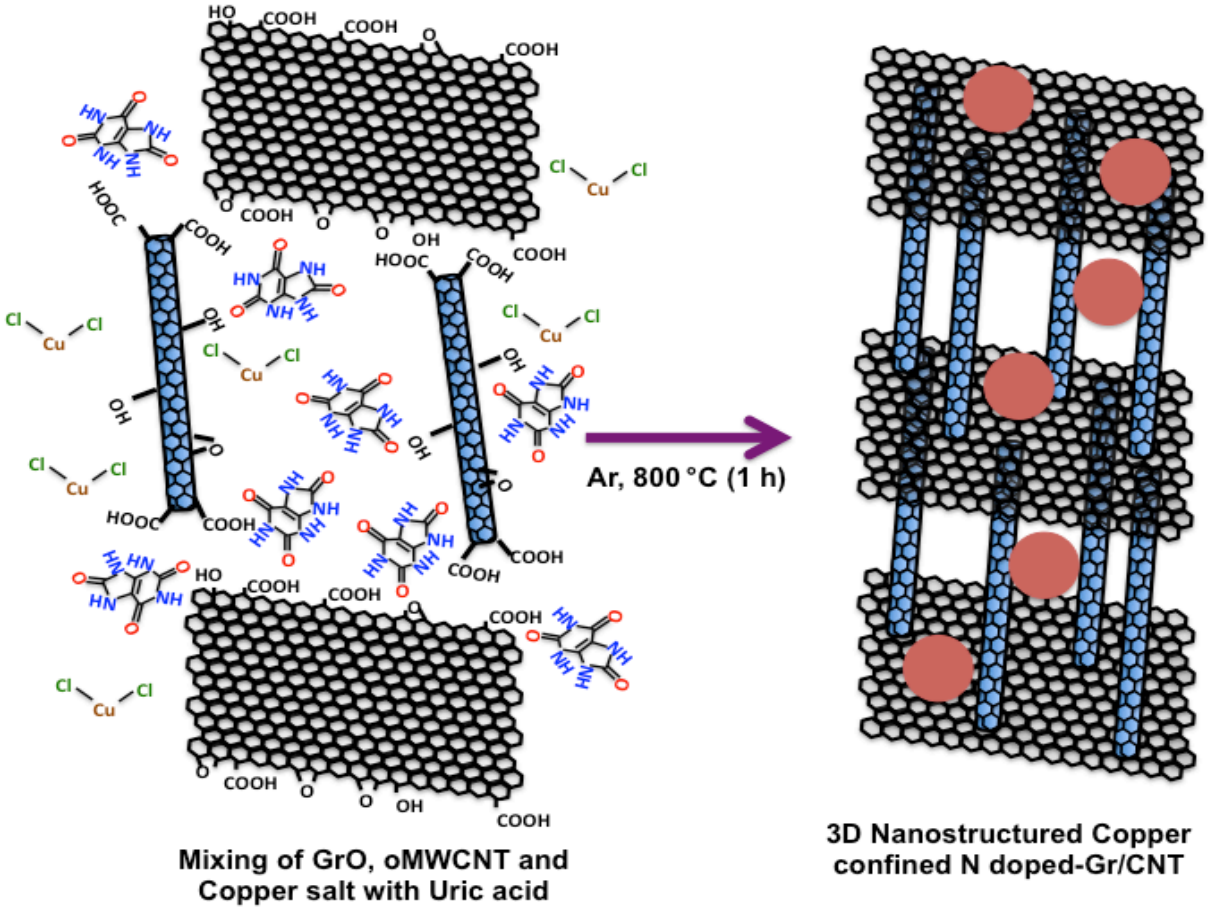

Figure 1: Schematic diagram of the single pot synthesis of copper confined nitrogen-doped graphene/ carbon nanotube three dimensional nanostructure.

The morphology and structure of the obtained composite after pyrolysis was characterized by scanning electron microscopy (SEM) and transmission electron microscopy (TEM). The SEM images of Cu-[N-Gr/CNT] revealed the presence of copper nanoparticles intercalated CNT networks inside the graphene layers. (Figure 2a). The three-dimensional structure and the intercalation of carbon nanotubes and copper nanoparticles inside the graphene layers were clearly visible. For further confirmation, low magnification TEM was used. The TEM image confirms the 3D structures of the composites by forming the CNT networks and copper nanoparticles ranging from 5- 50 nm diameter on the walls of carbon nanotube as well as decorated on the graphene lattice (Figure 2b). The conformation of the nanoparticles and the

distance between the layers of graphene were characterized with the XRD. (Figure 2c) The evaluation of the peak position indicated the slight shifting of the peaks of the composites than the peak for NGr and almost similar position to N-Gr/CNT, indicates the increment of interlayer spacing due to the insertion of carbon nanotube and copper nanoparticles. The calculated interlayer spacing found from the peak position was 0.374 nm, slightly lower than the N-Gr/CNT (0.38 nm) but higher than the average layer-to-layer spacing of nitrogen-doped graphene (0.352). [28, 29] The three major peaks of Cu-[N-Gr/CNT] at 43.5^{O}, 50.5^{O} and 74.5^{O} in the range of $40\text{-}80^{O}$ correspond to the (111), (200) and (220) planes of copper with cubic phase. [30] These peaks were absence for N-Gr/CNT and NGr.

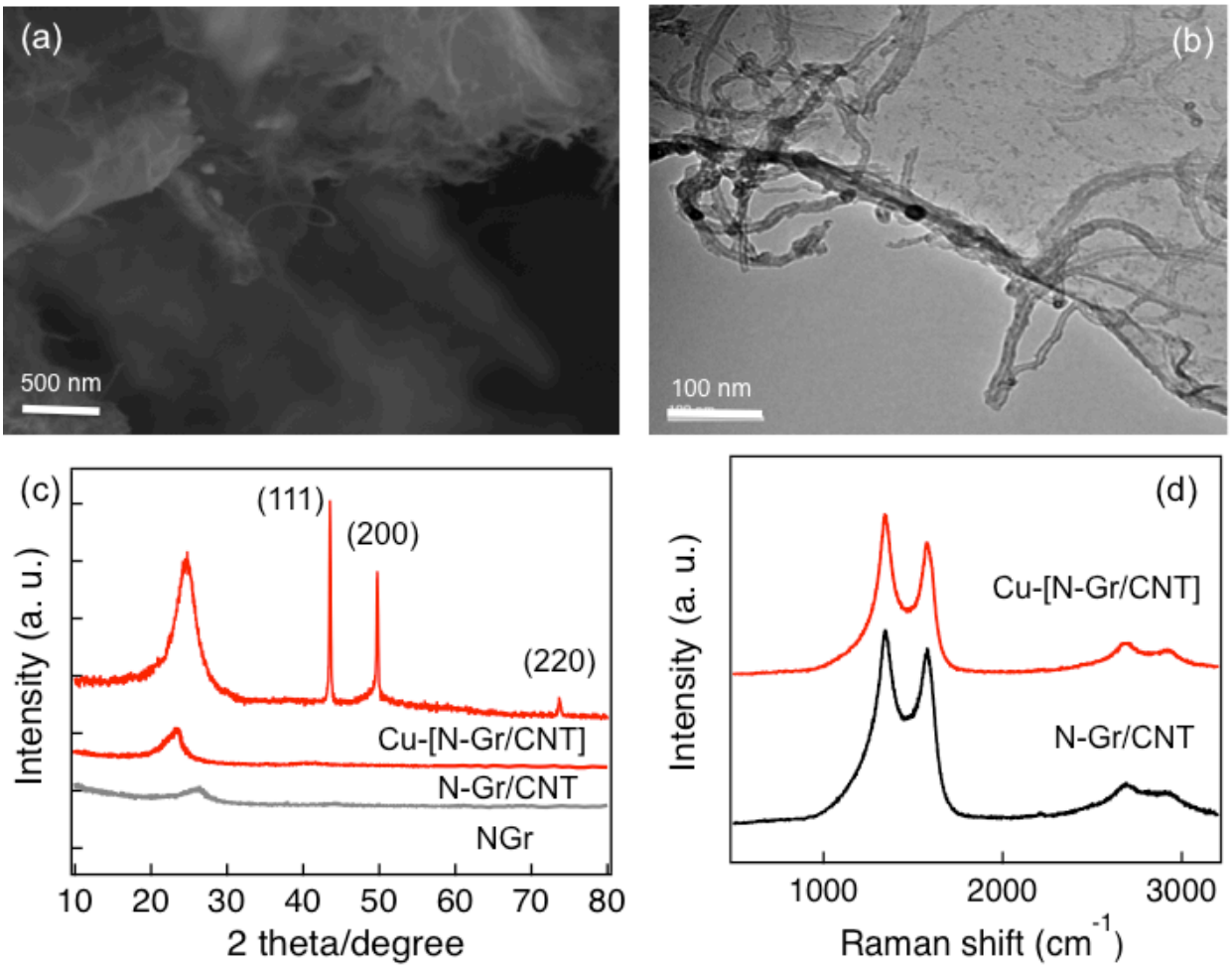

Figure 2: (a) SEM image of Cu-[N-Gr/CNT], (b) TEM image of Cu-[N-Gr/CNT], (c) XRD patterns of Cu-[N-Gr/CNT], N-Gr/CNT and NGr. (d) Raman Spectra of Cu-[N-Gr/CNT] and N-Gr/CNT.

The graphitic nature of both of composites of Cu-[N-Gr/CNT] and N-Gr/CNT were characterized by Raman spectroscopy at an excitation wavelength of 514 nm under ambient conditions. As shown in Figure 2d, the G peaks of both the composites were present at 1578 cm^{-1}. The position of the G peak of Cu-[N-Gr/CNT] was shifted towards down than the G peak of N-Gr/NCNT indicated the creation of more defects possibly due to the formation of metallic nanoparticle during the thermal annealing as well doping of copper atom on the carbon lattice of graphene. The distinguishable 2D peaks of both the composites were observed at 2688 cm^{-1} 2722 cm^{-1}, which confirmed the state of the composites as lamellar bilayers or few layers graphene flakes. [31]

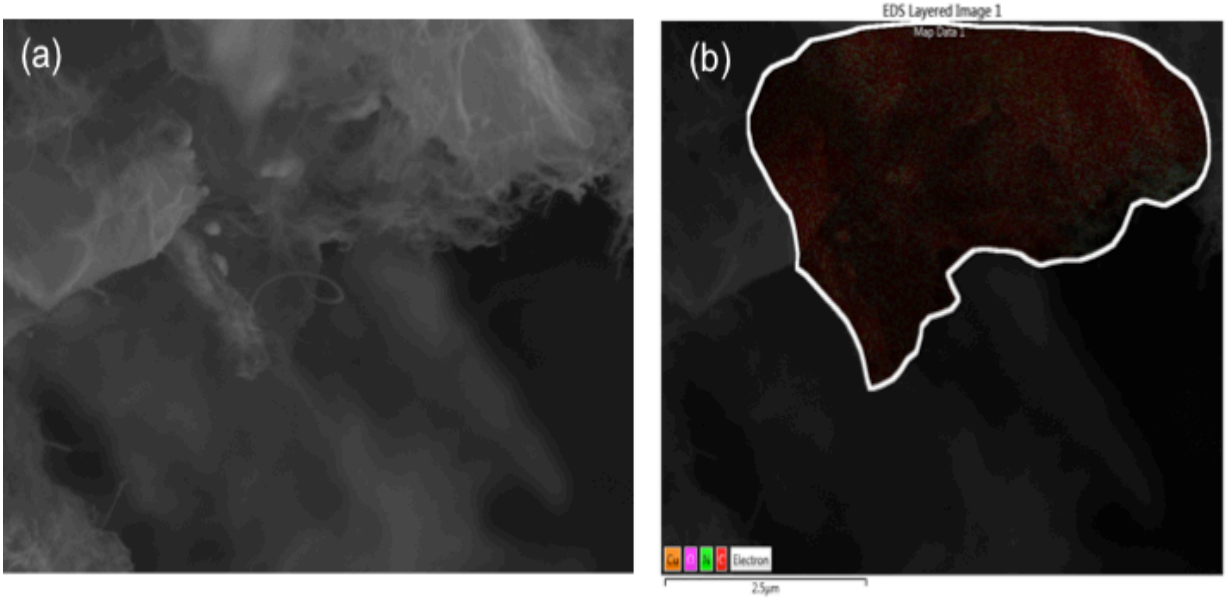

Figure 3: (a) SEM image of Cu-[N-Gr/CNT] (b) SEM-EDS mapping of selected area for the image of Cu-[N-Gr/CNT].

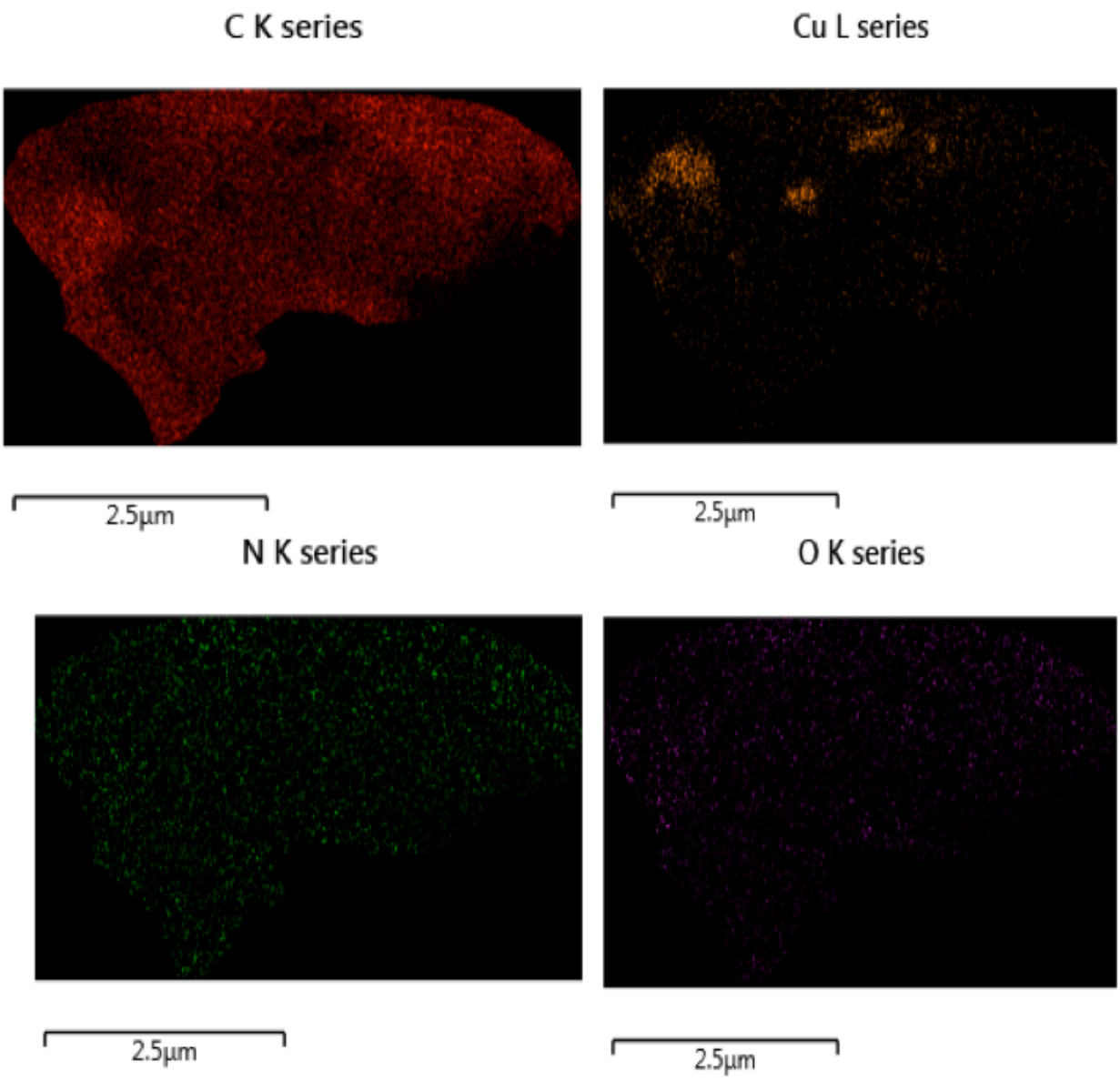

Figure 4: SEM-EDS mapping of the distribution of elements (C, Cu, N and O)

SEM-EDS was applied to further confirmation of elemental distribution (Figure 3). The SEM image of Cu-[N-Gr/CNT] (Figure 3a) and selected EDS layered image (Figure 3b) show the elemental distribution of C, N, O and Cu on the surface. The mapping of each elements shows the presence of C as primary element and overall distribution of N, small amount of distribution of O mostly with the C and presence of Cu embedded on the graphene layers (Figure 4). The percentage of elemental distribution was found from the peak analysis generated from the

corresponding EDS mapping (Figure 5). According to the peak analysis, the percentages of the elements are C (72.4 wt.%), N (13.2 wt.%), O (2.6 wt.%) and Cu (11.8 wt.%).

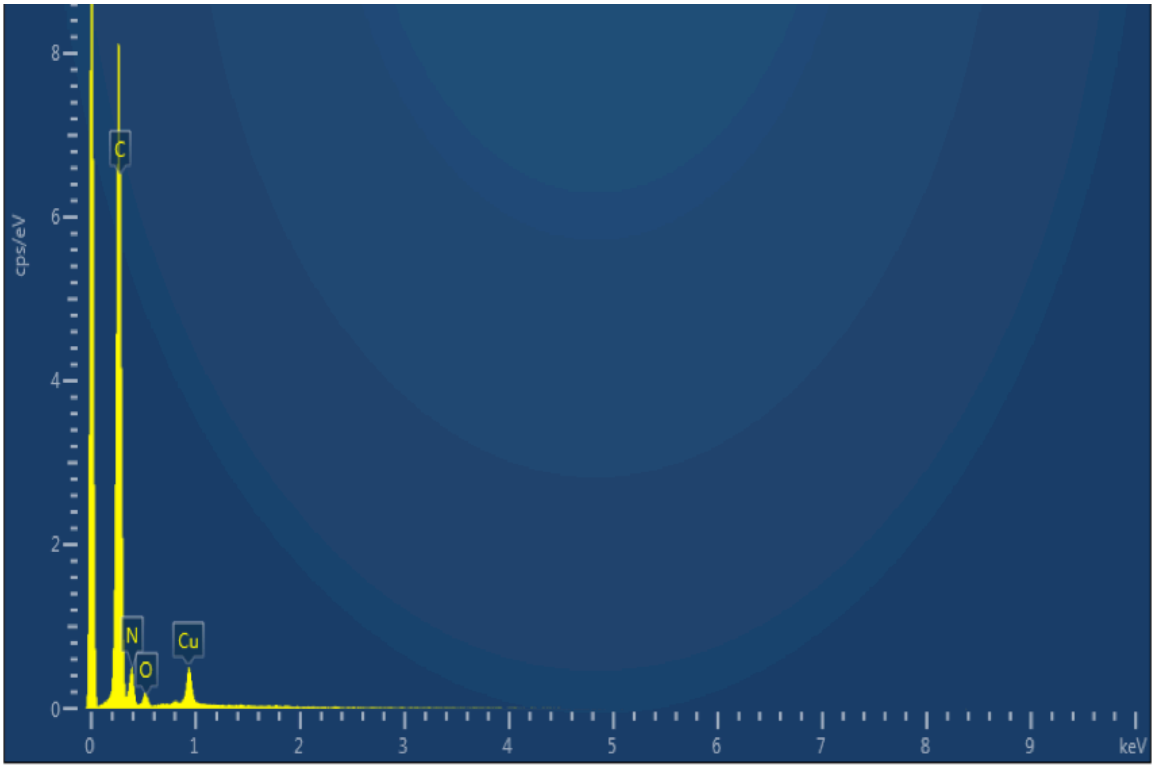

Figure 5: Peak analysis of SEM-EDS mapping.

To further characterize the elemental composition and content of nitrogen in the composites, X-ray photoelectron spectroscopy (XPS) measurements were carried out on Cu-[N-Gr/CNT]. From the XPS measurements of Cu-[N-Gr/CNT], the survey spectra of the composite revealed the presence of C, O, N and Cu. (Figure 6a) In the composite, the high-resolution C1s peak was centered at 284.4 eV tailing at higher binding energies, indicating the connection of carbon atoms with N and O heteroatoms. The peak deconvolution of C1s shows significant amount of sp2 and sp3 carbons and sp3 bonded carbons with nitrogen, oxygen and possibly with copper (Figure 6b). The peak deconvolution of N1s showed (Figure 6c) five possible nitrogen configurations in Cu-[N-Gr/CNT]. These included 49.4% pyridinic N (N1, N in 6-member ring), 10.6% pyrrolic N (N2, N in 5-member ring), 28.5% graphitic N (N3, N in graphene basal plane), 9.3% oxidized N (N4, N-O) and 2.2% protonated N (N5, N-H) in the total nitrogen content of

12.1%. The atomic percentage of copper doping in the carbon lattice is quite high (2.41 at.%) which can modulate the intrinsic electrical properties of the composite.

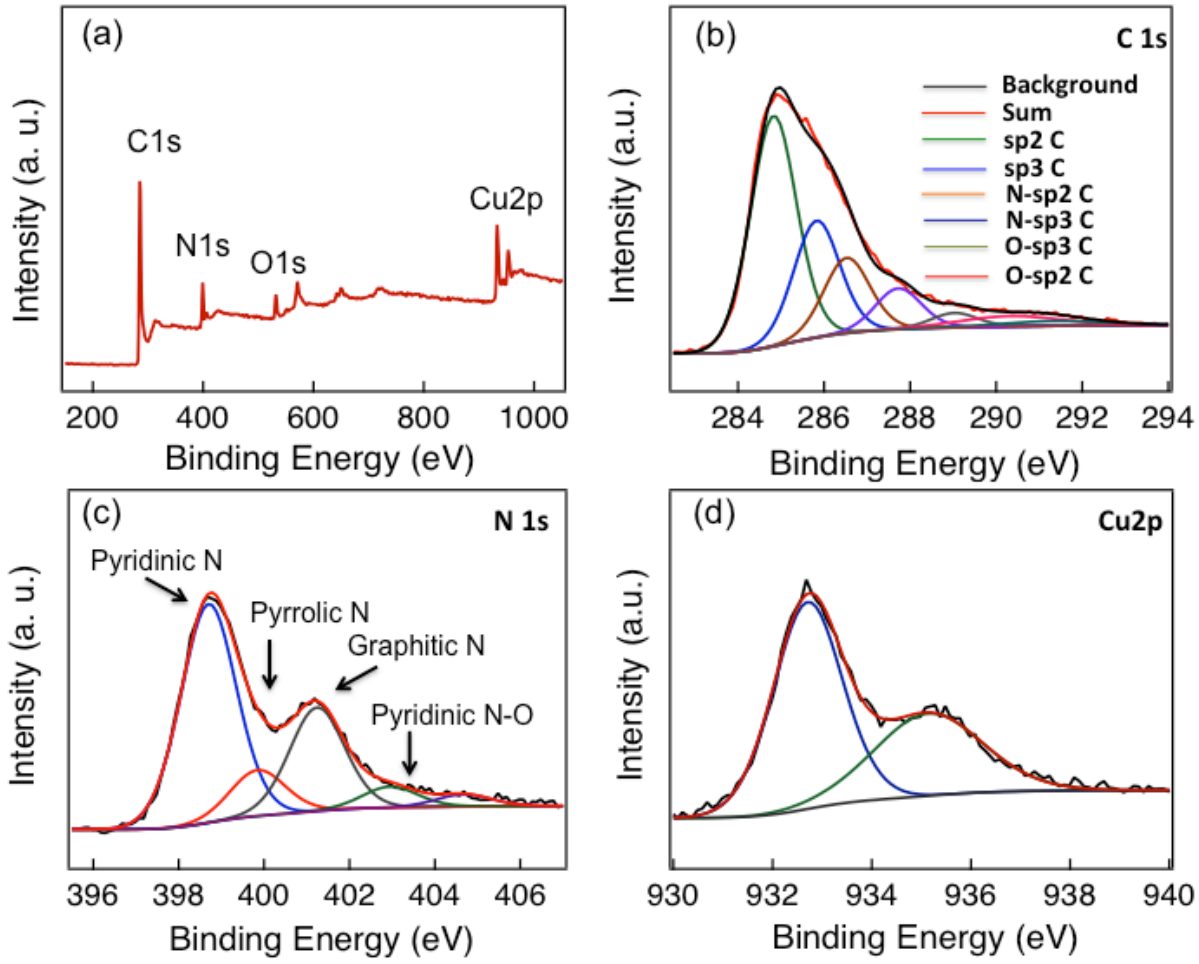

Figure 6: (a) XPS survey of Cu-[N-Gr/CNT], (b) C 1s XPS peak of Cu-[N-Gr/CNT], (c) N 1s XPS peak of Cu-[N-Gr/CNT], (d) Cu2p XPS peak of Cu-[N-Gr/CNT].

Electrochemical Performance of N-Gr/CNT as Anode for Li-Ion Battery.

The incorporation of nitrogen doping in the three-dimensional structure has exhibited superior performance in LIBs by increasing the Li-ion storage capacity, facilitating Li-ion adsorption, enhancing ion diffusion through the structural defects and increasing the stability and cycle life. [32, 33] After observing the remarkable performance of the three-dimensional active material N-Gr/CNT, [29] the copper-confined N-Gr/CNT composite has been utilized to explore the

electrochemical properties as anode for Li-ion battery as this material enriched with copper nanoparticles embedded into graphene surface and a lamellar structure with large surface area with efficient pore volume and high atomic percentage of nitrogen. The cyclic voltammograms profiles from 0 to 3 V exhibits the activity of the composite for lithium-ion batteries (Figure 7a). The CV curves were quite similar after the second cycle indicating a stable state. The capacity above 0.5 V is associated with defects, 3D architectures and layers, pores and Li binding with heteroatom [34, 35] and from the CV curves the peak at 1.1 V indicates the binding of Li ions with heteroatom. During the Li-extraction process, the potential hysteresis showing the removal of inserted lithium ions at a wide potential of 0.1 to 3 V with the associated peaks of 0.1, 0.7 and 1.6 V for lithium extraction from graphene layers and pore structures/defects. [36, 37] The charge-discharge current densities from the capacity over cycling initiating from 0.1 to 10 A/g showing the reversible capacities of 1250, 550, 400, 320, 290 and 230 mA h/g at 0.1, 0.5, 1, 3, 5 and 10 A/g (60 cycle) (Figure 7b). After cycling at various rates, the specific capacity can still be recovered to 1350 mA h/g, implying high stability and reversibility as well as increment of capacitance due to improvement of conductivity by better ion permeation after cycling. The specific capacitance of 1250 mA h/g obtained at 0.1 A/g is 3.36 times greater compared to the theoretical capacity of graphite (372 mA h/g) as well as higher than the metal-free N-Gr/CNT (1150 mA h/g) [29, Chapter 5)]

The cycling stability with reversible battery capacity were observed 500 and 400 mA h/g at current density of 0.5 and 1 A/g in the first cycle .The rapid increment of capacitance were observed at high current density of 0.5 and 1 A/g with the cycling number (Figure 7c). The three-dimensional structure, high nitrogen-doped graphene/carbon nanotube network with highly conductive copper nanoparticles tailor the intrinsic electrical conductivity of the composite and ease the ion diffusion through its porous structures created by the defects and efficiently recovered the large initial loss of capacity and enhanced the lithium storage performance storage at high rates. [34]

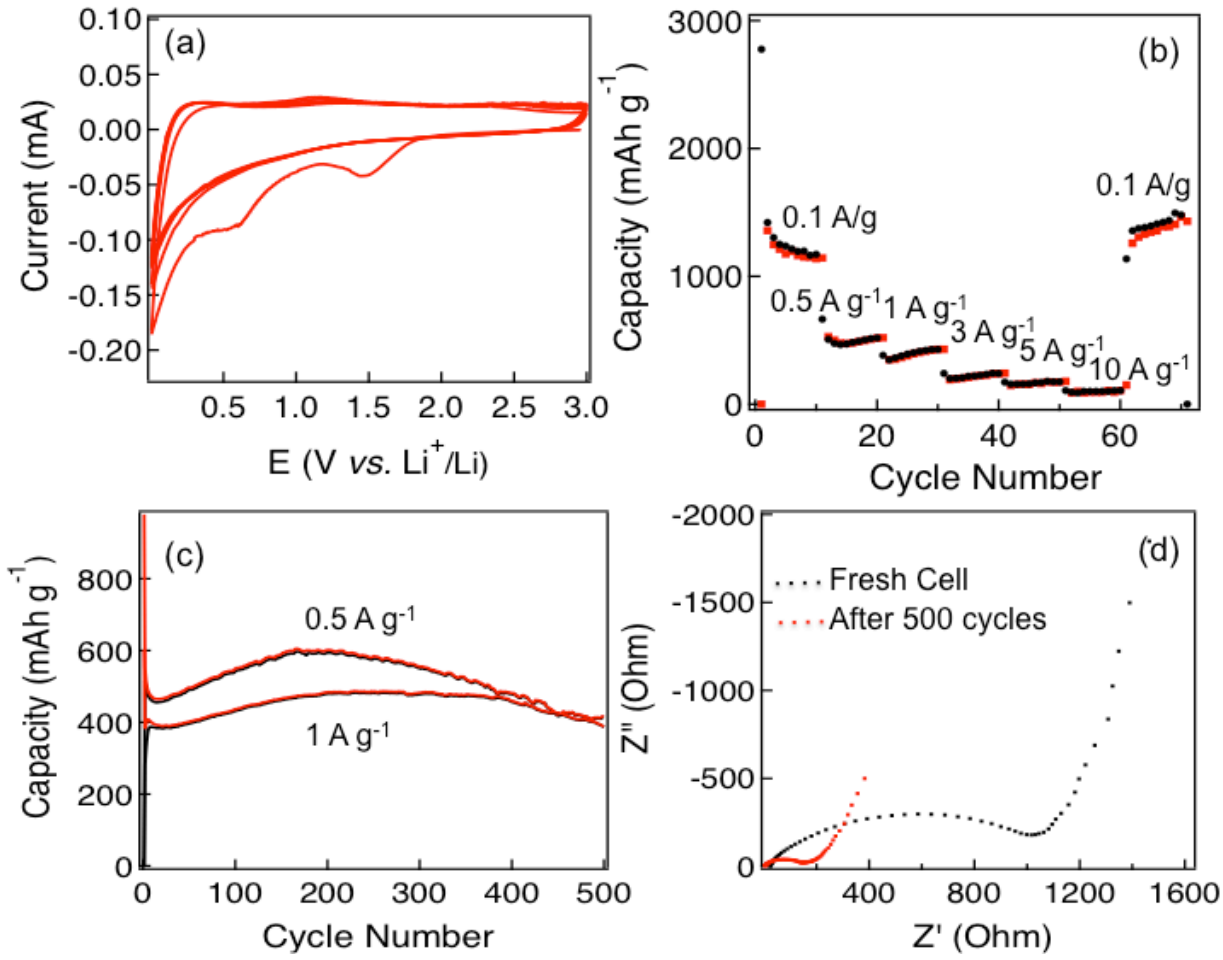

Figure 7. (a) CV curves (1st to 5th cycles) of Cu-[N-Gr/CNT] cell at a scan rate of 0.1 mV s^{-1}, (b) Rate performance at various current densities, (c) High-rate cycling performance in the voltage range from 0.01 to 3.0 V at current densities of 0.5 A/ g and 1 A/g for 500 cycles, (d) EIS of the cell at initial and after 500 cycles.

The electrode exhibits efficient stability by retaining to its initial capacitance after long cycle life of 500 cycles at high current density. The EIS results in Figure 7d, shows the comparison of Nyquest plots of initial and after 500 cycles, explaining the reason of increment of capacitance with the cycle number due to the improvement of conductivity possibly due to the better ion penetration into the highly conductive three-dimensional structure of the composite.

6. 4. CONCLUSION.

In conclusion, we report a facile synthesis method of copper nanoparticle confined-three-dimensional lamellar structured nitrogen-doped graphene/ carbon nanotube hybrid containing high atomic percentage of nitrogen. The synthesized Cu-[N-Gr/CNT] showed excellent capacitive properties and high rate capability anode in lithium-ion battery. This composite can be applied as an electrocatlyst for glucose oxidation and electrocatalytical application utilizing the electrocatalytical properties of copper nanoparticles. Nevertheless, other transition metal or noble metal nanoparticles can be introduced in the three-dimensional graphene/ carbon nanotube composite to explore the properties for different electrocatalytical activities.

REFERENCES

1. Liu, C.; Li, F.; Ma, L. P.; Cheng H. M. Advanced Materials for Energy Storage. *Adv. Mater*. **2010**, *22*, E28-E62.

2. Candelaria, S. L.; Shao, Y.; Zhou, W. Li, W.; Li, X.; Xiao, J.; Zhang, J. –G.; Wang, Y.; Liu, J.; Li, J.; Cao, G. Nanostructured carbon for Energy Storage and Conversion. *Nano Energy* **2012,** *1,* 195-220.

3. Cheg. F. Y.; Liang, J.; Tao, Z. L.; Chen, J. Functional materials for Rechargable Batteries. *Adv. Mater*. **2011**, *23*, 1695-1715.

4. Sun, W. W.; Wang, Y.; Graphene-Based Nanocomposites Anodes for Lithium-Ion Batteries. *Nanoscal*e **2014,** *6,* 11528-11552.

5. Geim, A. K., K. S. K. S. The Rise of Graphene. *Nat. Mater*. **2007,** *6,* 183–191.

6. Choi, H. –J., Jung, S. -M. Seo, J. M., Chang, D. W., Dai, L., Baek, J. –B. Graphene for Energy Conversion and Storage in Fuel Cells and Supercapacitors. *Nano Energy* **2012,** *1,* 534–551.

7. Sun, Y., Wu, Q., Shi, G. Graphene based New Energy Materials. *Energy Environ. Sci*. **2011**, *4,* 1113-1132.

8. Li, D.; Muller, M. B.; Gilje, S.; Kaner, R. B.; Wallace, G. G. Processable Aqueous Dispersions of Graphene Nanosheets. *Nature Nanotechnol*. **2008,** *3,* 101-105.

9. Zhang, J.; Xia, Z.; Dai, L. Carbon-based Electrocataysts for Advanced Energy Conversion and Storage. *Sci. Adv.* **2015,** *1*, 1500564-1500583.

10. Kaskhedikar, N. A.; Maier, J. Lithium Storage in carbon nanostructures. *Adv. Mater.* **2009,** *21,* 2664-2680.

11. Mukherjee, R.; Thomas, A. V.; Datta, D.; Singh, E.; Li, J. W.; Eksik, O.; Shenoy, V. B.; Koratkar, N. Defect-Induced Plating of Lithium Metal within Porous Graphene Networks. *Nat. Commun.* **2014,** *5,* 3710-3719.

12. Chabi, S.; Peng, C.; Hu, D.; Zhu, Y. Ideal Three-dimensional Electrode Structures for Electrochemical Energy Storage. *Adv. Mater.* **2014,** *26,* 2440-2445.

13. Chen, Y.; Li, X.; Prak, K.; Song, J.; Hong, J.; Zhou, L.; Mai, Y. W.; Huang, H.; Goodenough, J. B. Hollow Carbon-Nanotube/Carbon-Nanofiber Hybrid Anodes for Li-Ion Batteries. *J. Am. Chem. Soc.* **2013,** *135,* 16280-16283.

14. Zhang, L.; Huang, Y.; Zhang, Y.; Fan, W.; Liu, T. Three-Dimensional Nanoporous Graphene-Carbon Nanotube Hybrid Frameworks for Confinement of SnS_2 Nanosheets: Flexible and Binder-Free Papers with Highly Reversible Lithium Storage. *ACS Appl. Mater. Interfaces* **2015**, *7,* 27823-27830.

15. Reddy, A. L. M.; Srivastava, A.; Gowda, S. R.; Gullapalli, H.; Dubey, M.; Ajayan, P. M. Synthesis of Nitrogen-Doped Graphene Films for Lithium Battery Application. *ACS Nano* **2010,** *4(11),* 6337-6342.

16. Wu, Z. S.; Ren, W. C.; Xu, L.; Li, F.; Cheng, H. M. Doped Graphene Sheets as Anode Materials with Superhigh Rate and Large Capacity for Lithium Ion Batteries. *ACS Nano* **2011,** *5,* 5463-5471.

17. Tang, C.; Zhang, Q.; Zhao, M. –Q.; Huang, J. –Q.; Cheng, X. –B.; Tan, G. –L.; Peng, H. –J.; Wei, F. Nitrogen-doped Aligned Carbon Nanotube/Graphene Sandwiches: Facile Catalytic Growth on Bifunctional Natural Catalysts and Their Applications as Scaffolds for High-Rate Lithium-Sulfur Batteries. *Adv. Mater.* **2014**, *26,* 6100-6105.

18. Hou, J.; Cao, C.; Idrees, F. Ma, X. Hierarchical Porous Nitrogen-doped Carbon nanosheets Derived from Silk for Ultrahigh-capacity battery Anodes and Supercapacitors. *ACS Nano,* **2015,** *9,* 2556-2564.

19. Zhu, Z.; Wang, S.; Du, J.; Zhang, T.; Cheng, F.; Chen, J. Ultrsmall Sn Nanoparticles Embedded in Nitrogen-Doped Porous Carbon as High-Performance Anode for Lithium-Ion Batteries. *Nano Lett.* **2014,** *14*, 153-157.

20. Xiao, Y.; Sun, P.; Cao, M. Core-Shell Bimetallic Carbide Nanoparticles Confined in a Three-Dimensional N-doped Carbon Conductive Network for Efficient Lithium Storage. *ACS Nano* **2014,** *8,* 7846-7857.

21. Pan, Y.; Ye, K.; Cao, D.; Li, Y.; Dong, Y.; Niu, T.; Zeng, W.; Wang, G. Nitrogen-Doped Graphene Oxide/Cupric Oxide as an Anode Material for Lithium Ion Batteries. *RSC Adv*. **2014**, *4,* 64756-64762.

22. Xu, Y. T.; Guo, Y.; Jiang, H.; Xie, X. B.; Zhao, B.; Zhu, P. L.; Fu, X. Z.; Sun, R.; Wong, C. –P. Enhanced Performance of Lithium-Ion Batteries with Copper Oxide Microspheres@Graphene Oxide Micro/Nanocomposite Electrodes. *Energy Technol*. **2015,** *3*, 488-495.

23. Lu, L. Q.; Wang, Y. Sheet-like and Fusiform CuO Nanostructures Grown on Graphene by Rapid Microwave Heating for High Li-Ion Storage Capacities.

24. Liu, L.; Choi, B. G.; Tung, S. O.; Hu, T.; Liu, Y.; Li, T.; Zhao, T.; Kotov, N. A. Low-Current Field-Assisted Assembly of Copper Nanoparticles for Current Collectors. *Faraday Discuss*. **2015,** *181,* 383-401.

25. Guo, K.; Pan, Q.; Wang, L. Fang, S. Nano-scale Copper-coated Graphite as Anode Material for Lithium-Ion Batteries. *J. Appl. Electrochem*. **2002,** *32,* 679-685.

26. Polat, D. B.; Keles, O.; Amine, K. Silicon-Copper Helical Arrays for New Generation Lithium Ion Batteries. *Nano Lett*. **2015,** *15,* 6702-6708.

27. Polat, D. B.; Lu, J.; Abouimrane, A.; Keles, O.; Amine, K. Nanocolumnar Structured Porous Cu-Sn Thin Film as Anode Material for Lithium-Ion batteries. *ACS Appl. Mater. Interfaces*, **2014,** *6(14),* 10877-10885.

28. Faisal, S. N.; Haque, E.; Noorbehesht, N.; Zhang, W.; Harris, A. T.; Church, T. L.; Minett, A. I. N-Doped Graphene with High Atomic Percentages of Pyridinic N and Graphitic N as Electrode for High-Performance Supercapacitor and Efficient Bifunctional Electrocatalyst for ORR and OER**.** *Carbon*, **2016** (under review).

29. Faisal, S. N.; Subramaniyam, C. M.; Newman,P.; Haque, E.; Noorbehesht, N.; Roy, A. K.; Islam, M. M.; Yuen, A. K. L.; Liu, H. K.; Dou, S. X.; Harris A. T.; Minett, A. I. 3D Nanostructured Nitrogen-Doped Graphene/Carbon Nanotube Composites for Large Volumetric Solid State Supercapacitor, Highly Stable Anode for Li-Ion Battery and Metal-Free Bifunctional Electrocatalyst, *ACS Nano*, **2016** (Submitted).

30. Jiang, D.; Liu, Q.; Wang, K.; Qian, J.; Dong, W.; Yang, Z.; Du, X.; Qiu, B. Enhanced Non-Enzymatic Glucose Sensing Based on Copper Nanoparticles Decorated Nitrogen-doped Graphene. *Biosens. Bioelectron*. **2014,** *54,* 273-278.

31. C. Ferrari, D. M. Basko, Raman spectroscopy as a versatile tool for studying the properties of graphene, *Nat. Nanotechnol.* **2013,** *8,* 235–246.

32. Tang, C.; Zhang, Q.; Zhao, M. –Q.; Huang, J. –Q.; Cheng, X. –B.; Tan, G. –L.; Peng, H. –J.; Wei, F. Nitrogen-doped Aligned Carbon Nanotube/Graphene Sandwiches: Facile Catalytic Growth on Bifunctional Natural Catalysts and Their Applications as Scaffolds for High-Rate Lithium-Sulfur Batteries. *Adv. Mater.* **2014***, 26,* 6100-6105.

33. Lee, W. J.; Maiti, U. N.; Lee, J. M.; Lim, J.; Han, T. H.; Kim, S. O. Nitrogen-doped Carbon Nanotubes and Graphene Composites Structures for Energy and Catalytic Applications. *Chem. Commun.* **2014,** *50,* 6818-6830.

34. Hou, J.; Cao, C.; Idrees, F. Ma, X. Hierarchical Porous Nitrogen-doped Carbon nanosheets Derived from Silk for Ultrahigh-capacity battery Anodes and Supercapacitors. *ACS Nano,* **2015,** *9,* 2556-2564.

35. Xiao, Y.; Sun, P.; Cao, M. Core-Shell Bimetallic Carbide Nanoparticles Confined in a Three-Dimensional N-doped Carbon Conductive Network for Efficient Lithium Storage. *ACS Nano* **2014,** *8,* 7846-7857.

36. Guo, B.; Wang, X.; Fulvio P. F.; Chi, M.; Mahurin, S. M.; Sun, X.-G.; Dai, S.; Soft-Templated Mesoporous Carbon-Carbon Nanotube Composites for High Performance Lithium-ion Batteries. *Adv. Mater.* **2011,** *5,* 3710-3719.

37. Hu, C.; Wang, L.; Zhao, Y.; Ye, M.; Chen, Q.; Feng, Z.; Qu, L.; Designing Nitrogen-Enriched Echinus-like Carbon Capsules for Highly Efficient Oxygen Reduction Reaction and Lithium Ion Storage. *Nanoscale,* **2014,** *6*, 8002-8009.

* THIS CHAPTER HAS BEEN SUBMITTED AS A FULL PAPER IN THE FOLLOWING JOURNAL;

Three-dimensional Copper-confined Nitrogen-Doped Graphene/Carbon Nanotube Composites as High Performance Anode for Li-Ion Battery. **S. N. Faisal**, C. M. Subramaniyam, E. Haque, N. Noorbehesht, A. K. Roy, M. M. Islam, H. K. Liu, S. X. Dou, A. T. Harris and A. I. Minett, *ACS Applied Material & Interfaces*, 2016 (Manuscript under preparation)

Chapter: 7

Future Works and Conclusions

7. 1. Future Works

7.1.1 Synthesis of Nickel Embedded Nitrogen-doped Graphene/Carbon nanotube for Metal-Air battery

Observing the superior OER properties of Ni/NGr (Chapter 4) and N-Gr/CNT (chapter-5) led to focus on the development of Ni-embedded N-Gr/CNT electrode for metal-air batteries. The N-Gr/CNT shows remarkable rate capability in lithium ion battery as well as bifunctional electrocatalytic properties, which are crucial for next generation metal-air batteries. The composite may have a synergistic effect on catalysis and will provide better ORR activity closer to Pt/C and better OER activity than Ru/C. The active material has been already synthesized and under electrochemical characterization for application in metal-air battery.

7.1.2 Synthesis of Cobalt decorated Nitrogen-doped Graphene/Carbon nanotube and Nickel Embedded Nitrogen-doped Graphene/Carbon nanotube for Complete Water Splitting

Cobalt nanoparticles confined with nitrogen-doped graphene exhibits remarkable hydrogen evolution reaction for water splitting (Fei *et al*., Nat. Commun. 2015, 6, 8668-1674). On the other side nickel embedded nitrogen-doped graphene shows better OER activity compare to Ru/C (Chapter-4). The synthesis of Cobalt embedded N-Gr/CNT and Ni-embedded N-Gr/CNT and use as electrodes for HER and OER respectively can perform as complete water splitting at comparatively low energy. This can be a promising method to replace noble metal electrocatalyst for water splitting.

7.1.3 Copper-confined Nitrogen-doped Graphene/Carbon nanotube as Electrode for Developing Non-Enzymatic Glucose Fuel Cell

Copper nanoparticles and copper-graphene hybrid has shown excellent electrocatalytical properties for glucose oxidation. The three-dimensional structure of active material also facilitates the electrocatalysis of glucose. (Zaidi *et.al*. Talanta, 2016, 149, 30-42.) The synthesized Copper confined nitrogen-doped graphene/carbon nanotube Cu-[N-Gr/CNT] composite shows remarkable electrochemical properties (Chapter-6) and utilizing the three-

dimensional structure with copper nanoparticles can be able to oxidize glucose at high current which can led to fabricate a single compartment non-enzymatic glucose fuel cell.

7.1.4 Development of Electrode for Hydrogen Peroxide Fuel Cell for Aerospace applications

Hydrogen peroxide has gained attention as a liquid oxidant for the recent developments of rechargeable fuel cell, single compartment fuel cell and fuel cell without oxygen chamber. (An *et al*. Sci. Bull. 2015, 60, 55-64) The electrocatalytic activity of Ni/NG for HPOR (Chapter-4) led to design a hydrogen per oxide fuel cell using Ni-[N-Gr/CNT] composite as electrode material which is under investigation.

7. 2. Conclusions

The objective of this thesis is to develop graphene-based nanocomposites to improve the electrochemical properties comparable to commercially applied materials and develop energy storage and conversion devices for next generation. The significant results from each of the chapters of this thesis are outlined below:

i) Nitrogen-doped graphene with high atomic percentage of nitrogen has been synthesized in a facile thermal annealing process using uric acid as a new solid nitrogen precursor. The resultant composite shows high percentages of different nitrogen configurations on carbon lattice of graphene, which are crucial for electrochemical performance. Efficient capacitance properties (230 F/g at a current density of 1 A/g) in a T-Cell device are observed. In addition the material shows metal-free bifunctional electrocatalysis for ORR and OER closer to the commercial electrocatalysts of Pt/C and Ru/C.

ii) To enhance the electrocatalytical properties of the nitrogen-doped graphene, nickel nanoparticles has been co-pyrolysis from the nickel salt following similar synthesis procedure by adding the nickel salt in the solution before thermal annealing. The resultant composite shows high distribution of nickel nanoparticles on the graphene

layers and improves the electrocatalytical properties by utilizing the electrocatalytical properties of nickel nanoparticles. The synergistic electrocatalytical activities demonstrate not only intensify the ORR and OER but also HER and HPOR comparable to noble metal electrocataysts.

iii) The energy storage properties of the nitrogen-doped graphene have been developed by fabricating a three-dimensional nanostructure of nitrogen-doped graphene/carbon nanotube composite. The solid nitrogen precursor, uric acid not only acts as a source of nitrogen but also helps to create a structure by attaching the oxygen groups of graphene oxide and oxidized CNTs. And thus, form a lamellar structure of inserted CNTs in graphene layers upon thermal annealing. The composites shows high capacitance properties (324 F/g at current density of 1 A/g) and high rate capability in lithium-ion battery (1150 mA h g^{-1} at o.1 A/g) as well as cycle life up to 1250 cycles at high current density of 1 A/g. In addition, it shows superior metal-free bifunctional electrocatalytical activity for ORR and OER.

iv) The combination of metal nanoparticles and three-dimensional nitrogen-doped graphene/ carbon nanotube nanostructure can lead to develop electrode materials with high energy storage performance and electrocatalytical activity to replace the noble metal electrocatalyst and fabricating devices of advanced energy storage and conversions. The copper confined-N-Gr/CNT shows increment of capacitance after inserting copper nanoparticles than the metal-free N-Gr/CNT. It can also play crucial role to develop non-enzymatic glucose fuel cell and conductive transparent electrodes using high opacity of graphene. The electrocatalytical properties can be manipulated by tailoring different nanoparticles with different electrocatalytical activity. As example inserting cobalt nanoparticle in N-Gr/CNT can improve HER properties, nickel nanoparticles can improve OER properties for metal-air batteries, tin nanoparticles can improve metal-ion storage properties in lithium-ion batteries and silver nanoparticle can improve opacity for transparent conductive electrode.